Universita' degli Studi di Milano-Bicocca

Doctorate School of Science

Ph.D. in Physics and Astronomy - XXII Cycle

Coordinator: Prof. Claudio Destri

Matching Next-to-Leading-Order QCD Calculations with Shower Monte Carlo Simulations: Single Vector Boson and Higgs Boson Productions in POWHEG

Ph.D. Dissertation of Simone Alioli - Matr. 032874

Supervisor: Prof. Paolo Nason

Academic Year 2008–2009

Contents

Contents iii

Introduction

In the past years, next-to-leading order (NLO) QCD computations have become standard tools for phenomenological studies at lepton and hadron colliders. QCD tests have been mainly performed by comparing NLO results with experimental measurements, after the inclusion of corrections due to detector effects in the latter.

On the the other hand, from the experimental point of view, general purpose Shower Monte Carlo (SMC) programs have become the main tools used in the analysis. SMC programs usually include leading order (LO) calculations and account for dominant QCD effects at the leading logarithmic level, but do not enforce NLO accuracy. These programs were routinely used to simulate background processes and signals in physics searches. When a precision measurement was needed, to be compared with a NLO calculation, one could not directly compare the experimental output with the SMC output, since the SMC does not have the required accuracy. The SMC output was used in this case to correct the measurement for detector effects, and the corrected result was compared to the NLO calculation.

In view of increasing precision required to disentangle signals from backgrounds at present and future colliders, it has become clear that SMC programs should be improved, when possible, with NLO results. In this way a large amount of the acquired knowledge on QCD corrections would be made directly available to the experimentalists, in a flexible form that they could easily use for simulations.

The problem of merging NLO calculations with parton shower simulations is basically that of avoiding overcounting, since the SMC programs already implement approximate NLO corrections. Several proposals have appeared in the literature [1, 2, 3, 4] that can be applied to both e^+e^- and hadronic collisions, and two approaches [5, 6] suitable for e^+e^- annihilation. Furthermore, proposals for new shower algorithms, that should be better suited for merging with NLO results, have appeared during past years (see refs. [7, 8, 9, 10, 11, 12, 13]).

However, the first general solution to the overcounting problem was the `MC@NLO` proposal [2]. The basic idea of `MC@NLO` is to avoid the overcounting by subtracting from the exact NLO cross section its approximation, as implemented in the SMC program to which the NLO computation is then matched. Such approximated cross section is computed analytically, and is SMC dependent. On the other hand, the MC subtraction terms are process-independent, and thus, for a given SMC, can be computed once and for all. In the current version of the `MC@NLO` code, the MC subtraction terms have been computed for `HERWIG` [14, 15, 16]. In turns out, however, that in general, the exact NLO cross section minus the MC subtraction terms does not need to be positive. Therefore `MC@NLO` can generate events with negative weights. For the processes implemented so far, negative-weighted events may reach about 10–15% of the total. Their presence does not imply a negative cross section, since at the end physical distributions must turn out to be positive. However, the probabilistic interpretation of events is somewhat spoiled. The `MC@NLO` proposal is based upon the requirement that: infrared-safe observables have NLO accuracy, collinear enhanced emissions are summed at the leading-logarithmic level, and the double logarithmic region (i.e. soft and collinear gluon emission) is treated correctly, if the SMC code used for showering has this capability. In the case of `HERWIG` this last requirement is satisfied, owing to the fact that its shower is based upon an angular-ordered branching. The generality of the method has been explicitly proven by its application to processes of increasing complexity, such as heavy-flavour-pair [17] and single-top [18] production.

In ref. [4] a method, named `POWHEG` (for Positive Weight Hardest Emission Generator), that overcomes the problem of negative weighted events, and that is not SMC dependent, was proposed. In the `POWHEG` method the hardest radiation is generated first, with a technique that yields only positive-weighted events using the exact NLO matrix elements. The `POWHEG` output can then be interfaced to any SMC program that is either p_{T}-ordered, or allows the implementation of a p_{T} veto. All SMC programs compatible with the *Les Houches Interface for User Processes* [19] should comply with this requirement. However, when interfacing `POWHEG` to angular-ordered SMC programs, the double-log accuracy of the SMC is not sufficient to guarantee the double-log accuracy of the whole result. Some extra soft radiation (technically called vetoed-truncated shower in ref. [4]) must also be included in order to recover double-log accuracy. In fact, angular ordered SMC programs may generate soft radiation before generating the radiation with the largest p_{T}, while `POWHEG` generates it

first. In any case, recent versions of angular ordered SMC's, such as HERWIG++ [20], do implement soft-truncated showers. On the other hand, when POWHEG is interfaced to shower programs that use transverse-momentum ordering, the double-log accuracy should be correctly retained, if the SMC is double-log accurate. The ARIADNE program [21] and PYTHIA 6.4 [22] (when used with the new showering formalism), both adopt transverse-momentum ordering, in the framework of dipole-shower algorithm [23, 24, 25], and aim to have accurate soft resummation approaches, at least in the large N_c limit, N_c being the number of colours.

A proof of concept for the POWHEG method has been given in ref. [26], for ZZ production in hadronic collisions. In ref. [27] the method was also applied to $Q\bar{Q}$ hadroproduction. Detailed comparisons have been carried out between the POWHEG and MC@NLO results, and reasonable agreement has been found, which nicely confirms the validity of both approaches. In ref. [28] the POWHEG method, interfaced to the HERWIG Monte Carlo, has been applied to e^+e^- annihilation, and compared to LEP data. The method yields better fits compared to HERWIG with matrix-element corrections. The authors of ref. [28] have also provided an estimate of the effects of the soft-truncated shower, which turned out to be small. Furthermore, they have also applied the POWHEG method to top pairs production and decay, always from e^+e^- annihilation [29].

In ref. [30] a general description of the method was given, and in particular its implementation within the Catani-Seymour (CS) subtraction scheme [31] and within the Frixione-Kunszt-Signer (FKS) [32, 33] approach. We will follow the same approach and notation outlined in this work throughout the first part of this thesis.

Apart those mentioned above, the list of processes implemented according to the POWHEG method includes, up to now, Drell-Yan vector boson production [34, 35], W' production [36], Higgs boson production via gluon fusion [37, 38], Higgs boson production associated with a vector boson (Higgs-strahlung) [38] and single top, both in the s- and t-channel production mechanism [39].

Outline

In the present work we give a detailed description of the POWHEG method and an overview of two specific applications: single vector boson and Higgs boson production via gluon fusion. This thesis is organized as follows.

In the first chapter, after a brief introduction to QCD in sec. 1.1, we summarize in sec. 1.2 the general features of a NLO computations and of the subtraction formalisms. We first present the features of a general subtraction scheme. Then, we illustrate in detail two such schemes, which we adopted in calculations appearing in this thesis: the Catani and Seymour (CS) [31] and the Frixione, Kunszt and Signer (FKS) [32, 33] one. The CS method has been widely used in the literature. On the other hand, the FKS method has already been used extensively in the `MC@NLO` implementations. Furthermore, the NLO cross sections for vector-boson and heavy-quark pair production used in the `POWHEG` implementations of refs. [26, 27] have a treatment of initial-state radiation that is essentially the same one used in FKS. We thus review these two subtraction procedures separately in subsections 1.2.3 and 1.2.4.

In chapter 2 we turn to Shower Monte Carlo programs, with a general discussion about their features in sec. 2.1. The basis and the formulation of the shower algorithm are then presented in detail in sec. 2.1.1. The matching with matrix elements corrections is instead briefly surveyed in sec. 2.2.

In chapter 3 we discuss the inclusion of NLO corrections in a parton shower framework, together with a basic introduction of the `POWHEG` and `MC@NLO` methods, in sec. 3.1. Then we present the `MC@NLO` method in sec. 3.2, while in sec. 3.3 we go through all the details of the `POWHEG` method. This last is presented in its full generality, and it is shown how to apply it within any subtraction framework. Thus, this section does not refer in particular to either the FKS or the CS method.

In chapter 4 we deal with the application of the `POWHEG` method to the process of single vector boson production, according to the CS subtraction formalism. Both Tevatron and LHC collider configurations are discussed. Formulas and results of this chapter have already been published in

1. *NLO vector-boson production matched with shower in POWHEG*,
   Simone Alioli, Paolo Nason, Carlo Oleari and Emanuele Re.
   NSF-KITP-08-74, May 2008. 35pp.
   Published in *JHEP* **07** (2008) 060.
   e-Print: `arXiv:0805.4802[hep-ph]` .

Higgs boson production via gluon fusion process is then presented in chapter 5, with applications to both Tevatron and LHC colliders. In this case, the `POWHEG` implementation according to the FKS subtraction formalism has been chosen. Part

of the formulas and results of this chapter have already been published in

2. *NLO Higgs boson production via gluon fusion matched with shower in POWHEG*,
   Simone Alioli, Paolo Nason, Carlo Oleari and Emanuele Re.
   Dec. 2008. 26pp.
   Published in *JHEP* **04** (2009) 002.
   e-Print: `arXiv:0812.0578[hep-ph]` .

   With respect to these articles much emphasis on the calculations and more details are given in this thesis. In particular, we deepen the study of some aspects of Higgs boson production, presenting results concerning the high-p_{T} distribution, the renormalization and factorization scales dependence and the dip in the central rapidity region issues, that have not been published in the reference above. Some of this final considerations have instead been published, adapted for the single-top production case, in

3. *NLO single-top production matched with shower in POWHEG:*
   s- and t-channel contributions,
   Simone Alioli, Paolo Nason, Carlo Oleari and Emanuele Re.
   Jul. 2009. 37pp.
   Published in *JHEP* **09** (2009) 111.
   e-Print: `arXiv:0907.4076[hep-ph]` .

   Finally, we summarize our work and give our conclusion in the final chapter. We have also collected symbols, notations, useful formulas and explicit calculations not appearing in the aforementioned papers in the Appendixes A through C.

Perturbative QCD

1.1 Quantum Chromo-Dynamics

1.1.1 $SU(3)$ Algebra and the QCD Lagrangian

Strong interactions are one of the four fundamental forces in Nature. They account for the interactions between quarks and gluons, explaining how to they bind together to form ordinary hadronic matter, of which protons and neutrons are common examples. In the Standard Model of elementary particles (SM from now on), they are described by means of the Quantum Chromo-Dynamics (QCD). The basic idea of QCD is that hadronic matter is made of constituents: *quarks*, *anti-quarks* or *gluons*, and that there is a new degree of freedom, which results in a new conserved quantum number, the *color*. Each (anti-) quark, or gluon, can thus carry a different color index. Experimental evidences limit the total number of colors to three for (anti-) quarks and to eight for gluons. Furthermore, no observation of the color quantum number by means of free quark or gluons has ever been made, yielding to postulate the *confinement* of ordinary hadronic matter particles into states that behave as singlets under the color group action. Mathematically, QCD is a local gauge theory based on the non-abelian, compact and simple Lie group $SU(3)$, the group of 3×3 complex unitary matrices $U(x)$, with unit determinant

$$U^\dagger(x)U(x) = U(x)U^\dagger(x) = 1, \qquad \det U(x) = \exp\left[\mathrm{Tr}\{\log U(x)\}\right] = 1 \, . \qquad (1.1)$$

One can always write the generic element of the group in a exponential form

$$U(x) = \exp\left[i\,\omega_a(x)\,t^a\right], \quad \text{with} \quad a = 1, \, \ldots \, , N_{\mathrm{c}}^2 - 1 \quad \text{and} \quad N_{\mathrm{c}} = 3 \, . \qquad (1.2)$$

The index a runs on the degrees of freedom of the adjoint representation, $\omega_a(x)$ are the real phase parameters of the local gauge transformation and t^a the group generators in the same representation of the objects onto which the transformation is acting. These generators may be expressed by means of hermitian and traceless matrices,

$$t^a = (t^a)^\dagger \qquad \text{and} \qquad \text{Tr}\{t^a\} = 0\,, \tag{1.3}$$

from which it follows that the number of generators, i.e. the dimension of the adjoint representation, is $N_\mathrm{c}^2 - 1 = 8$. The group algebra is then further specified by the commutation relation

$$\left[t^a, t^b\right] = i\, f^{abc}\, t^c\,, \tag{1.4}$$

where f^{abc} are the group structure constants. From the usual normalization

$$\text{Tr}\{t^a t^b\} = T_\mathrm{F}\, \delta^{ab}\,, \qquad \text{with} \qquad T_\mathrm{F} = \frac{1}{2}\,, \tag{1.5}$$

it follows that the structure constants f are reals and antisymmetric. The commutation relation of eq. (1.4) also implies that the structure constants must satisfy a set of identities known as Jacobi identities, for example

$$f^{ade} f^{bcd} + f^{bde} f^{cad} + f^{cde} f^{abd} = 0\,. \tag{1.6}$$

A common choice for $SU(3)$ generators in the fundamental representation is provided by the Gell-Mann matrices λ^a, by the definition

$$t^a = \frac{\lambda^a}{2}\,. \tag{1.7}$$

Using Jacobi identities it is also possible to define the adjoint representation by means of matrices T, built by structure constants

$$\left(T^b\right)_{ac} = i f^{abc}\,, \tag{1.8}$$

in such a way that they always satisfy $\left[T^a, T^b\right] = i f^{abc}\, T^c$. It is also important to remark that the color matrices and the structure constants must satisfy the following relations

$$t^a_{ij}\, t^a_{jk} = C_\mathrm{F}\, \mathbb{1}_{ik}\,, \tag{1.9}$$

$$i f^{abc}\, i f^{cbd} = \left(T^b\right)_{ac} \left(T^b\right)_{cd} = C_\mathrm{A}\, \mathbb{1}^{ad}\,, \tag{1.10}$$

where we have indicated with i, j, k the color degrees of freedom in the fundamental representation $(i, j, k = 1, \ldots, 3)$ and with $\mathbb{1}$ the identity matrix. For the $SU(3)$ gauge group their values are

$$C_{\mathrm{F}} = 3 \qquad \text{and} \qquad C_{\mathrm{A}} = \frac{4}{3}. \tag{1.11}$$

The quantum QCD Lagrangian may be written as the sum of different Lorentz scalar invariants contributions

$$\mathcal{L}_{\mathrm{QCD}} = \mathcal{L}_{flavour} + \mathcal{L}_{gauge} + \mathcal{L}_{gauge-fixing} + \mathcal{L}_{Fadeev-Popov}. \tag{1.12}$$

At the classical level, one would simply have the sum of the flavour contribution plus the pure gauge one. The former is given by

$$\mathcal{L}_{flavour} = \sum_f \bar{\psi}_f^i \left(i\slashed{D}^{ij} - m_f \delta^{ij} \right) \psi_f^j, \tag{1.13}$$

with $\slashed{D} = D_\mu \gamma^\mu$, the covariant derivative defined as

$$D_\mu^{ij} = \delta^{ij} \, \partial_\mu + \ i \ g \ t_{ij}^c \ A_\mu^c, \tag{1.14}$$

when acting on fields in the fundamental representation and

$$D_\mu^{ab} = \delta^{ab} \, \partial_\mu - \ g \ f^{acb} \ A_\mu^c, \tag{1.15}$$

when acting on the adjoint. The pure gauge contribution

$$\mathcal{L}_{gauge} = -\frac{1}{4} \ F_{\mu\nu}^a \ F^{a\,\mu\nu} \tag{1.16}$$

is instead built from the A_μ^a field strength tensor, defined as

$$F_{\mu\nu}^a = \partial_\mu A_\nu^a - \partial_\nu A_\mu^a + g f^{abc} A_\mu^b A_\nu^c. \tag{1.17}$$

Quark fields ψ_i transform in the fundamental representation $\mathbf{3}$ of $SU(3)$, anti-quarks $\bar{\psi}_i$ in the anti-fundamental $\bar{\mathbf{3}}$ and gluons A_μ^a in the adjoint $\mathbf{8}$. Their transformation formulas read respectively

$$\psi_i'(x) = U_{ij}(x)\psi_j(x) \tag{1.18}$$

$$\bar{\psi}_i'(x) = \bar{\psi}_j(x)U_{ji}^\dagger(x) \tag{1.19}$$

$$A_\mu'^a(x) \ t_{ij}^a = U_{ii'}(x) \left(A_\mu^a(x) \ t_{i'j'}^a \right) U_{j'j}^{-1}(x). \tag{1.20}$$

Color singlets can thus be formed out of a quark-antiquark pair via

$$\sum_i \psi_i^* \, \psi_i \rightarrow \sum_{i,j,k} U_{ij}^* \, \psi_j^* \, U_{ik} \, \psi_k = \sum_{j,k} \left(\sum_i U_{ji}^\dagger U_{ik} \right) \psi_j^* \, \psi_k \; = \sum_k \psi_k^* \, \psi_k \,, \quad (1.21)$$

but it's also possible to form color singlet from three quarks (or anti-quarks) using

$$\sum_{i,j,k} \epsilon^{ijk} \, \psi_i \, \psi_j \, \psi_k \; \rightarrow \; \sum_{i,j,k,\ell,m,n} \epsilon^{ijk} U_{i\ell} U_{jm} U_{kn} \, \psi_\ell \, \psi_m \, \psi_n = \sum_{\ell,m,n} \det U \; \epsilon^{\ell m n} \, \psi_\ell \, \psi_m \, \psi_n \,.$$
$$(1.22)$$

In this way one can accommodate all observed hadrons and mesons in color invariant states. Furthermore, since in a system with n_q quarks and $n_{\bar{q}}$ anti-quarks it's possible to form color singlet only if

$$(n_q - n_{\bar{q}}) \mod 3 = 0 \,, \quad (1.23)$$

it is easy to see that all these invariant states must have integer electric charge, provided the usual charges assignments, i.e. $\frac{2}{3}$ of the electron charge e for up-type quarks and $-\frac{1}{3}e$ for down-type ones.

At the quantum level, the requirement of local gauge invariance results in a large degeneration between gauge-field configurations which are equivalent under a gauge transformation. Thus, to quantize the theory, this problem must be solved making a choice for the gauge. Adopting the path integral functional formalism, this corresponds to integrate only over inequivalent gauge configurations. Our choice for the gauge-fixing contribution to the quantum Lagrangian is

$$\mathcal{L}_{gauge-fixing} = -\frac{1}{2\lambda} \left(\partial^\mu A_\mu^a \right)^2 \,, \quad (1.24)$$

where λ fixes the class of covariant gauges into which the theory is defined. In a non-abelian theory like the QCD, the gauge-fixing Lagrangian must be supplemented by the Fadeev-Popov contributions, often called ghost contributions. This is not true in general, since for a particular class of gauges, the axial gauges, defined in terms of the four-vector η^μ by

$$\mathcal{L}_{gauge-fixing} = -\frac{1}{2\lambda} \left(\eta^\mu A_\mu^a \right)^2 \,, \quad (1.25)$$

there is no need to introduce ghost contributions to the Lagrangian. In these gauges, it is sufficient to trade the gluon propagator in Appendix A with

$$\delta^{ab} \frac{i}{p^2 + i\epsilon} \left(-g^{\alpha\beta} + \frac{p^\alpha \eta^\beta + \eta^\alpha p^\beta}{p \cdot \eta} - \lambda p^2 \frac{p^\alpha p^\beta}{(p \cdot \eta)^2} \right) \,, \quad (1.26)$$

where we have imposed $\eta^2 = 0$ for simplicity. However, since we choose to adopt the covariant gauge-fixing condition eq. (1.24), the ghost contribution reads

$$\mathcal{L}_{Fadeev-Popov} = \partial^\mu \bar{\chi}^a D_\mu^{ab} \chi^b \,. \tag{1.27}$$

The χ^a fields transform in the adjoint representation of the gauge group and they are complex, Lorentz scalar fields which obeys Fermi statistics, being anti-commuting. From this, we deduce that they cannot be real particles since they violate the spin-statistic theorem. These ghost fields are necessary in order to cancel the unphysical degrees of freedom which would otherwise propagate in covariant gauges. They couple only to gluon and they appear only as internal line or as being pair-produced in the final state. For ease of reference, we have reported their Feynman rules, together with all other QCD Feynman rules, in Appendix A.

1.1.2 Asymptotic freedom and the running of $\alpha_{\rm S}$

One of the most striking features of non-abelian gauge theories is the decreasing of the coupling constant as the scale of the theory increase, or as the distance under inspection become shorter. This effect, which goes under the name of *asymptotic freedom*, was originally proved for the QCD by Gross, Wilczek and Politzer [40, 41]. They derived the asymptotic freedom by showing the negativity of the β-function,

$$\beta(\alpha_{\rm s}) = \mu^2 \frac{\partial \alpha_{\rm s}}{\partial \mu^2} \,, \tag{1.28}$$

that accounts for the variation of the theory's coupling constant under the renormalization group. An important consequence of the negativity of β is that, for sufficiently short distances or, equivalently, large momenta exchange, an asymptotically free theory can be reliably studied by means of perturbative expansion, evaluating Feynman diagrams. This situation is therefore more theoretically tractable than the long-distance, strong-coupling behavior of QCD, which is thought to produce confinement, and for which an approximate expansion is not amenable.

Calculating the β-function is a matter of evaluating the relevant Feynman diagrams. In QCD it has the following perturbative expansion

$$\beta(\alpha_{\rm s}) = -b_0 \alpha_{\rm s}^2 \left(1 + b' \alpha_{\rm s} + b'' \alpha_{\rm s}^2 + O(\alpha_{\rm s}^3)\right) \,, \tag{1.29}$$

where the coefficients b_0, b', b'', ... and the related ones

$$b_1 = b_0 \, b' \,, \tag{1.30}$$

$$b_2 = b_0 \, b'' \,, \tag{1.31}$$

$$\vdots$$

depend on the gauge group $SU(3)$ and, apart from b_0 and b_1 (and thus b') that are universal, from the renormalization scheme adopted. One such scheme is the *minimal subtraction* scheme, denoted with MS. In this approach, ultraviolet divergences appearing in loop calculations are regulated reducing the number of space-time dimensions to $d = 4 - 2\epsilon$, such that they appear as $1/\epsilon^2$ or $1/\epsilon$ poles. The MS prescription consists in subtracting off these poles and in replacing the *bare* coupling with the renormalized one. In the *modified minimal subtraction* ($\overline{\text{MS}}$) scheme, one subtract also a common finite part. In this last scheme, the b coefficients read [42]

$$b_0 = \frac{33 - 2n_{\text{f}}}{12\pi} \,,$$

$$b' = \frac{153 - 19n_{\text{f}}}{2\pi(33 - 2n_{\text{f}})} \,,$$

$$b''_{\overline{\text{MS}}} = \frac{77139 - 15099n_{\text{f}} + 325n_f^2}{288\pi^2 \, (33 - 2n_{\text{f}})} \,,$$

$$b'''_{\overline{\text{MS}}} = \frac{36389979 + 5196312\zeta_3 - (351432\zeta_3 + 9705249)n_{\text{f}}}{31104\pi^3(33 - 2n_{\text{f}})}$$

$$+ \frac{(116496\zeta_3 + 450585)n_{\text{f}}^2 + 2186n_{\text{f}}^3}{31104\pi^3(33 - 2n_{\text{f}})} \,,$$

where n_{f} is the number of flavour that may be considered light at the scale Q and ζ is the Riemann ζ-function, with $\zeta_3 = 1.202056903\ldots$.

In non-abelian gauge theories such as QCD, the existence of asymptotic freedom depends on the gauge group and number of flavors of interacting particles. From the previous equations, it follows that, for the $SU(3)$ gauge group, the negativity of the β function at lowest nontrivial order, and consequently the asymptotic freedom, is guaranteed, provided that the number of light flavour n_{f} that may flow in quark loops is lower than $33/2$.

However, perturbative QCD tells us only how the coupling constant change varying the scale, it does not give us information concerning its value. To obtain it one

must instead rely on experimental observations, for example measuring the value of α_s at a certain scale, that depends on the particular process one is studying. Values of α_s measured at different scales are then evolved to the reference scale via the evolution equations, to perform comparisons. Usually, a common reference scale is the mass of the Z boson.

An alternative approach is to introduce a further parameter, Λ_{QCD}, into the definition of the coupling constant, in such a way that the equation

$$
\begin{aligned}
\log \frac{Q^2}{\Lambda^2_{QCD}} &= -\int_{\alpha_s(Q^2)}^{\infty} \frac{dx}{\beta(x)} \\
&= \int_{\alpha_s(Q^2)}^{\infty} \frac{dx}{b_0 \, x^2(1 + b'x + \dots)}
\end{aligned} \tag{1.32}
$$

holds. Keeping only the first order in the expansion of β, it is thus possible to re-express the coupling constant α_s as

$$
\alpha_s(Q^2) = \frac{1}{b_0 \log(Q^2/\Lambda^2_{QCD})} \, . \tag{1.33}
$$

The parameter Λ_{QCD} represent thus the scale at which the QCD becomes a strongly interacting theory, since the coupling there diverges. The phenomenology of strong interactions gives us only hints that this scale is of the order of some hundreds MeV (≈ 200 MeV), i.e. that is a scale comparable with light hadron masses (≈ 1 GeV).

In this thesis, and in the related computer codes, the value of the strong coupling constant α_s and the five-flavour $\overline{\text{MS}}$ value of Λ_{QCD}, denoted by $\Lambda^{(5)}_{\overline{\text{MS}}}$, are each time consistently taken from the set of the parton distribution functions adopted during the calculation. Furthermore, their values are correctly matched at heavy-quark thresholds, due to the change in the number of active flavours. Nevertheless, for ease of reference, we report here their current world averages [43]

$$
\alpha_s(M_Z) = 0.1184 \pm 0.0007 \, , \qquad \Lambda^{(5)}_{\overline{\text{MS}}} = 213 \pm 9 \text{ MeV} \, . \tag{1.34}
$$

1.2 Next-to-Leading Order computations

In this section, we describe the general features of a next-to-leading order (NLO) calculation for a generic hadron-hadron collision process. In case of a lepton-hadron

or a lepton-lepton collision, the treatment is similar, but simpler, since the parton-distribution functions for the incoming leptons may be thought as delta functions. Most of the following discussion can be found, in greater detail, in sec. 2.1 of ref. [30]. Here we report similar definitions and results, in a language that is more suited to this thesis.

1.2.1   Generalities and notations

We start considering $2 \to n$ processes at the leading-order (LO), by which we mean the lowest order in the strong coupling α_s expansion to which an hard process contributes to the total cross section. Throughout this thesis, we depart slightly from the notation of ref. [30], keeping, where useful, the distinction between parton momenta and kinematic variables that are related to the n-parton phase space and those related to the $n+1$-parton real emission phase space. We choose to denote the formers with barred symbols. Hence, momentum conservation for the LO hard process is written as

$$\bar{x}_\oplus K_\oplus + \bar{x}_\ominus K_\ominus = \bar{k}_1 + \ldots + \bar{k}_n \,, \tag{1.35}$$

where $\bar{x}_\oplus$ are the momentum fractions of the incoming partons, and $K_\oplus$ are the four-momenta of the incoming hadrons. We also indicate with

$$\bar{k}_\oplus = \bar{x}_\oplus K_\oplus \,, \qquad\qquad \bar{k}_\ominus = \bar{x}_\ominus K_\ominus \,, \tag{1.36}$$

the momenta of the incoming partons. In the following, we define

$$S = (K_\oplus + K_\ominus)^2 \,, \qquad \bar{s} = (\bar{k}_\oplus + \bar{k}_\ominus)^2 \tag{1.37}$$

the usual hadronic and the partonic centre-of-mass energy squared, respectively. To fully characterize the n-parton phase space, we introduce the set of variables

$$\bar{\boldsymbol{\Phi}}_n = \left\{ \bar{x}_\oplus, \bar{x}_\ominus, \bar{k}_1, \ldots, \bar{k}_n \right\} \,. \tag{1.38}$$

These are constrained by momentum conservation, eq. (1.35), and by the on-shell conditions $\bar{k}_i^2 = m_i^2$ for final-state particles.

The LO squared matrix elements, after spin and color sums and averages, and the inclusion of the appropriate flux factor, are collectively denoted by $\mathcal{B}$. The total cross section at the leading-order is thus given by

$$\sigma_\mathrm{LO} = \int d\bar{\boldsymbol{\Phi}}_n \, f_\oplus(\bar{x}_\oplus) \, f_\ominus(\bar{x}_\ominus) \, \mathcal{B}(\bar{\boldsymbol{\Phi}}_n) \tag{1.39}$$

where we have indicated with $f_\oplus$ the parton density functions (pdf), dropping, for ease of notation, their dependence on parton flavours, hadron type and on the factorization scale μ_{F}. We can introduce the parton luminosity as their product

$$\bar{\mathcal{L}} = \mathcal{L}(\bar{x}_\oplus, \bar{x}_\ominus) = f_\oplus(\bar{x}_\oplus)\, f_\ominus(\bar{x}_\ominus)\,. \tag{1.40}$$

As already stressed above, in case of an initial-state lepton, the corresponding parton distribution function $f_\oplus(\bar{x}_\oplus)$ is replaced by $\delta(1 - \bar{x}_\oplus)$.[1] Then, we define

$$d\bar{\bar{\Phi}}_n = d\bar{x}_\oplus\, d\bar{x}_\ominus\, d\Phi_n\left(\bar{k}_\oplus + \bar{k}_\ominus; \bar{k}_1, \ldots, \bar{k}_n\right)\,, \tag{1.41}$$

where $d\Phi_n$ is the usual n-body phase space

$$d\Phi_n\left(q; \bar{k}_1, \ldots, \bar{k}_n\right) = (2\pi)^4\, \delta^4\left(q - \sum_{i=1}^n \bar{k}_i\right) \prod_{i=1}^n \frac{d^3\bar{k}_i}{(2\pi)^3\, 2\bar{k}_i^0}\,. \tag{1.42}$$

The next-to-leading contributions in the strong coupling α_{S} expansion are given by reals, virtuals and collinear counterterms.

- The real contributions arise from the squared amplitudes for the $2 \to n+1$ parton process. We denote by $\mathcal{R}$ the real squared matrix elements, after spin and color sums and averages, and the inclusion of the appropriate flux factor. These contributions contain infrared divergences that need to be dealt with consistently, if one wants to obtain meaningful results. As before, to fully characterize the real emission phase space, we also introduce the set of variables

$$\mathbf{\Phi}_{n+1} = \{x_\oplus, x_\ominus, k_1, \ldots, k_{n+1}\}\,, \tag{1.43}$$

constrained by momentum conservation

$$x_\oplus K_\oplus + x_\ominus K_\ominus = k_1 + \ldots + k_{n+1}\,, \tag{1.44}$$

and on-shell conditions $k_i^2 = m_i^2$. The differential phase space for these contributions can be written as

$$d\mathbf{\Phi}_{n+1} = dx_\oplus\, dx_\ominus\, d\Phi_{n+1}\left(k_\oplus + k_\ominus; k_1, \ldots, k_{n+1}\right)\,, \tag{1.45}$$

with

$$d\Phi_{n+1}\left(q; k_1, \ldots, k_{n+1}\right) = (2\pi)^4\, \delta^4\left(q - \sum_{i=1}^{n+1} k_i\right) \prod_{i=1}^{n+1} \frac{d^3 k_i}{(2\pi)^3\, 2k_i^0}\,. \tag{1.46}$$

---

[1]In general, $f_\oplus(\bar{x}_\oplus)$ may be a more complicate function that effectively describes the energy loss of the incoming particle. An example is provided by the Weiszäcker-Williams function if the incoming particle is an electron turning into a photon.

- The virtual contributions arise from the interference of the amplitudes with one further loop times the LO amplitudes. These contributions may present both infrared and ultraviolet divergences. In the conventional dimensional regularization (CDR) approach, they are dealt with going in $d = 4 - 2\epsilon$ dimensions, where the divergences appear as single $1/\epsilon$, or double poles $1/\epsilon^2$. However, after all ultraviolet divergences are removed by the renormalization procedure, only infrared poles are left. We denote by $\mathcal{V}_{\rm b}$ the renormalized virtual corrections, where the subscript b (from "bare") remind us of the presence of infrared divergences in the amplitude. Owing to the same kinematics, the differential phase space for these contributions is the the n-parton one, i.e. $d\bar{\bar{\mathbf{\Phi}}}_n$ of eq. (1.41). We will see in the following how, for suitable defined quantities, the infrared divergences combines between reals and virtual contributions and concoct to cancel.

- In hadronic collisions, the inclusion of only real and virtual contributions is not enough to obtain a complete cancellation. Extra infrared divergences still remain. These are related to configurations where the emitted parton is collinear to one of the two initial-state partons. The lack of cancellations may be naively attributed to the different momentum flowing into the hard subprocess for collinear parton emissions amplitudes, compared to that for virtual contributions. In fact, while in the latter ones the amplitudes are evaluated for pure Born-like kinematics, in the formers the emission of a collinear parton lowers the momentum entering the hard scattering. In going from the parton-level cross section to the hadron-level one, these initial-state collinear divergences are usually absorbed into the definition of the parton density functions, causing their well-known dependence on the factorization scale $\mu_{\rm F}$. However, in our approach, we always understood the use of $\mu_{\rm F}$-dependent *pdf*'s and achieve the complete cancellation of IR singularities in the differential partonic cross section adding further contributions, which we call collinear remnants. We denote them with $\mathcal{G}_{\oplus,{\rm b}}$ and $\mathcal{G}_{\ominus,{\rm b}}$, each one related to the corresponding incoming parton. These counterterms are infrared divergent in four dimensions. Therefore, they are computed in $d = 4 - 2\epsilon$ dimensions, where the divergences appear as $1/\epsilon$ poles. To remind this fact, the subscript b has been included for them too. As already stressed, if one or both the incoming particles are leptons, the corresponding $\mathcal{G}_{\rm b}$ is zero.

The collinear configurations associated to $\mathcal{G}_{\oplus,\mathrm{b}}$ have effectively n-body final-state kinematics, except for the energy degree of freedom of the parton collinear to the beam. Their phase space is characterized by the sets of variables and momentum conservations

$$\boldsymbol{\Phi}_{n,\oplus} = \{x_\oplus, x_\ominus, z, k_1, \ldots, k_n\} \; , \quad z\, x_\oplus K_\oplus + x_\ominus K_\ominus = \sum_{i=1}^n k_i \; , \quad (1.47)$$

$$\boldsymbol{\Phi}_{n,\ominus} = \{x_\oplus, x_\ominus, z, k_1, \ldots, k_n\} \; , \quad x_\oplus K_\oplus + z\, x_\ominus K_\ominus = \sum_{i=1}^n k_i \; , \quad (1.48)$$

where z is the fraction of momentum of the incoming parton after radiation. Anyway, these variables may be related to those of the underlying n-parton configurations, obtained by merging the two collinear partons, by

$$\bar{\boldsymbol{\Phi}}_n = \{\bar{x}_\oplus, \bar{x}_\ominus, \bar{k}_1, \ldots \bar{k}_n\}, \qquad \bar{x}_\oplus = zx_\oplus \; , \qquad \bar{x}_\ominus = x_\ominus \; , \qquad \bar{k}_i = k_i \; . \quad (1.49)$$

The values of $\bar{x}_\oplus$ are only constrained by n-parton momentum conservation, and thus they do not depend upon z. The differential phase space for these contributions is denoted by

$$d\boldsymbol{\Phi}_{n,\oplus} = dx_\oplus \, dx_\ominus \, dz \, d\Phi_n \left(z\, k_\oplus + k_\ominus; k_1, \ldots, k_n \right) \; , \quad (1.50)$$

$$d\boldsymbol{\Phi}_{n,\ominus} = dx_\oplus \, dx_\ominus \, dz \, d\Phi_n \left(k_\oplus + z\, k_\ominus; k_1, \ldots, k_n \right) \; . \quad (1.51)$$

Having defined all of its contributions, the total NLO cross section can be written as

$$\sigma_{\mathrm{NLO}} = \int d\bar{\boldsymbol{\Phi}}_n \, \bar{\mathcal{L}} \left[\mathcal{B}(\bar{\boldsymbol{\Phi}}_n) + \mathcal{V}_{\mathrm{b}}(\bar{\boldsymbol{\Phi}}_n) \right] + \int d\boldsymbol{\Phi}_{n+1} \, \mathcal{L} \, \mathcal{R}(\boldsymbol{\Phi}_{n+1})$$

$$+ \int d\boldsymbol{\Phi}_{n,\oplus} \, \mathcal{L} \, \mathcal{G}_{\oplus,\mathrm{b}}(\boldsymbol{\Phi}_{n,\oplus}) + \int d\boldsymbol{\Phi}_{n,\ominus} \, \mathcal{L} \, \mathcal{G}_{\ominus,\mathrm{b}}(\boldsymbol{\Phi}_{n,\ominus}) \; , \quad (1.52)$$

where we have introduced the $\mathcal{L}$ symbol to denote the parton luminosity in the $n+1$-parton phase space of real contributions $\boldsymbol{\Phi}_{n+1}$ (and also in the phase space of collinear remnants $\boldsymbol{\Phi}_{n,\oplus}$). Without loosing generality, $\mathcal{L}$ can be easily obtained with the appropriate substitution $\bar{x}_\oplus \to x_\oplus$ in eq. (1.40).[2]

---

[2]For collinear remnants a precision relation between $\bar{x}_\oplus$ and $x_\oplus$ entering the luminosity $\mathcal{L}$ holds. We show it in sec. 1.2.2, when presenting the subtraction formalism for initial-state collinear configurations (see eq. (1.70)).

With the aid of eq. (1.52) it is possible to evaluate the NLO expectation value for a generic infrared safe observable O. By infrared safety we mean the lack of sensitivity to the presence of a soft or a collinear parton in the final state, i.e. we require

$$O_{n+1}(\mathbf{\Phi}_{n+1}) \to O_n(\bar{\mathbf{\Phi}}_n) \quad \text{when} \quad \mathbf{\Phi}_{n+1} \to \bar{\mathbf{\Phi}}_n \,, \tag{1.53}$$

where O_n and O_{n+1} are the expressions of the observable O in terms of n- and $(n+1)$-parton phase space variables, and $\bar{\mathbf{\Phi}}_n$ is the underlying n-parton configuration corresponding to $\mathbf{\Phi}_{n+1}$ (or $\mathbf{\Phi}_{n,\oplus}$) set. The Bloch-Nordsieck [44], Yennie-Frautschi-Suura [45] and Kinoshita-Lee-Nauenberg (KLN) [46, 47] theorems guarantee that these quantities are free of infrared singularities in the massless limit, both in QED and in QCD. The requirement of infrared safety is thus necessary to obtain meaningful results. With these assumptions, the expected value $\langle O \rangle$ is a finite quantity and can be calculated by means of

$$\langle O \rangle = \int d\bar{\mathbf{\Phi}}_n \, \bar{\mathcal{L}} \, O_n(\bar{\mathbf{\Phi}}_n) \left[\mathcal{B}(\bar{\mathbf{\Phi}}_n) + \mathcal{V}_{\mathrm{b}}(\bar{\mathbf{\Phi}}_n) \right] + \int d\mathbf{\Phi}_{n+1} \, \mathcal{L} \, O_{n+1}(\mathbf{\Phi}_{n+1}) \, \mathcal{R}(\mathbf{\Phi}_{n+1})$$

$$+ \int d\mathbf{\Phi}_{n,\oplus} \, \mathcal{L} \, O_n(\bar{\mathbf{\Phi}}_n) \, \mathcal{G}_{\oplus,\mathrm{b}}(\mathbf{\Phi}_{n,\oplus}) + \int d\mathbf{\Phi}_{n,\ominus} \, \mathcal{L} \, O_n(\bar{\mathbf{\Phi}}_n) \, \mathcal{G}_{\ominus,\mathrm{b}}(\mathbf{\Phi}_{n,\ominus}) \,. \tag{1.54}$$

In previous formula the implicit requirement that the Born contribution, i.e. the term proportional to $\mathcal{B}$, is infrared finite is understood. This can always be achieved by a suitable choice of the observable O, that must suppress regions where the $\mathcal{B}$ contribution may be plagued by infrared divergences. Moreover, thanks to eq. (1.53), the arguments of O in the last two terms on the right hand side of eq. (1.54) may be set equal to $\bar{\mathbf{\Phi}}_n$, rather than $\mathbf{\Phi}_{n,\oplus}$.

Notice that the different contributions of r.h.s. of eq. (1.54) are all separately infrared divergent. In fact, as already mentioned, the real matrix elements, i.e. the term proportional to $\mathcal{R}$, and the virtual contributions, i.e. that proportional to $\mathcal{V}_{\mathrm{b}}$, are singular in the soft and collinear limits. In this last limit, also collinear remnants diverge. All these divergences can be integrated, for example in $d = 4 - 2\epsilon$ dimensions, and yield $1/\epsilon^2$ and $1/\epsilon$ poles. However, when all these contributions are combined, these divergences cancel and the result turns out to be finite. Nevertheless, the integrals in eq. (1.54) are usually too difficult to be performed analytically, because of the involved functional form of O. Furthermore, they are not even suited for numerical computations, being them divergent in four dimensions. For these reasons, different strategies have been proposed for the computation of observables in QCD.

One of these is the so-called *slicing method* [48]. Its idea is to divide the real emission phase space between regions that are sensible to infrared divergences and infrared safe ones, by means of a small parameter δ, and then to calculate the integrals in $d = 4$ dimensions in terms of this parameter. At the end, results are combined to cancel the divergences, but a dependence on δ remains. Clearly, the smaller the δ the better the approximation, but in the limit $\delta \to 0$ one would re-obtain separately divergent contributions. Another idea, that does not involve any approximation and it is thus very largely adopted, goes under the name of *subtraction method* [49]. We shall discuss it in detail in the next section.

1.2.2 The subtraction method

The subtraction method relies on the introduction of a set of functions $\mathcal{C}^{(\alpha_{\rm r})}$, the real counterterms, that are summed and subtracted back from the differential cross section formula, in order to deal with integrable quantities only. Each of these counterterms is associated with a particular singular region $\alpha_{\rm r}$, i.e. with a configuration that has either a final-state soft parton, or a final-state massless parton which is collinear to another massless one. Furthermore, for each $\alpha_{\rm r}$, a new set of variables

$$\tilde{\mathbf{\Phi}}_{n+1}^{(\alpha_{\rm r})} = \left\{ \tilde{x}_{\oplus}^{(\alpha_{\rm r})}, \tilde{x}_{\ominus}^{(\alpha_{\rm r})}, \tilde{k}_1^{(\alpha_{\rm r})}, \ldots, \tilde{k}_{n+1}^{(\alpha_{\rm r})} \right\} \tag{1.55}$$

is introduced, in such a way that a mapping between these singular configurations and the real phase space variables $\mathbf{\Phi}_{n+1}$ can always be defined. This mapping must be smooth near the singular region, and it must become the identity there. Each singular region $\alpha_{\rm r}$ is characterized by a different mapping, but, in some approaches, the same mapping may be used to describe more than one singular region. Furthermore, the mapping may be defined only locally, with vanishing real counterterms outside a finite neighborhood of the singular region considered. However, to avoid loosing generality, we will neglect these complications in the following. For ease of notation, we also use the following *context convention*: if an expression is enclosed in the subscripted squared brackets

$$\left[\cdots \right]_{\alpha_{\rm r}}, \tag{1.56}$$

we mean that all variables appearing inside have, when applicable, the superscripts corresponding to the subscript of the bracket, *e.g.*

$$\tilde{\mathbf{\Phi}}_{n+1}^{(\alpha_{\rm r})} = \left[\left\{ \tilde{x}_{\oplus}, \tilde{x}_{\ominus}, \tilde{k}_1, \ldots, \tilde{k}_{n+1} \right\} \right]_{\alpha_{\rm r}}. \tag{1.57}$$

The singular configurations $\tilde{\mathbf{\Phi}}_{n+1}^{(\alpha_{\mathrm{r}})}$ differs according to the nature of the singular region:

-   In case of a soft (S) singularity, the singular configuration has a final-state parton with vanishing four-momentum.

-   In case of a final-state collinear singularity (FSC), the singular configuration has two massless final-state partons with parallel three-momenta.

-   In case of a initial-state collinear (ISC) singularity, the singular configuration has a massless outgoing parton with three-momentum parallel to the momentum of one incoming parton.

It is understood that there are regions of the phase space where singular configurations may overlap, for example a FSC configuration may contain part the soft region S associated to a collinear gluon becoming soft.

As already done for collinear configurations (eqs. (1.47) and (1.48)), we associate with each $\tilde{\mathbf{\Phi}}_{n+1}^{(\alpha_{\mathrm{r}})}$ configuration an n-body configuration $\bar{\mathbf{\Phi}}_n^{(\alpha_{\mathrm{r}})}$, that we call the *underlying n-body configuration*

$$\bar{\mathbf{\Phi}}_n^{(\alpha_{\mathrm{r}})} = \left[\left\{\bar{x}_\oplus, \bar{x}_\ominus, \bar{k}_1, \ldots, \bar{k}_n\right\}\right]_{\alpha_{\mathrm{r}}} . \tag{1.58}$$

This association goes as follows

-   If α is a soft region, $\bar{\mathbf{\Phi}}_n^{(\alpha_{\mathrm{r}})}$ is obtained by deleting the zero momentum parton from the $\tilde{\mathbf{\Phi}}_{n+1}^{(\alpha_{\mathrm{r}})}$ configuration.

-   If α is a final-state collinear region, $\bar{\mathbf{\Phi}}_n^{(\alpha_{\mathrm{r}})}$ is obtained by merging the momenta of the two collinear partons in $\tilde{\mathbf{\Phi}}_{n+1}^{(\alpha_{\mathrm{r}})}$.

-   If α is an initial state collinear region, $\bar{\mathbf{\Phi}}_n^{(\alpha_{\mathrm{r}})}$ is obtained by deleting the radiated collinear parton from $\tilde{\mathbf{\Phi}}_{n+1}^{(\alpha_{\mathrm{r}})}$, and by replacing the momentum fraction of the initial-state radiating parton with its momentum fraction after radiation.

In all of the cases above, at the end we are left with n final-state partons, constrained by momentum conservation

$$\bar{x}_\oplus K_\oplus + \bar{x}_\ominus K_\ominus = \sum_{j=1}^n \bar{k}_j . \tag{1.59}$$

Furthermore, for S or FSC regions, we have

$$\bar{x}_{\oplus} = \tilde{x}_{\oplus}\,, \tag{1.60}$$

and thus the luminosity is

$$\tilde{\mathcal{L}} = \mathcal{L}(\tilde{x}_{\oplus}, \tilde{x}_{\ominus}) = \bar{\mathcal{L}}\,. \tag{1.61}$$

This is not true for ISC regions, where

$$\bar{x}_{\oplus} < \tilde{x}_{\oplus}\,, \qquad \bar{x}_{\ominus} = \tilde{x}_{\ominus}\,, \tag{1.62}$$

for $\mathrm{ISC}_{\oplus}$ and the analogous one for $\mathrm{ISC}_{\ominus}$. In both cases,

$$\tilde{\mathcal{L}} \neq \bar{\mathcal{L}}\,. \tag{1.63}$$

In the subtraction method one rewrites the real contribution appearing in the r.h.s. of eq. (1.54) as follows

$$\int d\Phi_{n+1} \, \mathcal{L} \, O_{n+1}(\Phi_{n+1}) \, \mathcal{R}(\Phi_{n+1}) = \sum_{\alpha_{\mathrm{r}}} \int d\Phi_{n+1} \left[\tilde{\mathcal{L}} \, O_n(\bar{\bar{\Phi}}_n) \, \mathcal{C}(\Phi_{n+1})\right]_{\alpha_{\mathrm{r}}} +$$

$$\int d\Phi_{n+1} \left\{ \mathcal{L} \, O_{n+1}(\Phi_{n+1}) \, \mathcal{R}(\Phi_{n+1}) - \sum_{\alpha_{\mathrm{r}}} \left[\tilde{\mathcal{L}} \, O_n(\bar{\bar{\Phi}}_n) \, \mathcal{C}(\Phi_{n+1})\right]_{\alpha_{\mathrm{r}}} \right\}. \tag{1.64}$$

For any infrared-safe observable $O_{n+1}(\Phi_{n+1})$, that vanishes fast enough if Φ_{n+1} approaches more than one singular regions at the same time, the real counterterms $\mathcal{C}^{(\alpha_{\mathrm{r}})}$ have the property that

$$\mathcal{R}(\Phi_{n+1}) \, O_{n+1}(\Phi_{n+1}) - \sum_{\alpha_{\mathrm{r}}} \mathcal{C}^{(\alpha_{\mathrm{r}})}(\Phi_{n+1}) \, O_{n+1}\left(\tilde{\tilde{\Phi}}_{n+1}\right) \tag{1.65}$$

has at most integrable singularities in the Φ_{n+1} space. Notice that the previous requirement does not also imply that

$$\mathcal{R}(\Phi_{n+1}) - \sum_{\alpha_{\mathrm{r}}} \mathcal{C}^{(\alpha_{\mathrm{r}})}(\Phi_{n+1}) \tag{1.66}$$

is integrable. This instead happens only if the corresponding n-body process has no infrared singularities, *e.g.* for single vector boson or Higgs boson production processes studied in this thesis. Under these assumptions, and thanks to the infrared safety of O, the second term on the r.h.s. of eq. (1.64) is integrable in $d = 4$ dimensions. However, the first term on the r.h.s. of eq. (1.64) is still divergent. In order to deal

with it, we define, for each $\alpha_{\rm r}$, a parametrization of the $(n+1)$-phase space in terms of the underlying n-body phase space $\bar{\bar{\mathbf{\Phi}}}_n^{(\alpha_{\rm r})}$, plus three further variables that describe the radiation process $\Phi_{\rm rad}^{(\alpha_{\rm r})}$. The range of the radiation variables in $\Phi_{\rm rad}^{(\alpha_{\rm r})}$ may depend upon $\bar{\bar{\mathbf{\Phi}}}_n^{(\alpha_{\rm r})}$. The phase-space element can be written in a factorized form

$$d\mathbf{\Phi}_{n+1} = d\bar{\bar{\mathbf{\Phi}}}_n^{(\alpha_{\rm r})}\, d\Phi_{\rm rad}^{(\alpha_{\rm r})}\,, \tag{1.67}$$

that implicitly defines a ($\bar{\bar{\mathbf{\Phi}}}_n^{(\alpha_{\rm r})}$-dependent) Jacobian. We conventionally include it into $d\Phi_{\rm rad}^{(\alpha_{\rm r})}$. In case of a S or a FSC singular region, defining

$$\left[\bar{\mathcal{C}}\left(\bar{\mathbf{\Phi}}_n\right) = \int d\Phi_{\rm rad}\, \mathcal{C}(\mathbf{\Phi}_{n+1}) \right]_{\alpha_{\rm r}\in\{{\rm FSC,S}\}}, \tag{1.68}$$

the generic term in the first sum on the r.h.s. of eq. (1.64) reads

$$\left[\int d\mathbf{\Phi}_{n+1}\, \tilde{\mathcal{L}}\, O_n\left(\bar{\mathbf{\Phi}}_n\right)\, \mathcal{C}(\mathbf{\Phi}_{n+1}) = \int d\bar{\mathbf{\Phi}}_n\, \bar{\mathcal{L}}\, O_n\left(\bar{\mathbf{\Phi}}_n\right)\, \bar{\mathcal{C}}\left(\bar{\mathbf{\Phi}}_n\right) \right]_{\alpha_{\rm r}\in\{{\rm FSC,S}\}}. \tag{1.69}$$

In the ISC case, we cannot factor out the luminosity any longer, so we introduce the momentum fraction z and write

$$\tilde{\mathcal{L}} = \mathcal{L}(\tilde{x}_{\oplus}, \tilde{x}_{\ominus}) = \begin{cases} \mathcal{L}(\bar{x}_{\oplus}/z, \bar{x}_{\ominus}) & \text{for} \quad \alpha \in {\rm ISC}_{\oplus} \\ \mathcal{L}(\bar{x}_{\oplus}, \bar{x}_{\ominus}/z) & \text{for} \quad \alpha \in {\rm ISC}_{\ominus} \end{cases}. \tag{1.70}$$

This leads to the definition

$$\left[\bar{\mathcal{C}}\left(\bar{\mathbf{\Phi}}_n, z\right) = \int d\Phi_{\rm rad}\, \mathcal{C}(\mathbf{\Phi}_{n+1})\; z\, \delta\left(z - \bar{x}_{\circleddash}/\tilde{x}_{\circleddash}\right) \right]_{\alpha_{\rm r}\in\{{\rm ISC}_{\circleddash}\}}, \tag{1.71}$$

so that

$$\left[\int d\mathbf{\Phi}_{n+1}\, \tilde{\mathcal{L}}\, O_n\left(\bar{\mathbf{\Phi}}_n\right)\, \mathcal{C}(\mathbf{\Phi}_{n+1}) = \int d\bar{\mathbf{\Phi}}_n\, \frac{dz}{z}\, \tilde{\mathcal{L}}\, O_n\left(\bar{\mathbf{\Phi}}_n\right)\, \bar{\mathcal{C}}\left(\bar{\mathbf{\Phi}}_n, z\right) \right]_{\alpha_{\rm r}\in\{{\rm ISC}\}}. \tag{1.72}$$

Hence, we may identify the two ${\rm ISC}_{\circleddash}$ configurations with those of eqs. (1.47) and (1.48), thus equating the z variables of eqs. (1.49) and (1.71). From eqs. (1.50) and (1.51), we have

$$d\bar{\mathbf{\Phi}}_n \frac{dz}{z} = d\mathbf{\Phi}_{n,\circleddash}\,. \tag{1.73}$$

When integrated in d dimensions, the $\bar{\mathcal{C}}$ terms contain explicit poles in ϵ. These are the collinear divergences left over by the subtraction between reals and virtual contributions. We can calculated them choosing the counterterms in eq. (1.65) in

such a way that the integrals in eqs. (1.68) and (1.71) are easily performed analytically. It it thus possible to rewrite eq. (1.54) adding and subtracting back these real counterterms, so that

$$
\begin{aligned}
\langle O \rangle \;=\;& \int d\bar{\boldsymbol{\Phi}}_n\, \bar{\mathcal{L}}\, O_n(\bar{\boldsymbol{\Phi}}_n) \left[\mathcal{B}(\bar{\boldsymbol{\Phi}}_n) + \mathcal{V}_{\mathrm{b}}(\bar{\boldsymbol{\Phi}}_n) \right] \\[4pt]
&+ \int d\boldsymbol{\Phi}_{n+1} \left\{ \mathcal{L}\, O_{n+1}(\boldsymbol{\Phi}_{n+1})\, \mathcal{R}(\boldsymbol{\Phi}_{n+1}) - \sum_{\alpha_{\mathrm{r}}} \left[\tilde{\mathcal{L}}\, O_n(\bar{\boldsymbol{\Phi}}_n)\, \mathcal{C}(\boldsymbol{\Phi}_{n+1}) \right]_{\alpha_{\mathrm{r}}} \right\} \\[4pt]
&+ \sum_{\alpha_{\mathrm{r}} \in \{\mathrm{FSC,S}\}} \left[\int d\bar{\boldsymbol{\Phi}}_n\, \bar{\mathcal{L}}\, O_n(\bar{\boldsymbol{\Phi}}_n)\, \bar{\mathcal{C}}\left(\bar{\boldsymbol{\Phi}}_n\right) \right]_{\alpha_{\mathrm{r}}} \\[4pt]
&+ \sum_{\alpha_{\mathrm{r}} \in \{\mathrm{ISC}_{\circleddash}\}} \left[\int d\boldsymbol{\Phi}_{n,\circleddash}\, \tilde{\mathcal{L}}\, O_n(\bar{\boldsymbol{\Phi}}_n)\, \bar{\mathcal{C}}\left(\boldsymbol{\Phi}_{n,\circleddash}\right) \right]_{\alpha_{\mathrm{r}}} \\[4pt]
&+ \int d\boldsymbol{\Phi}_{n,\oplus}\, \tilde{\mathcal{L}}\, O_n(\bar{\boldsymbol{\Phi}}_n)\, \mathcal{G}_{\oplus,\mathrm{b}}(\boldsymbol{\Phi}_{n,\oplus}) + \int d\boldsymbol{\Phi}_{n,\ominus}\, \tilde{\mathcal{L}}\, O_n(\bar{\boldsymbol{\Phi}}_n)\, \mathcal{G}_{\ominus,\mathrm{b}}(\boldsymbol{\Phi}_{n,\ominus}) \,. \quad (1.74)
\end{aligned}
$$

With respect to eq. (1.54), in the last line we have traded $\mathcal{L} \to \tilde{\mathcal{L}}$, since, as pointed out above, in the phase space of collinear remnants they are the same. In addiction, if we combine the infrared divergent contributions coming from ISC regions, we may single out divergences writing

$$
\mathcal{G}_{\circleddash,\mathrm{b}}(\boldsymbol{\Phi}_{n,\circleddash}) + \sum_{\alpha_{\mathrm{r}} \in \{\mathrm{ISC}_{\circleddash}\}} \bar{\mathcal{C}}^{(\alpha_{\mathrm{r}})}(\boldsymbol{\Phi}_{n,\circleddash}) = \mathcal{G}_{\circleddash}(\boldsymbol{\Phi}_{n,\circleddash}) + \delta(1-z)\, \mathcal{G}_{\circleddash}^{\mathrm{div}}\left(\bar{\boldsymbol{\Phi}}_n\right) \,. \quad (1.75)
$$

The first term of the r.h.s. $\mathcal{G}_{\circleddash}(\boldsymbol{\Phi}_{n,\circleddash})$ is finite in $d = 4$ dimensions, even if it may contain distributions associated to the soft limit $z \to 1$. The second term $\mathcal{G}_{\circleddash}^{\mathrm{div}}$ accounts instead for the divergent poles in ϵ, of soft origin. To reach the complete cancellation of all ϵ poles, we combine these last terms with the virtual contribution, to obtain the so-called soft-virtual term

$$
\mathcal{V}(\bar{\boldsymbol{\Phi}}_n) = \mathcal{V}_{\mathrm{b}}(\bar{\boldsymbol{\Phi}}_n) + \left[\sum_{\alpha_{\mathrm{r}} \in \{\mathrm{FSC,S}\}} \bar{\mathcal{C}}^{(\alpha_{\mathrm{r}})}(\bar{\boldsymbol{\Phi}}_n) + \mathcal{G}_{\oplus}^{\mathrm{div}}\left(\bar{\boldsymbol{\Phi}}_n\right) + \mathcal{G}_{\ominus}^{\mathrm{div}}\left(\bar{\boldsymbol{\Phi}}_n\right) \right] \,, \quad (1.76)
$$

which is finite in $d = 4$ dimensions. In the previous formula the phase-space variables $\bar{\boldsymbol{\Phi}}_n$ appearing inside the square bracket are always implicitly assumed to correspond to those of the $\mathcal{V}_{\mathrm{b}}$ term, i.e. to the underlying Born n-parton configuration.

Defining now the following abbreviations

$$
R = \mathcal{L}\,\mathcal{R}, \qquad C^{(\alpha_{\mathrm{r}})} = \tilde{\mathcal{L}}^{(\alpha_{\mathrm{r}})}\,\mathcal{C}^{(\alpha_{\mathrm{r}})}, \qquad G_{\circleddash} = \tilde{\mathcal{L}}\,\mathcal{G}_{\circleddash}, \qquad B = \bar{\mathcal{L}}\,\mathcal{B}, \qquad V = \bar{\mathcal{L}}\,\mathcal{V} \,,
$$

$$
(1.77)
$$

equation (1.74) becomes

$$
\begin{aligned}
\langle O \rangle \;\; = &\;\; \int d\bar{\boldsymbol{\Phi}}_n \, O_n(\bar{\boldsymbol{\Phi}}_n) \left[B(\bar{\boldsymbol{\Phi}}_n) + V(\bar{\boldsymbol{\Phi}}_n) \right] \\
&+ \int d\boldsymbol{\Phi}_{n+1} \left\{ O_{n+1}(\boldsymbol{\Phi}_{n+1}) \, R(\boldsymbol{\Phi}_{n+1}) - \sum_{\alpha_{\mathrm{r}}} \left[O_n(\bar{\boldsymbol{\Phi}}_n) \, C(\boldsymbol{\Phi}_{n+1}) \right]_{\alpha_{\mathrm{r}}} \right\} \\
&+ \int d\boldsymbol{\Phi}_{n,\oplus} \, O_n(\bar{\boldsymbol{\Phi}}_n) \, G_\oplus(\boldsymbol{\Phi}_{n,\oplus}) + \int d\boldsymbol{\Phi}_{n,\ominus} \, O_n(\bar{\boldsymbol{\Phi}}_n) \, G_\ominus(\boldsymbol{\Phi}_{n,\ominus}) \; . \quad (1.78)
\end{aligned}
$$

This is the final result of the subtraction method: a formula for the expectation value of any infrared-safe quantity which is suited to be integrated numerically, being all the integrals that appear in it finite when evaluated in 4 dimensions.

Up to now, we have discussed of the general features of a subtraction method, without entering into the details of the definitions of the real counterterms $\mathcal{C}^{(\alpha_{\mathrm{r}})}$. Throughout the past years, two general procedures to define these counterterms established in the literature and has been used extensively in NLO calculations. These are commonly referred as as the Catani and Seymour (CS) method and the Frixione, Kunszt and Signer (FKS) one. In the following we shall analyze them separately.

1.2.3 Catani-Seymour subtraction

In this section we review the general subtraction formalism proposed by Catani and Seymour (CS) in ref. [31], called *dipole subtraction*. This method is based on the observation that the real counterterms $\mathcal{C}^{(\alpha_{\mathrm{r}})}$ can be constructed out from more fundamental objects, dubbed *dipoles*, built in a completely process independent way. This, in turn, is possible since the singular structure of a $n+1$ parton amplitude $\mathcal{M}_{n+1}$ is universal, in the sense that one can always obtain it by the insertion of an extra parton over all the possible external legs of an underlying amplitude $\mathcal{M}_n$, with n QCD partons. For each of these insertions, the soft or collinear behaviour of $\mathcal{M}_{n+1}$ is basically factorisable with respect to $\mathcal{M}_n$ and a singular factor, that only depends on the momenta and quantum numbers of three partons: the parton that undergoes the insertion and a pair of partons in $\mathcal{M}_n$. We call the former the emitted parton, while the latter two, which form the dipole, are dubbed respectively the emitter and the spectator parton. The whole factorization process is called then *dipole factorization*.

These names are inherited from the singular behaviour of emissions amplitudes in the soft limit. In fact, labeling the set of all the $n + 2$ partons of the underlying n-body process as

$$\mathcal{I} = \{\oplus, \ominus, 1, \ldots, n\} \,, \tag{1.79}$$

when the energy k^0 of the emitted parton tends to zero, the real contribution behaves, in presence of massless partons only, as follows (see, for example refs. [50, 51])

$$\mathcal{R} \xrightarrow[k^0 \to 0]{} 4\pi\alpha_{\mathrm{S}} \sum_{\substack{i,j \in \mathcal{I} \\ i \neq j}} \mathcal{B}_{ij} \, \frac{p_i \cdot p_j}{(p_i \cdot k)(p_j \cdot k)} \; = \; 8\pi\alpha_{\mathrm{S}} \sum_{i \in \mathcal{I}} \frac{1}{p_i \cdot k} \sum_{j \neq i} \mathcal{B}_{ij} \, \frac{p_i \cdot p_j}{(p_i + p_j) \cdot k} \tag{1.80}$$

Each term on the r.h.s. of eq. (1.80) depends thus on the radiated momentum k, on the emitter momentum p_i and on the spectator momentum p_j. Notice that the emitter signals the presence of a collinear singularity, while the spectator is necessary to account for color correlations: $\mathcal{B}_{ij}$ are indeed the so-called color-correlated Born amplitudes. They are simply built from products of Born matrix elements, keeping the color matrices exposed

$$\mathcal{B}_{ij} = -\frac{1}{2s} \frac{1}{N_{\mathrm{sym}} D_\oplus D_\ominus S_\oplus S_\ominus} \sum_{\substack{\text{spins} \\ \text{colors}}} \mathcal{M}_{\{c_k\}} \left(\mathcal{M}^\dagger_{\{c_k\}}\right)_{\substack{c_i \to c'_i \\ c_j \to c'_j}} T^a_{c_i, c'_i} \, T^a_{c_j, c'_j} \,. \tag{1.81}$$

The factor $1/(2s)$ is the flux factor, N_{sym} is the symmetry factor for identical particles in the final state, $D_\oplus$ are the dimension of the color representations of the incoming partons (3 for quarks and 8 for gluons), and $S_\oplus$ are the number of spin states. We have also introduced the symbols $\mathcal{M}_{\{c_k\}}$ to identify the Born amplitude, and $\{c_k\}$ to label the color indexes of all partons in $\mathcal{I}$. The suffix on the parentheses that enclose $\mathcal{M}^\dagger_{\{c_k\}}$ indicates that the color indexes of partons $i, j \in \mathcal{I}$ are substituted with primed indexes in $\mathcal{M}^\dagger_{\{c_k\}}$. We assume summation over repeated color indexes (c_k for $k \in \mathcal{I}$, c'_i, c'_j and a) and spin indexes. For gluons $T^a_{cb} = if^{cab}$, where f^{abc} are the structure constants of the $SU(3)$ algebra. For incoming quarks $T^a_{ij} = t^a_{ij}$, where t's are the color matrices in the fundamental representation. For antiquarks $T^a_{ij} = -t^a_{ij}$. From color conservation, it is easy to show that $\mathcal{B}_{ij}$ satisfy

$$\sum_{i \in \mathcal{I}, i \neq j} \mathcal{B}_{ij} = C_{f_j} \mathcal{B} \,. \tag{1.82}$$

The symbol f_i denotes the flavour of the parton i, i.e. $f_i = g$ for a gluon, $f_i = q$ for a quark and $f_i = \bar{q}$ for an antiquark. We have

$$C_g = C_{\mathrm{A}} \qquad \text{and} \qquad C_q = C_{\bar{q}} = C_{\mathrm{F}} \,. \tag{1.83}$$

From the previous discussion it is easy to see that several dipoles, differing among each other only for the spectator parton, can give contributions to the same singular region α_{r}. In the CS approach, it is thus better to refine singular regions associating the index α_{r}, and thus the real counterterm $\mathcal{C}^{(\alpha_{\mathrm{r}})}$, to a dipole, rather than to a singular region. This is necessary since a different mapping of the real phase space is necessary for each dipole structure. These mappings are constructed in such a way that, in most cases, they affect only the momenta of the dipole partons, and all other momenta remain unchanged. The only exception is when the emitter and the spectator are the two incoming partons, since one always wants to preserve the momenta of identified partons. These parametrization formulas, that connects the phase space for real emissions to the dipoles phase space, are derived in sec. 6 of ref. [30]. The definitions of the dipole formulas can be found instead in the original ref. [31]. Due to their large number and length, we do not report them here explicitly, but only give their references in a schematic way:

- Initial-state singularity, initial-state spectator

Kinematics	Dipole Formulas
eqs. (6.80)-(6.86) of ref. [30]	eqs. (5.136) and (5.145) - (5.148) of ref. [31]

- Initial-state singularity, final-state spectator

Kinematics	Dipole Formulas
eqs. (6.57)-(6.63) of ref. [30]	eqs. (5.114) and (5.117) - (5.120) of ref. [31]

- Final-state singularity, initial-state spectator

Kinematics	Dipole Formulas
eqs. (6.33)-(6.41) of ref. [30]	eqs. (5.36) and (5.39) - (5.41) of ref. [31]

- Final-state singularity, final-state spectator

Kinematics	Dipole Formulas
eqs. (6.5)-(6.14) of ref. [30]	eqs. (5.2) and (5.7) - (5.9) of ref. [31]

However, when complete formulas are needed, as in Chapter 4, we report explicitly either the parametrization formulas linking real emissions kinematics to the dipole kinematics, either the counterterms obtained.

The previous ingredients (and the inclusion of the flux factor) fulfill the definition of real counterterms $\mathcal{C}^{(\alpha_{\mathrm{r}})}$'s in terms of the dipoles $\mathcal{D}^{\alpha_{\mathrm{r}}}$. The real counterterms have then to be subtracted, after being opportunely convolved with the correct parton luminosity $\tilde{\mathcal{L}}^{(\alpha_{\mathrm{r}})}$, with the real contributions R, opportunely projected onto the α_{r} regions, in order to obtain the cancellation of infrared divergences (see eq. (1.78)).

According to eq. (1.78), the last two missing ingredients are the soft-virtual term V, and the collinear remnants $G_\oplus$. In the following we report explicitly the form of these terms, expressed in our notation.

To obtain $\mathcal{V}$ (and consequently V) we start considering the virtual term $\mathcal{V}_{\mathrm{b}}$ in eq. (1.74). Assuming the validity of the KLN theorem, the most general form of the divergent part of the one-loop contribution $\mathcal{V}_{\mathrm{b}}$ must be equal and opposite in sign to the real emissions divergences. Thus, one can easily compute the divergent contributions coming from real emissions diagrams in $d = 4 - 2\epsilon$ dimensions and then simply change the signs in front of the ϵ poles obtained in this way. For massless parton, this can be done straightforwardly. The resulting virtual contribution $\mathcal{V}_{\mathrm{b}}$ is given by

$$\mathcal{V}_{\mathrm{b}} = \mathcal{N} \frac{\alpha_{\mathrm{S}}}{2\pi} \left[-\sum_{i\in\mathcal{I}} \left(\frac{1}{\epsilon^2} C_{f_i} + \frac{1}{\epsilon} \gamma_{f_i} \right) \mathcal{B} + \frac{1}{\epsilon} \sum_{\substack{i,j\in\mathcal{I} \\ i\neq j}} \log \frac{2k_i{\cdot}k_j}{Q^2} \mathcal{B}_{ij} + \mathcal{V}_{\mathrm{fin}} \right], \qquad (1.84)$$

where we have factored out

$$\mathcal{N} = \frac{(4\pi)^\epsilon}{\Gamma(1-\epsilon)} \left(\frac{\mu_{\mathrm{R}}^2}{Q^2} \right)^\epsilon, \qquad (1.85)$$

and where the factor of 2, due to the interference of the virtual amplitude with the Born term, has already been included in $\mathcal{V}_{\mathrm{b}}$. In the previous formula, μ_{R} is the renormalization scale, and Q is an arbitrary scale that is extracted from the virtual amplitude in order to make the normalization $\mathcal{N}$ dimensionless. The finite part $\mathcal{V}_{\mathrm{fin}}$ depends upon these two scales trough the definition of the normalization factor $\mathcal{N}$ in eq. (1.85), and from the regularization scheme, which we assume to be the standard conventional dimensional regularization (CDR). In case the dimensional reduction (DR) scheme is adopted, the definition of the finite part would change according to

$$\mathcal{V}_{\mathrm{fin}} = \mathcal{V}_{\mathrm{fin}}^{\mathrm{DR}} - \alpha_{\mathrm{S}}/(2\pi) \mathcal{B} \sum_{i\in\mathcal{I}} \tilde{\gamma}(f_i), \qquad (1.86)$$

where, $\tilde{\gamma}(g) = N_c/6$ and $\tilde{\gamma}(q) = (N_c^2 - 1)/(4N_c)$, with $N_c = 3$.

The symbol f_i denotes again the flavour of the parton i. We have C_{f_i} defined as in eq. (1.83) and

$$\gamma_g = \frac{11C_A - 4T_F\, n_f}{6}\,, \qquad\qquad \gamma_q = \gamma_{\bar{q}} = \frac{3}{2}C_F\,, \qquad\qquad (1.87)$$

$$\gamma_g' = \left(\frac{67}{9} - \frac{2\pi^2}{3}\right)C_A - \frac{23}{9}T_F\, n_f\,, \qquad \gamma_q' = \gamma_{\bar{q}}' = \left(\frac{13}{2} - \frac{2\pi^2}{3}\right)C_F\,. \qquad (1.88)$$

Notice also that, since $\mathcal{B}_{ij}$ is symmetric, when we sum over $i \neq j$ in the second sum on the r.h.s. of eq. (1.84), each term appears twice in the sum.

In the Catani-Seymour subtraction method, the soft-virtual contribution $\mathcal{V}$ is obtained summing, to the (negative) divergent virtual term $\mathcal{V}_b$, the d-dimensional integrals of the real counterterms $\mathcal{C}^{(\alpha_r)}$. In the notation of sec. 1.2.2, these integrated terms correspond to $\bar{\mathcal{C}}^{(\alpha_r)}$ and the sum that regularize the virtual contribution follows the lines of eqs. (1.76) and (1.75). Here, we do not report the full calculations of the original paper [31], but we start from the results reported in eqs. (C.27) and (C.28) of ref. [31]. After a suitable manipulation to bring them in our notation, we obtain for $\mathcal{V}$ the formula

$$\mathcal{V} = \frac{\alpha_S}{2\pi}\left\{\sum_{\substack{i,j\in\mathcal{I}\\i\neq j}}\left[\frac{1}{2}\log^2\frac{Q^2}{2k_i\cdot k_j} + \frac{\gamma_{f_i}}{C_{f_i}}\log\frac{Q^2}{2k_i\cdot k_j}\right]\mathcal{B}_{ij} + \sum_{i\in\mathcal{I}}\left[-\frac{\pi^2}{3}C_{f_i} + \gamma_{f_i} + K_{f_i}\right]\mathcal{B} + \mathcal{V}_{\text{fin}}\right\}\,.$$
$$(1.89)$$

The value of the finite part $\mathcal{V}_{\text{fin}}$ appearing above is fixed by eq. (1.84).

To complete the ingredients of eq. (1.78), we report the initial-state collinear remnants. At each collinear singular configuration is associated either $G_\oplus = \tilde{\mathcal{L}}\,\mathcal{G}_\oplus$ or $G_\ominus = \tilde{\mathcal{L}}\,\mathcal{G}_\ominus$. Considering a process in which an incoming parton $\oplus$ of flavour $f_\oplus$ splits into a parton $f_\oplus'$, which brings the fraction z of the incoming momentum, that enters the Born process $\mathcal{B}$, we have

$$
\mathcal{G}_{\oplus}^{f_\oplus f_\ominus}(z) \;=\; \frac{\alpha_{\mathrm{S}}}{2\pi} \sum_{f'_\oplus} \left\{ \left[\overline{K}^{f_\oplus f'_\oplus}(z) - K_{\mathrm{F.S.}}^{f_\oplus f'_\oplus}(z) \right] \mathcal{B}^{f'_\oplus f_\ominus}(z) \right.
$$

$$
- \;\delta^{f_\oplus f'_\oplus} \sum_{i=1}^{n} \frac{\gamma_{f_i}}{C_{f_i}} \left[\left(\frac{1}{1-z} \right)_+ + \delta(1-z) \right] \mathcal{B}_{i\oplus}^{f'_\oplus f_\ominus}(z) + \frac{1}{C_{f'_\oplus}} \widetilde{K}^{f_\oplus f'_\oplus}(z)\, \mathcal{B}_{\ominus\oplus}^{f'_\oplus f_\ominus}(z)
$$

$$
- \left. P^{f_\oplus f'_\oplus}(z) \frac{1}{C_{f'_\oplus}} \sum_{\substack{i\in\mathcal{I}\\ i\neq\oplus}} \mathcal{B}_{i\oplus}^{f'_\oplus f_\ominus}(z) \log \frac{\mu_{\mathrm{F}}^2}{2\, z\, k_\oplus \cdot k_i} \right\}. \tag{1.90}
$$

The superscripts on $\mathcal{B}$ denote the flavours of the incoming parton, while its z dependence reminds that reduced momenta enters it. As before, we obtain this formula after the translation in our notation of eq. (10.30) of ref. [31]. All the "plus" distribution appearing above and in the following are dealt with according to the general rule

$$
\int_0^1 dz\, f(z) \Big(g(z) \Big)_+ \;=\; \int_0^1 dz\, [f(z) - f(1)] \Big(g(z) \Big). \tag{1.91}
$$

The original definitions of the functions $\overline{K}$, $\widetilde{K}$, $K_{\mathrm{F.S.}}$ and P can be found in Appendix C of ref. [31]. Here, we report them in our notation. In particular, the functions $P^{f_\oplus f'_\oplus}(z)$ appearing above, are the *regularized* AP kernels. They can be obtained from the (averaged) *unregularized* leading order d-dimensional Altarelli-Parisi splitting functions

$$
\hat{P}^{qq}(z, \epsilon) \;=\; C_{\mathrm{F}} \left[\frac{1+z^2}{1-z} - \epsilon(1-z) \right], \tag{1.92}
$$

$$
\hat{P}^{qg}(z, \epsilon) \;=\; C_{\mathrm{F}} \left[\frac{1+(1-z)^2}{z} - \epsilon z \right], \tag{1.93}
$$

$$
\hat{P}^{gq}(z, \epsilon) \;=\; T_{\mathrm{F}} \left[1 - \frac{2z(1-z)}{1-\epsilon} \right], \tag{1.94}
$$

$$
\hat{P}^{gg}(z, \epsilon) \;=\; 2\, C_{\mathrm{A}} \left[\frac{z}{1-z} + \frac{1-z}{z} + z(1-z) \right], \tag{1.95}
$$

after expanding them according to

$$
\hat{P}^{f_\oplus f'_\oplus}(z, \epsilon) \;=\; \hat{P}^{f_\oplus f'_\oplus}(z) - \epsilon \hat{P}'^{f_\oplus f'_\oplus}(z) + \mathcal{O}(\epsilon^2), \tag{1.96}
$$

and adding the virtual corrections. In eq. (1.96) we have implicitly defined $\hat{P}'^{\ f_{\oplus}f'_{\oplus}}(z)$ and identified the four dimensional part as $\hat{P}^{f_{\oplus}f'_{\oplus}}(z) = \hat{P}^{f_{\oplus}f'_{\oplus}}(z, 0)$. The final results, in four dimensions, are the *regularized* AP kernels

$$P^{qg}(z) = P^{\bar{q}g}(z) = C_{\mathrm{F}} \frac{1 + (1-z)^2}{z} \ , \tag{1.97}$$

$$P^{gq}(z) = P^{g\bar{q}}(z) = T_{\mathrm{F}} \left[z^2 + (1-z)^2 \right] \ , \tag{1.98}$$

$$P^{qq}(z) = P^{\bar{q}\bar{q}}(z) = C_{\mathrm{F}} \left(\frac{1 + z^2}{1 - z} \right)_+ \ , \tag{1.99}$$

$$P^{gg}(z) = 2 C_{\mathrm{A}} \left[\left(\frac{1}{1-z} \right)_+ + \frac{1-z}{z} - 1 + z(1-z) \right] + \delta(1-z) \left(\frac{11}{6} C_{\mathrm{A}} - \frac{2}{3} n_{\mathrm{f}} T_{\mathrm{F}} \right) \ . \tag{1.100}$$

Their regular parts are denoted as follows

$$P_{\mathrm{reg}}^{f_{\oplus}f'_{\oplus}}(z) = P^{f_{\oplus}f'_{\oplus}}(z) \qquad \text{if} \ \ f_{\oplus} \neq f'_{\oplus} \ ,$$

$$P_{\mathrm{reg}}^{qq}(z) = -C_{\mathrm{F}} \left(1 + z \right) \ , \quad P_{\mathrm{reg}}^{gg}(z) = 2 \, C_{\mathrm{A}} \left[\frac{1-z}{z} - 1 + z(1-z) \right] \ . \tag{1.101}$$

Then, we have introduced the functions

$$\overline{K}^{f_{\oplus}f'_{\oplus}}(z) = \hat{P}'^{\ f_{\oplus}f'_{\oplus}}(z) + P_{\mathrm{reg}}^{f_{\oplus}f'_{\oplus}}(z) \, \log \frac{1-z}{z} \tag{1.102}$$

$$+ \ \delta^{f_{\oplus}f'_{\oplus}} \left[C_{f_{\oplus}} \left(\frac{2}{1-z} \log \frac{1-z}{z} \right)_+ - \delta(1-z) \left(\gamma_{f_{\oplus}} + K_{f_{\oplus}} - \frac{5}{6}\pi^2 \, C_{f_{\oplus}} \right) \right] \ ,$$

where

$$K_q = K_{\bar{q}} = \left(\frac{7}{2} - \frac{\pi^2}{6} \right) C_{\mathrm{F}} \ , \quad K_g = \left(\frac{67}{18} - \frac{\pi^2}{6} \right) C_{\mathrm{A}} - \frac{10}{9} T_{\mathrm{F}} n_{\mathrm{f}} \ . \tag{1.103}$$

Their explicit values are

$$\overline{K}^{qg}(z) \;=\; \overline{K}^{\bar{q}g}(z) \;=\; P^{qg}(z) \log \frac{1-z}{z} + C_{\mathrm{F}}\, z \;,\tag{1.104}$$

$$\overline{K}^{gq}(z) \;=\; \overline{K}^{g\bar{q}}(z) \;=\; P^{gq}(z) \log \frac{1-z}{z} + T_{\mathrm{F}}\, 2z(1-z) \;,\tag{1.105}$$

$$\overline{K}^{qq}(z) \;=\; \overline{K}^{\bar{q}\bar{q}}(z) \;=\; C_{\mathrm{F}} \left[\left(\frac{2}{1-z} \log \frac{1-z}{z} \right)_{+} - (1+z) \log \frac{1-z}{z} + (1-z) \right]$$
$$-\; \delta(1-z)\left(5-\pi^2\right) C_{\mathrm{F}} \;,\tag{1.106}$$

$$\overline{K}^{gg}(z) \;=\; 2C_{\mathrm{A}} \left[\left(\frac{1}{1-z} \log \frac{1-z}{z} \right)_{+} + \left(\frac{1-z}{z} - 1 + z(1-z) \right) \log \frac{1-z}{z} \right]$$
$$-\; \delta(1-z)\left[\left(\frac{50}{9} - \pi^2 \right) C_{\mathrm{A}} - \frac{16}{9}T_{\mathrm{F}}n_{\mathrm{f}} \right] \;,\tag{1.107}$$

In addition, eq. (1.90) also depends on the scheme-dependent flavour functions $K^{ab}_{\mathrm{F.S}}(z)$. We do not report their definition here, since being identically zero in $\overline{\mathrm{MS}}$, they are not relevant to this thesis. Finally, we have only the additional function

$$\widetilde{K}^{f_{\oplus}f'_{\oplus}}(z) \;=\; P^{f_{\oplus}f'_{\oplus}}_{\mathrm{reg}}(z) \,\log(1-z)$$
$$+\; \delta^{f_{\oplus}f'_{\oplus}}\, C_{f_{\oplus}} \left[\left(\frac{2}{1-z} \log(1-z) \right)_{+} - \frac{\pi^2}{3}\delta(1-z) \right] \;.\tag{1.108}$$

The analogous formulas, for the $\mathcal{G}_{\ominus}$ case, can be obtained by simply exchanging $\oplus \to \ominus$ in the previous equations.

Separation of singular regions

We now return to the issue of separating R into singular components $R^{\alpha_{\mathrm{r}}}$, which may require particular attention. One may start considering a projective formula like

$$R^{\alpha_{\mathrm{r}}} = \frac{\mathcal{D}_{\alpha_{\mathrm{r}}}}{\sum_{\alpha'_r} \mathcal{D}_{\alpha'_r}} \, R \,,\tag{1.109}$$

where the sum in the denominator runs over all dipoles. In this case, a problem may arise due to zeros in the denominator (in fact, the CS counterterms are not necessarily positive). However, the problem is easily solved by using instead (for example)

$$R^{\alpha_{\mathrm{r}}} = \frac{\mathcal{D}^2_{\alpha_{\mathrm{r}}}}{\sum_{\alpha'_r} \mathcal{D}^2_{\alpha'_r}} \, R \,.\tag{1.110}$$

However, in case the n-body cross section possesses singular regions, as discussed in section 1.2.2, a further problem arises. Formula (1.109) may not be adequate to partition the different singular components of R. This is better seen with an example. Consider the $Z +$ jet production process. The n-body process corresponds to a $Z + 1$ jet final state, and the $(n + 1)$-body process corresponds to a $Z + 2$ jets final state. Consider now the counterterm corresponding to the second jet becoming collinear to an initial-state parton. It is proportional to the underlying $Z + 1$ jet parton cross section. It is therefore also singular when the first jet becomes collinear to an initial-state parton, since the $Z + 1$ jet cross section is singular in this limit. This problem in a standard NLO calculation is solved by the fact that an infrared-safe observable O, that vanishes fast enough when two singular regions are approached at the same time, suppresses the singular regions of the underlying Born process in the counterterm (see eq. (1.65)). Here, one can instead write

$$R^{\alpha_\mathrm{r}} = \frac{H\left(\bar{\bar{\Phi}}_n^{(\alpha_\mathrm{r})}\right) \mathcal{D}_{\alpha_\mathrm{r}}}{\sum_{\alpha_r'} H\left(\bar{\bar{\Phi}}_n^{(\alpha_r')}\right) \mathcal{D}_{\alpha_r'}} \, R \,, \tag{1.111}$$

where H is a positive function that vanishes when its argument approaches an n-body singular configuration. We again have

$$\sum_{\alpha_\mathrm{r}} R^{\alpha_\mathrm{r}} = R \,, \tag{1.112}$$

and now R^{α_r} is singular only in the α_r region.

1.2.4 Frixione-Kunszt-Signer subtraction

In this section, we review the Frixione-Kunszt-Signer (FKS) general subtraction formalism, proposed in refs. [32, 33], including a few modifications that have been introduced recently in refs. [18] and [30].

In the FKS method, the real-emission cross section is separated into a sum of terms, each of them having at most one collinear and one soft singularity associated with a given parton, which is called the FKS parton. Since all massless partons in the final state may induce a divergence of the real matrix elements, the role of FKS parton is given to each parton in turn.

The $\mathcal{S}$ functions

For each singular region, positive semidefinite functions $\mathcal{S}$ of the $(n+1)$-body phase space are introduced, in order to project real contributions onto singular regions. The sum of the $\mathcal{S}$ functions over singular regions satisfy

$$\sum_i \mathcal{S}_i + \sum_{ij} \mathcal{S}_{ij} = 1 \,, \tag{1.113}$$

where, in the previous equation and in the following of this section, we have labeled by i those regions associated with the final-state parton i becoming soft or collinear to one of the incoming partons ($\oplus$ or $\ominus$), and with the pair ij those regions associated with the final-state parton i becoming soft or collinear to a final-state parton j. In eq. (1.113), the sums are intended to run over $i, j = 1, \ldots, n+1$, excluding, of course, $i = j$. Alternatively, $\mathcal{S}_i$ and $\mathcal{S}_{ij}$ may also be set to zero if the corresponding regions are not singular. This is, for example, the case if i and j are two quarks of different flavour, since neither a soft or a collinear singularity is associated to this configuration. Observe, however, that if i and j are both gluons, both terms $\mathcal{S}_{ij}$ and $\mathcal{S}_{ji}$ must appear in the sum, since there is a soft singularity for either parton becoming soft. Hence, in a given soft region (*e.g.* assuming that the parton m becomes soft), all the $\mathcal{S}_i$ and $\mathcal{S}_{ij}$ with $i \neq m$ vanish. In a given initial-state collinear region instead, *e.g.* if parton m becomes collinear to an initial state parton, only $\mathcal{S}_m$ is non-zero and equal to one. Finally, in a given final-state collinear region, *e.g.* if partons i and j are collinear, only $\mathcal{S}_{ij}$ and $\mathcal{S}_{ji}$ can differ from zero, their sum being 1. All these considerations are summarized by the following properties of the $\mathcal{S}$ functions

$$\lim_{k_m^0 \to 0} \left(\mathcal{S}_i + \sum_j \mathcal{S}_{ij} \right) = \delta_{im} \,, \tag{1.114}$$

$$\lim_{\vec{k}_m \| \vec{k}_\ominus} \mathcal{S}_i = \delta_{im} \,, \tag{1.115}$$

$$\lim_{\vec{k}_m \| \vec{k}_l} (\mathcal{S}_{ij} + \mathcal{S}_{ji}) = \delta_{im}\delta_{jl} + \delta_{il}\delta_{jm} \,, \tag{1.116}$$

$$\lim_{\vec{k}_m \| \vec{k}_\ominus} \mathcal{S}_{ij} = 0 \,. \tag{1.117}$$

In the original FKS formulation [32, 33] these functions were chosen as sets of θ functions, to separate the phase space into non-overlapping regions. In more recent approaches of refs. [18, 30], they were instead chosen to be smooth functions, more

suited to numerical integrations required for Monte Carlo implementations. In this thesis we follow this last approach.

Formulas eqs. (1.114) to (1.117), together with the completeness relation eq. (1.113), are the only requirements for the analytic definition of the $\mathcal{S}$ functions. Their actual functional forms is left to one's taste, but away from the infrared limits it is only relevant to numerical integrations. Here, we follow ref. [30] and define the $\mathcal{S}$ functions as

$$\mathcal{S}_i = \frac{1}{\mathcal{D}\, d_i}\,, \tag{1.118}$$

$$\mathcal{S}_{ij} = \frac{1}{\mathcal{D}\, d_{ij}}\, h\left(\frac{E_i}{E_i + E_j}\right)\,, \tag{1.119}$$

where we have introduced the quantity

$$\mathcal{D} = \sum_k \frac{1}{d_k} + \sum_{kl} \frac{1}{d_{kl}}\,, \tag{1.120}$$

and where h is a function, whose precise definition is left to the user's choice, that is only required to satisfy

$$\lim_{z\to 0} h(z) = 1\,, \qquad \lim_{z\to 1} h(z) = 0\,, \qquad h(z) + h(1-z) = 1\,. \tag{1.121}$$

The functions d_i and d_{ij}, appearing in eqs. (1.118) and (1.119), are defined by

$$
\begin{aligned}
d_i = 0 &\quad \text{if and only if} \quad E_i = 0 \quad \text{or} \quad \vec{k}_i \parallel \vec{k}_\oplus \quad \text{or} \quad \vec{k}_i \parallel \vec{k}_\ominus\,, \\
d_{ij} = 0 &\quad \text{if and only if} \quad E_i = 0 \quad \text{or} \quad E_j = 0 \quad \text{or} \quad \vec{k}_i \parallel \vec{k}_j\,,
\end{aligned} \tag{1.122}
$$

where energies and three-momenta are computed in the centre-of-mass frame of the incoming partons. The d's are defined as

$$d_i = \left(\frac{\sqrt{s}}{2} E_i\right)^a \left(1 - \cos^2\theta_i\right)^b\,, \tag{1.123}$$

$$d_{ij} = \left(E_i E_j\right)^a \left(1 - \cos\theta_{ij}\right)^b\,, \tag{1.124}$$

where θ_i is the angle between $\vec{k}_i$ and $\vec{k}_\oplus$, θ_{ij} the angle between $\vec{k}_i$ and $\vec{k}_j$, $s = (k_\oplus + k_\ominus)^2$, and a, b are positive real numbers. Their actual values are relevant only for numerical integration issues, the physical cross sections being independent from this choice. In

this thesis, we have assumed $a = b = 1$. In terms of invariants, one can rewrite eqs. (1.123) and (1.124) using

$$k_{\oplus} = \frac{\sqrt{s}}{2}(1,0,0,1)\,, \quad k_{\ominus} = \frac{\sqrt{s}}{2}(1,0,0,-1)\,, \tag{1.125}$$

which imply

$$E_i \;=\; \frac{1}{\sqrt{s}}\,(k_{\oplus} + k_{\ominus})\!\cdot\! k_i\,, \tag{1.126}$$

$$\cos\theta_i \;=\; 1 - \frac{2k_i\!\cdot\! k_{\oplus}}{E_i\sqrt{s}}\,, \tag{1.127}$$

$$\cos\theta_{ij} \;=\; 1 - \frac{k_i\!\cdot\! k_j}{E_i E_j}\,. \tag{1.128}$$

In the original FKS approach, the $\oplus$ and $\ominus$ collinear regions are both singled out by the same $\mathcal{S}_i$ function. However, sometimes one may want to treat the two initial collinear regions separately. Thus, as already done in ref. [30], we separate

$$\mathcal{S}_i = \mathcal{S}_i^{\oplus} + \mathcal{S}_i^{\ominus}\,, \tag{1.129}$$

with the properties

$$\lim_{\vec{k}_m \| \vec{k}_{\oplus}} \mathcal{S}_i^{\oplus} = \delta_{im}\,, \qquad \lim_{\vec{k}_m \| \vec{k}_{\oplus}} \mathcal{S}_i^{\ominus} = 0\,, \tag{1.130}$$

that refine eq. (1.115). To do so, we introduce

$$d_i^{\oplus} = \left(\frac{\sqrt{s}}{2} E_i \right)^a 2^b (1 \mp \cos\theta_i)^b\,, \tag{1.131}$$

instead of d_i of eq. (1.123). The definition of $\mathcal{D}$ in eq. (1.120) becomes

$$\mathcal{D} = \sum_k \left(\frac{1}{d_k^{\oplus}} + \frac{1}{d_k^{\ominus}} \right) + \sum_{kl} \frac{1}{d_{kl}}\,, \tag{1.132}$$

and, at the end, we are left with

$$\mathcal{S}_i^{\oplus} = \frac{1}{\mathcal{D}\, d_i^{\oplus}}\,. \tag{1.133}$$

Contributions to the cross section

The projection of real contributions onto different singular regions proceeds then by multiplying the $\mathcal{R}$ term for the corresponding $\mathcal{S}$ function. One thus define

$$\mathcal{R}_i^{\oplus} = \mathcal{S}_i^{\oplus} \mathcal{R} , \qquad \mathcal{R}_{ij} = \mathcal{S}_{ij} \mathcal{R} , \tag{1.134}$$

which obviously obeys

$$\mathcal{R} = \sum_i \left(\mathcal{R}_i^{\oplus} + \mathcal{R}_i^{\ominus} \right) + \sum_{ij} \mathcal{R}_{ij} = \sum_i \mathcal{R}_i + \sum_{ij} \mathcal{R}_{ij} . \tag{1.135}$$

The $\mathcal{R}_i^{\oplus}$ terms (or the not-separated contributions $\mathcal{R}_i$) need now to be subtracted only in the regions in which parton i is soft and/or collinear to one of the initial-state partons, and the $\mathcal{R}_{ij}$ terms are divergent only in the regions in which parton i is soft and/or collinear to final-state parton j.

At this point, a different parametrization of the real phase space is assumed for each $\mathcal{R}_i^{\oplus}$ or $\mathcal{R}_{ij}$. This parametrization is chosen in such a way that one can easily perform the corresponding analytical and numerical integrations. Radiation variables involved in the phase-space parametrization are

- the energy of parton i, which is related to soft singularities both in $\mathcal{R}_i$ and $\mathcal{R}_{ij}$.

- the angle between parton i and one of the initial-state partons, which is related to initial-state collinear singularities in $\mathcal{R}_i$.

- the angle between parton i and j, which is related to a final-state collinear singularity for $\mathcal{R}_{ij}$.

Therefore, only two independent functional forms for phase spaces in FKS are sufficient, one for initial- and one for final-state emissions.

In practice, assuming that i is the FKS parton, we introduce the following variables

$$\xi_i = \frac{2k_i^0}{\sqrt{s}} , \qquad y_i = \cos\theta_i , \qquad y_{ij} = \cos\theta_{ij} , \qquad \phi , \tag{1.136}$$

where θ_i is the angle of parton i with the incoming parton $\oplus$, θ_{ij} is the angle of parton i with parton j, and ϕ is an azimuthal variable. All variables are computed in the centre-of-mass frame of the incoming partons. The singular regions (soft and collinear) are associated with $\xi_i \to 0$ and $y_i \to \pm 1$ ($y_{ij} \to 1$) respectively.

We have that, in $d = 4 - 2\epsilon$ dimensions,

$$\frac{d^{d-1}k_i}{2k_i^0(2\pi)^{d-1}} = \frac{s^{1-\epsilon}}{(4\pi)^{d-1}} \, \xi_i^{1-2\epsilon} \left(1 - y^2\right)^{-\epsilon} d\xi_i \, dy \, d\Omega^{d-2} \,, \qquad (1.137)$$

where

$$d\Omega^{d-2} = (\sin\phi)^{-2\epsilon} \, d\phi \, d\Omega^{d-3} \,, \qquad \int d\Omega^{d-3} = \frac{2\pi^{\frac{d-3}{2}}}{\Gamma\left(\frac{d-3}{2}\right)} \,. \qquad (1.138)$$

In the formulas above, the pair y, Ω stands for either y_i, Ω_i or y_{ij}, Ω_{ij}. The transverse angular variables $d\Omega_i^{d-2}$ are relative to the collision axis, while $d\Omega_{ij}^{d-2}$ are relative to the direction of parton j. In any case, the phase space for the $\mathcal{R}_i$ and $\mathcal{R}_{ij}$ contributions may be written as

$$\begin{aligned} d\Phi_{n+1} &= (2\pi)^d \, \delta^d\!\left(k_\oplus + k_\ominus - \sum_{i=1}^{n+1} k_i\right) \left[\prod_{l\neq i} \frac{d^{d-1}k_l}{(2\pi)^{d-1} \, 2k_l^0}\right] \\ &\times \frac{s^{1-\epsilon}}{(4\pi)^{d-1}} \, \xi_i^{1-2\epsilon} \left(1 - y^2\right)^{-\epsilon} d\xi_i \, dy \, d\Omega^{d-2} \,. \end{aligned} \qquad (1.139)$$

Other parametrization of the phase space are acceptable, provided that they allow a simple handling of the distributions appearing in the following.

The singularities for $\xi \to 0$, $y_i \to \pm 1$ or $y_{ij} \to 1$ are treated by rewriting

$$\mathcal{R}_i = \left(\frac{1}{\xi_i^2}\right) \frac{1}{2} \left[\left(\frac{1}{1 - y_i}\right) + \left(\frac{1}{1 + y_i}\right)\right] \left[\left(1 - y_i^2\right) \xi_i^2 \, \mathcal{R}_i\right] \,, \qquad (1.140)$$

$$\mathcal{R}_{ij} = \left(\frac{1}{\xi_i^2}\right) \left(\frac{1}{1 - y_{ij}}\right) \left[\left(1 - y_{ij}\right) \xi_i^2 \, \mathcal{R}_{ij}\right] \,, \qquad (1.141)$$

where now $\left[\left(1 - y_i^2\right) \xi_i^2 \, \mathcal{R}_i\right]$ and $\left[\left(1 - y_{ij}\right) \xi_i^2 \, \mathcal{R}_{ij}\right]$ are regular in the corresponding singular limits. Anyhow, the phase space integrals of $\mathcal{R}_i$ and $\mathcal{R}_{ij}$ are still infrared divergent. Going in $d = 4 - 2\epsilon$ dimensions, with $\epsilon < 0$, we have that the singular parts contain the integrals

$$\int_{-1}^{1} dy_i \left(1 - y_i^2\right)^{-1-\epsilon} \int_0^1 d\xi_i \, \xi_i^{-1-2\epsilon} \left[\xi_i^2 \left(1 - y_i^2\right) \mathcal{R}_i\right] , \qquad (1.142)$$

$$\int_{-1}^{1} dy_{ij} \left(1 - y_{ij}\right)^{-1-\epsilon} \int_0^1 d\xi_i \, \xi_i^{-1-2\epsilon} \left[\xi_i^2 \left(1 - y_{ij}\right) \mathcal{R}_{ij}\right] . \qquad (1.143)$$

In order to deal with these singularities, we make use of the following identities

$$\xi_i^{-1-2\epsilon} = -\frac{(\xi_c)^{-2\epsilon}}{2\epsilon}\delta(\xi_i) + \left(\frac{1}{\xi_i}\right)_{\xi_c} - 2\epsilon\left(\frac{\log\xi_i}{\xi_i}\right)_{\xi_c} + \mathcal{O}(\epsilon^2), \quad (1.144)$$

$$(1-y_i^2)^{-1-\epsilon} = -\frac{(2\delta_\mathrm{I})^{-\epsilon}}{2\epsilon}[\delta(1-y_i) + \delta(1+y_i)]$$

$$+ \frac{1}{2}\left[\left(\frac{1}{1-y_i}\right)_{\delta_\mathrm{I}} + \left(\frac{1}{1+y_i}\right)_{\delta_\mathrm{I}}\right] + \mathcal{O}(\epsilon), \qquad (1.145)$$

$$(1-y_{ij})^{-1-\epsilon} = -\frac{(\delta_\mathrm{O})^{-\epsilon}}{\epsilon}\delta(1-y_{ij}) + \left(\frac{1}{1-y_{ij}}\right)_{\delta_\mathrm{O}} + \mathcal{O}(\epsilon), \qquad (1.146)$$

where we have introduced the parameters ξ_c, δ_I and δ_O, with

$$0 < \xi_c \leq 1 \qquad \text{and} \qquad 0 < \delta_\mathrm{I}, \delta_\mathrm{O} \leq 2. \qquad (1.147)$$

The distributions appearing above are defined in terms of their action on a test function f, as follows

$$\int_0^1 d\xi_i\, f(\xi_i)\left(\frac{1}{\xi_i}\right)_{\xi_c} = \int_0^1 d\xi_i\, \frac{f(\xi_i) - f(0)\,\theta(\xi_c - \xi_i)}{\xi_i}, \qquad (1.148)$$

$$\int_0^1 d\xi_i\, f(\xi_i)\left(\frac{\log\xi_i}{\xi_i}\right)_{\xi_c} = \int_0^1 d\xi_i\left[f(\xi_i) - f(0)\,\theta(\xi_c - \xi_i)\right]\frac{\log\xi_i}{\xi_i}, \qquad (1.149)$$

$$\int_{-1}^1 dy_i\, f(y_i)\left(\frac{1}{1\mp y_i}\right)_{\delta_\mathrm{I}} = \int_{-1}^1 dy_i\, \frac{f(y_i) - f(\pm 1)\,\theta(\pm y_i - 1 + \delta_\mathrm{I})}{1\mp y_i}, \qquad (1.150)$$

$$\int_{-1}^1 dy_{ij}\, f(y_{ij})\left(\frac{1}{1-y_{ij}}\right)_{\delta_\mathrm{O}} = \int_{-1}^1 dy_{ij}\, \frac{f(y_{ij}) - f(1)\,\theta(y_{ij} - 1 + \delta_\mathrm{O})}{1-y_{ij}}. \qquad (1.151)$$

Applying eqs. (1.144)-(1.146) to the integrals in eqs. (1.142) and (1.143), different contributions appear when distributions eqs. (1.148)-(1.151) are expanded. Some of them have the same structure as the virtual term, some other are proportional to the collinear counterterms. They are treated combining each of these contributions with the term to which it is proportional (i.e. virtual or collinear remnants). In any case, we do not need to know the explicit formulas for the d-dimensional real emissions cross sections $\mathcal{R}_i$ or $\mathcal{R}_{ij}$, that appear in these terms, since either it is enough to know their soft limits $\xi \to 0$, which can be easily obtained using the eikonal approximation for soft emissions in d dimensions, either their d-dimensional collinear approximation

when $y_i \to \pm 1$ or $y_{ij} \to 1$. Finally, terms of the form

$$
\int_{-1}^{1} dy_i \int_0^1 d\xi_i \left(\frac{1}{\xi_i}\right)_{\xi_c} \frac{1}{2} \left[\left(\frac{1}{1-y_i}\right)_{\delta_I} + \left(\frac{1}{1+y_i}\right)_{\delta_I}\right] \left[(1-y_i^2)\,\xi_i^2\,\mathcal{R}_i\right]
$$
$$
= \int_{-1}^{1} dy_i \int_0^1 d\xi_i\, \xi_i\, \hat{\mathcal{R}}_i \qquad (1.152)
$$

or

$$
\int_{-1}^{1} dy_{ij} \int_0^1 d\xi_i \left(\frac{1}{\xi_i}\right)_{\xi_c} \left(\frac{1}{1-y_{ij}}\right)_{\delta_O} \left[(1-y_{ij})\,\xi_i^2\,\mathcal{R}_{ij}\right] = \int_{-1}^{1} dy_{ij} \int_0^1 d\xi_i\, \xi_i\, \hat{\mathcal{R}}_{ij}
$$
$$
(1.153)
$$

are left, where we have defined

$$
\hat{\mathcal{R}}_i \;=\; \frac{1}{\xi_i}\left\{\frac{1}{2}\left(\frac{1}{\xi_i}\right)_{\xi_c}\left[\left(\frac{1}{1-y_i}\right)_{\delta_I} + \left(\frac{1}{1+y_i}\right)_{\delta_I}\right]\left[(1-y_i^2)\,\xi_i^2\,\mathcal{R}_i\right]\right\}, \quad (1.154)
$$

$$
\hat{\mathcal{R}}_{ij} \;=\; \frac{1}{\xi_i}\left\{\left(\frac{1}{\xi_i}\right)_{\xi_c}\left(\frac{1}{1-y_{ij}}\right)_{\delta_O}\left[(1-y_{ij})\,\xi_i^2\,\mathcal{R}_{ij}\right]\right\}. \qquad (1.155)
$$

Observe that the $1/\xi_i$ factors in front of eqs. (1.154) and (1.155) cancel against the phase-space ξ_i factor in eqs. (1.152) and (1.153), and that $[\xi_i^2(1-y_i^2)\,\mathcal{R}_i]$ and $[\xi_i^2(1-y_{ij})\,\mathcal{R}_{ij}]$ are not singular at $\xi_i = 0$ and $y_i = \pm 1$, $y_{ij} = 1$, so that distributions in $\hat{\mathcal{R}}_i$ and $\hat{\mathcal{R}}_{ij}$ always act on a regular functions.

The procedure above is fully general. It can be shown that, defining

$$
\hat{\mathcal{R}} = \sum_i \hat{\mathcal{R}}_i + \sum_{ij} \hat{\mathcal{R}}_{ij}, \qquad (1.156)
$$

and $\hat{R} = \mathcal{L}\,\hat{\mathcal{R}}$, one can rewrite eq. (1.78) in the form

$$
\begin{aligned}
\langle O \rangle \;=\; & \int d\mathbf{\Phi}_n\, O_n(\mathbf{\Phi}_n)\left[B(\mathbf{\Phi}_n) + V(\mathbf{\Phi}_n)\right] \\
& + \int d\mathbf{\Phi}_{n+1}\, O_{n+1}(\mathbf{\Phi}_{n+1})\,\hat{R}(\mathbf{\Phi}_{n+1}) \\
& + \int d\mathbf{\Phi}_{n,\oplus}\, O_n(\bar{\mathbf{\Phi}}_n)\,G_\oplus(\mathbf{\Phi}_{n,\oplus}) + \int d\mathbf{\Phi}_{n,\ominus}\, O_n(\bar{\mathbf{\Phi}}_n)\,G_\ominus(\mathbf{\Phi}_{n,\ominus}). \quad (1.157)
\end{aligned}
$$

By handling the distributions in $\hat{R}$ according to the prescriptions (1.148)-(1.151), one thus automatically generates the real counterterms. Therefore, the final expression for

the differential cross section in the FKS formalism involves only non-divergent terms, since the cancellation of the infrared singularities takes place in the intermediate steps of the computation. For these reasons, any term appearing in eq. (1.157) can safely be evaluated in $d = 4$ dimensions.

In case one want to separate the $\oplus$ and $\ominus$ collinear regions, as outlined in eq. (1.129), we define

$$\hat{\mathcal{R}} = \sum_i \left(\hat{\mathcal{R}}_i^{\oplus} + \hat{\mathcal{R}}_i^{\ominus} \right) + \sum_{ij} \hat{\mathcal{R}}_{ij} \,, \tag{1.158}$$

$$\hat{\mathcal{R}}_i^{\oplus} = \frac{1}{\xi_i} \left\{ \left(\frac{1}{\xi_i} \right)_{\xi_c} \left(\frac{1}{1 \mp y_i} \right)_{\delta_{\mathrm{I}}} \left[(1 \mp y_i) \, \xi_i^2 \, \mathcal{R}_i^{\oplus} \right] \right\} \,, \tag{1.159}$$

and proceed just like before.

Then, the soft-virtual term in eq. (1.157) is given by

$$V = \mathcal{L} \mathcal{V} \,, \qquad \mathcal{V} = \frac{\alpha_{\mathrm{S}}}{2\pi} \left(\mathcal{Q} \mathcal{B} + \sum_{\substack{i,j \in \mathcal{I} \\ i \neq j}} \mathcal{I}_{ij} \, \mathcal{B}_{ij} + \mathcal{V}_{\mathrm{fin}} \right) \,, \tag{1.160}$$

with $\mathcal{V}_{\mathrm{fin}}$ defined by eq. (1.84) and where $\mathcal{Q}$ and $\mathcal{I}_{ij}$ depend on the flavours and momenta of the incoming and outgoing partons. They read

$$
\begin{aligned}
\mathcal{Q} = \sum_{i=1}^{n} \Bigg[& \gamma'_{f_i} - \log \frac{s \delta_{\mathrm{O}}}{2Q^2} \left(\gamma_{f_i} - 2 C_{f_i} \log \frac{2E_i}{\xi_c \sqrt{s}} \right) \\
& + 2 C_{f_i} \left(\log^2 \frac{2E_i}{\sqrt{s}} - \log^2 \xi_c \right) - 2 \gamma_{f_i} \log \frac{2E_i}{\sqrt{s}} \Bigg] \\
& - \log \frac{\mu_{\mathrm{F}}^2}{Q^2} \left[\gamma_{f_{\oplus}} + 2 C_{f_{\oplus}} \log \xi_c + \gamma_{f_{\ominus}} + 2 C_{f_{\ominus}} \log \xi_c \right] \,,
\end{aligned}
\tag{1.161}
$$

and

$$
\begin{aligned}
\mathcal{I}_{ij} = \; & \frac{1}{2} \log^2 \frac{\xi_c^2 s}{Q^2} + \log \frac{\xi_c^2 s}{Q^2} \log \frac{k_j \cdot k_i}{2 E_j E_i} - \mathrm{Li}_2 \left(\frac{k_j \cdot k_i}{2 E_j E_i} \right) \\
& + \frac{1}{2} \log^2 \frac{k_j \cdot k_i}{2 E_j E_i} - \log \left(1 - \frac{k_j \cdot k_i}{2 E_j E_i} \right) \log \frac{k_j \cdot k_i}{2 E_j E_i} \,,
\end{aligned}
\tag{1.162}
$$

where E_i is the energy of parton i in the partonic centre-of-mass frame.

The collinear remnants are instead given by

$$
\begin{aligned}
\mathcal{G}_{\oplus}^{f_\oplus f_\ominus}(z) \;=\; & \frac{\alpha_{\mathrm{S}}}{2\pi} \sum_{f'_\oplus} \Bigg\{ (1-z)\,\hat{P}^{f_\oplus f'_\oplus}(z,0) \left[\left(\frac{1}{1-z}\right)_{\!\xi_c} \log\frac{s\delta_{\mathrm{I}}}{2\mu_{\mathrm{F}}^2} + 2\left(\frac{\log(1-z)}{1-z}\right)_{\!\xi_c} \right] \\
& - \left[\frac{\partial\hat{P}^{f_\oplus f'_\oplus}(z,\epsilon)}{\partial\epsilon}\right]_{\epsilon=0} - K^{f_\oplus f'_\oplus}(z) \Bigg\} \mathcal{B}^{f'_\oplus f_\ominus}(z)\,,
\end{aligned}
\tag{1.163}
$$

In the previous equation, $s = (k_\oplus + k_\ominus)^2$. Furthermore, the distributions are defined as in eqs. (1.148) and (1.149), with $\xi_i = 1-z$. The functions $\hat{P}(z,\epsilon)$ are the leading order *unregularized* Altarelli-Parisi splitting functions in $d = 4 - 2\epsilon$ dimensions, reported in eqs. (1.92)-(1.95). The distributions $K^{ff'}$ are instead related to the change of the scheme in the evolution of parton distribution functions. Their precise definition can be found in the original ref. [32]. They are equivalent to $K_{\mathrm{F.S.}}^{ff'}$ of sec. 1.2.3 (see also Appendix C of ref. [31]), and thus identically zero in $\overline{\mathrm{MS}}$.

In eq. (1.163), $\mathcal{G}_{\oplus}^{f_\oplus f_\ominus}$ is the collinear remnant contribution for flavours $f_\oplus, f_\ominus$ of the incoming partons. Analogously, the superscripts in $\mathcal{B}$ (and $\mathcal{B}_{ij}$) single out a given flavour combination for the incoming partons in the Born amplitudes and its color-correlated components. The formula for $\mathcal{G}_\ominus$ can be obtained from eq. (1.163) by analogy, with the exchange $\oplus \to \ominus$.

It is important to observe that, up to now, we have presented the FKS method in the full generality. However, in the POWHEG framework, it is often useful to exploit the maximal range of integration, not limiting the $\xi_c, \delta_{\mathrm{I}}$ and δ_{O} parameter values. In this case, all the formulas presented in this section still hold, with the obvious identifications

$$
\left(\frac{1}{\xi}\right)_{\!+} = \left(\frac{1}{\xi}\right)_{\!\xi_c} \text{ with } \xi_c = 1\,, \qquad \left(\frac{1}{1\mp y}\right)_{\!+} = \left(\frac{1}{1\mp y}\right)_{\!\delta} \text{ with } \delta = \delta_{\mathrm{I}} = \delta_{\mathrm{O}} = 2\,.
\tag{1.164}
$$

The only missing ingredients one needs to construct a POWHEG generator in the FKS framework are the mappings between real phase space variables and underlying Born ones, for the two kind of possible singular regions (initial- or final-state). Examples of such mappings are given in due time in chapter 5, or may be found in sec. 5 of ref. [30].

<div align="right">

Chapter 2

</div>

Parton Showers

2.1 Shower Monte Carlo programs

In this section we present the general features of Shower Monte Carlo (SMC) programs. A SMC aims to a complete description of particle collisions from the high-energy perturbative domain down to the detector level, which is, in the end, what can be observed by experiments. In fact, even if for many processes and observables complete next-to-leading and also next-to-next-to-leading QCD calculations are available nowadays, these are usually not enough. There are indeed region of the phase space where higher-order terms are particularly enhanced and therefore these contributions must be accounted for and resummed properly to obtain consistent results. Furthermore, fixed order calculations, such those presented in sec. 1.2, have by definition a fixed, in most cases very low, number of final state particles. This contrasts with the large number of particles in the final state seen by detectors. Thus, a mechanism able to connect these two opposite features is needed, if a realistic description of collision processes is aimed. Such a task is performed by the so-called *parton shower algorithm*, from which SMC programs inherit the name.

Shower Monte Carlo programs are commonly formed by various components, or stages, all of which are needed to give an accurate description of the formation of the final state. A comprehensive list should contain

1. A large library of Standard Model, and also Beyond Standard Model (BSM), cross section formulas, usually calculated at the leading-order. The hard scattering process the user is interested into is chosen within this library.

2. A parton shower algorithm, for the generation of dominant QCD perturbative

<div align="center">

43

</div>

effects. This algorithm works by adding to the partons coming from the LO hard scattering process chosen a sequence of enhanced emissions of colored partons (quarks or gluons). The enhancement of these contributions is due to their behaviour in the soft or collinear limit, and appears as large logarithms of the ratio between the typical hard scale of the process over the strong interaction cutoff (*e.g.* Λ_{QCD}). These logarithms may grow up to the inverse of the strong coupling constant $\alpha_{\rm s}$, spoiling the perturbative expansion itself. Thus, their correct treatment is crucial.

3. Some phenomenological model of hadron formation, which is imposed upon the set of final state partons emerging from previous steps, in order to perform the partons-hadrons conversion, outside of the perturbative domain.

4. A library of unstable particle decays, by which weakly unstable hadrons are decayed and their decay products are available in the final state.

5. In hadronic collisions, a model for the *underlying event* (UE). We call underlying event the softer interactions, due to beam remnants, accompanying the hard one we are interested into. These usually do not include multi-particle interactions (MPI), which are instead due to the occurrence of more than one hard parton-parton interaction in the same hadronic collision. In most SMC programs these are accounted separately.

The core of a SMC program is the shower algorithm, item 2. This is nothing but a method to evaluate a potentially infinite class of Feynman diagrams, which, by virtue of infrared enhanced logarithms, gives contributions to the cross section that are comparable with those otherwise normally included.

For the purposes of this thesis, in the following we shall concentrate only on the shower algorithm description, leaving out the other issues (item 1 and 3-5). The interested reader can learn more about them looking into some other pedagogical reviews, for example refs. [52, 53]. The next discussion follows the lines of ref. [54], where more details and explanations can be found.

2.1.1 The shower algorithm

Collinear factorization

In sec. 1.2.3 it was shown that the matrix elements for soft emissions may be written in a factorized form. However, quark or gluons emissions from massless partons are also plagued by infrared singularities when the emitted particle becomes collinear to an incoming or outgoing parton in the scattering process. In this limit, the cross section can be pictorially seen as those for the production of a parent parton with small virtuality, that decays into the two collinear partons. The divergence is exactly due to the vanishing denominator in the propagator of this parent parton. In QCD there are three possible decays of this parent parton, commonly called *splitting* processes: $q \rightarrow qg$, $g \rightarrow q\bar{q}$ and $g \rightarrow gg$.

Like in the soft-emissions case, it happens that squared amplitudes near the collinear limit factorize. Here, this factorization is in terms of amplitudes for the production of the parent parton times a splitting factor, that does only depend on the particular splitting involved, and on its kinematics. Since also the phase space can always be written in a factorized form, this factorization applies to the whole cross section. For example, given a tree-level amplitude with $n+1$ final state particles and assuming that a final state quark goes collinear to a final state gluon, one has

$$|M_{n+1}|^2 d\Phi_{n+1} \;\Rightarrow\; |M_n|^2 d\Phi_n \;\times\; \frac{\alpha_{\rm s}}{2\pi} \frac{dt}{t} \, \hat{P}_{q,qg}(z) \, dz \, \frac{d\phi}{2\pi} \,, \qquad (2.1)$$

where M_{n+1} and M_n are the amplitudes for the $n+1$ and n body processes. The n particle phase spaces is defined, as usual, by

$$d\Phi_n = (2\pi)^4 \delta^4 \left(\sum_{i=1}^{n} k_i - q \right) \prod_{i=1}^{n} \frac{d^3 k_i}{2k_i^0 (2\pi)^3} \,, \qquad (2.2)$$

with q the total incoming momentum. An analogous formula holds for the $n+1$ particle phase space.

$\hat{P}_{q,qg}(z)$ in eq. (2.1) is the Altarelli-Parisi (AP) splitting function for the $q \rightarrow qg$ branching. Similar factorization formulas hold for the case of gg, and $q\bar{q}$ collinear

configurations too, the only difference being in the form of the splitting functions

$$\hat{P}_{q,qg}(z) \;=\; C_{\mathrm{F}}\,\frac{1+z^2}{1-z}\,,$$

$$\hat{P}_{g,gg}(z) \;=\; C_{\mathrm{A}}\left(\frac{z}{1-z}+\frac{1-z}{z}+z(1-z)\right),$$

$$\hat{P}_{g,q\bar{q}}(z) \;=\; T_{\mathrm{F}}\left(z^2+(1-z)^2\right). \tag{2.3}$$

Strictly speaking, the functions appearing here are the exclusive AP kernels, related to the usual four dimensional *unregularized* AP splitting functions of eq. (1.96) by

$$\hat{P}_{gg}(z) \;=\; 2\hat{P}_{g,gg}(z)\,, \qquad \hat{P}_{qq}(z) \;=\; \hat{P}_{q,qg}(z)\,,$$

$$\hat{P}_{qg}(z) \;=\; \hat{P}_{q,qg}(1-z)\,, \qquad \hat{P}_{gq}(z) \;=\; \hat{P}_{g,q\bar{q}}(z)\,. \tag{2.4}$$

The difference lies in the fact that the usual Altarelli-Parisi splitting functions tag a final state parton. From this the factor 2 in $\hat{P}_{gg}$ and the symmetry $(z) \leftrightarrow (1-z)$ in $\hat{P}_{qq}(z)$ and $\hat{P}_{qg}(1-z)$. Furthermore, in the discussion so far, we have completely ignored the azimuthal dependence of AP kernels. In fact, in the case of the $g \to gg$ and $g \to q\bar{q}$ splittings, an azimuthal dependent term, that has zero azimuthal average, should be added to eq. (2.1). This term comes from the interference of the two helicities that the intermediate gluon can have, at fixed helicities of the final state gg or $q\bar{q}$ partons. We will ignore this complication in the following, since the effects that arise are quite small, even if some shower algorithms account for this angular correlations to some extent.

Assuming the kinematics illustrated in the following figure
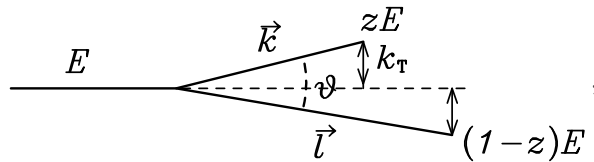
the parameters t, z and ϕ in eq. (2.1) describe the splitting process:

- t has the dimension of a mass and vanishes in the collinear limit. Since dt/t is invariant, several alternative definition of t can be accepted. Usually encountered ones are

$$\text{virtuality}: \quad t = \; (k+l)^2 \approx E^2\theta^2 z(1-z)\,, \tag{2.5}$$

$$\text{transverse momentum}: \quad t = \; k_\perp^2 = l_\perp^2 \approx E^2\theta^2 z^2(1-z)^2\,, \tag{2.6}$$

$$\text{angular variable}: \quad t = \; E^2\theta^2\,, \tag{2.7}$$

where $E \approx (k+l)^0$, θ is the angle between $\vec{k}$ and $\vec{l}$ and the $\approx$ relations hold for small θ.

- z is a variable that, in the collinear limit, yields the momentum fraction of the outgoing quark relative to the momentum of the quark that has split

$$k \rightarrow z(k+l) \quad \text{for} \quad t \rightarrow 0. \tag{2.8}$$

Alternative definitions of z can be chosen, provided that eq. (2.8) is satisfied in the collinear limit.

- ϕ is the azimuth of the $\vec{k}, \vec{l}$ plane around to the $\overrightarrow{k+l}$ direction.

In the following, we neglect complications due to the $z \rightarrow 0$ and $z \rightarrow 1$ soft divergences and postpone the treatment of the soft regions to sec. 2.1.2. Having this in mind, alternative choices in the definition of t and z make a difference only in subleading terms in eq. (2.1), i.e. for terms that are non-singular when $t \rightarrow 0$. The previous relation, eq. (2.1), can also be represented graphically as
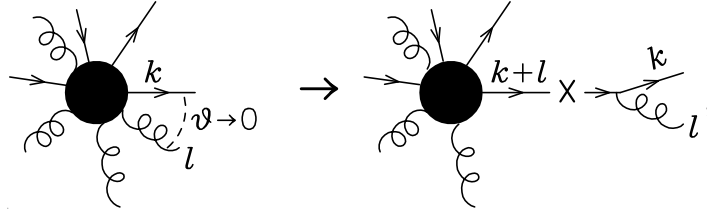
where squared amplitudes are represented by the black blobs, and we have chosen the angular variable for t.

The factorization of eq. (2.1) holds as long as the t variable (angle, virtuality or transverse momentum) between the two collinear partons is the smallest of the whole amplitude. This is, in some sense, expected since if the intermediate parent parton is almost on-shell, then its virtuality can be considered negligible compared to all other energy scales entering the amplitude. It follows then that factorization can be applied recursively to an amplitude, to obtain its most singular contribution. For example, in case of one further emission, one has

$$|M_{n+2}|^2 \, d\Phi_{n+2} \quad \Rightarrow \quad |M_n|^2 \, d\Phi_n \times \frac{\alpha_s}{2\pi} \frac{dt'}{t'} \hat{P}_{q,qg}(z') \, dz' \frac{d\phi'}{2\pi}$$

$$\times \, \theta(t'-t) \frac{\alpha_s}{2\pi} \frac{dt}{t} \hat{P}_{q,qg}(z) \, dz \frac{d\phi}{2\pi}, \tag{2.9}$$

or, pictorially,
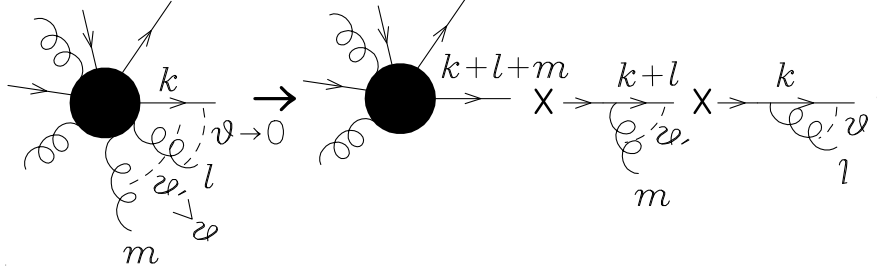
where we have the two angles becoming small, maintaining the strong ordering relation, $\theta' \gg \theta \to 0$.

Exclusive final states

In order to completely describe an exclusive final state, we should sum the perturbative expansion to all orders in α_s. Clearly, this is an impossible task. But, if we limit ourselves to the most singular terms in the perturbative expansion, that is to say, all terms that carry the collinear singularities dt/t in a strongly ordered sequence, we can apply recursively eq. (2.1), in the sense specified by eq. (2.9). Taking the qg ($\bar{q}g$) splitting as an example, one finds that the real emissions cross section for n splitting processes goes as

$$\sigma_0 \, \alpha_s^n \int \frac{dt_1}{t_1} \frac{dt_2}{t_2} \ldots \frac{dt_n}{t_n} \, \theta(Q^2 > t_1 > t_2 > \ldots > t_n > \lambda^2) = \sigma_0 \frac{1}{n!} \alpha_s^n \log^n \frac{Q^2}{\lambda^2}, \quad (2.10)$$

where σ_0 is the lowest-order cross section for the process at hand, Q is its hard scale (upper virtuality cutoff) and λ some infrared cut-off. The θ function here is assumed equal to 1 if its argument is true, zero otherwise. It is because of eq. (2.10) that the collinear approximation is sometimes called leading-log approximation.

As anticipated in sec. 1.2.1, one can easily see in eq. (2.10) that, when the gluon becomes collinear to the quark or to the antiquark, there is a divergent dt/t integration. This divergence is, of course, limited by the physical cutoff λ, which can be thought as a quark mass or, simply, Λ_{QCD}. But, even if we can reassure ourselves that no real infinity arises, the divergence implies that the real cross section is sensitive to low energy phenomena, that we cannot control or understand within perturbative QCD. Furthermore, if we consider that the coupling constant should be evaluated at the scale at which the emission occurs, the divergence yields a factor $\alpha_s(Q^2) \log (Q^2/\lambda^2)$, which is of order 1, since $\alpha_s(Q^2)$ is of order $1/\log (Q^2/\lambda^2)$.

Fortunately, the infrared safety of the total cross section guarantees that, if virtual corrections are included, these divergences cancel in the sum. In particular, virtual corrections to all orders in perturbation theory yield a term which is comparable with that of real emissions at all orders, i.e. eq. (2.10). Hence, in order to get sensible results, leading logarithmic virtuals must be included too in the computation of most singular contributions to cross sections. The inclusion of both leading logarithmic real and virtual contributions may be achieved by means of the shower.

Shower definition and evolution

The Shower Monte Carlo machinery for the calculation of the cross section of a given multi-particle final state can be summarized with the following recipe:

(a) The user chooses an hard interactions among those contained in the SMC library. The Born kinematics of this process must be fully specified. The weight associated to it is equal to its differential Born cross section.

(b) For each primary coloured parton present in the hard interaction, all possible tree-level graphs that can arise from it, obtained by letting the quark split into a qg pair, the gluon split into a gg or $q\bar{q}$ pair for any quark flavour, are considered. At each splitting occurred, one associates a t, z and ϕ value, defined by the splitting kinematics.

(c) Step (b) is iterated as many time as one wishes, for each possible coloured leg, present at any stage. One imposes that the t for splitting near the hard process must be less than the hard process scale Q^2, and all subsequent t's are in decreasing order as we go toward the branches of the tree-graph. Then :

   - Each vertex obtained in this way has the weight

$$\theta(t - t_0) \ \frac{\alpha_\mathrm{s}(t)}{2\pi} \frac{dt}{t} \ \hat{P}_{i,jl}(z) \, dz \ \frac{d\phi}{2\pi} \,, \tag{2.11}$$

   where $\alpha_\mathrm{s}(t)$ is the QCD running coupling (see eq. (1.33)), which we choose, for the moment, to evaluate at the scale t. A deeper discussion concerning the argument of α_s will follow in sec. 2.1.3. In order not to reach unphysical values of the running coupling constant, an infrared cutoff $t_0 > \Lambda_{QCD}^2$ is introduced. The upper bound on t is instead determined by the ordering imposed on it.

- Each line in the graph has weight $\Delta_i(t', t'')$, where t' is the t value associated with the upstream vertex, t'' with the downstream vertex, and

$$\Delta_i(t', t'') = \exp\left[-\sum_{(jl)} \int_{t''}^{t'} \frac{dt}{t} \int_0^1 dz \ \frac{\alpha_{\mathrm{s}}(t)}{2\pi} \ \hat{P}_{i,jl}(z)\right] . \qquad (2.12)$$

In case of a final state line t'' is replaced by the infrared cutoff t_0. The weights $\Delta_i(t', t'')$ are called Sudakov form factors. They represent all the dominant virtual corrections to our tree graph.

(d) Given the initial hard parton momenta, and the t, z and φ variables at each splitting vertex, one reconstructs all the momenta in the tree graph. Since a parton line, when followed by a splitting process, acquires a positive virtuality larger than its mass, the momenta of the partons must be adjusted, in order to conserve energy and momentum. This procedure is called *momentum reshuffling*.

Following this procedure, all possible partonic final state configurations may be generated and, furthermore, one can associate a weight at each of them. As a result, the shower will be pictorially see as a tree of splittings with decreasing angles (or virtuality, p_{T}), such that at a given splitting vertex, the splitting "angle" will be typically smaller by a factor α_{s} than the previous one. As the "angle" become smaller, at some point the scale t will be of the order of Λ_{QCD}, so that $\alpha_{\mathrm{s}} \approx 1$ and the whole picture breaks down. At this stage, some hadronization model need to be invoked, in order to convert the showered final state partons into hadrons, to complete the description of the formation of the final state. However, we neglected this further complication in the following and consider only partonic final states.

Notice that the Sudakov form factors of eq. (2.12) suppress the configurations containing lines with very large differences between upstream and downstream angles. This can be seen using eq. (1.33) to estimate $\Delta_i(t', t'') \approx 0$ if $t' \gg t''$. Hence, configurations that have no radiation down to very small scales are suppressed.

An alternative definition, more formal than the operative one given above, can be introduced by means of the function $\mathcal{S}_i(t, E)$, that represents the ensemble of all possible showers originating from parton i at a scale t, neglecting parton directions. Furthermore, with the notation

$$\sum_{\mathcal{F}} \mathcal{S}_i(t, E), \qquad (2.13)$$

we mean the sum over the final state $\mathcal{F}$, that is the sum over the number and type of final state particles and the integral over their momenta. We can easily convince ourselves that the recipe of points (a - d) may be translated into the recursive equation

$$
\mathcal{S}_i(t, E) = \Delta_i(t, t_0)\, \mathcal{S}_i(t_0, E) + \sum_{(jl)} \int_{t_0}^{t} \frac{dt'}{t'} \int_0^1 dz \int_0^{2\pi} \frac{d\phi}{2\pi}\ \frac{\alpha_{\mathrm{s}}(t')}{2\pi} \hat{P}_{i,jl}(z)
$$
$$
\times\ \Delta_i(t, t')\, \mathcal{S}_j(t', zE)\, \mathcal{S}_l(t', (1-z)E)\,, \quad (2.14)
$$

where the first term of the r.h.s. accounts for no branching from the scale t down to t_0, whilst the second one corresponds to one branching at the scale t' followed by two showers originating from it. We have indicated with $\mathcal{S}_i(t_0, E)$ the final state consisting of the incoming particle i alone.

We now take the derivative of both sides of eq. (2.14) with respect to t. The derivative can act on the upper limit of the integral in the second term in r.h.s. of eq. (2.14), or on the Sudakov form factors in both terms. At the end, we are left with the differential equation

$$
t\frac{\partial \mathcal{S}_i(t, E)}{\partial t} = \sum_{(jl)} \int_0^1 dz \int_0^{2\pi} \frac{d\phi}{2\pi}\ \frac{\alpha_{\mathrm{s}}(t)}{2\pi}\ \hat{P}_{i,jl}(z)\, \mathcal{S}_j(t, zE)\, \mathcal{S}_l(t, (1-z)E)
$$
$$
+ \left[-\sum_{(jl)} \int_0^1 dz\ \frac{\alpha_{\mathrm{s}}(t)}{2\pi}\ \hat{P}_{i,jl}(z) \right] \mathcal{S}_i(t, E)\,, \quad (2.15)
$$

that tells us how the shower changes under variations of the scale: if we raise the scale of the process by an infinitesimal amount, the shower has a larger probability to split into two sub-showers (the first term on the right hand side), and a smaller probability to remain the same (the second term). Defining now the *inclusive* shower as the sum over *all* possible final states

$$
\mathcal{S}_i^{\mathrm{inc}}(t, E) = \sum_{\substack{\text{final} \\ \text{states}}} \mathcal{S}_i(t, E)\,, \quad (2.16)
$$

we have that $\mathcal{S}_i^{\mathrm{inc}}(t, E)$ obeys the equation

$$
t\frac{\partial S_i^{\mathrm{inc}}(t, E)}{\partial t} = \sum_{(jl)} \int_0^1 dz\ \frac{\alpha_{\mathrm{s}}(t)}{2\pi}\ \hat{P}_{i,jl}(z)\, S_j^{\mathrm{inc}}(t, zE)\, S_l^{\mathrm{inc}}(t, (1-z)E)
$$
$$
+ \left[-\sum_{(jl)} \int_0^1 dz\ \frac{\alpha_{\mathrm{s}}(t)}{2\pi}\ \hat{P}_{i,jl}(z) \right] S_i^{\mathrm{inc}}(t, E)\,, \quad (2.17)
$$

which is analogous to eq. (2.15). An important consequence of this is the shower unitarity, that is $S_i^{\text{inc}}(t, E) = 1$. This solution indeed satisfies the above equation and is also consistent with the initial condition $S_i^{\text{inc}}(t_0, E) = 1$. This property, which is at the basis of the Shower Monte Carlo algorithms, tells us that the total cross section computed at the Born level is equal to the total multi-particle cross section. Of course, this statement holds in the approximation we are working with. Since we are only considering collinear-enhanced corrections, we should state more precisely that the effect of collinear-enhanced processes does not change the cross section, but distributes the total momentum between a different number of final-state partons according to the relative weight of the configuration they belong to.

Probabilistic interpretation

From what just exposed, it is apparent that the development of the shower can be computed numerically using a simple probabilistic algorithm. We interpret

$$\frac{\alpha_{\text{s}}(t')}{2\pi} \frac{dt'}{t'} \, \hat{P}_{i,jl}(z) \, dz \, \frac{d\phi}{2\pi} \,, \tag{2.18}$$

as the elementary branching probability in the phase space element $dt', dz, d\phi$. Hence, its integral over z (and ϕ) is the branching probability in the dt' interval

$$d\mathcal{P}_{\text{bran.}} = \frac{\alpha_{\text{s}}(t')}{2\pi} \frac{dt'}{t'} \int \frac{d\phi}{2\pi} \int_0^1 dz \, \hat{P}_{i,jl}(z) \,. \tag{2.19}$$

The complementary probability of not having a branching in the same interval, which corresponds to the sum of all leading-logs virtuals, is

$$d\mathcal{P}_{\text{no bran.}} = 1 - \frac{\alpha_{\text{s}}(t')}{2\pi} \frac{dt'}{t'} \int \frac{d\phi}{2\pi} \int_0^1 dz \, \hat{P}_{i,jl}(z) \,. \tag{2.20}$$

Dividing now the $[t, t']$ interval into N small subintervals of width δt, calling t_i the center of each subinterval, we have

$$\Delta_i(t, t') = \prod_{i=1}^N \left(1 - \frac{\alpha_{\text{s}}(t_i)}{2\pi} \frac{\delta t}{t_i} \int \hat{P}_{i,jl}(z) \, dz \, \frac{d\phi}{2\pi} \right) \,, \tag{2.21}$$

that is to say, taking the continuum limit $N \to \infty$ and $\delta t \to 0$ we get the Sudakov form factor of eq. (2.12), that thus corresponds to the non-emission probability in the

given $[t, t']$ interval. The probability that, starting at the scale t, the first branching is in the phase space element $dt', dz, d\phi$, is instead

$$d\mathcal{P}_{\text{first}} = \Delta_i(t, t') \frac{\alpha_{\text{s}}(t')}{2\pi} \frac{dt'}{t'} \hat{P}_{i,jl}(z) \, dz \, \frac{d\phi}{2\pi} \, . \qquad (2.22)$$

Hence, it is the product of the no-branching probability from the scale t down to t' times the branching probability in the interval $dt', dz, d\phi$. This is precisely equivalent to our shower recipe, if we remember that, because of unitarity, the total weight associated to further branchings of partons i and j is 1. Notice that the first emission probability, eq. (2.22), is the exact differential of the Sudakov form factor

$$d\mathcal{P}_{\text{first}} = d\Delta_i(t, t') \, . \qquad (2.23)$$

This means that the first emission is uniformly distributed with respect to the Sudakov form factor. We show in the following how this can be used to generate the shower very efficiently.

Initial state collinear singularities

Up to now, we have considered the problem of collinear splittings affecting final state partons only. The treatment of initial state radiation (ISR) in a Shower Monte Carlo is very similar to the case of final state radiation (FSR). The main difference is that the basic formula, analogous to eq. (2.1), now refers to the collinear emission off partonic leg j entering the graph that gives rise to the hard collision

$$d\sigma_j^{\text{ISR}}(p, \ldots) = \frac{\alpha_{\text{s}}}{2\pi} \frac{dt}{t} \, dz \, \hat{P}_{ij}(z) \, d\sigma_i(zp, \ldots) \, . \qquad (2.24)$$

In the previous formula, p is the momentum of the parton j that undergoes the splitting ij, with j entering the hard subprocess with momentum zp and i appearing as final state parton with momentum $(1-z)p$, or undergoing subsequent final state showers, as shown by
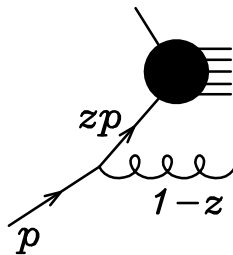
Contrarily to what happens for final state emissions, after the radiation the initial state parton is on-shell and the parton with reduced momentum zp acquires a space-like (negative) virtuality in this case. Iterating this process, multiple initial state emissions take place with the virtuality ordered from small absolute values, near the initial state parton, to large absolute values towards the hard scattering. The lower limit is the hardness of the scattering process $-Q^2$, while the upper one is the cutoff $-t_0$. In fact, as in the FSR case, factorization holds as long as the virtuality of the parton entering the hard scattering is negligible with respect to all the other scales entering the hard scattering amplitude.

The splitting functions and Sudakov form factors for initial state radiation splittings are the same that enter in the final state radiation process. On the other hand, if the shower is developed as in the FSR case, i.e. according to the forward evolution, one would waste a great amount of computing time generating configurations that does not end up in the hard scattering process chosen. It is thus preferable to solve the evolution equation in the opposite direction, in what is called the backward evolution method. The shower equation is thus represented with a recursive procedure that starts from the hard process at the lower scale, which is the largest in magnitude, and ends up to the infrared cutoff. In this case, by summing over all final states, one gets

$$\sum_{\substack{\text{final} \\ \text{states}}} \mathcal{S}_i(m,x,t,E) = f_m^{(i)}(x,t) , \qquad (2.25)$$

where we have slightly changed the previous notation. $\mathcal{S}_i(m,x,t,E)$ denotes now the ensemble of all possible states having a space-like parton of type m with an energy xE, at the scale t. The parton density functions $f_m^{(i)}(x,t)$ accounts instead for the probability to find the parton m inside the parton i with momentum fraction x, at the scale t. For FSR, the previous sum yielded 1, as have been shown after eq. (2.17). For ISR, the shower can thus be expressed by the following formula, which is the analogous of eq. (2.14)

$$f_m^{(i)}(x,t) = \delta_{mi}\,\delta(1-x)\,\Delta_m(t,t_0) + \int_{t_0}^{t} \frac{dt'}{t'} \int_x^1 \frac{dz}{z} \sum_j f_j^{(i)}(z,t')\frac{\alpha_{\mathrm{s}}(t')}{2\pi}\hat{P}_{jm}\left(\frac{x}{z}\right)\Delta_m(t,t') ,$$

$$(2.26)$$

where δ_{mi} is the usual Kronecker delta.

Taking the derivative of both sides with respect to t yields

$$
t\frac{\partial f_m^{(i)}(x,t)}{\partial t} = \frac{\alpha_{\rm s}(t)}{2\pi} \sum_j \int_x^1 \frac{dz}{z}\, \hat{P}_{jm}(x/z)\, f_j^{(i)}(z,t)
$$

$$
+ \left[-\sum_{(jl)} \int_0^1 dz\; \frac{\alpha_{\rm s}(t)}{2\pi}\, \hat{P}_{i,jl}(z) \right] f_m^{(i)}(x,t)\,, \qquad (2.27)
$$

which is equivalent to the ordinary Altarelli-Parisi equation for the parton densities

$$
t\frac{\partial f_m^{(i)}(x,t)}{\partial t} = \sum_j \int_x^1 \frac{dz}{z} \frac{\alpha_{\rm s}(t)}{2\pi}\, P_{jm}(z)\, f_j^{(i)}(x/z,t)\,, \qquad (2.28)
$$

where $P_{ij}(z)$ are the *regularized* AP splitting functions of eqs. (1.97) - (1.100) (see also eq. (2.4)).

The probability for the first backward branching thus reads

$$
d\mathcal{P}_{\rm first} = \sum_j f_j^{(i)}(z,t')\frac{\alpha_{\rm s}(t')}{2\pi}\hat{P}_{mj}(x/z)\Delta_m(t,t')\frac{dt'}{t'}\frac{dz}{z}\frac{d\phi}{2\pi}\,. \qquad (2.29)
$$

In order to generate the first branching, we must express eq. (2.29) as a differential in t'. Using the Altarelli-Parisi equation, from eq. (2.29) we obtain

$$
\frac{d\mathcal{P}_{\rm first}}{dt'} = \frac{\partial f_m^{(i)}(x,t')}{\partial t'}\Delta_m(t,t') + \left[\frac{1}{t'}\sum_{(jl)}\int_0^1 dz\; \frac{\alpha_{\rm s}(t)}{2\pi}\, \hat{P}_{i,jl}(z) \right] f_m^{(i)}(x,t')\Delta_m(t,t')
$$

$$
= \frac{\partial}{\partial t'}\left[f_m^{(i)}(x,t')\Delta_m(t,t') \right]\,, \qquad (2.30)
$$

which means that the probability distribution for the first branching is uniform in $f_m^{(i)}(x,t')\Delta_m(t,t')$.

Shower algorithm for processes with incoming hadrons

Collecting the previous considerations, the full recipe for the generation of a process with incoming hadrons can be written as follows:

(a) Generate a hard process configuration with a probability proportional to its parton level cross section. This cross section includes also the parton density functions. Both the cross section and the *pdf*'s are evaluated at the typical hard scale Q of the process.

(b) For each final state coloured parton, generate a shower in the following way

    1. Set the evolution variable $t = Q^2$.

    2. Generate a random number uniformly $0 < r < 1$.

    3. Solve the equation $r = \Delta_i(t, t')$ with respect to t'.

    4. If $t' < t_0$ then no further branching is generated, and the shower stops.

    5. If $t' \geqslant t_0$ then generate jl and z with a distribution proportional to $\hat{P}_{i,jl}(z)$, and a value for the azimuth ϕ with uniform probability in the interval $[0, 2\pi]$. Assign energies $E_j = zE_i$ and $E_l = (1 - z)E_i$ to partons j and l. The angle (or virtuality, transverse momentum) between them is fixed by the value of t'. Given the angle and the azimuth ϕ, the directions of j and l are fully reconstructed, since the sum of their momenta must equal the momentum of i.

    6. For each of the branched partons j and l, set $t = t'$ and go back to step (b-2).

(c) For each initial state coloured parton, generate a shower in the following way

    1. Set $t = Q^2$.

    2. Generate a random number $0 < r < 1$.

    3. Solve the equation $r = \Delta_i(t, t')$ for t'. In this case

$$r = \frac{f_i^{(h)}(x, t')\Delta_i(t, t')}{f_i^{(h)}(x, t)},$$

    where $f_i^{(h)}$ is the parton density for the hadron h where the parton i is found, and $x = E_i/E_h$ is the momentum fraction of the parton.

    4. If $t' < t_0$ then no further branching is generated, and the shower stops.

    5. If $t' \geqslant t_0$ then generate j and z with a distribution proportional to $\hat{P}_{ij}(z)$, and a value for the azimuth ϕ, with uniform probability in the interval $[0, 2\pi]$. Call l the radiated parton, and assign energies $E_j = zE_i$ and $E_l = (1 - z)E_i$ to partons j and l. The angle (virtuality, p_T) between their momenta is fixed by the value of t'. Given the angle and the azimuth ϕ (together with the fact that the sum of their momenta must equal to the momentum of i) the directions of j and l are fully reconstructed.

6. For parton j, set $t = t'$ and go back to step (c-2). For parton l, set $t = t'$ and go back to step (b-2).

The previous list exhausts the treatment of both initial- and final-state collinear enhanced emissions in QCD, at leading-log level.

2.1.2   Soft divergences

We turn now to the discussion of soft singularities. In fact, besides having collinear singularities, QCD amplitudes manifest soft singularities associated to gluon emissions at any angle. These can also appear, in some phase space regions, in conjunction with collinear singularities: we call these double-log singular regions. The divergences associated to the $z \to 1$ and $z \to 0$ limits in the branching $q \to qg$ or $g \to gg$, which we have neglected up to now, are in fact soft divergences, since z (or $(1 - z)$) is the energy fraction of the radiated gluon in AP splitting kernels of eq. (2.4). In full analogy to what happens for collinear singularities, also soft emissions are enhanced by large logarithms. This can be view considering the kinematic constraints upon the z integration, for example in a timelike splitting process. If t is the virtuality of the parent parton, one has

$$t \; = \; 2z(1 - z)E^2(1 - \cos\theta)\,, \qquad (2.31)$$

where θ is the angle between the two daughters. Thus, we must have

$$z(1 - z)E^2 \geq t/4\,, \qquad (2.32)$$

in order for the splitting to be possible. Thus, the z integration is (roughly) limited by

$$\frac{t}{4E^2} \leq z \leq 1 - \frac{t}{4E^2}\,. \qquad (2.33)$$

If there are no soft singularities, this complication can be neglected, since $\sqrt{t}/E$ is, at any stage of the branching, logarithmically subleading with respect to 1. This means that the unrestricted integral gives the same result of the restricted one, at the leading-log accuracy. However, being the splitting functions divergent for $z \to 0$ and $z \to 1$, these contributions from subleading logarithmic regions can raise to have order 1. Thus, in order to achieve logarithmic accuracy, soft divergences should be accounted for in a proper way. In the double logarithmic region then this problem is

even marked and a solution is needed in order to give a realistic description of the final state.

This problem is related to the choice of the hardness parameter t. In fact, the three different definitions of the ordering parameter given in eqs. (2.5), (2.6) and (2.7) yield a different double-log structure for the exponent of the Sudakov form factor. If t is the virtuality of the incoming line, then we must have $E^2 z(1-z) \gtrsim t$, in order for eq. (2.5) to hold for some value of θ, giving

$$\int \frac{dt}{t} \int_{t/E^2}^{1-t/E^2} \frac{dz}{1-z} \approx \frac{1}{2} \log^2 \frac{t}{E^2}. \tag{2.34}$$

If instead t is the transverse momentum, then $E^2 z^2 (1-z)^2 \gtrsim t$, and we get

$$\int \frac{dt}{t} \int_{\sqrt{t}/E}^{1-\sqrt{t}/E} \frac{dz}{1-z} \approx \frac{1}{4} \log^2 \frac{t}{E^2}. \tag{2.35}$$

Finally, if t is the angle, the value of z is not constrained by it, and we must impose a cutoff on z in such a way that the energy of the final state particles cannot become smaller than some typical hadronic scale Λ_{QCD}. In this case, we get yet another result

$$\int \frac{dt}{t} \int_0^1 \frac{dz}{1-z} \approx \log t \log \frac{E}{\Lambda_{QCD}}. \tag{2.36}$$

To find what is the correct choice, it is useful to look at the behaviour of soft gluons emitted at large angles: a soft gluon which is emitted from a bunch of partons with angular separation that is smaller then the soft gluon emission angle sees all the emitting partons as a single entity [55]. In other words, soft gluons at large angle adds up coherently. From a practical point of view, it is just as if the gluon was emitted from the parton that has originated the rest of the shower. Thin means that, if the emissions were angular ordered right from the beginning, one would obtain the correct behaviour for soft gluons at large angle. Thus, in order to treat correctly the double logarithmic region, one should use as ordering parameter the angular variable θ.

In the HERWIG SMC program [14, 15, 16], the ordering variable t is defined too be $E^2 \theta^2 / 2$, where E is the energy of the incoming parton, and θ is the angle of the two branched partons. The Sudakov form factor is

$$\Delta_i(t', t'') = \exp\left[-\sum_{(jl)} \int_{t''}^{t'} \frac{dt}{t} \int_0^1 dz \, \theta(t \, z^2 \, (1-z)^2 - t_0) \frac{\alpha_{\mathrm{s}} \, (t z^2 (1-z)^2)}{2\pi} \, \hat{P}_{i,jl}(z) \, dz \right]. \tag{2.37}$$

The argument of α_s is of the order of the transverse momentum. The integral in dz is limited by the θ function, that also avoids the region where the argument of α_s becomes smaller than the IR cutoff t_0, of the order of Λ_{QCD}. If a parton of energy E branches at a scale t into two partons of energies zE and $(1-z)E$, angular ordering is achieved by choosing as the initial condition for subsequent branchings the scales t/z and $t/(1-z)$.

The old versions of the PYTHIA SMC program [56, 57] are instead ordered in virtuality. This yields a more natural kinematics, since virtuality is kinematically ordered in a branching process. The lack of coherence, however, causes an unphysical increase in the number of soft partons, so that, for example, the particle multiplicity in e^+e^- annihilation processes does not have the correct growth with energy. The remedy in PYTHIA is to veto branchings that violate angular ordering. It was shown that in this way the correct multiplicity distributions could be recovered. Newer versions of PYTHIA [22, 58] implement a p_T-ordered shower, but also in this case an angular veto mechanism is at work to yield the correct soft gluons behaviour. We are not aware of any other relevant output differences between PYTHIA and HERWIG, due to the remaining differences in the treatment of soft radiation.

2.1.3   The argument of α_s

At this point, it is useful to re-examine carefully the argument of the running coupling constant entering into relevant formulas of this chapter. From the leading logarithm approximation point of view, the choice of the scale in α_s is formally an higher order problem, since it is related to the inclusion of higher-order logarithmic effects in the soft-collinear enhanced regions. However, its effects turn out to be numerically relevant and phenomenologically important. In the following, we limit ourself to report the relevant results, referring to ref. [20] for more comments and references to the original papers.

When calculating higher order corrections to splitting functions, one face the problem of ultraviolet and infrared divergent contributions. Assuming that the regularization procedure takes care of ultraviolet divergent poles, for example by the introduction of appropriate counterterms, the remaining poles are of infrared origin. In any case, for suitable define quantities, divergent virtual contributions must cancel against real emission contributions. This cancellation of infrared poles leaves,

however, a logarithm of the maximum possible virtuality of the daughter (i.e. the phase space boundary) over the renormalization scale μ_R, with the same coefficient of the canceled pole. It turns out that by choosing the argument of α_s to the maximum virtuality available for the outgoing gluon, one can reabsorb these higher order corrections into the definition of α_s. For instance, this corresponds to use the scale $(1-z)Q^2$ for a splitting $q \to gq$, where Q is the virtuality of the splitting parton, or $\mathrm{Min}(z, 1-z)Q^2$ for a splitting $g \to gg$, since in this case also the $z \to 0$ region may give rise to logarithmic enhanced contributions. In practice, however, one always choose to simultaneously include both type of corrections by using as argument of α_s the expression $z(1-z)Q^2$, that corresponds to use the transverse momentum of the emitted parton with respect to the splitting direction (see eqs. (2.6) and (2.37)).

Furthermore, it turns out that, by expanding the product of α_s expression within this scale choice times the 1-loop splitting kernel, one generates the soft-enhanced logarithmic terms present in the product of 2-loop splitting kernels times α_s with the usual scale choice (i.e. the virtuality of the splitting parton), up to a finite contribution. For example, in the soft limit, one has (see sec. 6.7.2 of ref.[20])

$$\lim_{z \to 1} \alpha_s((1-z)Q^2)P^{qg}(z) = \alpha_s(Q^2)\frac{2C_F}{1-z}\left(1 - b_0\alpha_s(Q^2)\log(1-z)\right) + \mathcal{O}(\alpha_s^3),$$

(2.38)

while

$$\lim_{z \to 1} \alpha_s(Q^2)P^{qg}_{2-\text{loop}}(z) = \alpha_s(Q^2)\frac{2C_F}{1-z}\left(1 - b_0\alpha_s(Q^2)\log(1-z) + \frac{\alpha_s(Q^2)}{2\pi}K_g\right) + \mathcal{O}(\alpha_s^3),$$

(2.39)

where $b_0 = (33 - 2n_f)/(12\pi)$ is defined as in eq. (1.32), $P^{qg}_{2-\text{loop}}(z)$ is the (up-to-)two loops expression for the splitting kernel [59, 60] and

$$K_g = C_A\left(\frac{67}{18} - \frac{\pi^2}{6}\right) - T_F n_f \frac{10}{9}.$$

(2.40)

Thus, the NLL accuracy may be achieved by incorporating this finite contribution into the definition of the strong coupling constant. This means replacing

$$\alpha_s \to A\left(\alpha_s\left(k_T^2\right)\right), \qquad A(\alpha_s) = \alpha_s\left\{1 + \frac{\alpha_s}{2\pi}K_g\right\},$$

(2.41)

where in the second formula above the $\overline{\mathrm{MS}}$, 1-loop expression of α_s should be used.

This corresponds to a redefinition of Λ_{QCD}, as shown in ref. [61]. One thus introduce a new scale

$$\Lambda_{\mathrm{MC}} = \Lambda_{\overline{\mathrm{MS}}} \, \exp\left(\frac{K_g}{4\pi b_0}\right) . \tag{2.42}$$

For $n_{\mathrm{f}} = 5$ light flavours, this gives

$$\Lambda_{\mathrm{MC}} = 1.569 \, \Lambda_{\overline{\mathrm{MS}}}^{(5)} . \tag{2.43}$$

So, by adopting Λ_{MC} as the strong scale and using the transverse momentum as the argument of the running coupling α_{s}, we keep track of, and correctly resum, all leading and next-to-leading logarithmic enhanced contributions, except those coming from wide angle soft emissions, that are, of course, not accounted for properly in the quasi-collinear approximation into which all results of this chapter are derived.

2.2 Improving Shower Monte Carlo programs

The picture resulting from previous sections is that a SMC program operates in the following way. First, it starts from a "hard" kinematic configuration, which is generated according to the exact LO computation for the given process (usually a $2 \rightarrow 2$ partonic process). The final-state multiplicity is then iteratively increased, by letting each initial- and final-state parton branch into a couple of partons with a probability related to a Sudakov form factor. Thus, if at a given stage of the shower, the scattering process is described by m partons, the algorithm decides with a certain probability whether branching is over at this stage, or further branchings will take place. In the latter case, one of the m partons splits into a pair, generating an $m + 1$ body final state. However, due to the fact that momentum conservation must be restored after branching, some "momentum reshuffling" is needed, that affects also the particles not directly involved in the branching. Since also the value of the momentum fraction of the incoming partons may undergo this reshuffling, the value of the luminosity used for the cross-section computation does not correspond exactly to what one would have used if the $(m + 1)$-particle matrix element had been computed with standard methods.

Furthermore, one should always remember that in a SMC the emissions beyond those belonging to the "hard" subprocess are generated by the shower, and therefore are correct only in the soft/collinear limits. Away from these limits, a better

description may be obtained using matrix elements (ME) corrections. In fact, matrix elements for process where one (or more) extra parton(s), with respect to the "hard" subprocess, is present are usually available. Clearly, these last cover the whole phase space of real emission(s) and give them the correct weight(s). The drawback is that, when one includes an extra emission into the "hard" subprocess description, he has to face the problem that the same configuration already included can be also generated by the shower. One has thus to avoid the double-counting of such events.

In order to merge the two approaches, to obtain a description as accurately as possible of both fixed order calculations and of Parton Shower-like evolution, with subsequent hadronization of the partonic event, one has thus to solve this double-counting problem. This may be reformulated in this context considering that a given $(n+1)$-jet event can be obtained in two ways: from the collinear/soft-radiation evolution of an appropriate $(n+1)$-parton final state (obtained from fixed order matrix elements), or from an n-parton configuration where a hard, large-angle emission during its evolution leads to the extra jet. One thus has to design a strategy, often called a "matching scheme" or "merging scheme", that defines, on an event-by-event basis, which of the two aforementioned paths should be followed. The primary goals of such a strategy are to avoid double counting, by preventing some events to appear twice, as well as dead regions, by ensuring that each configuration is generated by at least one of the allowed paths. In the past, several merging approaches have been proposed in the literature. Nowadays, the two widely used are the CKKW scheme [62, 63] (with some variants), and the MLM scheme [64]. These two approaches are implemented in currently used matrix element event generators, combined with parton showers tools, like SHERPA [65, 66], ALPGEN [67], MADGRAPH [68, 69] and HELAC [70, 71]. Any merging algorithm, however, is based on one or more *resolution parameters* which split the phase space into two regions: one of soft/collinear emissions to be described by Parton Shower (PS) evolution and the other one of hard and large angle emission to be described by fixed order calculations. These resolution parameters play the role of soft/collinear cut-off for fixed order calculations and it is therefore crucial to assess the (in)dependence of the algorithm on these parameters. In some specific case, it has been shown that the dependence on the choice of the resolution parameter is shifted beyond the Next-to-Leading-Log (NLL) accuracy (see, for example, ref. [62]), but, in general, an estimate of the independence of results from it is possible only empirically at present: one can check it varying the resolution parameters on the widest possible range (cfr. refs. [72, 73]).

This approach may be very fruitful, since one can include corrections of higher orders quite easily. However, one must remember, that in this way only real matrix elements of higher orders are added to the LO results. Hence, results will in general suffer from large scale variations dependence and, moreover, since this methods do not change the normalization, the resulting cross sections will be normalized only at the leading-order.

In the next chapter we will show how it is possible to include the full NLO result into the SMC framework, in a simple way that avoid overcounting and preserve the good features of the both the NLO accuracy and the (N)LL resummation.

Matching NLO Computations with Parton Showers

3.1 Introduction

In this chapter we discuss two different methods for the embedding of the full NLO computation[1] into SMC programs. The primary goal of this embedding is to reach the NLO accuracy when evaluating an inclusive observable and to maintain the leading logarithmic accuracy of the shower approach for exclusive ones. This may be translated into the requirements that the hardest emission, i.e. the one with the highest transverse-momentum, that is generated has the correct distribution also far from the soft or collinear regions, and that integrated quantities around the soft and collinear directions have NLO accuracy. All these features can be summarized as follows:

- Infrared-safe observables are required to have NLO accuracy.

- Collinear emissions must resummed at (least at) the leading-logarithmic level.

- The double logarithmic region (i.e. soft and collinear gluon emission) must be treated correctly, if the SMC code used for showering has this capability.

As in the matrix-element corrections approach discussed in sec. 2.2, the main problem of merging NLO calculations with parton shower simulations is basically that of avoiding overcounting, since the SMC programs already implements approximate NLO corrections. The first general solution to the overcounting problem in this

---

[1]With full NLO we mean both the real matrix element corrections for one further emission plus virtual contributions (plus eventual collinear remnants).

context was given in the `MC@NLO` proposal [2]. In the `MC@NLO` approach, the afore-mentioned requirements are met by evaluating the differences of the Shower Monte Carlo simulation relative to the exact NLO result. The shower algorithm is therefore analyzed to determine its own approximate NLO structure, in the FKS subtraction framework, in order to determine unambiguously the difference with the exact NLO formulas. These differences are subtracted from the NLO results, which are then showered by the SMC's shower algorithm. In this way, the (N)LL accuracy is restored by subsequent showering avoiding double-counting, and integrated quantities have NLO accuracy. Nonetheless, two major drawbacks are present. First, this approach is strongly dependent on the SMC's shower algorithm adopted, at the point that the difference between the shower NLO approximation and the exact NLO result must be recalculated every time the shower algorithm is changed. In the current version of the `MC@NLO` code, the MC subtraction terms have been computed for `HERWIG` [14, 15, 16] only. Secondly, due to subtraction of the shower approximated NLO results from the exact ones, it turns out that events may assume negative weights, which spoil their probabilistic interpretation.

In the `POWHEG` approach [4], instead, one performs the generation of the hardest event with NLO accuracy, in a framework that does not depend upon the SMC's shower algorithm. This is why it is fully independent from the SMC. Furthermore, the subsequent showers takes place at softer transverse momenta, and thus affects infrared-safe observables only at the next-to-next-to-leading order (NNLO). Thus, the matching problem considerably simplifies, since it no longer requires a detailed examination of the properties of the SMC. Finally, events produced according the `POWHEG` method always comes with a positive weight, as we will show later.

In the following two sections we analyze these two approaches in greater details.

3.2 The MC@NLO method

In this section we give an overview of the `MC@NLO` approach, the first method proposed to combine NLO matrix element contributions with parton shower algorithms, that overcomes the double-counting problem in a general way. A more accurate description and more references can be found on the original papers [2, 17, 18, 74]. The `MC@NLO` proposal consists basically in running the ordinary SMC (`HERWIG` up to now), with

initial conditions and weights determined by the NLO calculation. In the following, we explain how these initial conditions and weights are determined.

3.2.1 Definitions

Following refs. [2, 17], we distinguish two classes of events, depending upon the initial conditions. We denote the class where an emission, due to the NLO, occurs before the SMC run with "$\mathbb{H}$", for "hard". The other class is denoted by "$\mathbb{S}$", which stands for "standard", to remind us that it has the same initial conditions of ordinary SMC runs.

In `MC@NLO` the spectrum of the observable O resulting from $\mathbb{S}$ events is thus entirely due to SMC evolution of configurations whose initial conditions are identical to those of an ordinary SMC. On the contrary, the NLO hard emission contributes to the kinematics of $\mathbb{H}$ events. This kinematics, in turn, determines the initial conditions for the SMC evolution of events in this class. Thus, for $\mathbb{S}$ events, all terms of the NLO cross section calculation that do not contribute to the real emission serve only to fix the normalization of this class of events, relative to that of the class $\mathbb{H}$.

Recalling the formula (1.78), for the NLO expectation value of a generic observable O, which is infrared-safe and vanish fast enough if $\mathbf{\Phi}_{n+1}$ approaches two singular regions at the same time,

$$
\begin{aligned}
\langle O \rangle \;=\;& \int d\bar{\mathbf{\Phi}}_n \, O_n(\bar{\mathbf{\Phi}}_n) \left[B(\bar{\mathbf{\Phi}}_n) + V(\bar{\mathbf{\Phi}}_n) \right] \\
+\;& \int d\mathbf{\Phi}_{n+1} \left\{ O_{n+1}(\mathbf{\Phi}_{n+1}) \, R(\mathbf{\Phi}_{n+1}) - \sum_{\alpha_{\mathrm{r}}} \left[O_n(\bar{\mathbf{\Phi}}_n) \, C(\mathbf{\Phi}_{n+1}) \right]_{\alpha_{\mathrm{r}}} \right\} \\
+\;& \int d\mathbf{\Phi}_{n,\oplus} \, O_n(\bar{\mathbf{\Phi}}_n) \, G_{\oplus}(\mathbf{\Phi}_{n,\oplus}) + \int d\mathbf{\Phi}_{n,\ominus} \, O_n(\bar{\mathbf{\Phi}}_n) \, G_{\ominus}(\mathbf{\Phi}_{n,\ominus}) \;, \qquad (3.1)
\end{aligned}
$$

we introduce

$$
\int d\mathbf{\Phi}_{n+1} \;=\; \mathcal{I}_n \int d\bar{\mathbf{\Phi}}_n \qquad\qquad (3.2)
$$

$$
\int d\mathbf{\Phi}_{n,\oplus} \;=\; \mathcal{I}_n^{\oplus} \int d\bar{\mathbf{\Phi}}_n \qquad\qquad (3.3)
$$

$$
\qquad\qquad (3.4)
$$

and rewrite eq. (3.1) as

$$
\begin{aligned}
\langle O \rangle \;=\; & \int d\boldsymbol{\Phi}_{n+1} \left[O_n(\bar{\bar{\boldsymbol{\Phi}}}_n) \, \frac{1}{\mathcal{I}_n} \Big(B(\bar{\bar{\boldsymbol{\Phi}}}_n) + V(\bar{\bar{\boldsymbol{\Phi}}}_n) \Big) \right. \\
& + \left\{ O_{n+1}(\boldsymbol{\Phi}_{n+1}) \, R(\boldsymbol{\Phi}_{n+1}) - \sum_{\alpha_\mathrm{r}} \left[O_n(\bar{\bar{\boldsymbol{\Phi}}}_n) \, C(\boldsymbol{\Phi}_{n+1}) \right]_{\alpha_\mathrm{r}} \right\} \\
& \left. + \; O_n(\bar{\bar{\boldsymbol{\Phi}}}_n) \, \frac{1}{\mathcal{I}_n^{\oplus}} \, G_{\oplus}(\boldsymbol{\Phi}_{n,\oplus}) + O_n(\bar{\bar{\boldsymbol{\Phi}}}_n) \, \frac{1}{\mathcal{I}_n^{\ominus}} \, G_{\ominus}(\boldsymbol{\Phi}_{n,\ominus}) \right], \qquad (3.5)
\end{aligned}
$$

We remind the reader that, thanks to the FKS subtraction procedure adopted in `MC@NLO`, all the integrals appearing in eq. (3.1) are finite.

Next, we interface this to a SMC program. We need to introduce two different interfaces, one for the $n+1$ kinematics, which we denote with $\mathcal{F}_{\mathrm{MC}}^{(n+1)}$, and one for the n-body underlying Born kinematics, which we denote with $\mathcal{F}_{\mathrm{MC}}^{(n)}$. From a more formal point of view, $\mathcal{F}_{\mathrm{MC}}^{(n)}$ and $\mathcal{F}_{\mathrm{MC}}^{(n+1)}$ can be viewed as the SMC generating functionals when starting from a n-body kinematic configuration $\bar{\bar{\boldsymbol{\Phi}}}_n$ or a $n+1$-body one $\boldsymbol{\Phi}_{n+1}$, respectively. Interfacing a LO calculation to a SMC, i.e. performing what is usually done in a SMC program, may be easily translated in this notation as

$$
d\sigma_{\mathrm{LO+MC}} \;=\; B \, \mathcal{F}_{\mathrm{MC}}^{(n)} \,. \qquad (3.6)
$$

At this point, one could simply trade

$$
O_n \to \mathcal{F}_{\mathrm{MC}}^{(n)}, \qquad O_{n+1} \to \mathcal{F}_{\mathrm{MC}}^{(n+1)} \qquad (3.7)
$$

in eq. (3.5), performing what is called the *naïve* subtraction procedure. Unfortunately, this does not resolve the double-counting problem. This may be better explained considering that when evolving an event in the class $\mathbb{S}$ (i.e. starting from an n-body kinematics), the shower may produce some of the configurations in the class $\mathbb{H}$ (i.e. those starting from $n+1$-body kinematics), which are therefore double-counted. Moreover, the weights associated to events with or without a further emission are separately divergent, in the limit that no emissions occur.

However, one can modify the subtraction procedure in such a way that the double-counted configurations are subtracted at the short-distance cross section level, double counting is avoided and the requirement of sec. 3.1 for a NLO SMC generator are

fulfilled. This is the essence of the `MC@NLO` proposal. To do this, one modify the eq. (3.5) as follows

$$
\begin{aligned}
\mathcal{F}_{\text{MC@NLO}} \;=\;& \int d\mathbf{\Phi}_{n+1} \left\{ \mathcal{F}_{\text{MC}}^{(n+1)} \left[R(\mathbf{\Phi}_{n+1}) - R^{\text{MC}}(\mathbf{\Phi}_{n+1}) \right] \right. \\
&+\; \mathcal{F}_{\text{MC}}^{(n)} \left[\frac{1}{\mathcal{I}_n} \Big(B(\bar{\bar{\mathbf{\Phi}}}_n) + V(\bar{\bar{\mathbf{\Phi}}}_n) \Big) - \sum_{\alpha_{\text{r}}} [C(\mathbf{\Phi}_{n+1})]_{\alpha_{\text{r}}} \right. \\
&+\; \left. \left. R^{\text{MC}}(\mathbf{\Phi}_{n+1}) + \frac{1}{\mathcal{I}_n^{\oplus}} G_{\oplus}(\mathbf{\Phi}_{n,\oplus}) + \frac{1}{\mathcal{I}_n^{\ominus}} G_{\ominus}(\mathbf{\Phi}_{n,\ominus}) \right] \right\}, \qquad (3.8)
\end{aligned}
$$

where $\mathcal{F}_{\text{MC@NLO}}$ is the `MC@NLO` generating functional. We have performed the substitutions advocated in eq. (3.7), but we have also subtracted the quantity

$$
\mathcal{F}_{\text{MC}}^{(n+1)} R^{\text{MC}}(\mathbf{\Phi}_{n+1}) \;, \qquad (3.9)
$$

from the real emission contributions and added

$$
\mathcal{F}_{\text{MC}}^{(n)} R^{\text{MC}}(\mathbf{\Phi}_{n+1}) \;, \qquad (3.10)
$$

to the remaining terms. We have

$$
R^{\text{MC}}(\mathbf{\Phi}_{n+1}) \;=\; B(\bar{\bar{\mathbf{\Phi}}}_n) \, \frac{\alpha_{\text{s}}(t)}{2\pi} \frac{1}{t} \, P(z) \,, \qquad (3.11)
$$

where $P(z)$ are the Altarelli-Parisi splitting kernels and $d\mathbf{\Phi}_{n+1} = d\bar{\bar{\mathbf{\Phi}}}_n \, d\Phi_{\text{rad}}^{\text{MC}}$ with $d\Phi_{\text{rad}}^{\text{MC}} \equiv dz \, dt \, d\phi/(2\pi)$. Hence, R^{MC} is the collinear approximation of the real emission contributions, as implemented by the shower. The crucial point of the `MC@NLO` approach is thus the use of the $\mathcal{O}(\alpha_{\text{s}})$ terms in the expansions of the shower (of the SMC program which `MC@NLO` is interfaced to) to perform the *modified subtraction* procedure. This is also the reason why the `MC@NLO` method is so strongly dependent on the SMC.

Notice that the *modified subtraction* method requires to subtract eq. (3.9) and then add back eq. (3.10), which are *a priori* different. However, the difference between the twos does not contribute to the generic observable at the NLO, since $\mathcal{F}_{\text{MC}}^{(n+1)} - \mathcal{F}_{\text{MC}}^{(n)}$ starts at $\mathcal{O}(\alpha_{\text{s}})$ and $\mathcal{F}_{\text{MC}}^{(n+1)}$ multiplies R^{MC}, which already contains a further power of α_{s}.

3.2.2 Practical implementation

In order to efficiently implement formula (3.8) in a computer code, the total NLO
cross section is obtained evaluating separately the two integrals

$$
\mathbb{I}_{\mathbb{H}} \;=\; \int d\mathbf{\Phi}_{n+1} \left[R(\mathbf{\Phi}_{n+1}) - R^{\mathrm{MC}}(\mathbf{\Phi}_{n+1}) \right] , \tag{3.12}
$$

$$
\mathbb{I}_{\mathbb{S}} \;=\; \int d\mathbf{\Phi}_{n+1} \left[\frac{1}{\mathcal{I}_n} \Big(B(\bar{\mathbf{\Phi}}_n) + V(\bar{\mathbf{\Phi}}_n) \Big) \;-\; \sum_{\alpha_{\mathrm{r}}} [C(\mathbf{\Phi}_{n+1})]_{\alpha_{\mathrm{r}}} + R^{\mathrm{MC}}(\mathbf{\Phi}_{n+1}) \right.
$$

$$
\left. + \frac{1}{\mathcal{I}_n^{\oplus}} \, G_{\oplus}(\mathbf{\Phi}_{n,\oplus}) + \frac{1}{\mathcal{I}_n^{\ominus}} \, G_{\ominus}(\mathbf{\Phi}_{n,\ominus}) \right] . \tag{3.13}
$$

Observe that these two integrals are finite, owing to the behaviour of R^{MC} in the
singular limits, and that

$$
\sigma_{\mathrm{NLO}} = \mathbb{I}_{\mathbb{S}} + \mathbb{I}_{\mathbb{H}} . \tag{3.14}
$$

One also computes the integrals $\mathbb{J}_{\mathbb{S}}$ and $\mathbb{J}_{\mathbb{H}}$ that corresponds respectively to in
$\mathbb{I}_{\mathbb{S}}$ and $\mathbb{I}_{\mathbb{H}}$, with the only difference that the integrands are taken in absolute val-
ues. It is in fact possible for them to acquire non positive values, for example when
$R^{\mathrm{MC}}(\mathbf{\Phi}_{n+1}) > R(\mathbf{\Phi}_{n+1})$ in $\mathbb{I}_{\mathbb{H}}$. However, taking absolute values of the integrands
guarantees efficient generation, using standard techniques.[2]

In any case, the sign of the integrand function is stored, in order to perform the
unweighting of the event sample. The unweighting procedure is done separately for
positive and negative values of the integrand, for each class of events $\mathbb{S}$ or $\mathbb{H}$. It
involves comparing the integrand value of each event against the maximum absolute
value of the integrand, which is find scanning the phase space. Then a veto method is
applied: if the value of the integrand of the i-th event is less than a random number
$r \in (0,1)$ times the maximum value, the event is rejected. Otherwise, it is accepted
and it is given weight $w_i^{(\mathbb{S},\mathbb{H})} = +1$ if the integrand is positive, $w_i^{(\mathbb{S},\mathbb{H})} = -1$ if negative.
The presence of negative-weighted events is a distinctive feature of MC@NLO. Negative
weights imply larger statistical errors than in the case of ordinary SMC, if the total
number of events generated is the same. In the $\mathbb{S}$ and $\mathbb{H}$ samples, the fraction of

---

[2]For a thoughtful explanation of these techniques we address the reader to the discussion con-
cerning the integrator-unweighter routines BASES/SPRING in sec. 3.3.4

negative-weighted events is

$$f_{\mathbb{S}} = \frac{1}{2}\left(1 - \frac{\boldsymbol{I}_{\mathbb{S}}}{\boldsymbol{J}_{\mathbb{S}}}\right) \qquad f_{\mathbb{H}} = \frac{1}{2}\left(1 - \frac{\boldsymbol{I}_{\mathbb{H}}}{\boldsymbol{J}_{\mathbb{H}}}\right) \tag{3.15}$$

So, looking at eqs. (3.12) and (3.13), it is easy to see that the number of negative-weighted $\mathbb{S}$ events may be reduced, to some extent, by varying $\boldsymbol{J}_{\mathbb{S}}$, for example adjusting the free parameters in the FKS subtraction. On the other hand, the number of negative-weighted $\mathbb{H}$ events is fixed, after physical parameters on input were chosen.

Thus, one generates N_{TOT} unweighted events, with the number of events falling in the two classes $\mathbb{S}$ and $\mathbb{H}$ defined by

$$N_{\mathbb{S}} = N_{\mathrm{TOT}} \, \frac{\boldsymbol{J}_{\mathbb{S}}}{\boldsymbol{J}_{\mathbb{S}} + \boldsymbol{J}_{\mathbb{H}}} \qquad \text{and} \qquad N_{\mathbb{H}} = N_{\mathrm{TOT}} \, \frac{\boldsymbol{J}_{\mathbb{H}}}{\boldsymbol{J}_{\mathbb{S}} + \boldsymbol{J}_{\mathbb{H}}} \, . \tag{3.16}$$

The choice of the flavour associated to each of these events is a little involved. We do not want to enter into these details here. However, we only report that there is the possibility to compute the integrals in eqs. (3.12) and (3.13) summing over different flavour configurations at the integrand level and then compute the individual event flavours with statistical methods. This can give a wrong assignment of flavours on a event-by-event basis, but guarantees the correct distributions of different flavour configurations. This also saves from computing the integrals (3.12) and (3.13) for each possible flavour configurations.

As stated above, events are assigned weights that have the following properties:

$$\frac{\boldsymbol{J}_{\mathbb{S}}}{N_{\mathbb{S}}} \sum_{i=1}^{N_{\mathbb{S}}} w_i^{(\mathbb{S})} = \boldsymbol{I}_{\mathbb{S}} \, , \qquad \frac{\boldsymbol{J}_{\mathbb{H}}}{N_{\mathbb{H}}} \sum_{i=1}^{N_{\mathbb{H}}} w_i^{(\mathbb{H})} = \boldsymbol{I}_{\mathbb{H}} \, , \tag{3.17}$$

and thus, in the end,

$$\sigma_{\mathrm{NLO}} = \frac{\boldsymbol{J}_{\mathbb{S}} + \boldsymbol{J}_{\mathbb{H}}}{N_{\mathrm{TOT}}} \left(\sum_{i=1}^{N_{\mathbb{S}}} w_i^{(\mathbb{S})} + \sum_{i=1}^{N_{\mathbb{H}}} w_i^{(\mathbb{H})} \right) \tag{3.18}$$

Rescaling the event weights by a multiplicative factor

$$w_i = w_i^{(\mathbb{S},\mathbb{H})} \frac{\boldsymbol{J}_{\mathbb{S}} + \boldsymbol{J}_{\mathbb{H}}}{N_{\mathrm{TOT}}} \tag{3.19}$$

one gets that the sum of event weights gives the total cross section,

$$\sigma_{\mathrm{NLO}} = \sum_{i=1}^{N_{\mathrm{TOT}}} w_i \, , \tag{3.20}$$

as in standard SMC programs.

3.2.3 Hardest emission

In this section we want to report the formula for the `MC@NLO` cross section for the hardest emission, since it will result useful in the analysis of chapters 4 and 5.

According to ref. [4], we can schematically represent the `MC@NLO` cross section for the hardest emission with the following formula

$$
d\sigma = \underbrace{\bar{B}^{\mathrm{MC}}(\bar{\bar{\Phi}}_n)\,d\bar{\bar{\Phi}}_n}_{\mathbb{S}\ \mathrm{event}}\ \underbrace{\left[\Delta^{\mathrm{MC}}(\bar{\bar{\Phi}}_n,t_0) + \Delta^{\mathrm{MC}}(\bar{\bar{\Phi}}_n,t)\,\frac{R^{\mathrm{MC}}(\Phi_{n+1})}{B(\bar{\bar{\Phi}}_n)}\,d\Phi_{\mathrm{rad}}^{\mathrm{MC}}\right]}_{\mathrm{MC\ shower}}
$$
$$
+ \underbrace{\left[R(\Phi_{n+1}) - R^{\mathrm{MC}}(\Phi_{n+1})\right]d\bar{\bar{\Phi}}_n\,d\Phi_{\mathrm{rad}}^{\mathrm{MC}}}_{\mathbb{H}\ \mathrm{event}}, \tag{3.21}
$$

where $d\Phi_{n+1} = d\bar{\bar{\Phi}}_n\,d\Phi_{\mathrm{rad}}^{\mathrm{MC}}$ with $d\Phi_{\mathrm{rad}}^{\mathrm{MC}} \equiv dz\,dt\,d\phi/(2\pi)$ and have anticipated some of the `POWHEG` notation, defined in sec. 3.3. For the moment, it is sufficient to give the definitions

$$
\bar{B}^{\mathrm{MC}}(\bar{\bar{\Phi}}_n) = B(\bar{\bar{\Phi}}_n) + V(\bar{\bar{\Phi}}_n) + \int d\Phi_{\mathrm{rad}}^{\mathrm{MC}}\left[R^{\mathrm{MC}}(\Phi_{n+1}) - \sum_{\alpha_{\mathrm{r}}}\left[C(\Phi_{n+1})\right]_{\alpha_{\mathrm{r}}}\right], \tag{3.22}
$$

$$
\Delta^{\mathrm{MC}}(\bar{\bar{\Phi}}_n,t) = \exp\left\{-\int d\Phi_{\mathrm{rad}}^{\mathrm{MC}}\,\frac{\alpha_{\mathrm{S}}(t)}{2\pi}\frac{1}{t}\,P(z)\,\theta\left(k_{\mathrm{T}}(\Phi_{n+1})-t\right)\right\} \tag{3.23}
$$

only, where

$$
R^{\mathrm{MC}}(\Phi_{n+1}) = B(\bar{\bar{\Phi}}_n)\,\frac{\alpha_{\mathrm{S}}(t)}{2\pi}\frac{1}{t}\,P(z) \tag{3.24}
$$

is the $\mathcal{O}(\alpha_{\mathrm{S}})$ expansion of the shower, i.e. the same quantity defined in eq. (3.11). Notice that, on the right hand side of eq. (3.22), divergent quantities appear, and only their sum is finite. As already stated, in the `MC@NLO` framework, they are dealt with the FKS subtraction method. Notice also that the Sudakov form factor that appears here is different from the Sudakov of ordinary SMC's, because of the theta function on the transverse momentum, which insures the convergence of the integral at the exponent.

The "MC shower" factor in eq. (3.21) shows that the hardest emission is produced by running the `HERWIG` shower Monte Carlo, starting with the event kinematics $\bar{\bar{\Phi}}_n$. In fact, the Monte Carlo may not generate the hardest radiation as its first emission, especially in case of `HERWIG`, which is angular ordered. It was shown in ref. [4], however, that, owing to the k_{T}-vetoed Sudakov form factor in $\Delta^{\mathrm{MC}}(\bar{\bar{\Phi}}_n,t)$ of eq. (3.23),

formula (3.21) does correctly represent the hardest emission probability up to sub-leading effects.

3.3 The POWHEG method

3.3.1 Definitions

In this section we present the `POWHEG` method in its full generality. In the `POWHEG` formalism, the generation of the hardest emission is performed first, using full NLO accuracy. Subsequent radiation is then generated by a SMC, just like in the `MC@NLO` approach. In order to built a `POWHEG` implementation one must specify the separation of the singular regions, and the kinematics that associates a given $(n+1)$-body singular region with an n-body one. In the following, we discuss `POWHEG` in the framework of a generic subtraction formalism, distinguishing between the FKS or CS approaches only when needed.

Flavour separation

The first problem one encounters during the construction of an event generator, is that flavour should be carefully tracked, since different flavour structures give rise to different events. We thus need to introduce an index to distinguish the contributions to the cross section, depending on their flavour structures. These, in turn, are determined by the flavours of the incoming and outgoing partons. We thus introduce the index f_b to denote the flavour structure of the n-body processes and write B^{f_b} and V^{f_b} for the various Born and soft-virtual contributions. It should be notice that, for all practical purposes, two flavour configurations are equivalent if they differ only by a permutation of final-state partons, or other colorless particles. Thus, in the following, the index f_b is assumed to run over inequivalent configurations only.

Given a flavour structure and a region of singularity, the real contribution that is singular in that region and that has the given underlying Born flavour structure may be unambiguously determined. We label it with α_r. The association of a specific flavour structure f_b of the underlying n-body process with a given singular region α_r of the real contribution is performed as follows:

- If the singular region is collinear, the two collinear particles are merged into a single particle in such a way that flavour is conserved. In particular, a gg pair is merged into a g, a $q\bar{q}$ pair is merged into a g, and a qg ($\bar{q}g$) pair is merged into a q ($\bar{q}$).

- If the singular region is soft, the soft gluon is removed and the flavour structure is not changed.

Observe also that there is no need to define the flavour structure of the underlying n-body process in case of non singular limits (for example, in case two quarks, or a quark and an antiquark of different flavour become collinear, or in case a quark becomes soft).

We then separate the real correction into terms

$$R = \sum_{\alpha_{\mathrm{r}}} R^{\alpha_{\mathrm{r}}}, \tag{3.25}$$

that are singular in one and only one singular region. A similar separation is also performed for the counterterms, so that they are also labeled by an index α_{r}. For the collinear remnants instead we use the notation $\alpha_{\oplus}$.

In the FKS case, for example, the α_{r} contributions are obtained by first separating the real contribution R into the sum of all its flavour components. For each flavour component, one constructs the $\mathcal{S}$ functions, according to the procedure of section 1.2.4, and then multiplies it by the factors $\mathcal{S}_i$ or $\mathcal{S}_{ij}$. In the CS case, for each flavour component of the real contribution, one may instead define

$$\mathcal{S}_{\alpha_{\mathrm{r}}} = \frac{\mathcal{D}_{\alpha_{\mathrm{r}}}}{\sum_{\alpha'_r} \mathcal{D}_{\alpha'_r}}, \tag{3.26}$$

where α_{r} ranges in the set of dipoles $\mathcal{D}$ with the same flavour structure.

However, as explained in sec.1.2.3, in order to avoid possible zeros and/or divergences in the dipoles in the denominator of the previous formula, it is better to adopt a formula analogous to that in eq. (1.111)

$$\mathcal{S}_{\alpha_{\mathrm{r}}} = \frac{H\left(\bar{\mathbf{\Phi}}_n^{(\alpha_{\mathrm{r}})}\right) \mathcal{D}_{\alpha_{\mathrm{r}}}^2}{\sum_{\alpha'_r} H\left(\bar{\mathbf{\Phi}}_n^{(\alpha'_r)}\right) \mathcal{D}_{\alpha'_r}^2}, \tag{3.27}$$

where H is a positive function that vanishes when its argument approaches an n-body singular configuration.

$\bar{B}$ function and Sudakov form factor

At this point we are ready to generalize the formula for the expectation value of a generic IR safe observable O within the subtraction method (see eq. (1.78)), according to the separation of flavour structures. As discussed at the beginning of section 1.2.2, in case the n-body cross section possesses singular regions, the observable O_{n+1} should vanish fast enough if $\mathbf{\Phi}_{n+1}$ approaches two singular regions at the same time. We have

$$\langle O \rangle \; = \; \sum_{f_b} \left[\langle O \rangle_B^{f_b} + \sum_{\alpha_\mathrm{r} \in \{\alpha_\mathrm{r}|f_b\}} \langle O \rangle_R^{\alpha_\mathrm{r}} + \sum_{\alpha_\oplus \in \{\alpha_\oplus|f_b\}} \langle O \rangle_{G_\oplus}^{\alpha_\oplus} + \sum_{\alpha_\ominus \in \{\alpha_\ominus|f_b\}} \langle O \rangle_{G_\ominus}^{\alpha_\ominus} \right] ,$$
(3.28)

$$\langle O \rangle_B^{f_b} \; = \; \int d\bar{\mathbf{\Phi}}_n \, O_n \big(\bar{\mathbf{\Phi}}_n \big) \left[B^{f_b} \big(\bar{\mathbf{\Phi}}_n \big) + V^{f_b} \big(\bar{\mathbf{\Phi}}_n \big) \right] ,$$
(3.29)

$$\langle O \rangle_{G_\oplus}^{\alpha_\oplus} \; = \; \int d\mathbf{\Phi}_{n,\oplus} \, O_n \big(\bar{\mathbf{\Phi}}_n \big) \, G_\oplus^{\alpha_\oplus} (\mathbf{\Phi}_{n,\oplus}) \; ,$$
(3.30)

$$\langle O \rangle_R^{\alpha_\mathrm{r}} \; = \; \int d\mathbf{\Phi}_{n+1} \left[O_{n+1}(\mathbf{\Phi}_{n+1}) \, R(\mathbf{\Phi}_{n+1}) - O_n \big(\bar{\mathbf{\Phi}}_n \big) \, C(\mathbf{\Phi}_{n+1}) \right]_{\alpha_\mathrm{r}} ,$$
(3.31)

where we have indicated with $\{\alpha_\mathrm{r}|f_b\}$ (and $\{\alpha_\oplus|f_b\}$) the set of all values of the indexes α_r (and $\alpha_\oplus$) that have the flavour structure of the underlying n-body-configuration equal to f_b.

Then, we further separate

$$\langle O \rangle_R^{\alpha_\mathrm{r}} = \langle O \rangle_{R,n}^{\alpha_\mathrm{r}} + \langle O \rangle_{R,n+1}^{\alpha_\mathrm{r}} ,$$
(3.32)

$$\langle O \rangle_{R,n}^{\alpha_\mathrm{r}} \; = \; \left[\int d\mathbf{\Phi}_{n+1} \, O_n \big(\bar{\mathbf{\Phi}}_n \big) \left\{ R \left(\mathbf{\Phi}_{n+1} \right) - C \left(\mathbf{\Phi}_{n+1} \right) \right\} \right]_{\alpha_\mathrm{r}} ,$$
(3.33)

$$\langle O \rangle_{R,n+1}^{\alpha_\mathrm{r}} \; = \; \left[\int d\mathbf{\Phi}_{n+1} \, R \left(\mathbf{\Phi}_{n+1} \right) \left\{ O_{n+1}(\mathbf{\Phi}_{n+1}) - O_n \big(\bar{\mathbf{\Phi}}_n \big) \right\} \right]_{\alpha_\mathrm{r}} ,$$
(3.34)

by summing and subtracting back the same contribution, that is $R \left(\mathbf{\Phi}_{n+1} \right) O_n \big(\bar{\mathbf{\Phi}}_n \big)$.

Now the terms entering eq. (3.28) can be classified according to their kinematic structure: $\langle O \rangle_B^{f_b}$ (eq. (3.29)), $\langle O \rangle_{G_\oplus}^{\alpha_\oplus}$ (eq. (3.30)) and $\langle O \rangle_{R,n}^{\alpha_\mathrm{r}}$ (eq. (3.33)) have n-body kinematics and, according to ref.[4], they should be all included into the $\bar{B}$ function. The term $\langle O \rangle_{R,n+1}^{\alpha_\mathrm{r}}$ of eq. (3.34) involves instead real radiation and must be treated separately.

Exploiting phase space factorization, eqs. (3.30), (3.33) and (3.34) may be rewritten as

$$\langle O \rangle_{G_\oplus}^{\alpha_\oplus} = \int d\bar{\boldsymbol{\Phi}}_n \, O_n\big(\bar{\boldsymbol{\Phi}}_n\big) \, \frac{dz}{z} \, G_\oplus^{\alpha_\oplus}\big(\boldsymbol{\Phi}_{n,\oplus}\big) \; , \tag{3.35}$$

$$\langle O \rangle_{R,n}^{\alpha_r} = \left[\int d\bar{\boldsymbol{\Phi}}_n \, O_n\big(\bar{\boldsymbol{\Phi}}_n\big) \, d\Phi_{\rm rad} \, \{ R\,(\boldsymbol{\Phi}_{n+1}) - C\,(\boldsymbol{\Phi}_{n+1}) \} \right]_{\alpha_r} , \tag{3.36}$$

$$\langle O \rangle_{R,n+1}^{\alpha_r} = \left[\int d\bar{\boldsymbol{\Phi}}_n \, d\Phi_{\rm rad} \, R\,(\boldsymbol{\Phi}_{n+1}) \, \{ O_{n+1}\,(\boldsymbol{\Phi}_{n+1}) - O_n\big(\bar{\boldsymbol{\Phi}}_n\big) \} \right]_{\alpha_r} . \tag{3.37}$$

Following ref. [4], we define the so-called $\bar{B}$ function, which is the integral over the radiation variables of the full NLO cross section. Thanks to our notation we can carefully distinguish the contributions to $\bar{B}$ according to their flavour structure. We thus define a different $\bar{B}$ function for each flavour configuration, as

$$\bar{B}^{f_b}(\bar{\boldsymbol{\Phi}}_n) = B^{f_b}\big(\bar{\boldsymbol{\Phi}}_n\big) + V^{f_b}\big(\bar{\boldsymbol{\Phi}}_n\big) + \sum_{\alpha_r \in \{\alpha_r | f_b\}} \int \left[d\Phi_{\rm rad} \, \{ R\,(\boldsymbol{\Phi}_{n+1}) - C\,(\boldsymbol{\Phi}_{n+1}) \} \right]_{\alpha_r}^{\bar{\boldsymbol{\Phi}}_n}$$

$$+ \sum_{\alpha_\oplus \in \{\alpha_\oplus | f_b\}} \int \left[\frac{dz}{z} \, G_\oplus^{\alpha_\oplus}\big(\boldsymbol{\Phi}_{n,\oplus}\big) \right]^{\bar{\boldsymbol{\Phi}}_n} + \sum_{\alpha_\ominus \in \{\alpha_\ominus | f_b\}} \int \left[\frac{dz}{z} \, G_\ominus^{\alpha_\ominus}\big(\boldsymbol{\Phi}_{n,\ominus}\big) \right]^{\bar{\boldsymbol{\Phi}}_n} . \tag{3.38}$$

Here, in analogy with eq. (1.56), we have explicitly introduced the *context convection*

$$[\dots]^{\bar{\boldsymbol{\Phi}}_n} \tag{3.39}$$

to indicate that all set of variables appearing inside the square brackets (i.e. $\boldsymbol{\Phi}_{n+1}$ or $\boldsymbol{\Phi}_{n,\oplus}$) have the same underlying Born variables $\bar{\boldsymbol{\Phi}}_n$ of the Born contribution.

It follows then that

$$\int d\bar{\boldsymbol{\Phi}}_n \, O_n\big(\bar{\boldsymbol{\Phi}}_n\big) \, \bar{B}^{f_b}(\bar{\boldsymbol{\Phi}}_n) = \langle O \rangle_B^{f_b} + \sum_{\alpha_r \in \{\alpha_r | f_b\}} \langle O \rangle_{R,n}^{\alpha_r} + \sum_{\alpha_\oplus \in \{\alpha_\oplus | f_b\}} \langle O \rangle_{G_\oplus}^{\alpha_\oplus} + \sum_{\alpha_\ominus \in \{\alpha_\ominus | f_b\}} \langle O \rangle_{G_\ominus}^{\alpha_\ominus} , \tag{3.40}$$

and

$$\langle O \rangle = \sum_{f_b} \int d\bar{\boldsymbol{\Phi}}_n \, O_n\big(\bar{\boldsymbol{\Phi}}_n\big) \, \bar{B}^{f_b}(\bar{\boldsymbol{\Phi}}_n)$$

$$+ \sum_{\alpha_r} \left[\int d\bar{\boldsymbol{\Phi}}_n \, d\Phi_{\rm rad} \, R\,(\boldsymbol{\Phi}_{n+1}) \, \{ O_{n+1}\,(\boldsymbol{\Phi}_{n+1}) - O_n\big(\bar{\boldsymbol{\Phi}}_n\big) \} \right]_{\alpha_r}^{\bar{\boldsymbol{\Phi}}_n} . \tag{3.41}$$

The next step is the definition of the (flavour dependent) Sudakov form factors

$$\Delta^{f_b}(\bar{\mathbf{\Phi}}_n, p_{\mathrm{T}}) = \exp\left\{ -\sum_{\alpha_{\mathrm{r}}\in\{\alpha_{\mathrm{r}}|f_b\}} \int \frac{\left[d\Phi_{\mathrm{rad}}\, R\left(\mathbf{\Phi}_{n+1}\right)\theta\left(k_{\mathrm{T}}(\mathbf{\Phi}_{n+1}) - p_{\mathrm{T}}\right)\right]_{\alpha_{\mathrm{r}}}^{\bar{\mathbf{\Phi}}_n}}{B^{f_b}\left(\bar{\mathbf{\Phi}}_n\right)} \right\}.$$

(3.42)

Notice that the argument of the $\theta\left(k_{\mathrm{T}}\left(\mathbf{\Phi}_{n+1}\right) - p_{\mathrm{T}}\right)$ function, which insure the convergence of the integral at the exponent, should be a function $k_{\mathrm{T}}\left(\mathbf{\Phi}_{n+1}\right)$, of the same order of the transverse momentum of the emitted parton relative to the emitting one, that becomes exactly equal to it when the singular limit is reached. This is necessary in order not to spoil the leading-log accuracy of the Sudakov form factor. Furthermore, $k_{\mathrm{T}}\left(\mathbf{\Phi}_{n+1}\right)$ is a function of the kinematics variables that depends upon the particular singular region we are considering, so is should be better to indicate it with $k_{\mathrm{T}}^{\alpha_{\mathrm{r}}}\left(\mathbf{\Phi}_{n+1}\right)$.[3] Assuming that the transverse momentum is computed in the CM frame of the colliding partons, we make the two choices:

- $k_{\mathrm{T}}^{\alpha_{\mathrm{r}}}\left(\mathbf{\Phi}_{n+1}\right)$ is proportional to the transverse momentum of the emitted parton with respect to the beam axis in the collinear limit and becomes exactly it in the limit, for ISC singular regions.

- $k_{\mathrm{T}}^{\alpha_{\mathrm{r}}}\left(\mathbf{\Phi}_{n+1}\right)$ is the (spatial) component of k_i or k_j orthogonal to the sum $\vec{k}_i + \vec{k}_j$, for FSC singular regions, where we have assumed that the singular region corresponds to momenta k_i and k_j becoming collinear.

Notice also that in eq. (3.42) the sum over α_{r} real configurations runs only on those whose underlying n-body-process flavour structure is equal to f_b.

The factorization and renormalization scales choice in the definition of $\bar{B}$, eq. (3.38), and in the definition of the Sudakov form factors, eq. (3.42), deserves further comments:

- In the definition of $\bar{B}$ one adopts a choice that is appropriate to the Born cross section, for example the virtuality of a resonance or a high mass that appears in the computation.

- In the Sudakov exponents one must instead adopt a scale of the order of $k_{\mathrm{T}}^{\alpha_{\mathrm{r}}}\left(\mathbf{\Phi}_{n+1}\right)$, for both the renormalization and factorization scales.

---

[3] In eq. (3.42) the α_{r} index is omitted on k_{T} thanks to the context convention.

It may be show that with this choices of scales, the Sudakov form factor of eq. (3.42) is equal, at least to the leading logarithmic (LL) level, to the DDT [75] Sudakov form factor, and that, in some cases, with a simple modification of Λ_{QCD}, one can reach NLL accuracy (see sec. 2.1.3 and sec. 3.3.3 and also ref. [30]).

Hardest emission

The `POWHEG` cross section for the generation of the hardest event is then

$$
\begin{aligned}
d\sigma \;=\; & \sum_{f_b} \bar{B}^{f_b}(\bar{\bm{\Phi}}_n)\, d\bar{\bm{\Phi}}_n \Bigg\{ \Delta^{f_b}\big(\bar{\bm{\Phi}}_n, p_{\mathrm{T}}^{\min}\big) \\
& + \sum_{\alpha_{\mathrm{r}} \in \{\alpha_{\mathrm{r}}|f_b\}} \frac{\left[d\Phi_{\mathrm{rad}}\, \theta\left(k_{\mathrm{T}} - p_{\mathrm{T}}^{\min}\right) \Delta^{f_b}\big(\bar{\bm{\Phi}}_n, k_{\mathrm{T}}\big)\ R\left(\bm{\Phi}_{n+1}\right) \right]_{\alpha_{\mathrm{r}}}^{\bar{\bm{\Phi}}_n}}{B^{f_b}(\bar{\bm{\Phi}}_n)} \Bigg\},
\end{aligned}
\tag{3.43}
$$

where it is assumed that $\bm{\Phi}_{n+1}$ is parametrized in terms of Φ_{rad} and $\bar{\bm{\Phi}}_n$, and, for ease of notation, we have dropped the $\bm{\Phi}_{n+1}$ argument in $k_{\mathrm{T}}^{\alpha_{\mathrm{r}}}$. The $p_{\mathrm{T}}^{\min}$ value introduced here is a lower cut-off on the transverse momentum, that is needed in order to avoid to reach unphysical values of the strong coupling constant and of the parton-density functions. It turns out that the cross section (3.43) fulfills all the requirement listed in the sec. 3.1 for the inclusion of NLO corrections into a SMC. Namely:

- At large values of k_{T}, it coincides with the NLO cross section, up to terms subleading in α_{s}.

- Owing to the overall weight $\bar{B}(\bar{\bm{\Phi}}_n) = \sum_{f_b} \bar{B}^{f_b}(\bar{\bm{\Phi}}_n)$, it reproduces correctly the value of infrared safe observables at the NLO. Hence, also its integral around the small k_{T} region has NLO accuracy.

- In the soft/collinear limit ($k_{\mathrm{T}} \to 0$) it behaves no worse than standard Shower Monte Carlo generators, that is it has the same (N)LL accuracy.

From eq. (3.43) it is also clear why the `POWHEG` method avoid to generate negative-weighted events. The overall weight of an events is, in fact, the term $\bar{B}(\bar{\bm{\Phi}}_n) = \sum_{f_b} \bar{B}^{f_b}(\bar{\bm{\Phi}}_n)$ that multiplies the large curly brackets in eq. (3.43). This happens because the content of curly brackets does not affect the total weight by virtue of unitarity. It thus follows that the region where $\bar{B}(\bar{\bm{\Phi}}_n)$ is negative is not admitted

since it signals the breakdown of the perturbative approach. This is easily explained since a negative value of $\bar{B}(\bar{\boldsymbol{\Phi}}_n)$ may only be obtained if NLO negative contributions overcome the Born approximation.

Interfacing to a SMC

The POWHEG formula (3.43) can be directly used to feed a SMC program, that will perform all subsequent (softer) showers and hadronization. If the SMC is ordered in p_{T}, we simply require that the shower is started with an upper limit on the scale equal to the k_{T} of the POWHEG event. In case the SMC uses a different ordering variable, a problem arises, since the POWHEG cross section requires the emissions with higher k_{T} to be suppressed in the SMC. This problem typically arises when interfacing POWHEG to angular ordered SMC's, *e.g.* HERWIG, since in those programs the largest-angle emission in not necessarily the hardest one. The solution is find by vetoing emissions with larger k_{T} in the subsequent shower, and by introducing vetoed truncated showers (see ref. [4]), that compensate for the fact that in angular ordered shower the hardest emission may not be the first.

Modern SMC programs, such as HERWIG and PYTHIA, have the capability of generating a vetoed shower. In fact, all SMC programs compatible with the *Les Houches Interface for User Processes* [19] (LHIUP from now on) should comply with this requirement. This is not the case for the vetoed truncated showers. However, recent versions of angular ordered SMC's, such as HERWIG++ [20], do implement them. The issue of the addition of soft-truncated showers have been addressed in refs. [28, 35, 38]. There, it was shown that their inclusion never affects the results heavily. In our codes we do not implement soft-truncated showers, and therefore we miss, to some extent, the color coherence effects due to soft wide-angle emissions. In any case, soft large-angle radiation does not appreciably alter the hardest emission.

We also point out that the need of vetoed truncated showers is not specific to the POWHEG method. As explained in ref. [4], it also emerges in the merging of matrix element corrections with parton shower, for example in the approach of ref. [62].

The POWHEG algorithm generates the kinematics and flavour configuration of the hardest-emission event. The event is then fed into a SMC using the LHIUP. In particular, the requirement that no events harder than the one generated by POWHEG can be generated by the SMC, is achieved by setting the variable SCALUP of the

LHIUP equal to the k_T of the `POWHEG` event. The LHIUP specifies also how to pass the kinematics and flavour structure of the hard event to the SMC. The LHIUP also requires that the color connections of the hard event (in the large N_c limit) should also be specified. `POWHEG` does not, in general, generate these large-N_c color structures.

They are needed (and can be generated) only if one wishes to reach large-N_c NLL accuracy of the Sudakov form factor, in events with more than 3 coloured partons at the Born level, as we discuss in section 3.3.3. If this is not the case, the generation of the color configuration should be performed after the `POWHEG` event has been generated. For example, one can generate the `POWHEG` events in the standard way, picking the different (planar) color contributions to the Born cross section, at the kinematics of the generated underlying Born configuration, with a probability proportional to the corresponding (planar) color Born contribution. Then retain that color structure only if there is no radiation. Otherwise, the planar color structure of the event, is fully specified by the singular region index α_r where the emission take place, under the assumption that the emitted parton is (planar) colour-connected to the emitter.

Singular regions and transverse momentum ordering

Some more comments are required concerning the separation of the various singular contributions in `POWHEG`, when the underlying n-body cross section also possesses singular regions. In standard NLO calculations, these regions are avoided by simply requiring that the physical observables one computes should be finite for the n-body term. As already stated, this is achieved requiring that the observable O_{n+1} should vanish fast enough if $\mathbf{\Phi}_{n+1}$ approaches two singular regions at the same time. In the `POWHEG` cross section given in eq. (3.43) instead, the dependence on the observable O is no longer evident. We thus should require that the $\bar{B}$ function is well-behaved when the underlying Born configuration approach one of its singular limits. Should it not be the case, for example for a process like $Z + jet$, whose underlying Born configuration diverges when the jet becomes soft or collinear to the beam, a damping factor that suppresses the regions where the n-body configuration becomes singular, must be added to $\bar{B}$, in order to get a finite result.

However, this requirement is in general not sufficient. We should also require that the k_T of the radiation generated by `POWHEG` should not be harder than all the k_T's associated with the underlying Born kinematics. More precisely, we should require

that radiation with k_T larger than the smallest k_T of the underlying n-body process should be suppressed. Notice that the separation of R into contributions singular only in one regions regions achieves to some extent this purpose, since R^{α_r} is suppressed away from the region α_r. The crucial point, however, is that this suppression should be based upon k_T, in order to have a consistent treatment of soft singularities. Thus, in the FKS case for example, a more appropriate choice for the $d_i^{\oplus}$ and the d_{ij}'s is

$$
d_i^{\oplus} = (E_i)^{2b} \, 2^b (1 \mp \cos\theta_i)^b \,, \tag{3.44}
$$

$$
d_{ij} = \left(\frac{E_i E_j}{E_i + E_j} \right)^{2b} 2^b \, (1 - \cos\theta_{ij})^b \,, \tag{3.45}
$$

that correspond, in the small θ limits, to the square of the transverse momentum to the power b, rather than the form suggested in eqs (1.131) and (1.124).

In the CS approach instead, one can first separate R as in eqs. (1.135) and (1.134), using the $\mathcal{S}$ functions defined in eqs. (1.119) and (1.133), with the d functions defined as in eqs. (3.44) and (3.45). The contributions to R corresponding to a given singular region can then be separated according to each possible spectator using a formula similar to eq. (3.27).

3.3.2 NLO accuracy of the POWHEG formula

In the previous section, it was argued that the POWHEG main formula eq. (3.43) yields NLO accuracy for infrared-finite observables. The proof goes as follows. Let's start applying the formula (3.43) to an infrared-safe observable O. We have

$$
\begin{aligned}
\langle O \rangle = \sum_{f_b} \int d\bar{\boldsymbol{\Phi}}_n \, \bar{B}^{f_b}(\bar{\boldsymbol{\Phi}}_n) \Bigg\{ & \Delta^{f_b}\left(\bar{\boldsymbol{\Phi}}_n, p_T^{\min}\right) O_n(\bar{\boldsymbol{\Phi}}_n) \\
& + \sum_{\alpha_r \in \{\alpha_r | f_b\}} \frac{\left[\int d\Phi_{\mathrm{rad}} \, \theta\left(k_T - p_T^{\min}\right) \, \Delta^{f_b}\left(\bar{\boldsymbol{\Phi}}_n, k_T\right) \, R\left(\boldsymbol{\Phi}_{n+1}\right) O_{n+1}(\boldsymbol{\Phi}_{n+1}) \right]_{\alpha_r}^{\bar{\boldsymbol{\Phi}}_n}}{B^{f_b}(\bar{\boldsymbol{\Phi}}_n)} \Bigg\} .
\end{aligned}
$$
$$\tag{3.46}$$

Now, with a simple manipulation eq. (3.46) can be written as

$$
\langle O \rangle = \sum_{f_b} \int d\bar{\bar{\Phi}}_n \, \bar{B}^{f_b}(\bar{\bar{\Phi}}_n) \left\{ \left[\Delta^{f_b}(\bar{\bar{\Phi}}_n, p_{\mathrm{T}}^{\min}) \right. \right.
$$

$$
+ \sum_{\alpha_{\mathrm{r}} \in \{\alpha_{\mathrm{r}}|f_b\}} \frac{\left[\int d\Phi_{\mathrm{rad}} \, \theta\left(k_{\mathrm{T}} - p_{\mathrm{T}}^{\min}\right) \, \Delta^{f_b}(\bar{\bar{\Phi}}_n, k_{\mathrm{T}}) \, R(\Phi_{n+1}) \right]_{\alpha_{\mathrm{r}}}^{\bar{\Phi}_n}}{B^{f_b}(\bar{\bar{\Phi}}_n)} \left. \right] O_n(\bar{\bar{\Phi}}_n)
$$

$$
+ \sum_{\alpha_{\mathrm{r}} \in \{\alpha_{\mathrm{r}}|f_b\}} \frac{\left[\int d\Phi_{\mathrm{rad}} \, \theta\left(k_{\mathrm{T}} - p_{\mathrm{T}}^{\min}\right) \Delta^{f_b}(\bar{\bar{\Phi}}_n, k_{\mathrm{T}}) \, R(\Phi_{n+1}) \left(O_{n+1}(\Phi_{n+1}) - O_n(\bar{\bar{\Phi}}_n)\right) \right]_{\alpha_{\mathrm{r}}}^{\bar{\Phi}_n}}{B^{f_b}(\bar{\bar{\Phi}}_n)} \left. \right\},
$$

$$(3.47)$$

where we have simply added and subtracted back the same term proportional to $R(\Phi_{n+1}) \, O_n(\Phi_n)$.

Then observe that

$$
\sum_{\alpha_{\mathrm{r}} \in \{\alpha_{\mathrm{r}}|f_b\}} \frac{\left[\int d\Phi_{\mathrm{rad}} \, \theta\left(k_{\mathrm{T}} - p_{\mathrm{T}}^{\min}\right) \, \Delta^{f_b}(\bar{\bar{\Phi}}_n, k_{\mathrm{T}}) \, R(\Phi_{n+1}) \right]_{\alpha_{\mathrm{r}}}^{\bar{\Phi}_n}}{B^{f_b}(\bar{\bar{\Phi}}_n)} =
$$

$$
= \int_{p_{\mathrm{T}}^{\min}}^{\infty} dp_{\mathrm{T}}' \sum_{\alpha_{\mathrm{r}} \in \{\alpha_{\mathrm{r}}|f_b\}} \frac{\left[\int d\Phi_{\mathrm{rad}} \, \theta\left(k_{\mathrm{T}} - p_{\mathrm{T}}^{\min}\right) \, \delta(k_{\mathrm{T}} - p_{\mathrm{T}}') \Delta^{f_b}(\bar{\bar{\Phi}}_n, p_{\mathrm{T}}') \, R(\Phi_{n+1}) \right]_{\alpha_{\mathrm{r}}}^{\bar{\Phi}_n}}{B^{f_b}(\bar{\bar{\Phi}}_n)}
$$

$$
= - \int_{p_{\mathrm{T}}^{\min}}^{\infty} dp_{\mathrm{T}}' \, \Delta^{f_b}(\bar{\bar{\Phi}}_n, p_{\mathrm{T}}') \, \frac{d}{dp_{\mathrm{T}}'} \sum_{\alpha_{\mathrm{r}} \in \{\alpha_{\mathrm{r}}|f_b\}} \frac{\left[\int d\Phi_{\mathrm{rad}} \, \theta\left(k_{\mathrm{T}} - p_{\mathrm{T}}^{\min}\right) \theta(k_{\mathrm{T}} - p_{\mathrm{T}}') \, R(\Phi_{n+1}) \right]_{\alpha_{\mathrm{r}}}^{\bar{\Phi}_n}}{B^{f_b}(\bar{\bar{\Phi}}_n)}
$$

$$
= \int_{p_{\mathrm{T}}^{\min}}^{\infty} dp_{\mathrm{T}}' \, \frac{d}{dp_{\mathrm{T}}'} \Delta^{f_b}(\bar{\bar{\Phi}}_n, p_{\mathrm{T}}') = 1 - \Delta^{f_b}(\bar{\bar{\Phi}}_n, p_{\mathrm{T}}^{\min}) \ , \tag{3.48}
$$

where we have used the fact that $\Delta^{f_b}(\bar{\bar{\Phi}}_n, \infty) = 1$. This shows that the term in the large square brackets on the r.h.s of eq. (3.47), which multiplies $O(\bar{\bar{\Phi}}_n)$, sums up to 1.

Furthermore, in the term into the last line of eq. (3.47), small k_{T} values in the integral are suppressed by the difference $O_{n+1}(\Phi_{n+1}) - O_n(\bar{\bar{\Phi}}_n)$, and therefore we can

replace $\Delta^{f_b}(\bar{\bar{\Phi}}_n, k_{\mathrm{T}}) \to 1$ and $B^{f_b}(\bar{\bar{\Phi}}_n) \to \bar{B}^{f_b}(\bar{\bar{\Phi}}_n)$, the difference introduced being of higher orders in α_{s}.

Equation (3.46) thus reduces to

$$
\begin{aligned}
\langle O \rangle \;=\; & \sum_{f_b} \int d\Phi_n \Bigg\{ \bar{B}^{f_b}(\Phi_n)\, O_n(\bar{\Phi}_n) \\
& + \sum_{\alpha_{\mathrm{r}} \in \{\alpha_{\mathrm{r}} | f_b\}} \left[\int d\Phi_{\mathrm{rad}}\, \theta(k_{\mathrm{T}} - p_{\mathrm{T}}^{\min})\, R\left(\Phi_{n+1}\right) \left(O_{n+1}(\Phi_{n+1}) - O_n(\bar{\Phi}_n) \right) \right]_{\alpha_{\mathrm{r}}}^{\bar{\bar{\Phi}}_n} \Bigg\} ,
\end{aligned}
$$

(3.49)

up to NLLO corrections. To conclude this proof, we can drop the restriction $\theta(k_{\mathrm{T}} - p_{\mathrm{T}}^{\min})$ from the $d\Phi_{\mathrm{rad}}$ integration, its effect being suppressed by powers of $p_{\mathrm{T}}^{\min}$. In this way, formula eq. (3.49) is immediately found to agree with eq. (3.41), thus concluding our proof.

It is worth noticing that subsequent showering performed by an SMC program does not spoil the NLO accuracy. This is a simple consequence of the fact that no radiation with k_{T} larger than that generated by POWHEG is allowed in the subsequent shower.

3.3.3   NLL accuracy of the Sudakov form factor

As shown in the previous section, the POWHEG method reach the NLO accuracy for inclusive quantities. The other requested feature is to enforce the leading logarithmic (LL) accuracy for exclusive final states. Since the POWHEG method deals with the hardest emission only and subsequent emissions are handled by the Shower Monte Carlo which POWHEG is interfaced to, in general, the emissions have the LL accuracy of the SMC. However, as discussed in sec. 2.1.3, for a SMC program a simple redefinition of Λ_{QCD} may result in achieving the NLL accuracy of the showered results. In this section we address the question how the NLL accuracy may be enforced into the POWHEG framework. Exclusive observables that are especially sensitive to the hardest emission will benefit from such an improved POWHEG accuracy.

In the following we simply collect the results of sec. 2.1.3, of sec. 4.4 of ref. [30] and of sec. 4. of ref. [26], referring the reader to those references for deeper explanations

on how these results are derived.

The `POWHEG` Sudakov form factor is accurate at the LL level, provided that the strong coupling constant and the parton density functions in the Sudakov exponent are evaluated at a scale of order k_{T}^2.

In case of processes involving no more than 3 coloured partons at the Born level (in the initial or final state), one can easily go even further. In fact, the NLL accuracy may be achieved in two simple steps. First one has to perform the replacement in eq. (2.41) for the strong coupling constant in the Sudakov exponent. The argument of α_{s} in eq. (2.41) must be taken equal to a function of the radiation variable that is of order k_{T}^2 in the soft or collinear limit, but becomes exactly equal to k_{T}^2 in the soft *and* collinear region. Then, the parton densities in the Sudakov exponent must be evaluated at a scale of order k_{T}^2, for both the real emission contributions (in the numerator) and the Born contribution (in the denominator).

In case of processes involving more than 3 coloured partons, the procedure just outlined is not sufficient to guarantee the NLL accuracy. There are in fact soft (NLL) contributions that do exponentiate only in a matrix sense, so that, in order to deal with them using standard Monte Carlo techniques suited for the evaluation of ordinary exponential, one should diagonalize their colour structure. These are soft-interference terms, due to the color correlation present in the soft limits, see eq. (1.80). However, their correct exponentiation of the soft (NLL) contributions can be easily recovered for the dominant terms in the large-N_{c} limit, as shown in sec. 4.4 of ref. [30].

3.3.4 Practical implementation

The `POWHEG` cross section (eq. (3.43)) looks very complex, but, in fact, from a numerical point of view, it is quite easy to implement using few well-known Monte Carlo techniques. We have collected an overview of those techniques in Appendix C.

The implementation issues can be easily reduced to the problem to generate consistently the relevant kinematic configurations: i.e. the Born variables and the radiative ones.

Generation of the Born variables

In a POWHEG implementation, following eq. (3.43), the first step is the generation of the Born-like kinematics $\bar{\bar{\mathbf{\Phi}}}_n$ and of the value of the index f_b, with a probability given by $\bar{B}^{f_b}(\bar{\bar{\mathbf{\Phi}}}_n) \, d\bar{\bar{\mathbf{\Phi}}}_n$. This is, in the end, the total weight of the generated event.

The standard Monte Carlo technique usually used in these cases is the hit-and-miss procedure: one finds an upper bound to the cross section, generates randomly the phase-space point, and then accepts it with a probability equal to the ratio of the value of the cross section at the given point over the upper bound value. However, this technique is tremendously inefficient in our case, since each evaluation of the $\bar{B}$ function requires an integration over $d\Phi_{\text{rad}}$.

A clever solution is to parametrize, for each singular region, the radiation variables Φ_{rad} in terms of a set of three variables in the unit cube, that we call $X_{\text{rad}} = \left\{ X_{\text{rad}}^{(1)}, X_{\text{rad}}^{(2)}, X_{\text{rad}}^{(3)} \right\}$. Also the z variable in the collinear remnants case is parametrized in terms of one of these three variables, that we choose to be $X_{\text{rad}}^{(1)}$. We then introduce the function

$$
\begin{aligned}
\tilde{B}^{f_b}(\bar{\bar{\mathbf{\Phi}}}_n, X_{\text{rad}}) \;=\;& B^{f_b}\left(\bar{\bar{\mathbf{\Phi}}}_n\right) + V^{f_b}\left(\bar{\bar{\mathbf{\Phi}}}_n\right) \\[2mm]
&+ \sum_{\alpha_{\text{r}} \in \{\alpha_{\text{r}} | f_b\}} \left[\left| \frac{\partial \Phi_{\text{rad}}}{\partial X_{\text{rad}}} \right| \left\{ R\left(\mathbf{\Phi}_{n+1}\right) - C\left(\mathbf{\Phi}_{n+1}\right) \right\} \right]_{\alpha_{\text{r}}}^{\bar{\bar{\mathbf{\Phi}}}_n} \\[2mm]
&+ \sum_{\alpha_{\oplus} \in \{\alpha_{\oplus} | f_b\}} \left[\frac{1}{z} \left| \frac{\partial z}{\partial X_{\text{rad}}^{(1)}} \right| G_{\oplus}^{\alpha_{\oplus}}\left(\mathbf{\Phi}_{n,\oplus}\right) \right]^{\bar{\bar{\mathbf{\Phi}}}_n} \\[2mm]
&+ \sum_{\alpha_{\ominus} \in \{\alpha_{\ominus} | f_b\}} \left[\frac{1}{z} \left| \frac{\partial z}{\partial X_{\text{rad}}^{(1)}} \right| G_{\ominus}^{\alpha_{\ominus}}\left(\mathbf{\Phi}_{n,\ominus}\right) \right]^{\bar{\bar{\mathbf{\Phi}}}_n} ,
\end{aligned}
\tag{3.50}
$$

so that

$$
\bar{B}^{f_b}(\bar{\bar{\mathbf{\Phi}}}_n) = \int_0^1 dX_{\text{rad}}^{(1)} \int_0^1 dX_{\text{rad}}^{(2)} \int_0^1 dX_{\text{rad}}^{(3)} \, \tilde{B}^{f_b}(\bar{\bar{\mathbf{\Phi}}}_n, X_{\text{rad}}),
\tag{3.51}
$$

and we define

$$
\tilde{B}(\bar{\bar{\mathbf{\Phi}}}_n, X_{\text{rad}}) = \sum_{f_b} \tilde{B}^{f_b}(\bar{\bar{\mathbf{\Phi}}}_n, X_{\text{rad}}).
\tag{3.52}
$$

Notice that, unlike the $\bar{B}\left(\bar{\bar{\mathbf{\Phi}}}_n\right)$ function, the $\tilde{B}(\bar{\bar{\mathbf{\Phi}}}_n, X_{\text{rad}})$ function is not guaranteed to be positive. Only its integral over radiation variables, which is in the end the

$\bar{B}(\bar{\boldsymbol{\Phi}}_n)$, has this property. Negative values of $\tilde{B}(\bar{\boldsymbol{\Phi}}_n, X_{\mathrm{rad}})$ corresponds to points in the full radiative phase space $\boldsymbol{\Phi}_{n+1}$ where negative NLO contributions overcome the Born terms.

At this point one can use a computer algorithm that, after performing a single integration on a given function, can generate points in the integration range, distributed according to the integrand function. One such popular program is the `BASES/SPRING` package [76]. Another possible choice is the integrator-unweighter `MINT` [77], which is a `BASES/SPRING` variant, that allows for folded integration. By this we mean that `MINT` folds the phase space, performing its integration stage collecting together different points of the phase space, in such a way that the occurrence of negative values of $\tilde{B}(\bar{\boldsymbol{\Phi}}_n, X_{\mathrm{rad}})$ is greatly reduced.

Both these programs starts with an adaptive Monte Carlo integration routine (`VEGAS` [78]), that performs the integration of the non-negative function and stores the intermediate results. Then, a generation routine uses these informations to generate unweighted events with the usual hit-and-miss technique. In the `POWHEG` case, the $\tilde{B}(\bar{\boldsymbol{\Phi}}_n, X_{\mathrm{rad}})$ function is first integrated over the full $(\bar{\boldsymbol{\Phi}}_n, X_{\mathrm{rad}})$ space, obtaining in this way the weight $\bar{B}(\bar{\boldsymbol{\Phi}}_n)$. Then one generate a phase-space point $(\bar{\boldsymbol{\Phi}}_n, X_{\mathrm{rad}})$ according to $\tilde{B}(\bar{\boldsymbol{\Phi}}_n, X_{\mathrm{rad}})$. For each generated phase-space point, one chooses an f_b value with a probability equal to $\tilde{B}^{f_b}(\bar{\boldsymbol{\Phi}}_n, X_{\mathrm{rad}})/\sum_{f_b} \tilde{B}^{f_b}(\bar{\boldsymbol{\Phi}}_n, X_{\mathrm{rad}})$. The final trick is to discard the X_{rad} generated values, which corresponds to integrate over them. Thus, by doing a single $(n+1)$-body phase-space integration, one is able to generate the Born configuration with reasonable efficiency.

As already pointed out, if the Born configuration possesses singular regions, for example when one deals with Born cross sections that include the production of a light parton, care should be taken in order to avoid these singularity during the n-body phase space integration. There are two ways of implementing this constrain:

- One may specify a transverse-momentum cut on the light parton momenta, in order to get a finite total cross section. This is what is usually implemented in standard SMC programs.

- Alternatively, one may weight the (divergent) cross section with a weight $W(\bar{\boldsymbol{\Phi}}_n)$ that suppresses the n-body singular regions, so that the integral of $W \times \tilde{B}$ is finite. Events are then generated using $W \times \tilde{B}$ instead of $\tilde{B}$, and a weight $W^{-1}(\bar{\boldsymbol{\Phi}}_n)$ should be attached to each event. At the end, an unweighting proce-

dure is performed to recover the correct results.

Generation of the hardest-radiation variables

Given the Born kinematics $\left(\bar{\bar{\Phi}}_n,\, f_b\right)$, we then generate the hardest-radiation configu-
ration, characterized by $(\alpha_{\mathrm{r}},\, \Phi_{\mathrm{rad}}^{\alpha_{\mathrm{r}}})$, with $\alpha_{\mathrm{r}} \in \{\alpha_{\mathrm{r}} | f_b\}$, with probability

$$\left[\frac{R\left(\Phi_{n+1}\right)}{B^{f_b}\left(\bar{\bar{\Phi}}_n\right)}\, \Delta^{f_b}\left(\bar{\bar{\Phi}}_n, k_{\mathrm{T}}\left(\Phi_{n+1}\right)\right) d\Phi_{\mathrm{rad}} \right]_{\alpha_{\mathrm{r}}}^{\bar{\bar{\Phi}}_n} . \tag{3.53}$$

The Sudakov form factor can be written as

$$\Delta^{f_b}(\bar{\bar{\Phi}}_n, p_{\mathrm{T}}) = \prod_{\alpha_{\mathrm{r}} \in \{\alpha_{\mathrm{r}} | f_b\}} \Delta^{f_b}_{\alpha_{\mathrm{r}}}(\bar{\bar{\Phi}}_n, p_{\mathrm{T}}) , \tag{3.54}$$

where

$$\Delta^{f_b}_{\alpha_{\mathrm{r}}}(\bar{\bar{\Phi}}_n, p_{\mathrm{T}}) = \exp\left\{ - \left[\int d\Phi_{\mathrm{rad}} \frac{R\left(\Phi_{n+1}\right)}{B^{f_b}\left(\bar{\bar{\Phi}}_n\right)}\, \theta\left(k_{\mathrm{T}}(\Phi_{n+1}) - p_{\mathrm{T}}\right) \right]_{\alpha_{\mathrm{r}}}^{\bar{\bar{\Phi}}_n} \right\} . \tag{3.55}$$

Under these conditions, the problem of generating the radiation variables according
to eq. (3.53) can be reduced to the problem of generating them with probabilities

$$\left[\frac{R^{\alpha_{\mathrm{r}}}\left(\Phi_{n+1}\right)}{B^{f_b}\left(\bar{\bar{\Phi}}_n\right)}\, \Delta^{f_b}_{\alpha_{\mathrm{r}}}\left(\bar{\bar{\Phi}}_n, k_{\mathrm{T}}\left(\Phi_{n+1}\right)\right) \right]^{\bar{\bar{\Phi}}_n} d\Phi_{\mathrm{rad}}^{\alpha_{\mathrm{r}}} , \tag{3.56}$$

by using the highest-bid method, illustrated in appendix C.2. We are thus left with
the problem of generating radiation variables according to eq. (3.56), for a fixed
value of α_{r}. This problem can be dealt with using the veto technique, illustrated in
appendix C.1. In order to use this technique, we need a sufficiently simple upper
bounding function

$$\left[\frac{R^{\alpha_{\mathrm{r}}}\left(\Phi_{n+1}\right)}{B^{f_b}\left(\bar{\bar{\Phi}}_n\right)} \right]^{\bar{\bar{\Phi}}_n} \leq U(\Phi_{\mathrm{rad}}^{\alpha_{\mathrm{r}}}, \Phi_n). \tag{3.57}$$

This can be found by taking the singular limit of the left hand side of eq. (3.57), that
has, in general, a form suggested by the factorization theorem, and by elementary
properties of the parton densities in the case of initial-state singular regions. Once
the functional form of F is guessed, its normalization is found by scanning the Φ_{n+1}
phase space.

Within a given subtraction method, one has typically two kinds of upper bounding functions: one for final-state radiation and one for initial-state radiation. In the following chapters we illustrate explicit forms for U in the CS and FKS frameworks, for the initial-state radiation cases that appear in this thesis.

Notice also that, in general, it is not necessary to separate out all α_r regions in order to apply the veto method. In many cases several regions can be group together, thus simplifying the generation algorithm.

3.3.5 Born zeros, remnants and regular contributions

In case the Born cross section vanishes in particular kinematics points, a problem arises in the POWHEG expression for the Sudakov form factor (3.42) and (3.55). It happens, in fact, that although B vanishes, $\bar{B}$ may differ from zero. Born kinematics configurations with a vanishing Born cross section may thus be generated and, at the stage of radiation generation, one would find very large ratios of the real-emission cross section over the Born cross section. It would thus prove difficult to find a reasonable upper bound for this ratio. If one tries to neglect the problem, radiation events with a vanishing underlying Born configuration would never be generated. We observe that, in the limit of small hardness parameter, the real cross also exhibit the same vanishing behaviour of the Born cross section. Loosely speaking, the problem arises when the distance of the underlying Born configuration from the zero configuration is smaller than the distance of the real emission cross section from the singular (i.e. zero hardness) configuration. In the following, we show that this problem has a simple solution, that can be easily generalized to all cases in which the Born cross section vanishes.

In order to solve this problem, in a completely general way, we further decompose the α_r contribution to the real cross section as

$$R^{\alpha_r} = R^{\alpha_r,s} + R^{\alpha_r,r}, \tag{3.58}$$

where

$$R^{\alpha_r,s} = R^{\alpha_r} \frac{Z}{Z+H}, \qquad R^{\alpha_r,r} = R^{\alpha_r} \frac{H}{Z+H}. \tag{3.59}$$

The suffixes s and r stand for "singular" and "regular" respectively, and Z is a function of the kinematics that vanishes like the Born cross section, evaluated at the

underlying Born kinematics of the given term. H is the hardness of radiation and it must vanish for vanishing transverse momentum of the radiation. The simplest possible choice would be

$$Z = \mathcal{B}\, \frac{k_{T,\mathrm{max}}^2}{\mathcal{B}_{\mathrm{max}}}, \qquad H = k_T^2 \,, \tag{3.60}$$

where k_T is some definition of the transverse momentum of the radiation. Notice now that $R^{\alpha_r,s}$ vanishes as fast as the Born term when its underlying Born kinematics approaches the Born zero. It can thus be used in the expression for the Sudakov form factor (eqs. (3.42) and (3.55)) without problems. The $R^{\alpha_r,r}$ is instead non-vanishing, but, on the other hand, it does not have collinear or soft singularities because of the H factor, and thus it can be computed directly, without any Sudakov form factor.

Thus, all the R^{α_r} terms in eq. (3.38) are replaced by the corresponding $R^{\alpha_r,s}$. The $R^{\alpha_r,r}$ terms are instead generated in a way similar to what was done for eq. (3.50). In other words one defines

$$
\begin{aligned}
\tilde{B}^r(\bar{\boldsymbol{\Phi}}_n, X_{\mathrm{rad}}) &= \sum_{f_b} \tilde{B}^{f_b,r}(\bar{\boldsymbol{\Phi}}_n, X_{\mathrm{rad}}) \\
&= \sum_{f_b} \sum_{\alpha_{\mathrm{r}} \in \{\alpha_{\mathrm{r}} | f_b\}} \left[\left| \frac{\partial \Phi_{\mathrm{rad}}}{\partial X_{\mathrm{rad}}} \right| R^r\left(\boldsymbol{\Phi}_{n+1}\right) \right]_{\alpha_{\mathrm{r}}}^{\bar{\boldsymbol{\Phi}}_n} ,
\end{aligned}
\tag{3.61}
$$

and integrates over the whole $\left(\bar{\boldsymbol{\Phi}}_n, X_{\mathrm{rad}}\right)$ phase space with the same method used for $\tilde{B}$ of eq. (3.50).

In general, the procedure outlined above is safe since one can always separate the real contributions into two parts: a reduced one

$$R^{\alpha_r,s} = R^{\alpha_r} \times F \,, \tag{3.62}$$

which is singular in the soft/collinear limits and the complementary one $R^{\alpha_r} \times (1 - F)$. The previous separation is a sensible one provided F is a function of the real phase space, with $F < 1$ everywhere, such that F approaches 1 for small transverse momenta, and approaches zero for large transverse momenta. The previous choice $F = Z/(Z + H)$ clearly satisfy these requirements.

Furthermore, within this approach, by carefully choosing the functional form of F one may tune the part of real contributions which is affected by shower effects (because it enters the Sudakov form factor), with respect to that part that is expected to be insensible to the shower, for example the high-transverse-momentum tail.

Thus, in general, one can perform the POWHEG generation using $R^{\alpha_r,s}$ instead of R^{α_r}, and treat the remaining $R^{\alpha_r} \times (1-F)$ contribution to the cross section with the same method that we used for the $R^{\alpha_r,r}$ contribution above (see eq. (3.61)). This can be done, since $R^{\alpha_r} \times (1-F)$ is damped by the $1-F$ factor in the singular region.

We call "remnants" these non singular contributions to the cross section, in order to distinguish them from purely "regular" contributions, which we mean to be those that do not have a valid underlying Born configuration, and are therefore not sensible to the collinear or soft limits. The "regular" contributions, if present, are dealt in full analogy to the "remnants" contributions. That is, they are collected into $\tilde{B}^r$ and generated with the same method outlined above.

A the end, in order to generate an event, we choose $\tilde{B}$ or $\tilde{B}^r$, with a probability proportional to their respective total integral. In case $\tilde{B}^r$ is chosen, one generates a kinematic configuration according to it. This kinematic configuration is a full $\mathbf{\Phi}_{n+1}$ configuration. The flavour f_b is chosen with a probability proportional the the value of $\tilde{B}^{f_b,r}$ for the particular kinematic point $\mathbf{\Phi}_{n+1}$ that has been generated, and the event is sent to the output. In case $\tilde{B}$ is chosen, a kinematic configuration and an underlying Born flavour is chosen in the same way. Then the radiation is generated according the Sudakov form factor.

Chapter 4

Single Vector Boson Production

4.1 Introduction

In this chapter we present an implementation of the W and Z hadroproduction cross section in the POWHEG framework, using the CS subtraction formalism. Its content is based on the work published in ref. [34], with minor modifications. In particular, a slight change in the notation is performed, in order to comply with sec. 1.2.1.

All previous next-to-leading-order calculations interfaced according to the POWHEG method have been performed in the FKS approach (see refs. [26, 27]). In view of the popularity of the CS scheme, we have found desirable to explore more in detail its use within POWHEG. In ref. [30] an outline of the implementation of the Drell-Yan production cross section in POWHEG in the CS scheme was already given. In the present chapter we depart slightly from that approach. In particular, we adopt a more appropriate form of the hardness variable used for the generation of radiation. As a further point, for the case of W production, if angular correlations in decay products are correctly taken into account, the problem of vanishing underlying Born configuration, discussed in sec. 3.3.5 is present. In fact, the Born-level W cross section vanishes when the fermion decay products are exactly in the opposite direction of the incoming quark-antiquark pair. This causes a problem in the generation of radiation within the POWHEG method, which may be solved in a general way.

The chapter is organized as follows. In sec. 4.2 we describe how we performed the calculation for the NLO W and Z cross sections. In sec. 4.3 we discuss the POWHEG implementation and how to deal with vanishing Born cross sections in the case of W production. In sec. 4.4 we show our results for several kinematic variables and

compare them with `MC@NLO` [2] and `PYTHIA` 6.4 [22]. Finally, in sec. 4.5, we give our conclusions.

4.2   Description of the calculation

4.2.1   Kinematics

Born kinematics

We begin by considering the Born process for the annihilation of a quark and an antiquark into a lepton-antilepton pair[1] $q + \bar{q} \rightarrow l + \bar{l}$. Following sec. 1.2.1, we denote by $\bar{k}_\oplus$ and $\bar{k}_\ominus$ the incoming quark momenta, and by $\bar{k}_1$ and $\bar{k}_2$ the outgoing fermion momenta. We call $K_\oplus$ and $K_\ominus$ the incoming hadron momenta and define the momentum fractions $\bar{x}_\oplus$ as

$$\bar{k}_\oplus = \bar{x}_\oplus K_\oplus \ . \tag{4.1}$$

We choose our reference frame with the z axis along the $\bar{k}_\oplus$ direction. We introduce the following variables

$$\bar{M}^2 = (\bar{k}_1 + \bar{k}_2)^2, \qquad \bar{Y} = \frac{1}{2} \log \frac{(\bar{k}_1 + \bar{k}_2)^0 + (\bar{k}_1 + \bar{k}_2)^3}{(\bar{k}_1 + \bar{k}_2)^0 - (\bar{k}_1 + \bar{k}_2)^3}, \tag{4.2}$$

that characterize the invariant mass and rapidity of the virtual vector boson.[2] We also introduce the angle $\bar{\theta}_l$ that represents the angle between the outgoing lepton and the $\bar{k}_\oplus$ momentum, in the centre-of-mass frame of the lepton pair. The azimuthal orientation of the decay products is irrelevant here, since the cross sections do not depend upon it. We thus fix it to zero. At the end of the generation of the event, we perform a uniform, random azimuthal rotation of the whole event, in order to cover all final-state phase space. The set of variables $\bar{M}^2$, $\bar{Y}$ and $\bar{\theta}_l$ fully parametrize the Born kinematics. From them we can reconstruct

$$\bar{x}_\oplus = \sqrt{\frac{\bar{M}^2}{S}} e^{\bar{Y}}, \qquad \bar{x}_\ominus = \sqrt{\frac{\bar{M}^2}{S}} e^{-\bar{Y}}, \tag{4.3}$$

---

[1]In case of W production the quark-antiquark and lepton-antilepton pairs have different flavour. We focus here for simplicity on leptonic decays of the vector bosons. Hadronic decays are treated similarly.

[2]The virtuality of the lepton pair $\bar{M}^2$ will be distributed according to a Breit-Wigner formula around the squared mass of the vector boson M_V^2 (where V stands for either the $W^\pm$ or the Z).

where $S = (K_\oplus + K_\ominus)^2$. The leptons' momenta are first reconstructed in the longitudinal rest frame of the lepton pair, where each lepton has energy equal to $\bar{M}/2$ and where the lepton momentum forms an angle $\bar{\theta}_l$ with the $\oplus$ direction and has zero azimuth (i.e. it lies in the z, x plane and has positive x component). The leptons' momenta are then boosted with boost angle $\bar{Y}$.

The Born phase space in terms of these variables is written as

$$
\begin{aligned}
d\bar{\Phi}_2 & = d\bar{x}_\oplus \, d\bar{x}_\ominus (2\pi)^4 \delta^4(\bar{k}_\oplus + \bar{k}_\ominus - \bar{k}_1 - \bar{k}_2) \frac{d^3\bar{k}_1}{(2\pi)^3 2\bar{k}_1^0} \frac{d^3\bar{k}_2}{(2\pi)^3 2\bar{k}_2^0} \\
& = \frac{1}{S}\frac{1}{16\pi} d\bar{M}^2 \, d\bar{Y} \, d\cos\bar{\theta}_l \frac{d\bar{\phi}_l}{2\pi} \, .
\end{aligned}
\tag{4.4}
$$

Real-emission kinematics

The real emission process is described by the final-state momenta k_1, k_2 and k_3, where k_1 and k_2 are the outgoing fermion momenta, and k_3 is the momentum of the radiated light parton. In the POWHEG framework, applied in the context of the CS subtraction method, one introduces a different real phase-space parametrization for each CS dipole. In the present case, we have two CS dipoles, with the two incoming partons playing the role of the emitter and the spectator. We consider the case of the $\oplus$ collinear direction. Thus, the emitter is the incoming parton with momentum $k_\oplus$. We introduce the variable

$$
x = 1 - \frac{(k_\oplus + k_\ominus) \cdot k_3}{k_\oplus \cdot k_\ominus},
\tag{4.5}
$$

and the momenta

$$
K = k_1 + k_2 = k_\oplus + k_\ominus - k_3
\tag{4.6}
$$

$$
\bar{K} = x \, k_\oplus + k_\ominus \, .
\tag{4.7}
$$

Observe that $K^2 = \bar{K}^2$, which is the condition that fixes the value of x. When k_3 is collinear to $k_\oplus$ we have

$$
x k_\oplus = k_\oplus - k_3,
\tag{4.8}
$$

and $K = \bar{K}$. Following ref. [31], we introduce the boost tensor

$$
\Lambda^\mu{}_\nu(K, \bar{K}) = g^\mu{}_\nu - \frac{2(K + \bar{K})^\mu (K + \bar{K})_\nu}{(K + \bar{K})^2} + \frac{2\bar{K}^\mu K_\nu}{K^2} \, ,
\tag{4.9}
$$

that gives the relation between the real and the underlying-Born kinematics (barred momenta)

$$\bar{k}_r^\mu = \Lambda^\mu{}_\nu(K, \bar{K})\, k_r^\nu \qquad\qquad r = 1, 2\,. \tag{4.10}$$

Then, the relation between momentum fractions is

$$\bar{x}_\oplus = x\, x_\oplus, \qquad\qquad \bar{x}_\ominus = x_\ominus\,, \tag{4.11}$$

and the incoming momenta are defined in terms of the barred ones as

$$\bar{k}_\oplus = x k_\oplus = \bar{x}_\oplus K_\oplus, \qquad\qquad \bar{k}_\ominus = k_\ominus = \bar{x}_\ominus K_\ominus\,. \tag{4.12}$$

We thus have that

$$\bar{M}^2 = (\bar{k}_1 + \bar{k}_2)^2 = (k_1 + k_2)^2\,. \tag{4.13}$$

The radiation variables are given by

$$x, \qquad\qquad v = \frac{k_\oplus \cdot k_3}{k_\oplus \cdot k_\ominus}, \qquad\qquad \phi, \tag{4.14}$$

where ϕ is the azimuth of k_3 around the z direction.

From the set of variables $\bar{M}^2$, $\bar{Y}$, x, v and ϕ we can reconstruct the full production kinematics for the real-emission cross section. We summarize the reconstruction procedure from ref. [30]. From $\bar{M}^2$ and $\bar{Y}$ we reconstruct the barred momenta, as for the Born kinematics case. Then we reconstruct immediately

$$k_\oplus = \frac{\bar{k}_\oplus}{x}, \qquad k_\ominus = \bar{k}_\ominus, \tag{4.15}$$

and then

$$k_3 = v k_\ominus + (1 - x - v) k_\oplus + k_T, \tag{4.16}$$

where k_T has only transverse components. Its magnitude is determined by the on-shell condition $k_3^2 = 0$, which yields

$$k_T^2 = 2 k_\oplus \cdot k_\ominus (1 - x - v) v \tag{4.17}$$

and its azimuth is ϕ. We then construct the vectors

$$K = k_\oplus + k_\ominus - k_3, \qquad\qquad \bar{K} = x k_\oplus + k_\ominus, \tag{4.18}$$

and the inverse boost

$$\Lambda^{-1}_{\mu\nu}(K, \bar{K}) = g_{\mu\nu} - \frac{2(K + \bar{K})_\mu (K + \bar{K})_\nu}{(K + \bar{K})^2} + \frac{2 K_\mu \bar{K}_\nu}{K^2}, \tag{4.19}$$

from which we can compute the leptons' momenta

$$k_r = \Lambda^{-1}(K, \bar{K}) \, \bar{k}_r, \qquad r = 1, 2. \tag{4.20}$$

The real-emission phase space can be expressed in a factorized form in terms of the underlying Born kinematics phase space and of the radiation variables

$$d\mathbf{\Phi}_3 = d\bar{\mathbf{\Phi}}_2 \, d\Phi_{\rm rad}, \tag{4.21}$$

with

$$d\Phi_{\rm rad} = \frac{\bar{M}^2}{16\pi^2} \frac{d\phi}{2\pi} \, dv \, \frac{dx}{x^2} \, \theta(v) \, \theta\left(1 - \frac{v}{1-x}\right) \theta(x(1-x)) \, \theta(x - \bar{x}_\oplus) \tag{4.22}$$

and

$$d\bar{\mathbf{\Phi}}_2 = \frac{1}{S} \frac{1}{16\pi} \, d\bar{M}^2 \, d\bar{Y} \, d\cos\bar{\theta}_l \,. \tag{4.23}$$

The kinematic variables corresponding to the $\ominus$ collinear direction are reconstructed in full analogy. Observe that starting from a real emission kinematics, the underlying-Born variables depend in general upon the collinear region that we are considering. In the present case, while $\bar{M}$, x and ϕ are obviously independent of the region we are considering, $\bar{Y}$, $\bar{\theta}_l$ and v do depend upon it. In order to avoid a too heavy notation, we have refrained from appending $\oplus$ or $\ominus$ indexes to the underlying Born and radiation variables. When necessary, we will put a $[\;]_\oplus$ "context" bracket around a formula, meaning that the underlying Born and radiation variables inside it should refer to the $\oplus$ direction.

4.2.2   Cross sections

We have used the helicity amplitude method of refs. [79, 80] in order to compute the cross sections including the vector-boson decay products, and checked our results with MadEvent [69]. For the W-boson propagator we have taken

$$\frac{-g_{\mu\nu} + q_\mu q_\nu / M_W^2}{q^2 - M_W^2 + i\Gamma_W M_W} \tag{4.24}$$

and for the Z/γ-boson propagators, multiplied by the corresponding couplings,

$$g_l \, g_q \, \frac{-g_{\mu\nu} + q_\mu q_\nu / M_Z^2}{q^2 - M_Z^2 + i\Gamma_Z M_Z} + e_l \, e_q \, \frac{-g_{\mu\nu}}{q^2}, \tag{4.25}$$

where g_l, g_q are the lepton and quark couplings to the Z (for given helicities), and e_l, e_q are their electric charges.

Following sec. 3.3.1 and ref. [30], we introduce the Born $\mathcal{B}_{q\bar{q}}$ and the real-emission cross sections $\mathcal{R}_{q\bar{q},g}$, $\mathcal{R}_{g\bar{q},q}$ and $\mathcal{R}_{qg,\bar{q}}$, that represent the contributions for quark-antiquark, gluon-antiquark and quark-gluon initiating processes. Notice that the flavour of the outgoing particle in the subscript of $\mathcal{R}$ is also taken to be incoming. In the case of Z production, q and $\bar{q}$ are conjugate in flavour. For $W^{\pm}$ production, because of flavour mixing, q and $\bar{q}$ may refer to different flavour species. We thus assume that, in general, q and $\bar{q}$ may both represent any flavour, but, in general, if q is a quark, $\bar{q}$ is an antiquark, and vice-versa. $\mathcal{B}$ and $\mathcal{R}$ are obtained by taking the absolute value squared of the corresponding helicity amplitude, summing over the helicities and colours of the outgoing particles, averaging over the helicities and colour of the initial partons, and multiplying by the flux factor $1/(2s)$ (see eq. (4.27)). The soft-virtual term in the CS approach is given by (see eq. (1.89) of the present thesis and eq. (7.104) of ref. [30])

$$\mathcal{V}_{q\bar{q}} = \frac{\alpha_S}{\pi} C_F \mathcal{B}_{q\bar{q}} . \tag{4.26}$$

Defining

$$s = (k_\oplus + k_\ominus)^2, \qquad u = (k_\oplus - k_3)^2 = -s\,v, \qquad t = (k_\ominus - k_3)^2 = -(1-x-v)\,s, \tag{4.27}$$

the CS subtraction terms are given by

$$\mathcal{C}_{q\bar{q},g}^{\oplus} = \left[-\frac{1}{u} 2\,g_s^2\,C_F \left\{ \frac{2}{1-x} - (1+x) \right\} \mathcal{B}_{q\bar{q}}(\bar{M}, \bar{Y}, \bar{\theta}_l) \right]_\oplus , \tag{4.28}$$

for gluon radiation from a $q\bar{q}$ initial-state, and

$$\mathcal{C}_{g\bar{q},q} = \left[-\frac{1}{u} 2\,g_s^2\,T_F \left\{ 1 - 2\,x\,(1-x) \right\} \mathcal{B}_{q\bar{q}}(\bar{M}, \bar{Y}, \bar{\theta}_l) \right]_\oplus , \tag{4.29}$$

for the $g\bar{q}$. Analogous formulas apply for the $q\bar{q}$ and the qg counterterms in the $\ominus$ collinear direction.

The collinear remnants are given by

$$
\begin{aligned}
\mathcal{G}_{\oplus}^{q\bar{q},g}(\mathbf{\Phi}_{2,\oplus}) &= \frac{\alpha_{\mathrm{S}}}{2\pi}C_{\mathrm{F}}\Bigg[\left(\frac{2}{1-z}\log\frac{(1-z)^2}{z}\right)_{+} - (1+z)\log\frac{(1-z)^2}{z} + (1-z) \\
&\quad + \left(\frac{2}{3}\pi^2 - 5\right)\delta(1-z) + \left(\frac{1+z^2}{1-z}\right)_{+}\log\frac{\bar{M}^2}{\mu_{\mathrm{F}}^2}\Bigg]\left[\mathcal{B}_{q\bar{q}}(\bar{M},\bar{Y},\bar{\theta}_l)\right]_{\oplus}, \quad (4.30)
\end{aligned}
$$

$$
\begin{aligned}
\mathcal{G}_{\oplus}^{g\bar{q},q}(\mathbf{\Phi}_{2,\oplus}) &= \frac{\alpha_{\mathrm{S}}}{2\pi}T_{\mathrm{F}}\left\{[z^2+(1-z)^2]\left[\log\frac{(1-z)^2}{z}+\log\frac{\bar{M}^2}{\mu_{\mathrm{F}}^2}\right]+2z(1-z)\right\} \\
&\quad \times \left[\mathcal{B}_{q\bar{q}}(\bar{M},\bar{Y},\bar{\theta}_l)\right]_{\oplus}. \quad (4.31)
\end{aligned}
$$

The $\mathbf{\Phi}_{2,\oplus}$ notation, represents here the set of variables

$$
\mathbf{\Phi}_{2,\oplus} = \{x_{\oplus}, x_{\ominus}, z, k_1, k_2\}, \qquad z\,x_{\oplus}K_{\oplus} + x_{\ominus}K_{\ominus} = k_1 + k_2. \quad (4.32)
$$

We also associate an underlying Born configuration $\bar{\mathbf{\Phi}}_2$ to the $\mathbf{\Phi}_{2,\oplus}$ kinematics, defined by

$$
\bar{k}_{\oplus} = z\,x_{\oplus}K_{\oplus}, \qquad \bar{k}_{\ominus} = x_{\ominus}K_{\ominus}, \qquad \bar{k}_1 = k_1, \quad \bar{k}_2 = k_2. \quad (4.33)
$$

The other two collinear remnants, $\mathcal{G}_{\ominus}^{q\bar{q},g}(\mathbf{\Phi}_{2,\ominus})$ and $\mathcal{G}_{\ominus}^{qg,\bar{q}}(\mathbf{\Phi}_{2,\ominus})$, are equal to $\mathcal{G}_{\oplus}^{q\bar{q},g}(\mathbf{\Phi}_{2,\oplus})$ and $\mathcal{G}_{\oplus}^{g\bar{q},q}(\mathbf{\Phi}_{2,\oplus})$ respectively, with $\left[\mathcal{B}_{q\bar{q}}(\bar{M},\bar{Y},\bar{\theta}_l)\right]_{\oplus}$ replaced by $\left[\mathcal{B}_{q\bar{q}}(\bar{M},\bar{Y},\bar{\theta}_l)\right]_{\ominus}$. We then introduce the notation B, V, R, C, G, to stand for $\mathcal{B}, \mathcal{V}, \mathcal{R}, \mathcal{C}, \mathcal{G}$, each multiplied by its appropriate parton densities. The differential cross section, multiplied by some infrared safe observable O, can then be written as

$$
\begin{aligned}
\langle O \rangle &= \sum_{q\bar{q}}\Bigg\{\int d\bar{\mathbf{\Phi}}_2 \left[B_{q\bar{q}}(\bar{\mathbf{\Phi}}_2) + V_{q\bar{q}}(\bar{\mathbf{\Phi}}_2)\right]O(\bar{\mathbf{\Phi}}_2) \\
&\quad + \int d\mathbf{\Phi}_3 \left\{R_{q\bar{q},g}(\mathbf{\Phi}_3)O(\mathbf{\Phi}_3) - C_{q\bar{q},g}^{\oplus}(\mathbf{\Phi}_3)\left[O(\bar{\mathbf{\Phi}}_2)\right]_{\oplus} - C_{q\bar{q},g}^{\ominus}(\mathbf{\Phi}_3)\left[O(\bar{\mathbf{\Phi}}_2)\right]_{\ominus}\right\} \\
&\quad + \int d\mathbf{\Phi}_3 \left\{R_{g\bar{q},q}(\mathbf{\Phi}_3)O(\mathbf{\Phi}_3) - C_{g\bar{q},q}(\mathbf{\Phi}_3)\left[O(\bar{\mathbf{\Phi}}_2)\right]_{\oplus}\right\} \\
&\quad + \int d\mathbf{\Phi}_3 \left\{R_{qg,\bar{q}}(\mathbf{\Phi}_3)O(\mathbf{\Phi}_3) - C_{qg,\bar{q}}(\mathbf{\Phi}_3)\left[O(\bar{\mathbf{\Phi}}_2)\right]_{\ominus}\right\} \\
&\quad + \int d\mathbf{\Phi}_{2,\oplus} \left[G_{\oplus}^{q\bar{q},g}(\mathbf{\Phi}_{2,\oplus}) + G_{\oplus}^{g\bar{q},q}(\mathbf{\Phi}_{2,\oplus})\right]O(\mathbf{\Phi}_{2,\oplus}) \\
&\quad + \int d\mathbf{\Phi}_{2,\ominus} \left[G_{\ominus}^{q\bar{q},g}(\mathbf{\Phi}_{2,\ominus}) + G_{\ominus}^{qg,\bar{q}}(\mathbf{\Phi}_{2,\ominus})\right]O(\mathbf{\Phi}_{2,\ominus})\Bigg\}. \quad (4.34)
\end{aligned}
$$

4.3 POWHEG implementation

The starting point of a `POWHEG` implementation is the inclusive cross section at fixed underlying-Born flavour and kinematics. For the soft-virtual and Born contributions the underlying Born kinematics is obviously given by the Born kinematics itself. For the collinear remnant, for example, in the $\oplus$ direction (see eq. 4.32) the underlying Born kinematics is given by

$$\bar{\bar{\Phi}}_2 = \{\bar{x}_\oplus, \bar{x}_\ominus, \bar{k}_1, \bar{k}_2\} = \{zx_\oplus, x_\ominus, \bar{k}_1, \bar{k}_2\}\,. \tag{4.35}$$

For the CS counterterms, the underlying Born kinematics is given by the corresponding $\bar{\Phi}_2$ variables defined in eqs. (4.11) and (4.12). In order to assign an underlying Born kinematics to the real term, one has to decompose it into contributions that are singular in only one kinematic region. Since $R_{g\bar{q},q}$ and $R_{qg,\bar{q}}$ are only singular in the $\oplus$ and $\ominus$ direction respectively, we assign their underlying Born to be the same of the corresponding CS subtraction term. For $R_{q\bar{q},g}$, on the other hand, we separate:

$$R_{q\bar{q},g} = R_{q\bar{q},g}^\oplus + R_{q\bar{q},g}^\ominus, \qquad R_{q\bar{q},g}^{\oplus} = R_{q\bar{q},g}\frac{C_{q\bar{q},g}^{\oplus}}{C_{q\bar{q},g}^\oplus + C_{q\bar{q},g}^\ominus}\,, \tag{4.36}$$

and assign to $R_{q\bar{q},g}^{\oplus}$ the same underlying Born kinematics of the corresponding CS counterterm $C_{q\bar{q},g}^{\oplus}$. The underlying Born flavour, on the other hand, is always $q\bar{q}$ in the notation we have adopted.

4.3.1 Generation of the Born variables

The primary ingredient for a `POWHEG` implementation is the $\bar{B}$ function, that is the inclusive cross section at fixed underlying Born variables. In our case, it is given by

$$\bar{B} \;=\; \sum_{q\bar{q}} \bar{B}_{q\bar{q}}\,, \tag{4.37}$$

$$\begin{aligned}
\bar{B}_{q\bar{q}} &= B_{q\bar{q}}(\bar{\bar{\Phi}}_2) + V_{q\bar{q}}(\bar{\bar{\Phi}}_2) + \sum_{\oplus} \int \left[d\Phi_{\mathrm{rad}} \left\{ R_{q\bar{q},g}^{\oplus}(\Phi_3) - C_{q\bar{q},g}^{\oplus}(\Phi_3) \right\} \right]_{\oplus}^{\bar{\Phi}_2} \\
&+ \int \left[d\Phi_{\mathrm{rad}} \left\{ R_{g\bar{q},q}(\Phi_3) - C_{g\bar{q},q}(\Phi_3) \right\} \right]_{\oplus}^{\bar{\Phi}_2} + \int \left[d\Phi_{\mathrm{rad}} \left\{ R_{qg,\bar{q}}(\Phi_3) - C_{qg,\bar{q}}(\Phi_3) \right\} \right]_{\ominus}^{\bar{\Phi}_2} \\
&+ \int_{\bar{x}_{\oplus}}^{1} \frac{dz}{z} \left[G_{\oplus}^{q\bar{q},g}(\Phi_{2,\oplus}) + G_{\oplus}^{g\bar{q},q}(\Phi_{2,\oplus}) \right]^{\bar{\Phi}_2} + \int_{\bar{x}_{\ominus}}^{1} \frac{dz}{z} \left[G_{\ominus}^{q\bar{q},g}(\Phi_{2,\ominus}) + G_{\ominus}^{qg,\bar{q}}(\Phi_{2,\ominus}) \right]^{\bar{\Phi}_2} .
\end{aligned}$$

$$(4.38)$$

In the previous formula, reals contributions, CS counterterms and collinear remnants appearing in terms inside square brackets are required to have the same underlying Born configurations $\bar{\bar{\Phi}}_2$ of the Born and virtual contributions, as explicitly indicated by the $\bar{\bar{\Phi}}_2$ superscript outside the square brackets.

The radiation variables Φ_{rad} are parametrized in terms of three variables that span the unit cube, $X_{\mathrm{rad}} = \{X_{\mathrm{rad}}^{(1)}, X_{\mathrm{rad}}^{(2)}, X_{\mathrm{rad}}^{(3)}\}$, while the z variable is parametrized in term of a single variable $X_{\mathrm{rad}}^{(1)}$ that ranges between 0 and 1. We then define the $\tilde{B}$ function

$$\begin{aligned}
\tilde{B}_{q\bar{q}} &= B_{q\bar{q}}(\bar{\bar{\Phi}}_2) + V_{q\bar{q}}(\bar{\bar{\Phi}}_2) + \sum_{\oplus} \left[\left| \frac{\partial \Phi_{\mathrm{rad}}}{\partial X_{\mathrm{rad}}} \right| \left\{ R_{q\bar{q},g}^{\oplus}(\Phi_3) - C_{q\bar{q},g}^{\oplus}(\Phi_3) \right\} \right]_{\oplus}^{\bar{\Phi}_2} \\
&+ \left[\left| \frac{\partial \Phi_{\mathrm{rad}}}{\partial X_{\mathrm{rad}}} \right| \left\{ R_{g\bar{q},q}(\Phi_3) - C_{g\bar{q},q}(\Phi_3) \right\} \right]_{\oplus}^{\bar{\Phi}_2} \\
&+ \left[\left| \frac{\partial \Phi_{\mathrm{rad}}}{\partial X_{\mathrm{rad}}} \right| \left\{ R_{qg,\bar{q}}(\Phi_3) - C_{qg,\bar{q}}(\Phi_3) \right\} \right]_{\ominus}^{\bar{\Phi}_2} \\
&+ \left[\frac{1}{z} \frac{\partial z}{\partial X_{\mathrm{rad}}^{(1)}} \left\{ G_{\oplus}^{q\bar{q},g}(\Phi_{2,\oplus}) + G_{\oplus}^{g\bar{q},q}(\Phi_{2,\oplus}) \right\} \right]_{\oplus}^{\bar{\Phi}_2} \\
&+ \left[\frac{1}{z} \frac{\partial z}{\partial X_{\mathrm{rad}}^{(1)}} \left\{ G_{\ominus}^{q\bar{q},g}(\Phi_{2,\ominus}) + G_{\ominus}^{qg,\bar{q}}(\Phi_{2,\ominus}) \right\} \right]_{\ominus}^{\bar{\Phi}_2}
\end{aligned}$$

$$(4.39)$$

so that defining $\tilde{B} = \sum_{q\bar{q}} \tilde{B}_{q\bar{q}}$, we have

$$\bar{B} = \int d^3 X_{\mathrm{rad}} \, \tilde{B} . \tag{4.40}$$

In practice, the $\tilde{B}$ function is integrated numerically over all $\bar{\bar{\Phi}}_2, X_{\mathrm{rad}}$ integration variables, using an integration program that can generate the set of kinematic variables

$\bar{\boldsymbol{\Phi}}_2, X_{\mathrm{rad}}$, with a probability proportional to $d\bar{\boldsymbol{\Phi}}_2 \, d^3 X_{\mathrm{rad}} \, \tilde{B}$ in the $d\bar{\boldsymbol{\Phi}}_2 \, d^3 X_{\mathrm{rad}}$ kinematic cell (see, for example, refs. [76, 77]). Once the $\bar{\boldsymbol{\Phi}}_2, X_{\mathrm{rad}}$ point is generated, the flavour $q\bar{q}$ is chosen with a probability proportional to the value of $\tilde{B}_{q\bar{q}}$ at that specific $\bar{\boldsymbol{\Phi}}_2, X_{\mathrm{rad}}$ point. At this stage, the radiation variables are disregarded, and only the underlying Born ones are kept. This corresponds to integrate over the radiation variables.

4.3.2   Generation of the radiation variables

Radiation kinematics is instead generated using the POWHEG Sudakov form factor

$$\Delta^{q\bar{q}}(\bar{\boldsymbol{\Phi}}_2, p_{\mathrm{T}}) = \prod_{\oplus} \Delta^{q\bar{q}}_{\oplus} \, , \tag{4.41}$$

where

$$\Delta^{q\bar{q}}_{\oplus}(\bar{\boldsymbol{\Phi}}_2, p_{\mathrm{T}}) = \exp \left\{ - \left[\int d\Phi_{\mathrm{rad}} \, \frac{R^{\oplus}_{q\bar{q},g}(\boldsymbol{\Phi}_3) + R_{g\bar{q},q}(\boldsymbol{\Phi}_3)}{B_{q\bar{q}}(\bar{\boldsymbol{\Phi}}_2)} \, \theta \left(k_{\mathrm{T}}(\boldsymbol{\Phi}_3) - p_{\mathrm{T}} \right) \right]_{\oplus}^{\bar{\boldsymbol{\Phi}}_2} \right\} , \tag{4.42}$$

$$\Delta^{q\bar{q}}_{\ominus}(\bar{\boldsymbol{\Phi}}_2, p_{\mathrm{T}}) = \exp \left\{ - \left[\int d\Phi_{\mathrm{rad}} \, \frac{R^{\ominus}_{q\bar{q},g}(\boldsymbol{\Phi}_3) + R_{qg,\bar{q}}(\boldsymbol{\Phi}_3)}{B_{q\bar{q}}(\bar{\boldsymbol{\Phi}}_2)} \, \theta \left(k_{\mathrm{T}}(\boldsymbol{\Phi}_3) - p_{\mathrm{T}} \right) \right]_{\ominus}^{\bar{\boldsymbol{\Phi}}_2} \right\} . \tag{4.43}$$

The function $k_T(\boldsymbol{\Phi}_3)$ measures the hardness of radiation in the real event. It is required to be of the order of the transverse momentum of the radiation in the collinear limit, and to become equal to it in the soft-collinear limit. In principle, the choice of $k_T(\boldsymbol{\Phi}_3)$ can differ in the two singular regions ($\oplus$ and $\ominus$) that we are considering. The choice adopted in the Examples section of ref. [30] had in fact this feature. We have found, however, that for practical reasons[3] it is better to adopt a different choice, namely to take $k_T(\boldsymbol{\Phi}_3)$ to coincide with that of eqs. (4.16) and (4.17).

The generation of radiation is performed individually for $\Delta^{q\bar{q}}_{\oplus}$ and $\Delta^{q\bar{q}}_{\ominus}$, and the highest generated k_T is retained. The upper bounding function for the application of

---

[3]The choice discussed in [30] is $k_T^2 = \bar{M}^2(1-x)v$, and is such that k_T^2 is always bound to be smaller than $\bar{M}^2$. Since the factorization and renormalization scales are taken equal to k_T, for vector-boson production at transverse momenta much larger than the vector-boson mass the coupling does not properly decrease.

the veto method is chosen to be[4]

$$\frac{R_{q\bar{q},g}^{\oplus} + R_{g\bar{q},q}}{B_{q\bar{q}}} \leq \frac{16\pi^2}{\bar{M}^2} N_{q\bar{q}}^{\oplus} \frac{\alpha_s(k_T^2)}{2v} \frac{x^2}{1 - x - v} , \tag{4.44}$$

and the analogous one for the $\ominus$ direction. The procedure used to generate radiation events according to this upper bounding function is described in Appendix C.3.

4.3.3 Born zeros

In the case of W production, we face the problem of vanishing underlying Born configurations, already discussed in sec. 3.3.5. The Born zero is associated to $\bar{\theta}_l = 0$ if q is an antiquark, and $\bar{\theta}_l = \pi$ if it is a quark. Hence, we choose to adopt the further separation advocated in eq. (3.59), taking

$$Z = \bar{M}^2 \left(1 + s_q \cos\bar{\theta}_l\right)^2 , \qquad H = k_T^2 , \tag{4.45}$$

with k_T^2 given by formula (4.17) and the factor s_q equals 1 for quarks, and -1 for antiquarks. The angle $\bar{\theta}_l$ is chosen according to the $\oplus$ parametrization (for $R^{\oplus}$) or the $\ominus$ parametrization (for $R^{\ominus}$) of the real-emission phase space.

In addition, all the R^{α_r} terms in eq. (4.38) are replaced by the corresponding $R^{\alpha_r,s}$ and the $R^{\alpha_r,r}$ terms are generated in a way similar to what was done for eq. (4.39), as illustrated in eq. (3.61). In this case, eq. (3.61) takes the form

$$\tilde{B}^r = \sum_{q\bar{q}} \tilde{B}_{q\bar{q}}^r = \sum_{q\bar{q}} \left\{ \left[\left| \frac{\partial\Phi_{\mathrm{rad}}}{\partial X_{\mathrm{rad}}} \right| R_{q\bar{q},g}^{\oplus,r}(\boldsymbol{\Phi}_3) \right]_{\oplus}^{\bar{\boldsymbol{\Phi}}_2} + \left[\left| \frac{\partial\Phi_{\mathrm{rad}}}{\partial X_{\mathrm{rad}}} \right| R_{q\bar{q},g}^{\ominus,r}(\boldsymbol{\Phi}_3) \right]_{\ominus}^{\bar{\boldsymbol{\Phi}}_2} \right.$$

$$\left. + \left[\left| \frac{\partial\Phi_{\mathrm{rad}}}{\partial X_{\mathrm{rad}}} \right| R_{g\bar{q},q}^r(\boldsymbol{\Phi}_3) \right]_{\oplus}^{\bar{\boldsymbol{\Phi}}_2} + \left[\left| \frac{\partial\Phi_{\mathrm{rad}}}{\partial X_{\mathrm{rad}}} \right| R_{qg,\bar{q}}^r(\boldsymbol{\Phi}_3) \right]_{\ominus}^{\bar{\boldsymbol{\Phi}}_2} \right\} , \tag{4.46}$$

At this point one integrates the previous formula over the whole $\bar{\boldsymbol{\Phi}}_2$, X_{rad} phase space with the same method used for $\tilde{B}$. As explained in sec. 3.3.5, one then chooses $\tilde{B}$ or $\tilde{B}^r$, with a probability proportional to their respective total integral. In case $\tilde{B}^r$ is chosen, one generates a kinematic configuration according to it. This kinematic configuration

---

[4]This upper bounding function differs from the ones of eqs. (7.163)–(7.166) in ref. [30], but is in fact equivalent to the bound of eq. (7.234) in the same reference, once the change of variables $\xi = 1 - x$, $y = (1 - 2v - x)/(1 - x)$ is performed, and the different definitions of $d\Phi_{\mathrm{rad}}$ are properly taken into account.

is a full 3-body configuration. The flavour $q\bar{q}$ is chosen with a probability proportional the the value of $\tilde{B}^r_{q\bar{q}}$ for the particular kinematic point that has been generated, and the event is sent to the output. In case $\tilde{B}$ is chosen, a kinematic configuration and an underlying Born flavour is chosen in the same way.

4.4 Results

The `MC@NLO` program provides an implementation of vector-boson production at the NLO level in a shower Monte Carlo framework. It should therefore be comparable to our calculation, and we thus begin by comparing `MC@NLO` and `POWHEG` distributions. In this comparison, the `POWHEG` code is interfaced to `HERWIG`, in order to minimize differences due to the subsequent shower in the two approaches. We choose as our default parton-density functions the CTEQ6M [81] package, and the corresponding value of Λ_{QCD}. The factorization and renormalization scales are taken equal to $M_V^2 + (p_T^V)^2$ in the calculation of the $\bar{B}$ function, where $V = W$ or Z. In the generation of radiation, the factorization and renormalization scales are taken equal to the transverse momentum of the vector boson V. We also account properly for the heavy-flavour thresholds, when the transverse momentum of the vector boson approaches the bottom and charm quark threshold. That is to say, when the renormalization scale crosses a heavy-flavour mass threshold, the QCD evolution of the running coupling is accordingly changed to the new number of active flavours. The other relevant parameters for our calculation are

M_z (GeV)	Γ_Z (GeV)	M_W (GeV)	Γ_W (GeV)	$\sin^2\theta_W^{\text{eff}}$	$\alpha_{\text{em}}^{-1}(M_Z)$
91.188	2.49	80.419	2.124	0.23113	127.934

The above values of masses and widths are used in eqs. (4.24) and (4.25). The W and Z couplings are given by

$$g = \frac{e}{\sin\theta_W^{\text{eff}}}, \quad g_{l/q} = \frac{e}{\sin\theta_W^{\text{eff}}\cos\theta_W^{\text{eff}}}\left[T_3^{(l/q)} - q_{l/q}\sin^2\theta_W^{\text{eff}}\right], \quad e = \sqrt{4\pi\alpha_{\text{em}}(M_Z)},$$

(4.47)

where l/q denotes the given left or right component of a lepton or a quark. For W production we used the following absolute values for the CKM matrix elements

ud	us	ub	cd	cs	cb	td	ts	tb
0.9748	0.2225	0.0036	0.2225	0.9740	0.041	0.009	0.0405	0.9992

.

In all figures shown in the following we do not impose any acceptance cut.

4.4.1 Z production at the Tevatron

In fig. 4.1 we show a comparison of the lepton transverse momentum and rapidity, and of the transverse momentum of the reconstructed lepton-antilepton pair at the Tevatron. We notice a larger cross section in POWHEG, when the Z transverse momentum
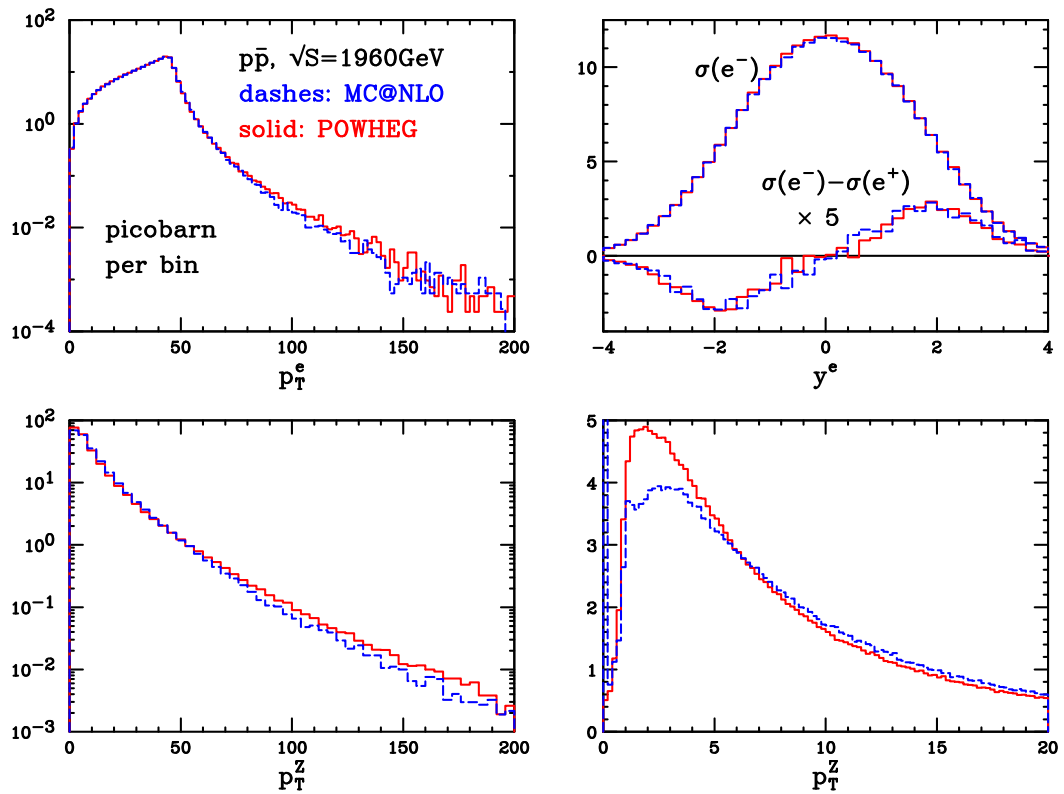
Figure 4.1: *Comparison between* POWHEG *and* MC@NLO *results for the transverse momentum and rapidity of the lepton coming from the decay of the Z boson, and for the transverse momentum of the Z, as reconstructed from its decay products. The lepton-rapidity asymmetry is also shown. Plots done for the Tevatron $p\bar{p}$ collider.*

becomes large. This is not unexpected, since for large momenta the POWHEG result

is larger than the standard NLO result by a factor $\bar{B}/B$ (this feature has also some impact upon the transverse-momentum distribution of the lepton). Once this fact is accounted for, the transverse-momentum distribution of the Z is in fair agreement, although we find observable shape differences at low transverse momenta. We also notice a peak at $p_T = 0$ in the `MC@NLO` distribution, that is not present in the `POWHEG` result. We expect this distribution to be affected by low transverse-momentum power-suppressed effects. In fact, the peak at zero transverse momentum in `MC@NLO` disappears if the primordial transverse momentum of the partons (the `PTRMS` variable in `HERWIG`) is set to a non-zero value. In fig. 4.2 we compare the rapidity distribution of the reconstructed Z, its invariant mass, the azimuthal distance of the e^+e^- pair coming from Z decays, and the transverse momentum of the radiated jet at the Tevatron. The jet is defined using the `SISCONE` algorithm [82] as implemented in the `FASTJET`
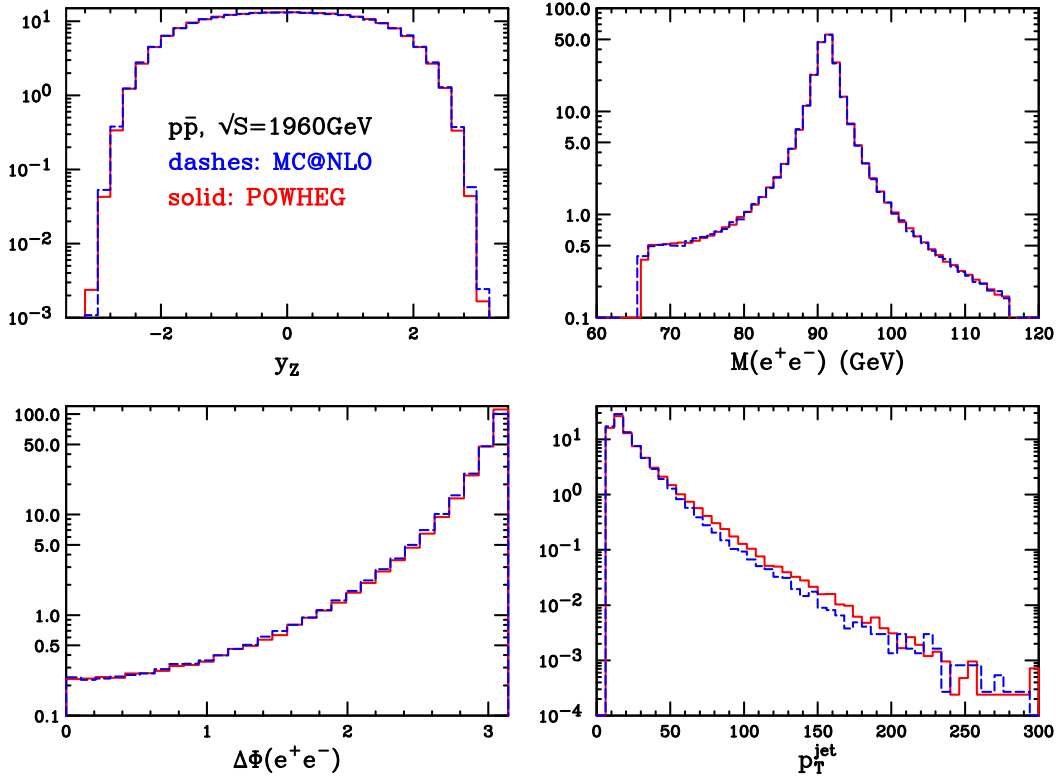
Figure 4.2: *Comparison between* `POWHEG` *and* `MC@NLO` *for the reconstructed* Z *rapidity, its invariant mass, the lepton-pair azimuthal distance and the transverse momentum of the reconstructed jet, above a 10 GeV minimum value.*

package [83], using $R = 0.7$. We find again fair agreement.

In ref. [73], a discrepancy was found in the rapidity distribution of the hardest

radiated jet as computed in `MC@NLO` and `ALPGEN`, for the case of top pair production at the Tevatron. The `MC@NLO` calculation shows there a dip at zero rapidity, not present in `ALPGEN`. In fact, the `POWHEG` calculation of this quantity does not display any dip. We thus examine the transverse momentum of the radiated jet in this case. Furthermore, we also plot the rapidity difference between the Z and the hardest radiated jet. The results are displayed in fig. 4.3. We have chosen different cuts for
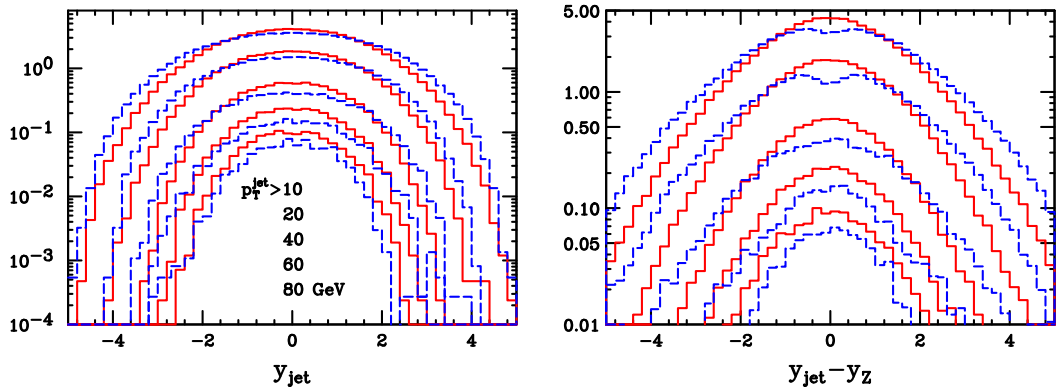
Figure 4.3: *Rapidity distribution of the hardest jet with different transverse-momentum cuts, and the rapidity distance between the hardest jet and the reconstructed Z boson.*

the minimum transverse momentum of the radiated jet, i.e. 10, 20, 40, 60 and 80 GeV. We observe noticeable differences in the rapidity distribution of the hardest jet in the two approaches. The `MC@NLO` result displays a dip at zero $y_{\text{jet}} - y_Z$.

In the following of this chapter, we limit ourselves to report results concerning rapidity distributions (and rapidity distribution differences) for the various processes and colliders under inspection, without entering into an explanation of the differences found between the `POWHEG` and `MC@NLO` results. A more accurate analysis and an explanation of these features is postponed to sec. 5.5, where we return to comment the relevant plots of this chapter and more comparisons, concerning also other processes implemented in the `POWHEG` and `MC@NLO` frameworks, are shown. Here, we only remark that these features may be attributed to effects beyond the NLO accuracy.

4.4.2 Z production at the LHC

Similar results are reported for the LHC in fig. 4.4 through 4.6. We notice less pronounced differences (with respect to the Tevatron case) in the p_T spectrum of the
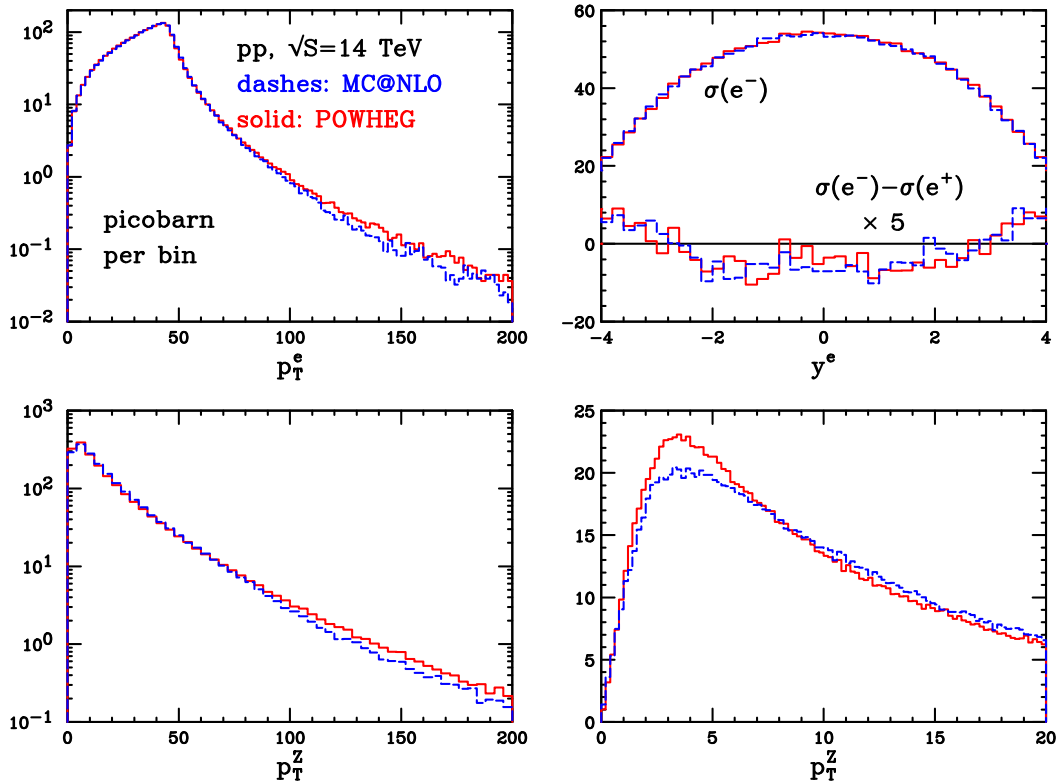
Figure 4.4: *Same as fig. 4.1 for the LHC at 14 TeV.*

Z boson. The discrepancy in the y_{jet} distribution is still evident, although the dip is barely noticeable in this case.

The same set of plots are also shown for a PYTHIA-POWHEG comparison in fig. 4.7 through 4.9. In this case the POWHEG code was interfaced with PYTHIA. Photon radiation from final-state leptons was switched off (MSTJ(41)=3), in order to simplify the analysis. Furthermore, the new transverse-momentum ordered shower was used (i.e the PYEVNW routine), since transverse-momentum ordering should be more appropriate in conjunction with POWHEG. In the plots, the PYTHIA output is normalized to the POWHEG total cross section. From fig. 4.7 through 4.8, we can see a remarkable agreement between the two calculations for the Tevatron results, the only visible discrepancy being given by the transverse-momentum distribution of the Z boson at small transverse momenta. We also notice that, unlike the case of the MC@NLO-POWHEG comparison, the transverse-momentum distribution of the Z is slightly harder in PYTHIA than in POWHEG. The rapidity distributions of the hardest jet are also in remarkable agreement.
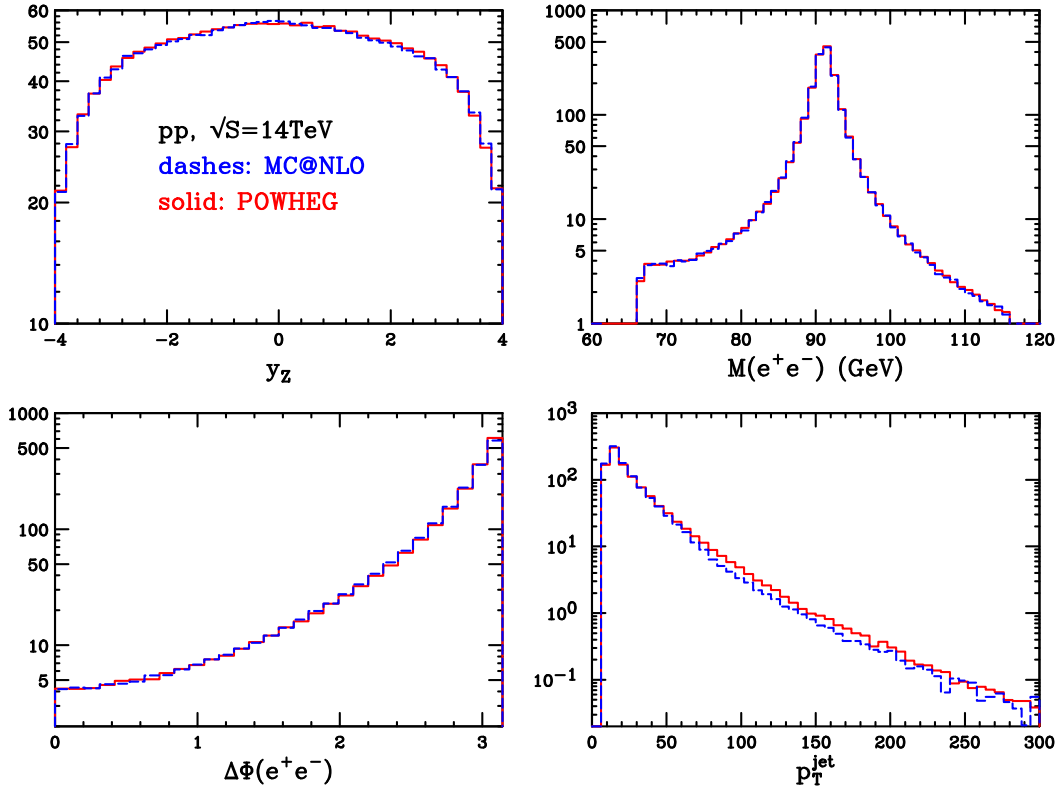
Figure 4.5: *Same as fig. 4.2 for the LHC at 14 TeV.*
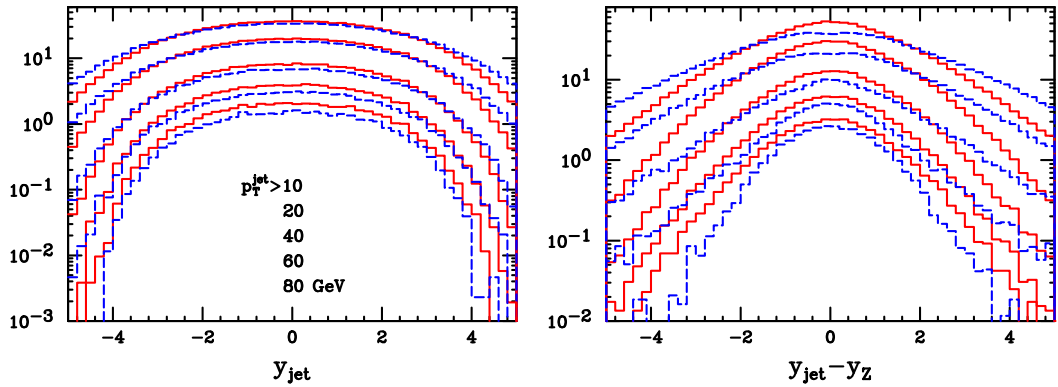
Figure 4.6: *Same as fig. 4.3 at the LHC at 14 TeV.*

In fig. 4.10 through 4.12, we carry out the same comparison in the LHC case. We notice here few important differences in the rapidity distribution of the Z boson, and, probably related to that, of the electron, the PYTHIA distribution being flatter in the central region. Both MC@NLO and POWHEG do not show this feature. As already pointed out in ref. [30], the generation of vector bosons in PYTHIA is not very different from the POWHEG generation. Radiation is generated with a very similar method [84, 53].
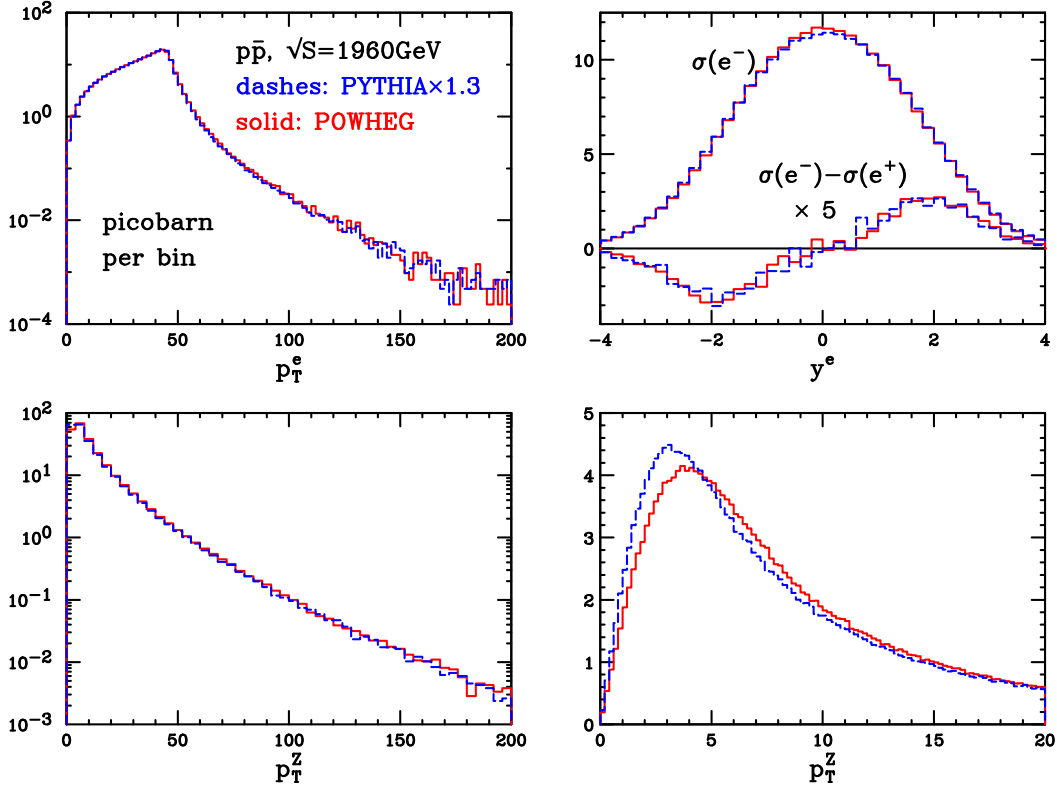
Figure 4.7: *Same as fig. 4.1 for a* PYTHIA *and* POWHEG *comparison at the Tevatron.*

There are however differences. In PYTHIA the Born inclusive cross section is used rather than our $\bar{B}$ function. Furthermore, our choice of scales is constrained by the requirement of next-to-leading logarithmic accuracy in the Sudakov form factor. The discrepancy in the transverse-momentum distribution of the Z may be due to different requirements for the choice of the scale in the generation of radiation in the two algorithms. The discrepancy in the rapidity distribution may be due to the lack of NLO corrections in PYTHIA, i.e. to the use of the Born cross section (rather than the $\bar{B}$ function) and LO parton densities. In fact, in fig. 3 of ref. [85], a comparison in the rapidity distribution of the Z at LO, NLO and NNLO, is shown for the LHC. One can notice from that figure that there is a difference in the LO and NLO shape of the distribution, the former being flatter. In order to elucidate this point, we show in fig. 4.13 the rapidity distribution of the Z boson computed at fixed order in QCD, at LO and NLO. With the LO calculation, we also show the result obtained using the same LO parton-distribution function (*pdf*) set used in PYTHIA, that is CTEQ5L [86].

The figure leads to the conclusion that the use of the LO parton-density set
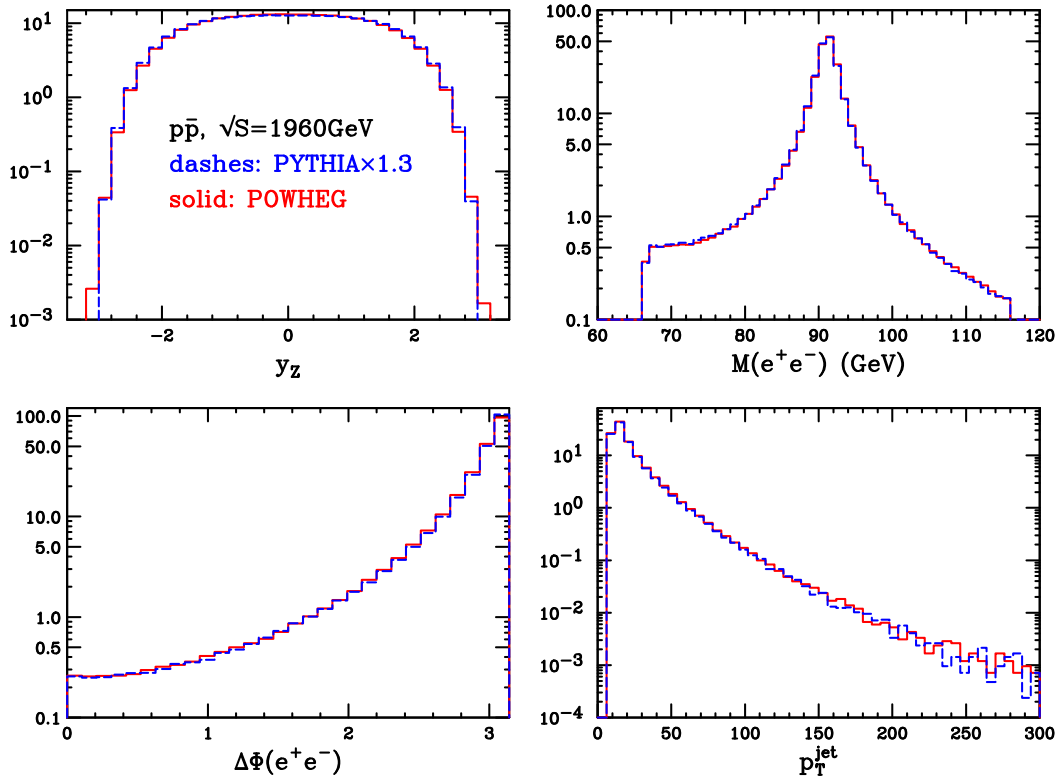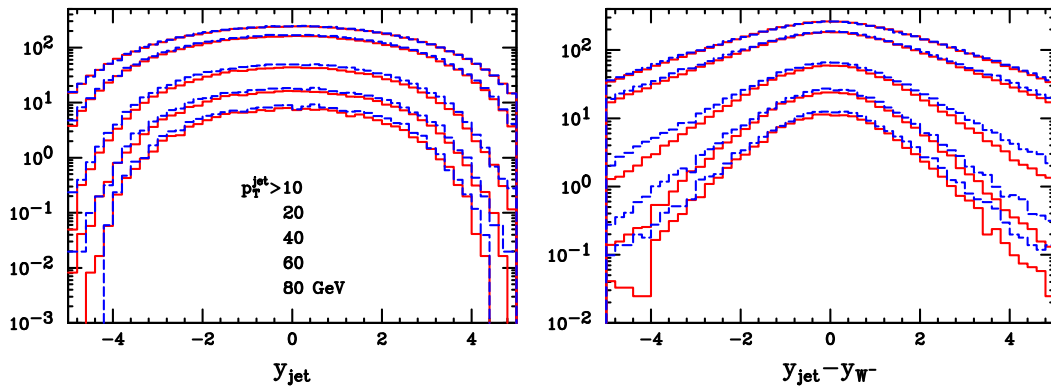
Figure 4.8: *Same as fig. 4.2 for a* PYTHIA *and* POWHEG *comparison at the Tevatron.*

CTEQ5L is the primary cause of this shape difference. We find, in fact, no difference in shape between the LO and NLO result if the same *pdf* set is used instead. We thus conclude that also the effect observed in fig. 3 of ref. [85] is due to the use of a LO parton-density set together with the LO result.[5]

The predictions for the transverse-momentum distribution of the Z boson are summarized in fig. 4.14, in comparison with data from ref. [87], at $\sqrt{S} = 1960$ GeV and from refs. [88, 89, 90] at $\sqrt{S} = 1800$ GeV. The POWHEG+HERWIG and the MC@NLO output are obtained with an intrinsic transverse momentum of the incoming partons equal to 2.5 GeV (HERWIG's PTRMS parameter). Both data and predictions are normalized to 1. The difference in the shape of the distributions at 1960 and 1800 GeV are only minimal. We see that POWHEG with PYTHIA is in remarkable agreement with the MC@NLO result. On the other hand, standalone PYTHIA is closer to the output of POWHEG with HERWIG.

---

[5]Some authors do prefer to use LO parton-density functions in LO calculations, although, in our opinion, there are no compelling reasons to do so.
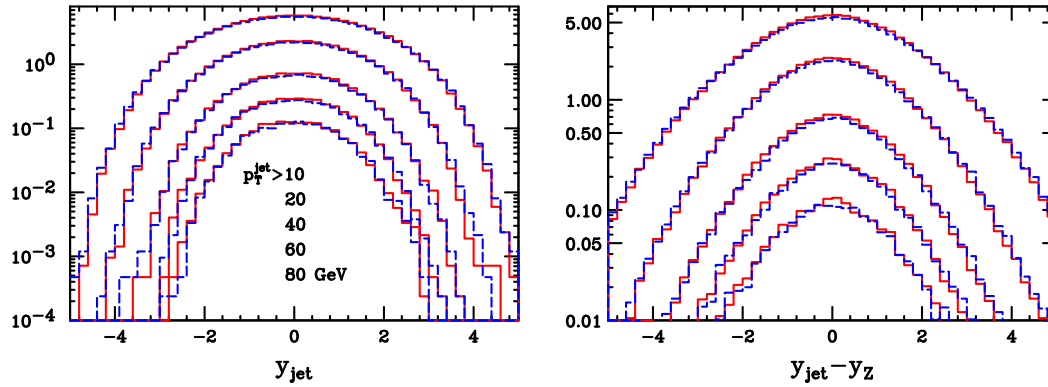
Figure 4.9: *Same as fig. 4.3 for a* PYTHIA *and* POWHEG *comparison at the Tevatron.*
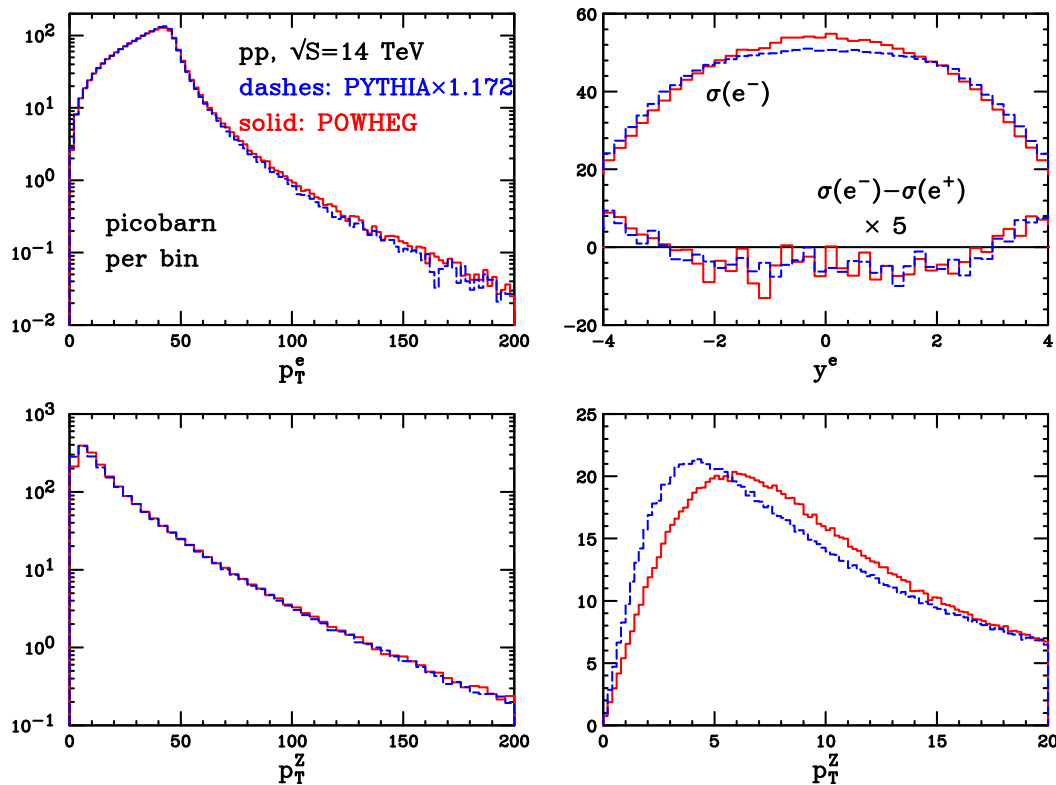
Figure 4.10: *Same as fig. 4.1 for a* PYTHIA *and* POWHEG *comparison at the LHC.*
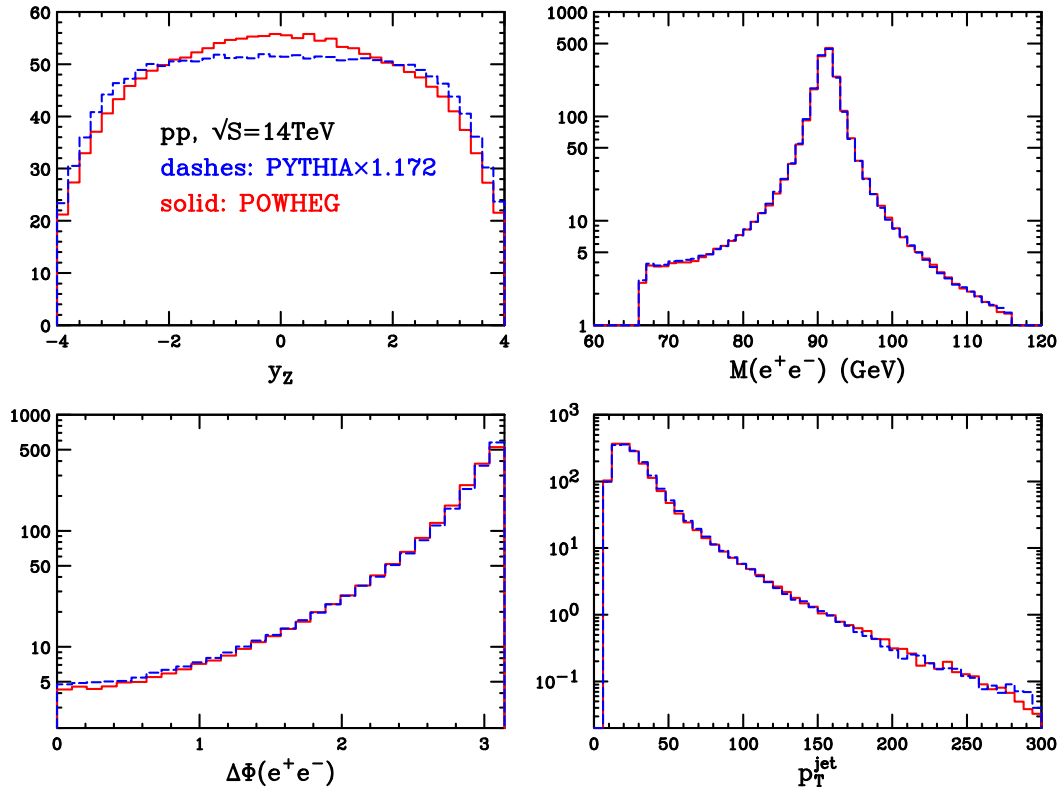
Figure 4.11: *Same as fig. 4.2 for a* PYTHIA *and* POWHEG *comparison at the LHC.*
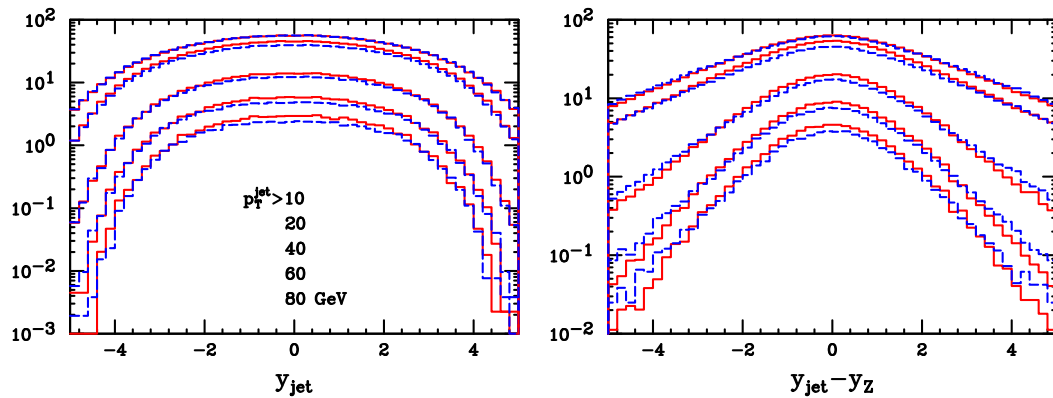
Figure 4.12: *Same as fig. 4.3 for a* PYTHIA *and* POWHEG *comparison at the LHC.*

In all cases, the agreement with data is not optimal. It is thus clear that this distributions is sensitive to long distance effects like hadronization and transverse-momentum smearing, and good agreement with data may only achieved by suitable tuning of the non-perturbative parameters of the shower Monte Carlo.
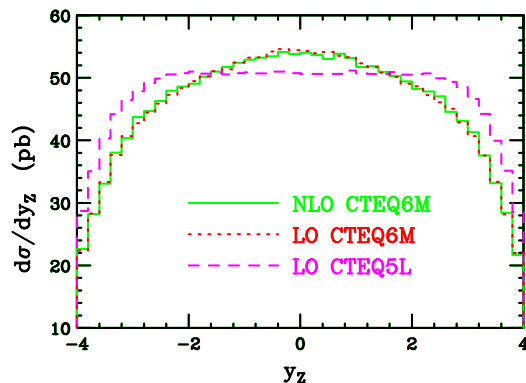
Figure 4.13: *Rapidity distribution for the Z boson, computed at fixed order at LO and NLO. For the LO result, both the CTEQ6M and the CTEQ5L parton-density set were used. The plots are normalized to the NLO total cross section.*
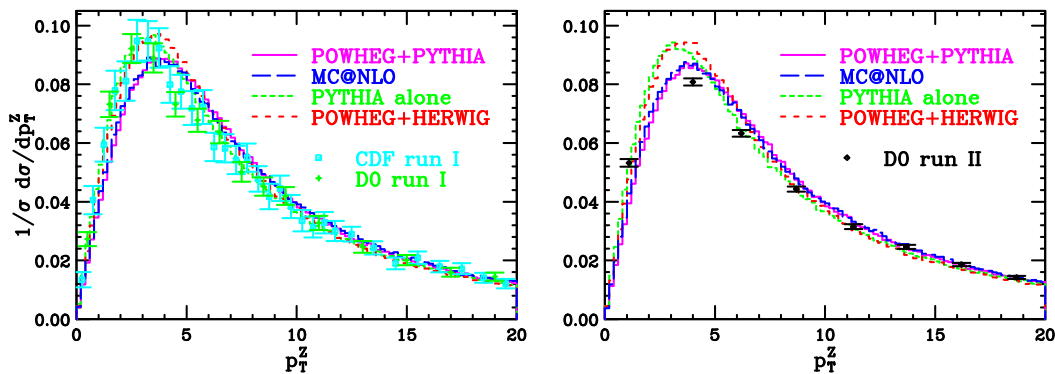
Figure 4.14: *Comparison of transverse-momentum distributions of the Z bosons with data from the Tevatron.*

4.4.3 W production at the Tevatron and LHC

All results presented so far are relative to Z boson production. In the case of W production we find similar features and the comparison between `MC@NLO` and `PYTHIA` presents very similar characteristics. For the sake of completeness, we present in fig. 4.15 through 4.32 plots of observables for W^- production at the Tevatron, and W^- and W^+ production at the LHC, comparing again the `POWHEG` output with `MC@NLO` and `PYTHIA`, and the observables for W^+ production at the LHC. We find again that `MC@NLO` displays dips in the rapidity distribution of the hardest jet at Tevatron energy. The comparison of the transverse-momentum distribution of the W shows the same differences found in the Z case. Furthermore, the rapidity distribution of the $W^\pm$ at the LHC differs in `PYTHIA`, showing a very marked difference in the W^+ case (see fig. 4.31), probably (as in the Z case) a consequence of the different *pdf* set.
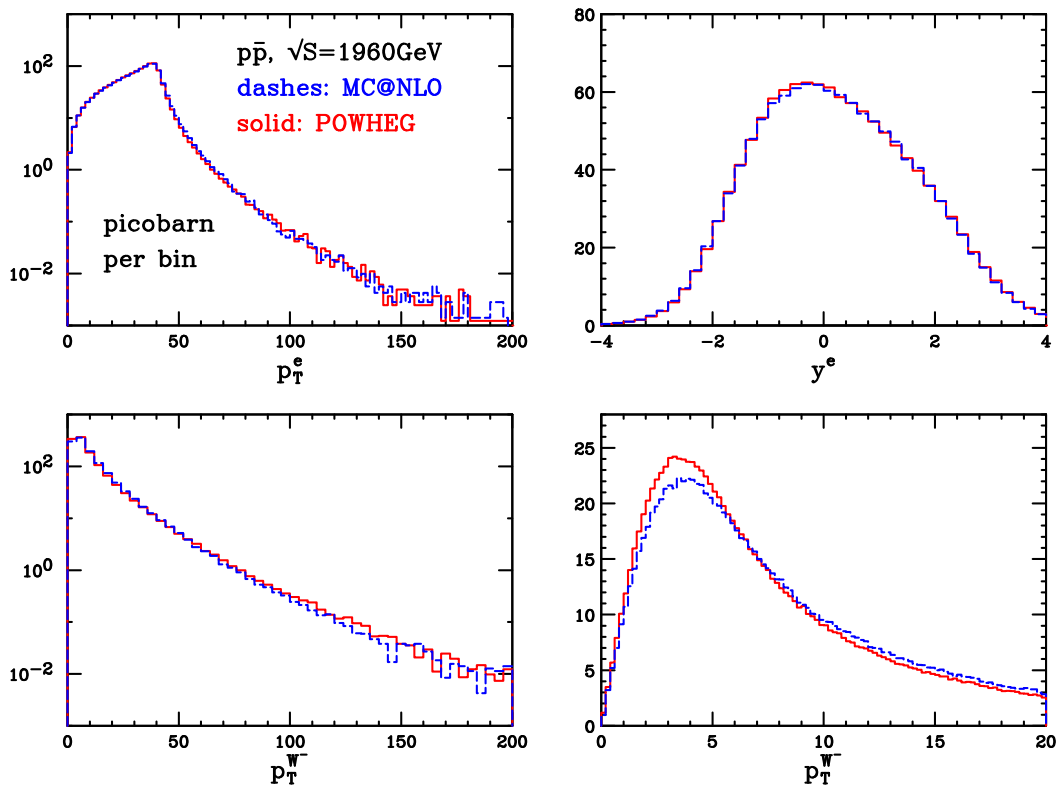
Figure 4.15: *Comparison of* `POWHEG` *and* `MC@NLO` *results for the transverse momentum and rapidity of the lepton coming from the decay of the W^- boson and for the transverse momentum of the W^-, as reconstructed from its decay product.*
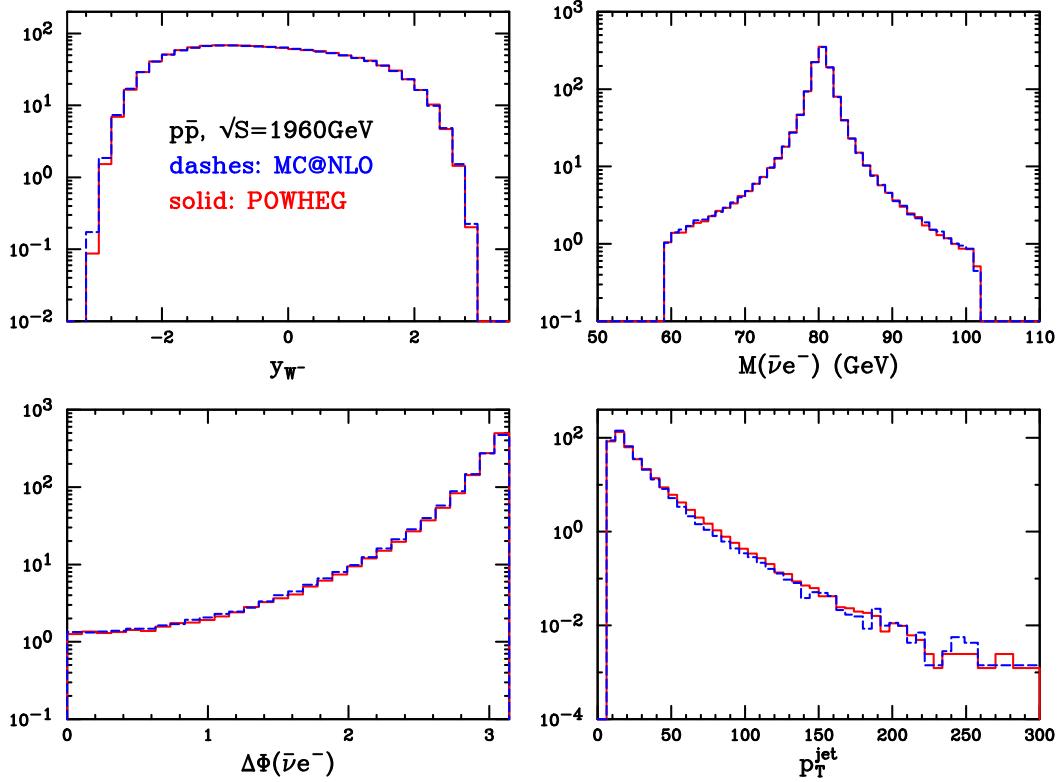
Figure 4.16: *Comparison of* `POWHEG` *and* `MC@NLO` *for the reconstructed* W^- *rapidity, its invariant mass, the lepton-pair azimuthal distance and the transverse momentum of the reconstructed jet, above a 10 GeV minimum value.*
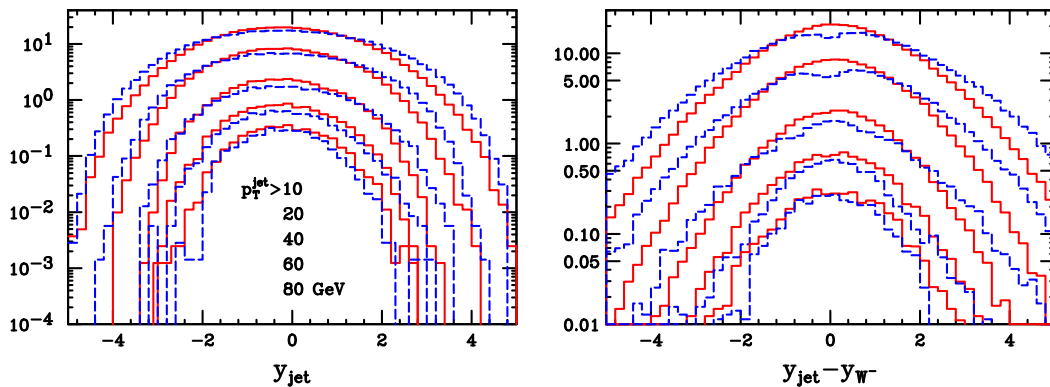
Figure 4.17: *Rapidity distribution of the hardest jet with different transverse-momentum cuts, and the rapidity distance between the hardest jet and the reconstructed* W^- *boson for* `POWHEG` *and* `MC@NLO` *at the Tevatron.*
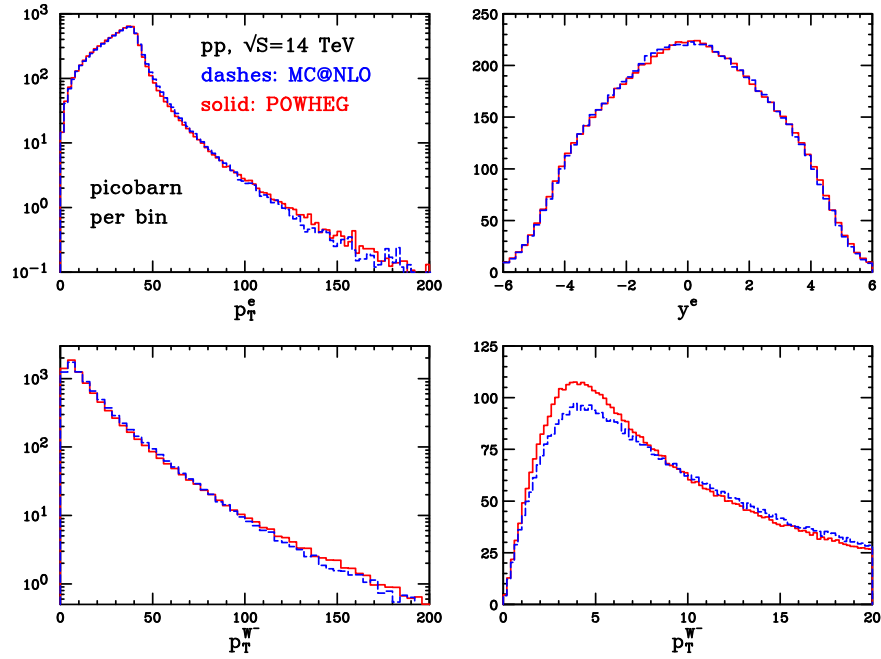
Figure 4.18: *Same as fig. 4.15 for the LHC at 14 TeV.*
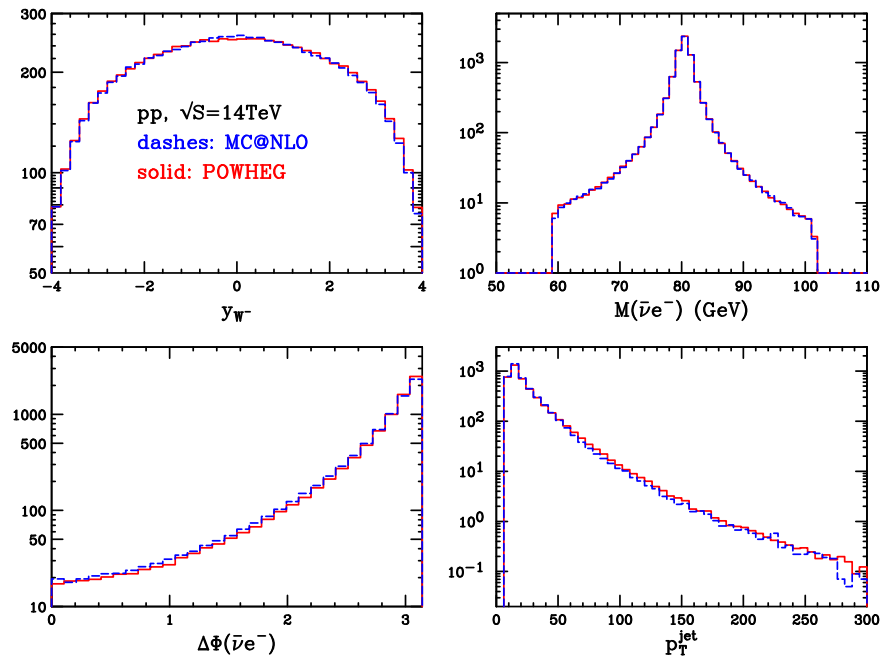
Figure 4.19: *Same as fig. 4.16 for the LHC at 14 TeV.*
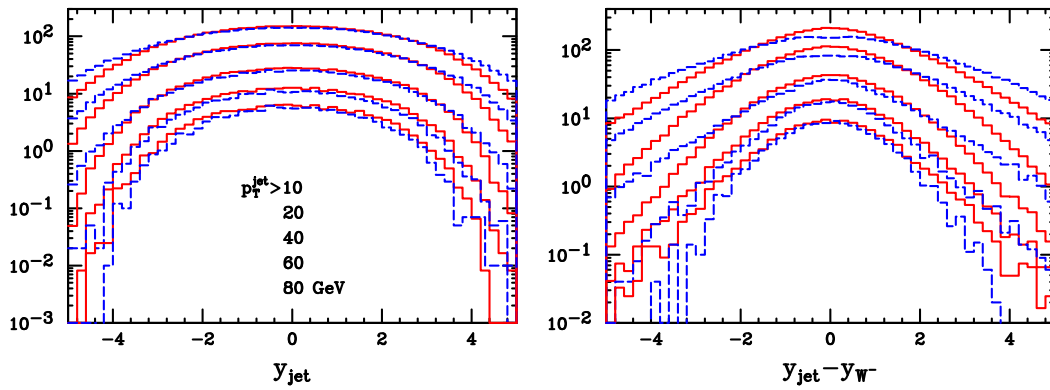
Figure 4.20: *Same as fig. 4.17 at the LHC at 14 TeV.*
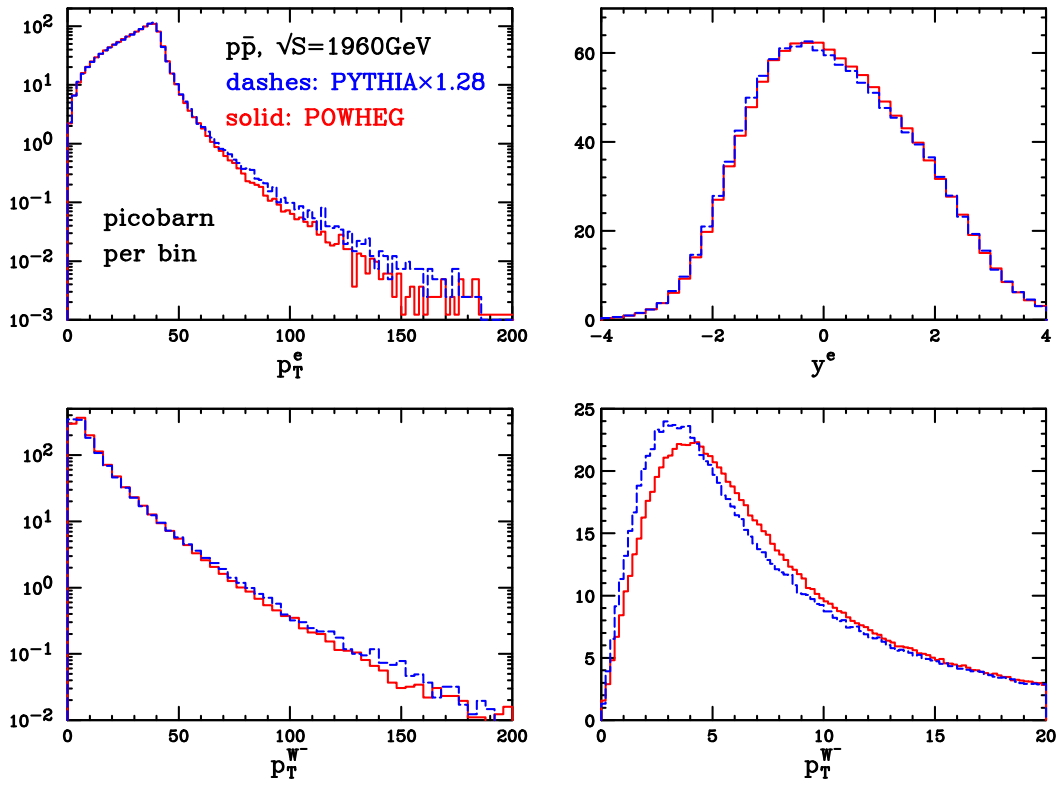
Figure 4.21: *Same as fig. 4.15 for a* PYTHIA *and* POWHEG *comparison at the Tevatron.*
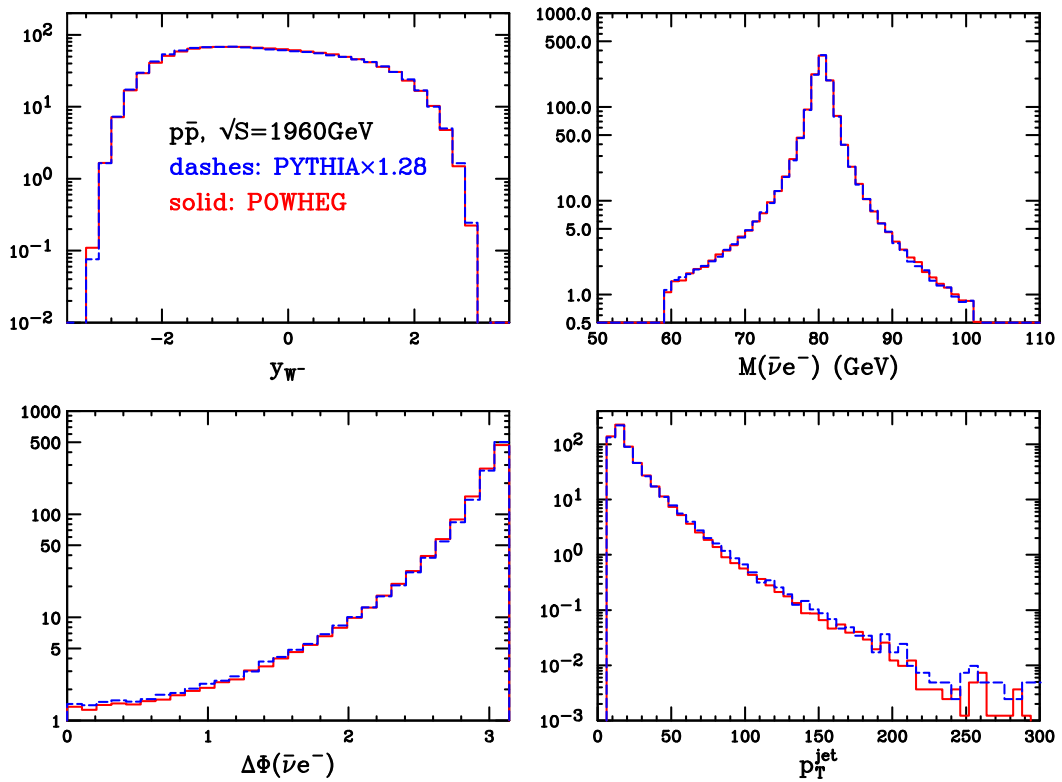
Figure 4.22: *Same as fig. 4.16 for a* PYTHIA *and* POWHEG *comparison at the Tevatron.*
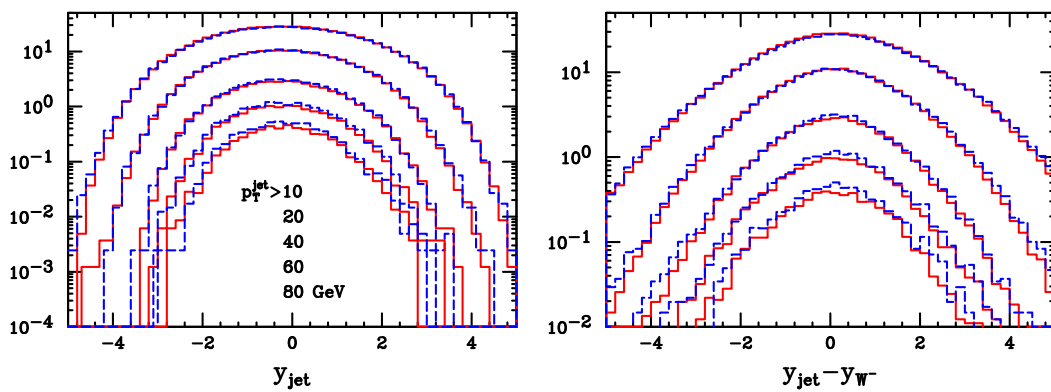
Figure 4.23: *Same as fig. 4.17 for a* PYTHIA *and* POWHEG *comparison at the Tevatron.*
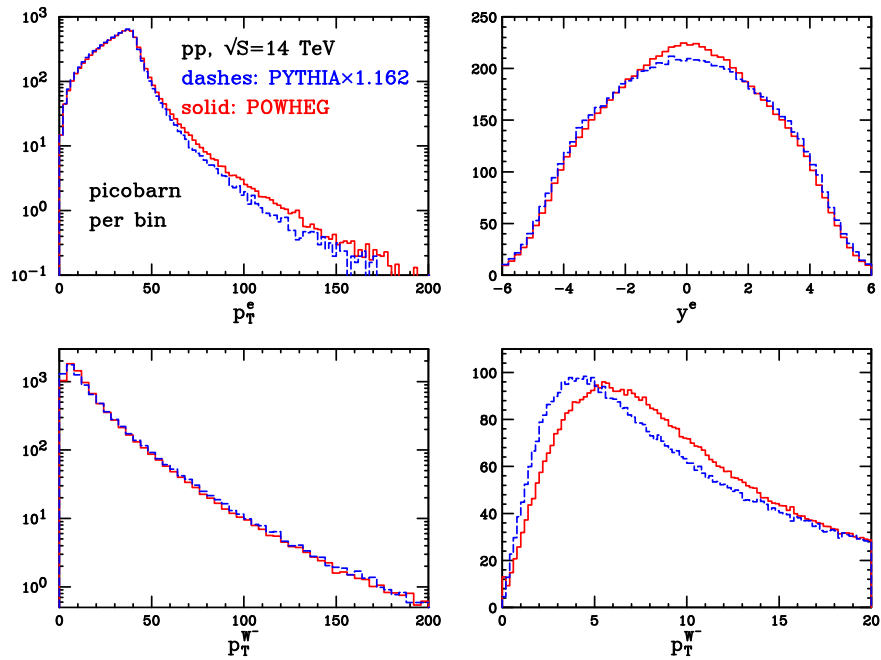
Figure 4.24: *Same as fig. 4.15 for a* `PYTHIA` *and* `POWHEG` *comparison at the LHC.*
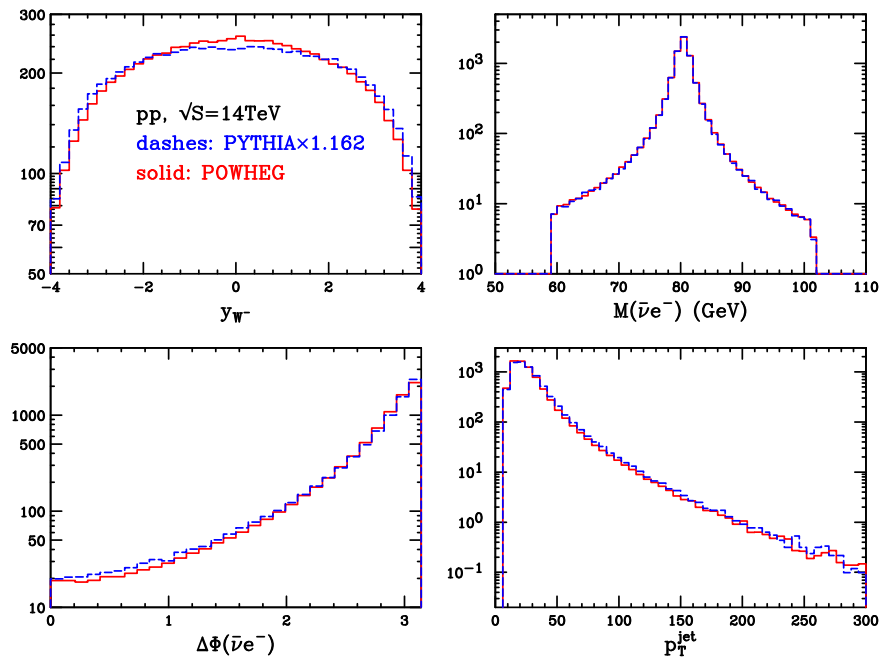
Figure 4.25: *Same as fig. 4.16 for a* `PYTHIA` *and* `POWHEG` *comparison at the LHC.*

Figure 4.26: *Same as fig. 4.17 for a* `PYTHIA` *and* `POWHEG` *comparison at the LHC*
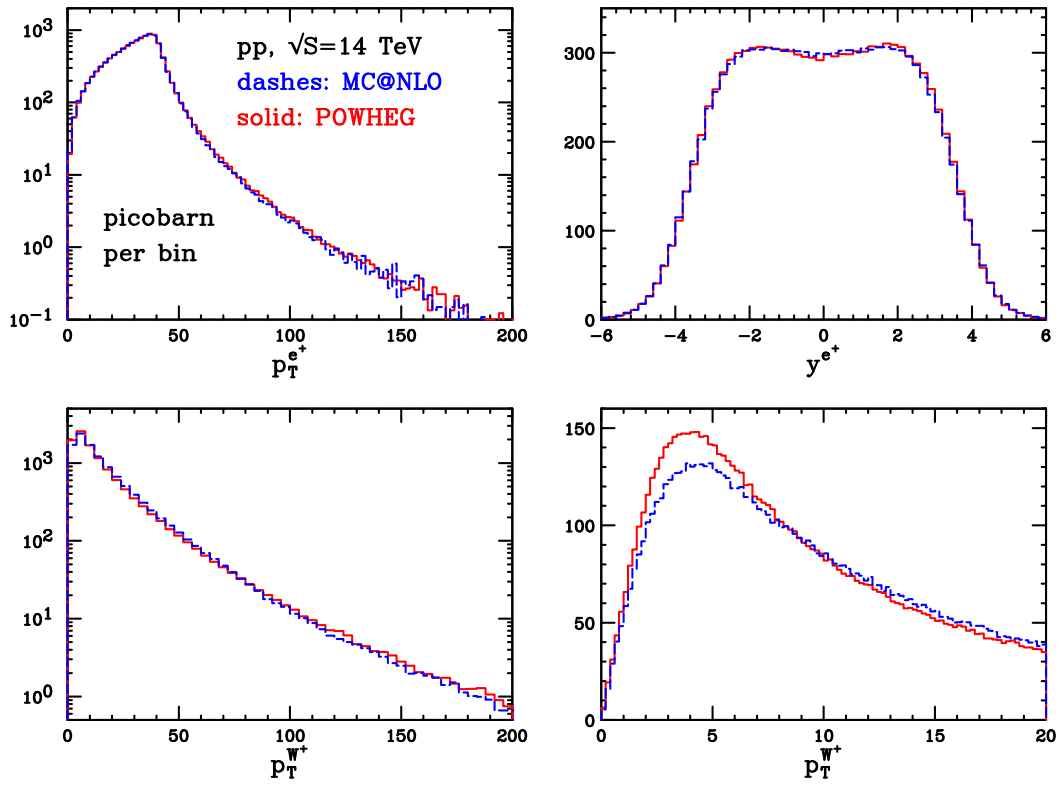
Figure 4.27: *Same as fig. 4.18 for W^+ production at the LHC.*
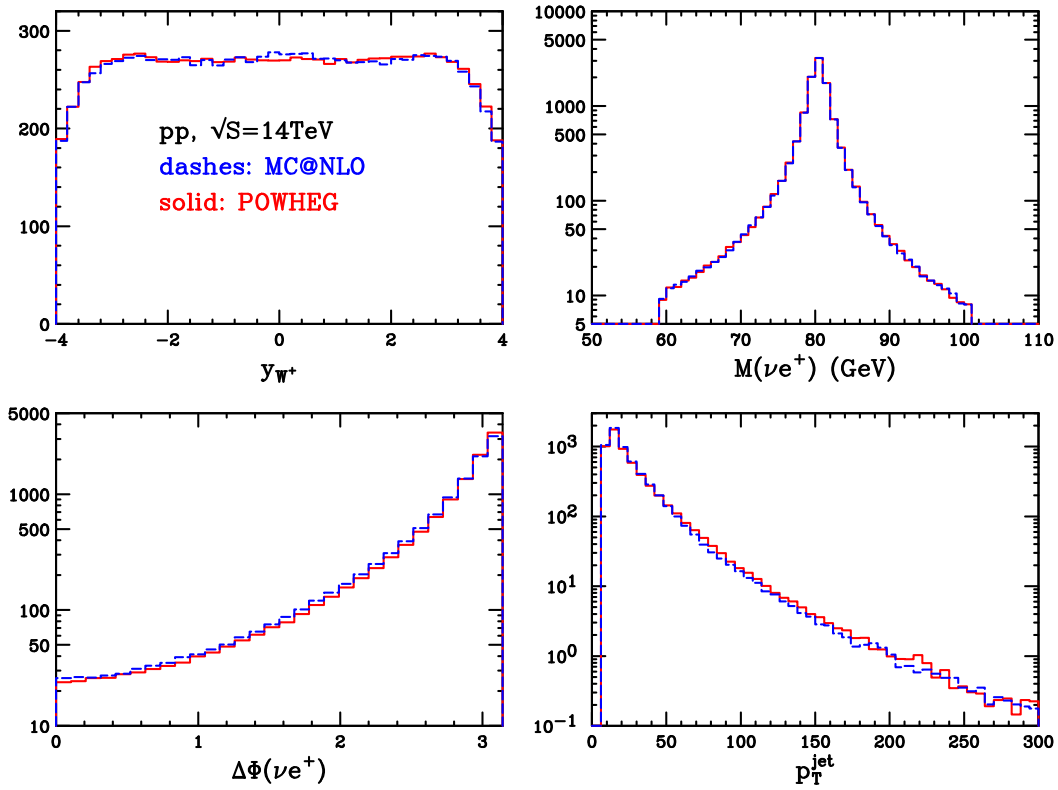
Figure 4.28: *Same as fig. 4.19 for W^+ production at the LHC.*
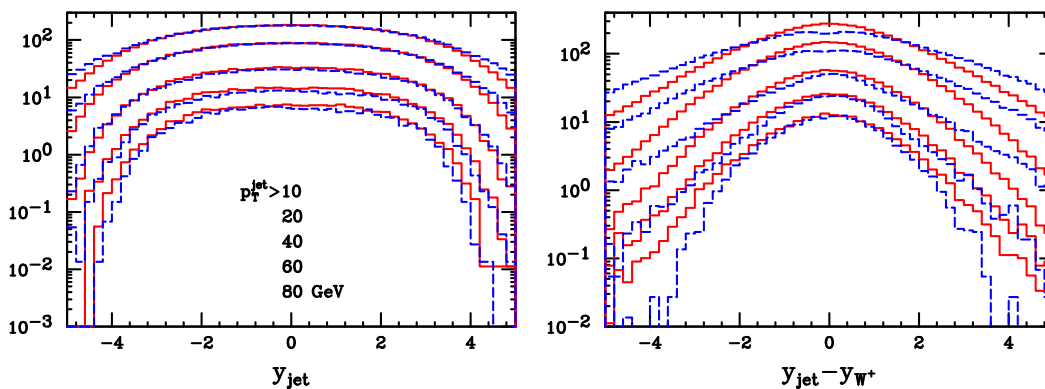
Figure 4.29: *Same as fig. 4.20 for W^+ production at the LHC.*
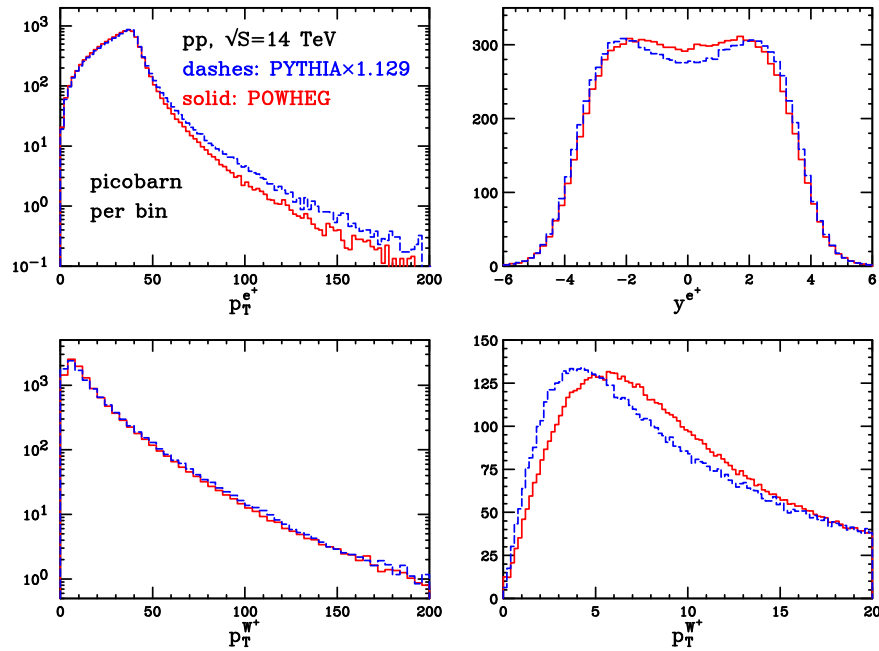
Figure 4.30: *Same as fig. 4.24 for W^+ production at the LHC.*
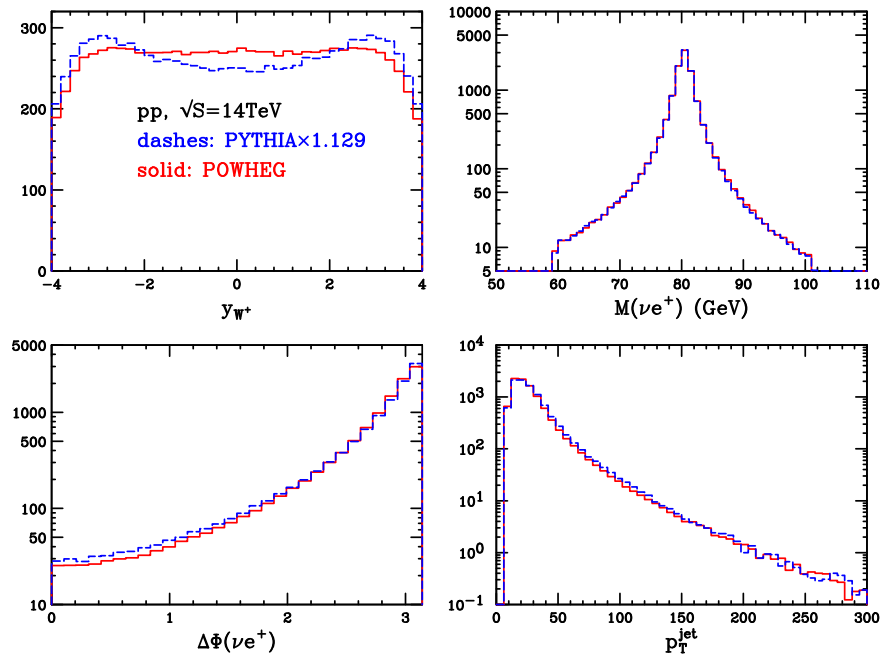
Figure 4.31: *Same as fig. 4.25 for W^+ production at the LHC.*
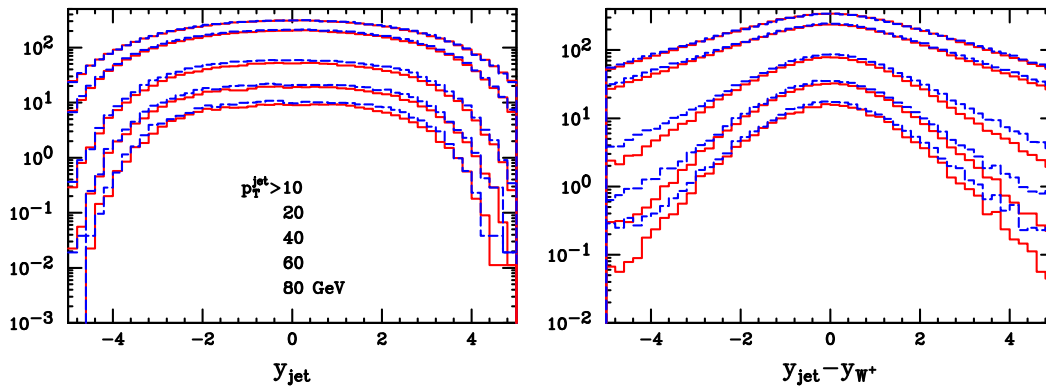
Figure 4.32: *Same as fig. 4.26 for W^+ production at the LHC.*

4.5   Conclusions

In this chapter we have reported on a complete implementation of vector-boson production at NLO in the POWHEG framework, following the work published in ref. [34]. The calculation was performed within the Catani-Seymour [31] dipole approach. To the best of our knowledge, this is the only POWHEG implementation within the Catani-Seymour framework at a hadronic collider. We have found that, at variance with what was proposed in sec. 7.3 of ref. [30], it is better to define the transverse momentum as the true transverse momentum for the initial-state singular region. Furthermore, we have shown how to perform a POWHEG implementation when the Born term vanishes.

The results of our work have been compared extensively with MC@NLO and PYTHIA. The PYTHIA result, rescaled to the full NLO cross section, is in good agreement with POWHEG, except for differences in the rapidity distribution of the vector boson, that may be ascribed to the use of a LO parton density in PYTHIA. The MC@NLO result is in fair agreement with POWHEG, except for the distribution of the hardest jet in the process, the MC@NLO distribution being generally wider. Furthermore, we have also examined the distributions in the difference of the hardest jet and the vector-boson rapidity. In the MC@NLO case, we have found that these distributions exhibit dips at zero rapidity, that POWHEG results do not show. We remark however that this differences may be ascribed to effect beyond the NLO accuracy, as we will show in sec. 5.5.

Higgs Boson Production

5.1 Introduction

In this chapter we present an implementation of the Higgs boson production via gluon fusion in the `POWHEG` framework, using the FKS subtraction formalism. Its content is based on the work published in ref. [37], with minor modifications.

Gluon fusion is the dominant Higgs boson production mechanism both at the Tevatron and at the LHC. Radiative corrections to this process are known to be large [91, 92, 93], and it is thus important that shower generators that do include them are made available to the experimental collaborations. In fact, one such generator already exists, namely the `MC@NLO` implementation [2] of Higgs boson production.

In the present chapter we describe a next-to-leading order (NLO) calculation of Higgs boson production via gluon fusion, interfaced to shower Monte Carlo programs according to the `POWHEG` method. We remark that, unlike the `MC@NLO` implementation, `POWHEG` produces events with positive (constant) weight, and, furthermore, it is not tied to the `HERWIG` shower Monte Carlo program. It can be easily interfaced to any modern shower generator and, in fact, we show results of `POWHEG` interfaced to `HERWIG` and to `PYTHIA`.

Much of the phenomenological section will be devoted to study the comparison of our result with that of `MC@NLO`. We find fair agreement between `MC@NLO` and `POWHEG` results, except for the p_{T} distribution of the Higgs boson, and consequently of the hardest jet, in the high-p_{T} region. In this region, the `POWHEG` distributions are generally harder. We show that this is due to next-to-next-to-leading order (NNLO) effects in the `POWHEG` formula for the differential cross section. We checked that these effects

actually bring our result closer to the NNLO one [94]. Other relevant discrepancies are found in the rapidity difference of the Higgs boson and the hardest jet. The dip produced by the `MC@NLO` program, found in previous implementations [26, 27, 34], is present also here. We remark that this seems to be a general feature of `MC@NLO`, since other calculations do not find effects of this kind [73, 95, 96].

The chapter is organized as follows. In sec. 5.2 we describe how we performed the calculation for the Higgs boson cross section at the next-to-leading order. In sec. 5.3 we discuss the `POWHEG` implementation. In sec. 5.4 we show our results for several kinematic variables and compare them with the `MC@NLO` [2] and `PYTHIA` 6.4 [22] shower Monte Carlo programs. In particular, a comparison with next-to-next-to-leading order results and a study on how the reduction of real contributions entering the Sudakov form factor, advocated in sec. 3.3.5, may be performed in the case at hand is presented in sec. 5.6. Differences in rapidity distributions between `POWHEG` and `MC@NLO`, already found in previous implementations, are further discussed in sec. 5.5, where a general explanation of these features of the `MC@NLO` approach is presented. In sec. 5.7 a comparison of our results with analytical resummed ones is also carried out. Then we address the renormalization and factorization scales dependence issue in sec. 5.8. Finally, in sec. 5.9, we give our conclusions.

5.2   Description of the calculation

In this section we fix our kinematic notation, and give the Higgs boson production differential cross sections up to next-to-leading order in the strong coupling $\alpha_{\rm s}$.

5.2.1   Kinematics

Born kinematics

The Born process has a single partonic contribution, $gg \to H$. Following the notation of sec. 1.2.1, we denote with $\bar{k}_\oplus$ and $\bar{k}_\ominus$ the incoming gluon momenta, aligned along the plus and minus direction of the z axis, and by $\bar{k}_1$ the outgoing Higgs boson

momentum. If $K_\oplus$ and $K_\ominus$ are the momenta of the incoming hadrons, then we have

$$\bar{k}_\oplus = \bar{x}_\oplus K_\oplus \,, \tag{5.1}$$

where $\bar{x}_\oplus$ are the momentum fractions, and momentum conservation reads

$$\bar{k}_\oplus + \bar{k}_\ominus = \bar{k}_1 \,. \tag{5.2}$$

We introduce the Higgs boson invariant mass squared and rapidity

$$\bar{M}^2 = \bar{k}_1^2, \qquad \bar{Y} = \frac{1}{2} \log \frac{\bar{k}_1^0 + \bar{k}_1^3}{\bar{k}_1^0 - \bar{k}_1^3} \,, \tag{5.3}$$

so that the set of variables $\bar{\bar{\Phi}}_1 \equiv \{\bar{M}^2, \bar{Y}\}$ fully parametrizes the Born kinematics. From them, we can reconstruct the momentum fractions

$$\bar{x}_\oplus = \sqrt{\frac{\bar{M}^2}{S}} e^{\bar{Y}}, \qquad \bar{x}_\ominus = \sqrt{\frac{\bar{M}^2}{S}} e^{-\bar{Y}}, \tag{5.4}$$

where $S = (K_\oplus + K_\ominus)^2$ is the squared center-of-mass energy of the hadronic collider. The Born phase space, in terms of these variables, can be written as

$$d\bar{\bar{\Phi}}_1 = d\bar{x}_\oplus \, d\bar{x}_\ominus (2\pi)^4 \delta^4(\bar{k}_\oplus + \bar{k}_\ominus - \bar{k}_1) \frac{d^3 \bar{k}_1}{(2\pi)^3 2 \bar{k}_1^0} = \frac{2\pi}{S} \delta(\bar{M}^2 - m_H^2) \, d\bar{M}^2 \, d\bar{Y} \,, \tag{5.5}$$

where m_H is the Higgs boson mass. We generate the Higgs boson virtuality according to a Breit-Wigner distribution, i.e. we make the replacement[1]

$$\delta(\bar{M}^2 - m_H^2) \rightarrow \frac{1}{\pi} \frac{\bar{M}^2 \, \Gamma_H / m_H}{(\bar{M}^2 - m_H^2)^2 + (\bar{M}^2 \, \Gamma_H / m_H)^2} \,. \tag{5.6}$$

The decay of the Higgs boson is left to the shower Monte Carlo program, since, being the Higgs boson a scalar, no spin correlation can arise.

Real-emission kinematics

The real emission processes have an additional final-state parton, so that momentum conservation reads

$$k_\oplus + k_\ominus = k_1 + k_2 \,, \tag{5.7}$$

---

[1] In order to compare our result with other programs, we have also used slightly different forms of the Breit-Wigner distribution, that will be illustrated in due time.

where k_1 is the Higgs boson momentum and k_2 is the momentum of the additional final-state parton in the laboratory frame and

$$k_\oplus = x_\oplus K_\oplus \, . \tag{5.8}$$

Since we regularize the infrared divergences in the Frixione, Kunszt and Signer (FKS) subtraction scheme [32, 33], we introduce the appropriate set of radiation variables. In the partonic center-of-mass frame, the final-state parton has momentum

$$k_2' = k_2'^0 \, (1, \sin\theta\sin\phi, \sin\theta\cos\phi, \cos\theta), \tag{5.9}$$

and we use the set $\Phi_{\rm rad} \equiv \{\xi, y, \phi\}$ as radiation variables, where

$$k_2'^0 = \frac{\sqrt{s}}{2}\xi, \qquad y = \cos\theta \, , \tag{5.10}$$

and

$$s = (k_\oplus + k_\ominus)^2 = \frac{\bar{M}^2}{1-\xi} \tag{5.11}$$

is the partonic center-of-mass energy squared. Since there are no final-state coloured partons at the Born level, we have to deal with initial-state singularities only. The soft singularity is characterized by $\xi \to 0$, while the collinear limits (k_2 parallel to the $\oplus$ or $\ominus$ incoming directions) are characterized by $y \to 1$ and $y \to -1$ respectively.

Inverse construction

The set of variables $\Phi_2 \equiv \left\{\bar{M}^2, \bar{Y}, \xi, y, \phi\right\}$ fully specifies the real-emission kinematics. In fact, given these variables, we can reconstruct all the momenta. Using eq. (5.4), we can compute the underlying Born momentum fractions $\bar{x}_\oplus$ and, following sec. 5 of ref [30], we have

$$x_\oplus = \frac{\bar{x}_\oplus}{\sqrt{1-\xi}}\sqrt{\frac{2-\xi(1-y)}{2-\xi(1+y)}}, \qquad x_\ominus = \frac{\bar{x}_\ominus}{\sqrt{1-\xi}}\sqrt{\frac{2-\xi(1+y)}{2-\xi(1-y)}}, \tag{5.12}$$

with the kinematics constraints

$$0 \le \xi \le \xi_{\rm M}(y) \, , \tag{5.13}$$

where

$$\xi_{\rm M}(y) = 1 - \max \left\{ \frac{2(1+y)\,\bar{x}_\oplus^2}{\sqrt{(1+\bar{x}_\oplus^2)^2(1-y)^2 + 16\,y\,\bar{x}_\oplus^2} + (1-y)(1-\bar{x}_\oplus^2)}, \right.$$
$$\left. \frac{2(1-y)\,\bar{x}_\ominus^2}{\sqrt{(1+\bar{x}_\ominus^2)^2(1+y)^2 - 16\,y\,\bar{x}_\ominus^2} + (1+y)(1-\bar{x}_\ominus^2)} \right\} . \tag{5.14}$$

The momentum of the final-state parton in the partonic center-of-mass frame is given by eqs. (5.9) and (5.10). We then make a longitudinal boost $\mathbb{B}_L$ from the center-of-mass frame back to the laboratory frame, with boost velocity

$$\beta = \frac{x_\oplus - x_\ominus}{x_\oplus + x_\ominus}\,, \tag{5.15}$$

to obtain k_2 from k_2'

$$k_2 = \mathbb{B}_L\,k_2'\,. \tag{5.16}$$

From momentum conservation, we reconstruct the Higgs boson momentum

$$k_1 = x_\oplus K_\oplus + x_\ominus K_\ominus - k_2\,. \tag{5.17}$$

Finally, the two-body phase space can be written in a factorized form in terms of the Born and radiation phase space

$$d\mathbf{\Phi}_2 = dx_\oplus\,dx_\ominus (2\pi)^4 \delta^4(k_\oplus + k_\ominus - k_1 - k_2)\frac{d^3k_1}{(2\pi)^3 2k_1^0}\frac{d^3k_2}{(2\pi)^3 2k_2^0} = d\bar{\bar{\mathbf{\Phi}}}_1\,d\Phi_{\text{rad}}\,, \tag{5.18}$$

where

$$d\Phi_{\text{rad}} = \frac{\bar{M}^2}{(4\pi)^3}\frac{\xi}{(1-\xi)^2}\,d\xi\,dy\,d\phi\,. \tag{5.19}$$

5.2.2 Cross sections

In order to apply the `POWHEG` method, we need the Born, real and virtual contributions to the differential cross section, i.e. the squared amplitudes, averaged over colours and helicities of the incoming partons, and multiplied by the appropriate flux factor.

Born contribution

At Born level, Higgs boson production via gluon fusion proceeds through the coupling of the Higgs boson to a heavy-quark loop. The squared matrix element for the lowest-order contribution, averaged over colours and helicities of the incoming gluons, and multiplied by the flux factor $1/(2\bar{M}^2)$, is given by

$$\mathcal{B}_{gg} = \frac{\alpha_s^2}{\pi^2}\frac{G_F\,\bar{M}^2}{576\,\sqrt{2}}\left|\frac{3}{2}\sum_Q \tau_Q\Big[1 + (1-\tau_Q)f(\tau_Q)\Big]\right|^2\,, \tag{5.20}$$

where $\tau_Q = 4m_Q^2/\bar{M}^2$, and the sum runs over the heavy flavours with mass m_Q circulating in the loop. The function f is given by

$$f(\tau_Q) = \begin{cases} \arcsin^2 \dfrac{1}{\sqrt{\tau_Q}} & \tau_Q \geq 1\,, \\[2ex] -\dfrac{1}{4}\left[\log\left(\dfrac{1+\sqrt{(1-\tau_Q)}}{1-\sqrt{(1-\tau_Q)}}\right) - i\pi\right]^2 & \tau_Q < 1. \end{cases} \qquad (5.21)$$

In our implementation we only retain the contribution coming from the top quark.

Virtual corrections

In the calculation of all NLO corrections, we have used an effective Lagrangian, where the heavy-quark degrees of freedom have been integrated out. This corresponds to take the $m_Q \to \infty$ limit.

We have regularized the infrared divergences according to the conventional dimensional regularization method, i.e. we have set the space-time dimensions $D = 4 - 2\epsilon$.

The finite soft-virtual term, obtained from the sum of the divergent virtual contributions and of the integral over the radiation variables of the counter-terms is given by (see eq. (1.160) of the present thesis and eq. (2.99) of ref. [30])

$$\mathcal{V}_{gg} = \frac{\alpha_{\mathrm{S}}}{2\pi}\left[-\left(\frac{11}{3}C_{\mathrm{A}} - \frac{4}{3}T_{\mathrm{F}}n_f\right)\log\frac{\mu_{\mathrm{F}}^2}{\mu_{\mathrm{R}}^2} + \frac{11}{3}C_{\mathrm{A}} + \frac{2\pi^2}{3}C_{\mathrm{A}}\right]\mathcal{B}_{gg}\,. \qquad (5.22)$$

In deriving this equation we have set $\xi_c = 1$. We indicate with μ_{R} and μ_{F} the renormalization and factorization scales, respectively.

Real corrections

At NLO, there are four subprocesses that contribute to Higgs boson production: $gg \to Hg$, $gq \to Hq$, $qg \to Hq$ and $q\bar{q} \to Hg$, where q runs over all possible quark and antiquark flavours and q and $\bar{q}$ are conjugate in flavour. The respective squared amplitudes, averaged over the incoming helicities and colours and multiplied by the

flux factor $1/(2s)$ are given by

$$\mathcal{R}_{gg} = \frac{\alpha_{\rm s}^3}{12\pi}\frac{G_F}{\sqrt{2}}\frac{1}{2s}\frac{s^4+t^4+u^4+\bar{M}^8}{stu}, \tag{5.23}$$

$$\mathcal{R}_{gq} = -\frac{\alpha_{\rm s}^3}{27\pi}\frac{G_F}{\sqrt{2}}\frac{1}{2s}\frac{s^2+u^2}{t}, \tag{5.24}$$

$$\mathcal{R}_{qg} = -\frac{\alpha_{\rm s}^3}{27\pi}\frac{G_F}{\sqrt{2}}\frac{1}{2s}\frac{s^2+t^2}{u}, \tag{5.25}$$

$$\mathcal{R}_{q\bar{q}} = \frac{8\,\alpha_{\rm s}^3}{81\pi}\frac{G_F}{\sqrt{2}}\frac{1}{2s}\frac{t^2+u^2}{s}, \tag{5.26}$$

where

$$s = (k_\oplus+k_\ominus)^2 = \frac{\bar{M}^2}{1-\xi}, \quad t = (k_\ominus-k_2)^2 = -\frac{s}{2}\,\xi\,(1+y), \quad u = (k_\oplus-k_2)^2 = -\frac{s}{2}\,\xi\,(1-y). \tag{5.27}$$

In terms of the FKS variables, we then have

$$\mathcal{R}_{gg} = \frac{\alpha_{\rm s}^3}{12\pi}\frac{G_F}{\sqrt{2}}\frac{1}{4}\left[8+\left(y^4+6y^2+1\right)\xi^4+8(1-\xi)^4\right]\frac{1}{\xi^2(1-y^2)}, \tag{5.28}$$

$$\mathcal{R}_{gq} = \frac{\alpha_{\rm s}^3}{27\pi}\frac{G_F}{\sqrt{2}}\frac{1}{4}\left[4+(1-y)^2\xi^2\right]\frac{1}{\xi(1+y)}, \tag{5.29}$$

$$\mathcal{R}_{qg} = \frac{\alpha_{\rm s}^3}{27\pi}\frac{G_F}{\sqrt{2}}\frac{1}{4}\left[4+(1+y)^2\xi^2\right]\frac{1}{\xi(1-y)}, \tag{5.30}$$

$$\mathcal{R}_{q\bar{q}} = \frac{8\,\alpha_{\rm s}^3}{81\pi}\frac{G_F}{\sqrt{2}}\frac{1}{4}\left[\xi^2\left(1+y^2\right)\right], \tag{5.31}$$

where the singular behavior for a soft ($\xi \to 0$) or collinear gluon ($y \to \pm 1$) is clearly manifest. Notice that the contribution $\mathcal{R}_{q\bar{q}}$ is not singular and has no underlying Born. It is thus a "regular" contribution, of the kind depicted in sec. 3.3.5.

Collinear remnants

After the subtraction of the initial-state collinear singularities into the parton distribution functions, finite collinear remnants are left over. The kinematics of these terms is Born-like. More precisely, we can introduce two sets of variables, $\mathbf{\Phi}_{1,\oplus} = \{\bar{M}^2, \bar{Y}, z\}$, such that momentum conservation reads

$$z\,x_\oplus K_\oplus + x_\ominus K_\ominus = k_1 \tag{5.32}$$

for the $\oplus$ direction and

$$x_\oplus K_\oplus + z\, x_\ominus K_\ominus = k_1 \tag{5.33}$$

for the $\ominus$ one. We can then associate an underlying Born configuration $\bar{\boldsymbol{\Phi}}_1$ such that

$$\bar{k}_\oplus = z\, x_\oplus K_\oplus\,, \qquad \bar{k}_\ominus = x_\ominus K_\ominus\,, \qquad \bar{k}_1 = k_1 \tag{5.34}$$

for the $\oplus$ direction, and

$$\bar{k}_\oplus = x_\oplus K_\oplus\,, \qquad \bar{k}_\ominus = z\, x_\ominus K_\ominus\,, \qquad \bar{k}_1 = k_1 \tag{5.35}$$

for the $\ominus$ one.

The collinear remnants are given in eq. (1.163), where we have fixed $\xi_c = 1$ and $\delta_I = 2$ and chosen the $\overline{\text{MS}}$ renormalization scheme. For the $\oplus$ direction and for the two different real-term contributions, they are given by

$$
\begin{aligned}
\mathcal{G}_\oplus^{qg}\left(\boldsymbol{\Phi}_{1,\oplus}\right) &= \frac{\alpha_{\text{s}}}{2\pi}\, C_{\text{F}}\left\{ (1-z)\frac{1+(1-z)^2}{z}\left[\left(\frac{1}{1-z}\right)_+ \log\left(\frac{\bar{M}^2}{z\mu_F^2}\right)\right.\right. \\
&\qquad\qquad \left.\left. + 2\left(\frac{\log(1-z)}{1-z}\right)_+ \right] + z \right\} \mathcal{B}_{gg}\,,
\end{aligned}
\tag{5.36}
$$

$$
\begin{aligned}
\mathcal{G}_\oplus^{gg}\left(\boldsymbol{\Phi}_{1,\oplus}\right) &= \frac{\alpha_{\text{s}}}{2\pi}\, 2C_{\text{A}}\left[z + \frac{(1-z)^2}{z} + z(1-z)^2 \right]\left[\left(\frac{1}{1-z}\right)_+ \log\left(\frac{\bar{M}^2}{z\mu_F^2}\right)\right. \\
&\qquad\qquad \left. + 2\left(\frac{\log(1-z)}{1-z}\right)_+ \right] \mathcal{B}_{gg}\,.
\end{aligned}
\tag{5.37}
$$

The other two collinear remnants, $\mathcal{G}_\ominus^{gq}(\boldsymbol{\Phi}_{1,\ominus})$ and $\mathcal{G}_\ominus^{gg}(\boldsymbol{\Phi}_{1,\ominus})$, have the same functional form of $\mathcal{G}_\oplus^{qg}\left(\boldsymbol{\Phi}_{1,\oplus}\right)$ and $\mathcal{G}_\oplus^{gg}\left(\boldsymbol{\Phi}_{1,\oplus}\right)$ respectively, since $\mathcal{B}_{gg}$ only depends upon $\bar{k}_1^2$.

5.3 POWHEG implementation

5.3.1 Generation of the Born variables

The first step in the POWHEG implementation is the generation of the Born kinematics. According to ref. [30], we introduce the $\bar{B}(\bar{\boldsymbol{\Phi}}_1)$ function, defined as

$$
\begin{aligned}
\bar{B}(\bar{\boldsymbol{\Phi}}_1) \;=\;& B_{gg}(\bar{\boldsymbol{\Phi}}_1) + V_{gg}(\bar{\boldsymbol{\Phi}}_1) + \int d\Phi_{\mathrm{rad}} \bigg\{ \hat{R}_{gg}\left(\bar{\boldsymbol{\Phi}}_1, \Phi_{\mathrm{rad}}\right) \\
& + \sum_q \left[\hat{R}_{qg}\left(\bar{\boldsymbol{\Phi}}_1, \Phi_{\mathrm{rad}}\right) + \hat{R}_{gq}\left(\bar{\boldsymbol{\Phi}}_1, \Phi_{\mathrm{rad}}\right) \right] \bigg\} \\
& + \int_{\bar{x}_\oplus}^1 \frac{dz}{z} \left[G_\oplus^{gg}(\boldsymbol{\Phi}_{1,\oplus}) + \sum_q G_\oplus^{qg}(\boldsymbol{\Phi}_{1,\oplus}) \right] + \int_{\bar{x}_\ominus}^1 \frac{dz}{z} \left[G_\ominus^{gg}(\boldsymbol{\Phi}_{1,\ominus}) + \sum_q G_\ominus^{gq}(\boldsymbol{\Phi}_{1,\ominus}) \right],
\end{aligned}
\tag{5.38}
$$

where

$$
B_{gg}(\bar{\boldsymbol{\Phi}}_1) \;=\; \mathcal{B}_{gg}(\bar{\boldsymbol{\Phi}}_1)\, \mathcal{L}_{gg}(\bar{x}_\oplus, \bar{x}_\ominus), \tag{5.39}
$$

$$
V_{gg}(\bar{\boldsymbol{\Phi}}_1) \;=\; \mathcal{V}_{gg}(\bar{\boldsymbol{\Phi}}_1)\, \mathcal{L}_{gg}(\bar{x}_\oplus, \bar{x}_\ominus), \tag{5.40}
$$

$$
\hat{R}_{gg}(\bar{\boldsymbol{\Phi}}_1, \Phi_{\mathrm{rad}}) \;=\; \hat{\mathcal{R}}_{gg}(\bar{\boldsymbol{\Phi}}_1, \Phi_{\mathrm{rad}})\, \mathcal{L}_{gg}(x_\oplus, x_\ominus), \tag{5.41}
$$

$$
\hat{R}_{gq}(\bar{\boldsymbol{\Phi}}_1, \Phi_{\mathrm{rad}}) \;=\; \hat{\mathcal{R}}_{gq}(\bar{\boldsymbol{\Phi}}_1, \Phi_{\mathrm{rad}})\, \mathcal{L}_{gq}(x_\oplus, x_\ominus), \tag{5.42}
$$

$$
\hat{R}_{qg}(\bar{\boldsymbol{\Phi}}_1, \Phi_{\mathrm{rad}}) \;=\; \hat{\mathcal{R}}_{qg}(\bar{\boldsymbol{\Phi}}_1, \Phi_{\mathrm{rad}})\, \mathcal{L}_{qg}(x_\oplus, x_\ominus), \tag{5.43}
$$

$$
G_\oplus^{gg}(\boldsymbol{\Phi}_{1,\oplus}) \;=\; \mathcal{G}_\oplus^{gg}(\boldsymbol{\Phi}_{1,\oplus})\, \mathcal{L}_{gg}\!\left(\frac{\bar{x}_\oplus}{z}, \bar{x}_\ominus\right), \tag{5.44}
$$

$$
G_\oplus^{qg}(\boldsymbol{\Phi}_{1,\oplus}) \;=\; \mathcal{G}_\oplus^{qg}(\boldsymbol{\Phi}_{1,\oplus})\, \mathcal{L}_{qg}\!\left(\frac{\bar{x}_\oplus}{z}, \bar{x}_\ominus\right), \tag{5.45}
$$

$$
G_\ominus^{gg}(\boldsymbol{\Phi}_{1,\ominus}) \;=\; \mathcal{G}_\ominus^{gg}(\boldsymbol{\Phi}_{1,\ominus})\, \mathcal{L}_{gg}\!\left(\bar{x}_\oplus, \frac{\bar{x}_\ominus}{z}\right), \tag{5.46}
$$

$$
G_\ominus^{gq}(\boldsymbol{\Phi}_{1,\ominus}) \;=\; \mathcal{G}_\ominus^{gq}(\bar{\boldsymbol{\Phi}}_{1,\ominus})\, \mathcal{L}_{gq}\!\left(\bar{x}_\oplus, \frac{\bar{x}_\ominus}{z}\right), \tag{5.47}
$$

with $x_\oplus, x_\ominus$ given in eq. (5.12) and the luminosity $\mathcal{L}$ is defined in terms of the parton distribution functions $f_f^\oplus(x_\oplus, \mu_{\mathrm{F}}^2)$

$$
\mathcal{L}_{ff'}(x_\oplus, x_\ominus) = f_f^\oplus(x_\oplus, \mu_{\mathrm{F}}^2)\, f_{f'}^\ominus(x_\ominus, \mu_{\mathrm{F}}^2). \tag{5.48}
$$

Observe that the $\mathcal{R}_{q\bar{q}}$ term does not appear in $\bar{B}$, since it does not have a valid underlying Born. It is just generated separately, as described in sec. 3.3.5 and at the end of this section.

All the integrals appearing in eq. (5.38) are finite. In fact, according the the FKS subtraction scheme, the hatted functions

$$\hat{\mathcal{R}}_{ij} = \frac{1}{\xi} \left\{ \frac{1}{2} \left(\frac{1}{\xi} \right)_+ \left[\left(\frac{1}{1-y} \right)_+ + \left(\frac{1}{1+y} \right)_+ \right] \right\} \left[(1-y^2)\, \xi^2\, \mathcal{R}_{ij} \right] \qquad (5.49)$$

have only integrable divergences. Some care should still be used when dealing with the plus distributions. In order to illustrate this, we explicitly show how to deal with the $\mathcal{R}_{gg}$ term, that is the most singular one. According to eq. (5.49), it can be written

$$\begin{aligned}
\widehat{\mathcal{R}}_{gg} &= \frac{\alpha_{\rm S}^3}{12\pi} \frac{G_F}{\sqrt{2}} \left[2 + \frac{y^4 + 6y^2 + 1}{4} \xi^4 + 2(1-\xi)^4 \right] \\
&\quad \times \left\{ \frac{1}{2} \left(\frac{1}{\xi} \right)_+ \left[\left(\frac{1}{1-y} \right)_+ + \left(\frac{1}{1+y} \right)_+ \right] \right\} \frac{1}{\xi}. \qquad (5.50)
\end{aligned}$$

Inserting now the expression (5.19) of $d\Phi_{\rm rad}$ into eq. (5.38), we have

$$\int d\Phi_{\rm rad}\, \mathcal{L}_{gg}(x_\oplus, x_\ominus)\, \widehat{\mathcal{R}}_{gg} = \frac{\bar{M}^2}{(4\pi)^3} \int_{-1}^{1} dy \int_{0}^{\xi_{\rm M}(y)} d\xi \frac{\xi}{(1-\xi)^2} \int_{0}^{2\pi} d\phi\, \mathcal{L}_{gg}(x_\oplus, x_\ominus)\, \widehat{\mathcal{R}}_{gg}\,, \qquad (5.51)$$

where $\xi_{\rm M}(y)$ is given in eq. (5.14). The integration over the azimuthal angle ϕ is straightforward, giving an overall multiplicative factor of 2π. Considering then the $(1/(1-y))_+$ term only, we get an integral of the form

$$I = \int_{-1}^{1} dy \int_{0}^{\xi_{\rm M}(y)} d\xi \left(\frac{1}{\xi} \right)_+ \left(\frac{1}{1-y} \right)_+ f(\xi, y)\, \mathcal{L}_{gg}(x_\oplus, x_\ominus) \qquad (5.52)$$

where

$$f(\xi, y) = \frac{\alpha_{\rm S}^3}{12\pi} \frac{G_F}{\sqrt{2}} \left[2 + \frac{y^4 + 6y^2 + 1}{4} \xi^4 + 2(1-\xi)^4 \right] \frac{1}{2} \frac{\bar{M}^2}{(4\pi)^3} \frac{2\pi}{(1-\xi)^2}. \qquad (5.53)$$

Recalling the definition of the plus distributions

$$\int_{0}^{1} d\xi \left(\frac{1}{\xi} \right)_+ f(\xi) = \int_{0}^{1} d\xi \frac{f(\xi) - f(0)}{\xi}\,, \qquad (5.54)$$

$$\int_{-1}^{1} dy \left(\frac{1}{1-y} \right)_+ f(y) = \int_{-1}^{1} dy \frac{f(y) - f(1)}{1-y}\,, \qquad (5.55)$$

and making the change of variable

$$\xi = \xi_{\mathrm{M}}(y)\,\tilde{\xi}\,, \tag{5.56}$$

we are left with

$$
\begin{aligned}
I &= \int_{-1}^{1} dy \left(\frac{1}{1-y}\right)_{+} \int_{0}^{1} d\tilde{\xi} \left(\frac{1}{\tilde{\xi}}\right)_{+} f\left(\xi,y\right)\, \mathcal{L}_{gg}\left(x_{\oplus},x_{\ominus}\right) \\
&\quad + \int_{-1}^{1} dy \left(\frac{1}{1-y}\right)_{+} f(0,y) \log \xi_{\mathrm{M}}(y)\, \mathcal{L}_{gg}(\bar{x}_{\oplus},\bar{x}_{\ominus}) \\
&= \int_{-1}^{1} dy \left(\frac{1}{1-y}\right)_{+} \int_{0}^{1} d\tilde{\xi}\, \frac{1}{\tilde{\xi}} \Big[f\left(\xi,y\right) \mathcal{L}_{gg}(x_{\oplus},x_{\ominus}) - f\left(0,y\right) \mathcal{L}_{gg}(\bar{x}_{\oplus},\bar{x}_{\ominus}) \Big] \\
&\quad + \int_{-1}^{1} dy\, \frac{1}{1-y} \Big[f(0,y) \log \xi_{\mathrm{M}}(y) - f(0,1) \log \xi_{\mathrm{M}}(1) \Big] \mathcal{L}_{gg}(\bar{x}_{\oplus},\bar{x}_{\ominus}) \\
&= \int_{0}^{1} d\tilde{y} \int_{0}^{1} d\tilde{\xi}\, \frac{1}{1-\tilde{y}}\, \frac{1}{\tilde{\xi}} \Bigg\{ \Big[f\left(\xi,y\right) \mathcal{L}_{gg}(x_{\oplus},x_{\ominus}) - f\left(0,y\right) \mathcal{L}_{gg}(\bar{x}_{\oplus},\bar{x}_{\ominus}) \Big] \\
&\qquad\qquad - \Big[f\left(\xi,1\right) \mathcal{L}_{gg}\left(\frac{\bar{x}_{\oplus}}{1-\xi},\bar{x}_{\ominus}\right) - f\left(0,1\right) \mathcal{L}_{gg}(\bar{x}_{\oplus},\bar{x}_{\ominus}) \Big] \Bigg\} \\
&\quad + \int_{0}^{1} d\tilde{y}\, \frac{1}{1-\tilde{y}} \Big[f(0,y) \log \xi_{\mathrm{M}}(y) - f(0,1) \log \xi_{\mathrm{M}}(1) \Big] \mathcal{L}_{gg}(\bar{x}_{\oplus},\bar{x}_{\ominus})\,, \tag{5.57}
\end{aligned}
$$

where we have used the expression of $x_{\oplus}$ of eq. (5.12) and $\xi_{\mathrm{M}}(1) = 1 - \bar{x}_{\oplus}$ (see eq. (5.14)). In the last line we have made the further change of variable

$$y = -1 + 2\,\tilde{y}\,, \tag{5.58}$$

so that all radiation variables are mapped into a cubic unit volume. The integral I is now manifestly finite and can be computed numerically.

The same manipulations should be applied to the z integration of the collinear remnants in eq. (5.38). For example, concentrating on the two plus distributions in the $\mathcal{G}_{\oplus}^{gg}$ term, we have to deal with integrals of the form

$$
\int_{\bar{x}_{\oplus}}^{1} dz \left(\frac{1}{1-z}\right)_{+} f(z) = \log(1-\bar{x}_{\oplus})f(1) + \int_{0}^{1} d\tilde{\xi}\, \frac{f(z)-f(1)}{1-\tilde{\xi}}\,, \tag{5.59}
$$

$$
\begin{aligned}
\int_{\bar{x}_{\oplus}}^{1} dz \left(\frac{\log(1-z)}{1-z}\right)_{+} f(z) &= \frac{1}{2}\log^2(1-\bar{x}_{\oplus})f(1) \\
&\quad + \int_{0}^{1} d\tilde{\xi}\, \frac{\log(1-z)}{1-\tilde{\xi}} \left[f(z)-f(1)\right], \tag{5.60}
\end{aligned}
$$

where $f(z)$ is finite in the $z \to 1$ limit and we have made the change of variable

$$z = \bar{x}_\oplus + \tilde{\xi}\left(1 - \bar{x}_\oplus\right) . \tag{5.61}$$

At the end of this procedure, the most general form one can obtain for $\bar{B}$ is

$$\bar{B}(\bar{\Phi}_1) = D(\bar{\Phi}_1) + \int_0^1 d\tilde{\xi}\, E\left(\bar{\Phi}_1, \tilde{\xi}\right) + \int_0^1 d\tilde{y} \int_0^1 d\tilde{\xi}\, F\left(\bar{\Phi}_1, \tilde{\xi}, \tilde{y}\right), \tag{5.62}$$

and we can define the function

$$\tilde{B}\left(\bar{\Phi}_1, \tilde{\xi}, \tilde{y}\right) = D(\bar{\Phi}_1) + E\left(\bar{\Phi}_1, \tilde{\xi}\right) + F\left(\bar{\Phi}_1, \tilde{\xi}, \tilde{y}\right) , \tag{5.63}$$

so that

$$\bar{B}(\bar{\Phi}_1) = \int_0^1 d\tilde{y} \int_0^1 d\tilde{\xi}\, \tilde{B}\left(\bar{\Phi}_1, \tilde{\xi}, \tilde{y}\right). \tag{5.64}$$

In order to generate the underlying Born kinematics, we first compute the two distinct contributions to the total cross section, defined by

$$\sigma_{\text{tot}} = \sigma_{\bar{B}} + \sum_q \sigma_{R_{q\bar{q}}}, \tag{5.65}$$

where

$$\sigma_{\bar{B}} = \int d\bar{\Phi}_1\, \bar{B}(\bar{\Phi}_1) ,$$

$$\sigma_{R_{q\bar{q}}} = \int d\bar{\Phi}_1\, d\Phi_{\text{rad}}\, R_{q\bar{q}}(\bar{\Phi}_1, \Phi_{\text{rad}}) , \tag{5.66}$$

and

$$R_{q\bar{q}}(\bar{\Phi}_1, \Phi_{\text{rad}}) = \mathcal{R}_{q\bar{q}}(\bar{\Phi}_1, \Phi_{\text{rad}})\, \mathcal{L}_{q\bar{q}}(x_\oplus, x_\ominus) . \tag{5.67}$$

We then decide whether the event is a $\bar{B}$ event or a $R_{q\bar{q}}$ one, with a probability equal to $\sigma_{\bar{B}}/\sigma_{\text{tot}}$ and $\sigma_{R_{q\bar{q}}}/\sigma_{\text{tot}}$ respectively. In case of a $\bar{B}$ event, the generation of the Born variables $\bar{\Phi}_1$ is performed by using the integrator-unweighter program MINT [77] that, after a single integration of the function $\tilde{B}(\bar{\Phi}_1, \tilde{\xi}, \tilde{y})$ over the Born and radiation variables, can generate a set of values for the variables $\{\bar{\Phi}_1, \tilde{\xi}, \tilde{y}\}$, distributed according to the weight $\tilde{B}(\bar{\Phi}_1, \tilde{\xi}, \tilde{y})$. We then keep the $\bar{\Phi}_1$ generated values only, and neglect all the others, which corresponds to integrate over them. The event is then further processed, to generate the radiation variables, as illustrated in the following section. In case of a $R_{q\bar{q}}$ event, one uses the same method used for the $\bar{B}$ case, except that, at the end, one keeps the whole set of Born plus radiation variables, that fully defines the kinematics of a real event. In this last case, one does not need to do anything else, and the event is passed to the Les Houches Interface, to be further showered by the Monte Carlo program.

5.3.2 Generation of the radiation variables

Radiation kinematics is generated using the POWHEG Sudakov form factor

$$\Delta\left(\bar{\bar{\mathbf{\Phi}}}_1, p_{\mathrm{T}}\right) \;\; = \;\; \exp\left\{ -\int d\Phi_{\mathrm{rad}} \frac{R\left(\bar{\bar{\mathbf{\Phi}}}_1, \Phi_{\mathrm{rad}}\right)}{B(\bar{\bar{\mathbf{\Phi}}}_1)} \, \theta(k_{\mathrm{T}} - p_{\mathrm{T}}) \right\}, \qquad (5.68)$$

where we have defined

$$R\left(\bar{\bar{\mathbf{\Phi}}}_1, \Phi_{\mathrm{rad}}\right) \;\; = \;\; R_{gg}\left(\bar{\bar{\mathbf{\Phi}}}_1, \Phi_{\mathrm{rad}}\right) + \sum_q \left[R_{qg}\left(\bar{\bar{\mathbf{\Phi}}}_1, \Phi_{\mathrm{rad}}\right) + R_{gq}\left(\bar{\bar{\mathbf{\Phi}}}_1, \Phi_{\mathrm{rad}}\right) \right], \quad (5.69)$$

$$B(\bar{\bar{\mathbf{\Phi}}}_1) \;\; = \;\; B_{gg}(\bar{\bar{\mathbf{\Phi}}}_1), \qquad (5.70)$$

and

$$k_{\mathrm{T}}^2 = \frac{s}{4} \xi^2 \left(1 - y^2\right) = \frac{\bar{M}^2}{4(1-\xi)} \xi^2 \left(1 - y^2\right) \qquad (5.71)$$

is the exact squared transverse momentum of the radiated parton. The factorization and renormalization scales in eq. (5.68) should be taken equal to k_{T}^2, in order to recover the correct leading logarithm (LL) Sudakov behavior[2].

To generate the radiation variables, we use the veto method. This requires to find a simple upper bound for the integrand in eq. (5.68)

$$\frac{\bar{M}^2}{(4\pi)^3} \frac{\xi}{(1-\xi)^2} \frac{R\left(\bar{\bar{\mathbf{\Phi}}}_1, \Phi_{\mathrm{rad}}\right)}{B\left(\bar{\bar{\mathbf{\Phi}}}_1\right)}. \qquad (5.72)$$

A suitable upper bounding function is given by

$$U = N \frac{\alpha_{\mathrm{s}}(k_{\mathrm{T}}^2)}{\xi\left(1 - y^2\right)}, \qquad (5.73)$$

where N is determined by spanning randomly the whole phase space and imposing that U is larger than the integrand function. The generation of the event according to the bound (5.73) follows the line depicted in Appendix C.3.

The POWHEG differential cross section for the generation of the hardest event is given by

$$d\sigma \;\; = \;\; \bar{B}(\bar{\bar{\mathbf{\Phi}}}_1) \, d\bar{\bar{\mathbf{\Phi}}}_1 \left\{ \Delta\left(\bar{\bar{\mathbf{\Phi}}}_1, p_{\mathrm{T}}^{\min}\right) + \Delta\left(\bar{\bar{\mathbf{\Phi}}}_1, p_{\mathrm{T}}\right) \frac{R\left(\bar{\bar{\mathbf{\Phi}}}_1, \Phi_{\mathrm{rad}}\right)}{B\left(\bar{\bar{\mathbf{\Phi}}}_1\right)} \, d\Phi_{\mathrm{rad}} \right\}$$

$$+ \sum_q R_{q\bar{q}}\left(\bar{\bar{\mathbf{\Phi}}}_1, \Phi_{\mathrm{rad}}\right) d\bar{\bar{\mathbf{\Phi}}}_1 d\Phi_{\mathrm{rad}}, \qquad (5.74)$$

---

[2]We will show in sec. 5.7 how it is possible to reach next-to-leading logarithmic accuracy for this particular process.

where the last term in the sum is the non-singular real contribution. In the $\bar{B}$ and $R_{q\bar{q}}$ functions, the renormalization and factorization scales, μ_{R} and μ_{F}, should be taken of the order of the hard scale of the process, i.e. the Higgs boson mass or its transverse mass. During the generation of radiation, the two scales should instead be taken equal to the transverse momentum of the produced radiation, in order to recover the correct Sudakov form factor.

We remark that, in the formula for the strong coupling constant used for the generation of radiation, we have properly taken into account the heavy-flavour thresholds. That is to say, when the renormalization scale μ_{R} crosses a heavy-flavour mass threshold, we change the number of active flavours accordingly. Furthermore, as discussed in refs. [30, 26], we use a rescaled value $\Lambda_{\mathrm{MC}} = 1.569\,\Lambda_{\overline{\mathrm{MS}}}^{(5)}$ in the expression for α_{S}, in order to achieve next-to-leading logarithmic accuracy in the Sudakov form factor (see sec. 5.7 for more details).

5.4   Results

In this section we present our results, obtained for the Tevatron and the LHC, and the comparison done with `MC@NLO` and `PYTHIA`. We have used the CTEQ6M [81] set for the parton distribution functions and the corresponding returned value $\Lambda_{\overline{\mathrm{MS}}}^{(5)} = 0.226$ GeV. In the generation of the radiation, we have fixed the lower cutoff of the transverse momentum to the value $p_{\mathrm{T}}^{\min} = \sqrt{5}\,\Lambda_{\mathrm{MC}}$. The renormalization and factorization scales have been taken equal to the Higgs boson transverse mass $m_{\mathrm{T}}^{H} = \sqrt{m_{H}^{2} + (p_{\mathrm{T}}^{H})^{2}}$.

No acceptance cuts have been applied in any of the following plots.

5.4.1   POWHEG - MC@NLO comparison

We have compared our results with `MC@NLO`, the only existing program where NLO Higgs boson production via gluon fusion is merged with a shower Monte Carlo program. Since `MC@NLO` uses only the `HERWIG` angular-ordered shower, we have also interfaced `POWHEG` with `HERWIG`, in order to minimize effects due to differences in the shower and hadronization algorithms.

`MC@NLO` generates the Higgs boson virtuality $\bar{M}^2$ according to the Breit-Wigner form

$$\frac{1}{\pi} \frac{m_H \, \Gamma_H}{\left(\bar{M}^2 - m_H^2\right)^2 + (m_H \, \Gamma_H)^2} \,. \tag{5.75}$$

For the purpose of this comparison we have thus used the same form. We have considered two different sets of values for the Higgs boson mass and width: $m_H = 120$ GeV with $\Gamma_H = 3.605$ MeV and $m_H = 400$ GeV with $\Gamma_H = 28.89$ GeV.

Both in `POWHEG` and in `MC@NLO` there is the option to retain the full top-mass dependence in the Born cross section, i.e. to use a finite τ_Q value in eq. (5.20). We have then the choice to generate our Born variables by fixing $m_t = 171$ GeV in the $\bar{B}$ term in eq. (5.38) or by sending $m_t \to \infty$. Since we have computed the real-radiation term only in the $m_t \to \infty$ limit, we have to use the same limit in the calculation of the Born term in the Sudakov form factor (5.68), in order to recover the correct Altarelli-Parisi behavior when the collinear limit is approached.
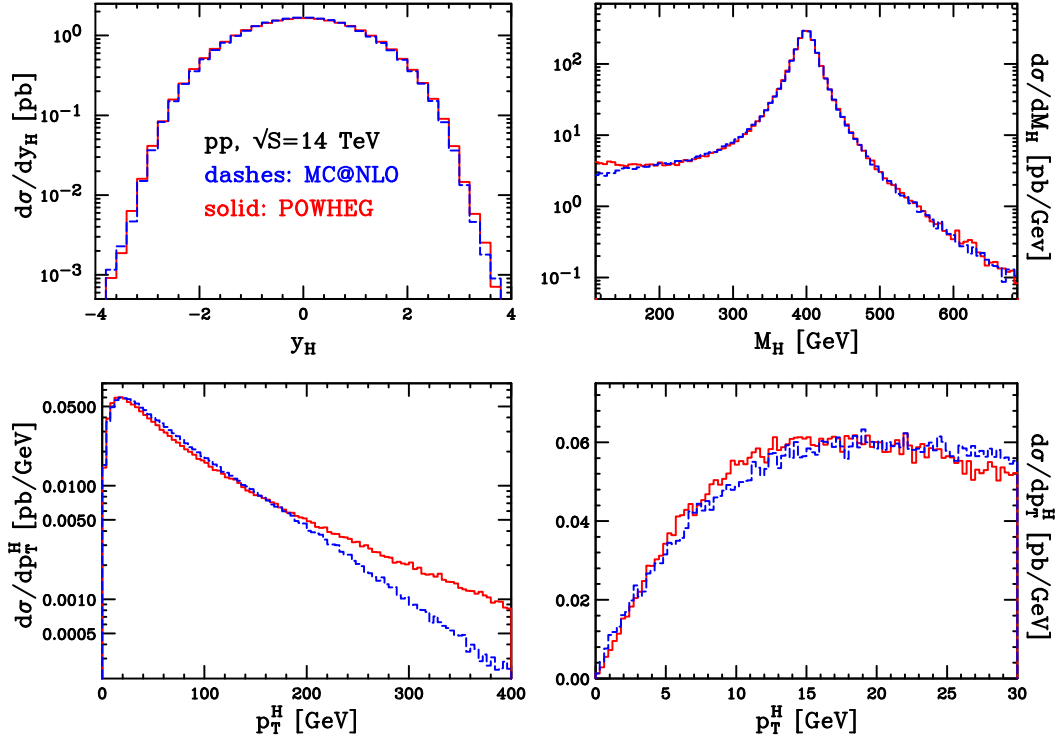
Tevatron results

In fig. 5.1 we show a comparison between `POWHEG` and `MC@NLO` for the rapidity, invariant mass and transverse-momentum distributions of a Higgs boson with mass $m_H = 120$ GeV, at the Tevatron $p\bar{p}$ collider. The lowest order m_t-dependence is retained. A blowup of the transverse-momentum distribution near the low-p_{T} region is also shown. There is good agreement between the two programs, except for the transverse momentum distribution at high p_{T} (we will comment more on this issue in sec. 5.6).

In fig. 5.2 we compare the leading jet rapidity and the difference in the rapidity of the leading jet and the Higgs boson. The jet is defined using the `SISCONE` algorithm [82] as implemented in the `FASTJET` package [83], setting the jet radius $R = 0.7$ and the overlapping fraction $f = 0.5$. As in previous `POWHEG` implementations, we notice a dip in the `MC@NLO` jet rapidity distribution, which is enhanced in the difference. We extensively discuss this feature in sec. 5.5.

In fig. 5.3, we compare the transverse-momentum distributions of the leading jet, reconstructed with the `SISCONE` and the k_T algorithms (included in `FASTJET`). A lower 10 GeV cut on jet transverse momentum is imposed. The high-p_{T} discrepancy reflects the same behavior found for the Higgs boson transverse-momentum distribution.
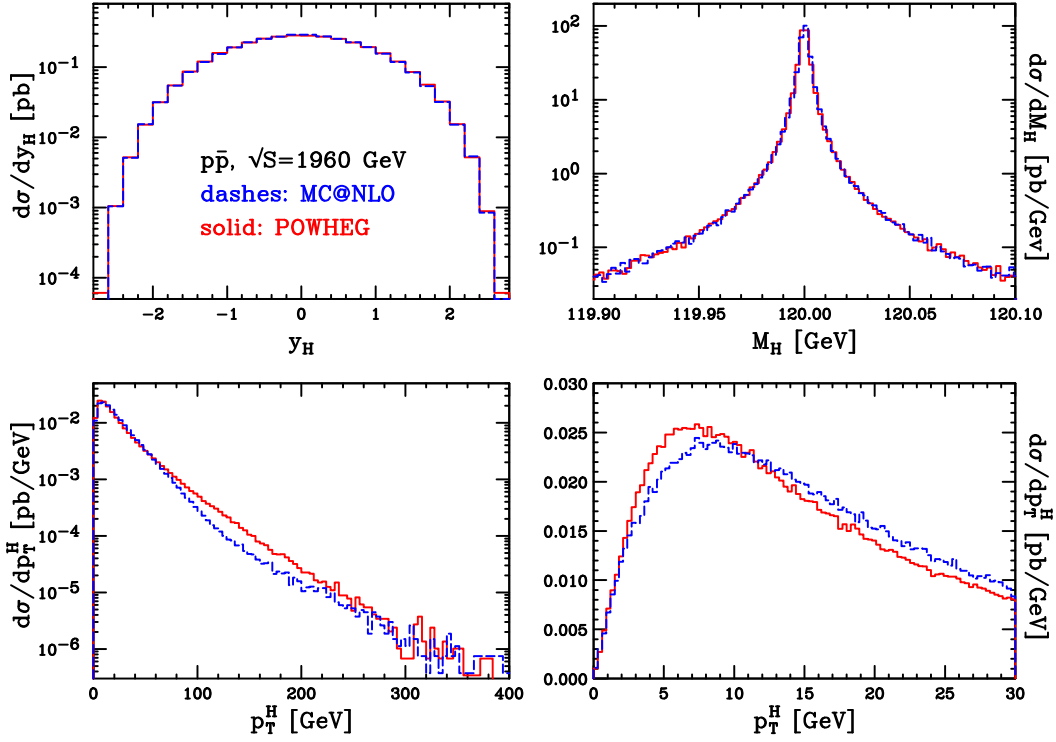
Figure 5.1: *Comparison between* POWHEG *and* MC@NLO *for the rapidity, in-variant mass and transverse-momentum distributions of a Higgs boson with* $m_H = 120$ *GeV, at Tevatron* $p\bar{p}$ *collider.*
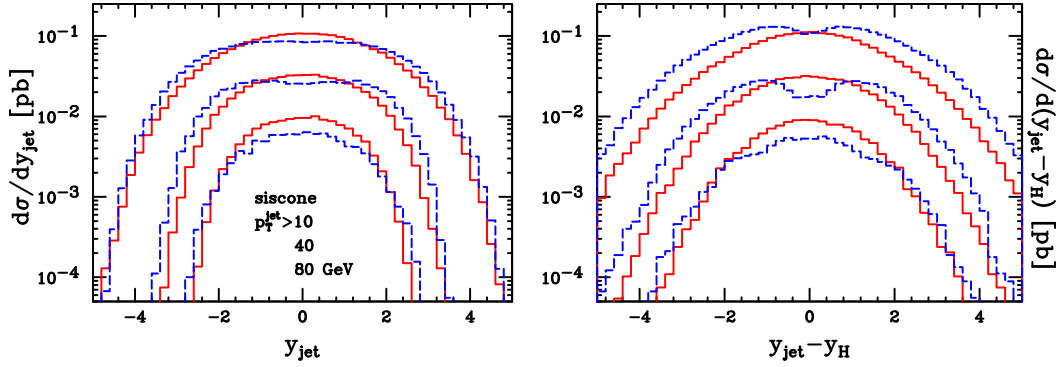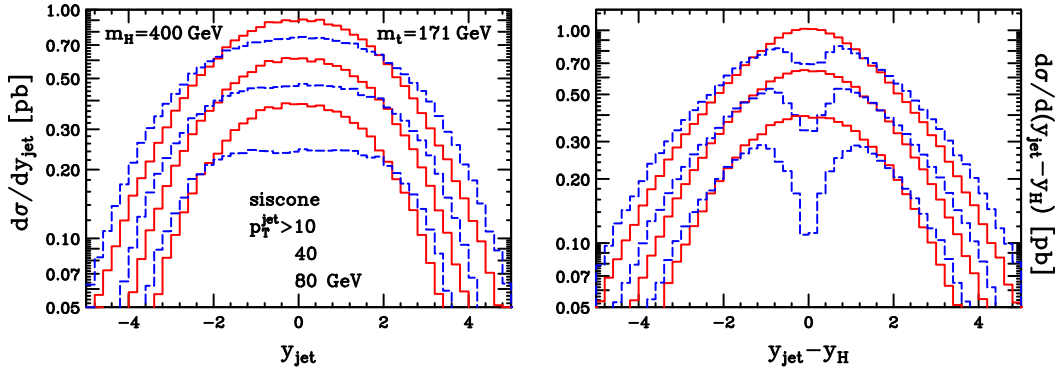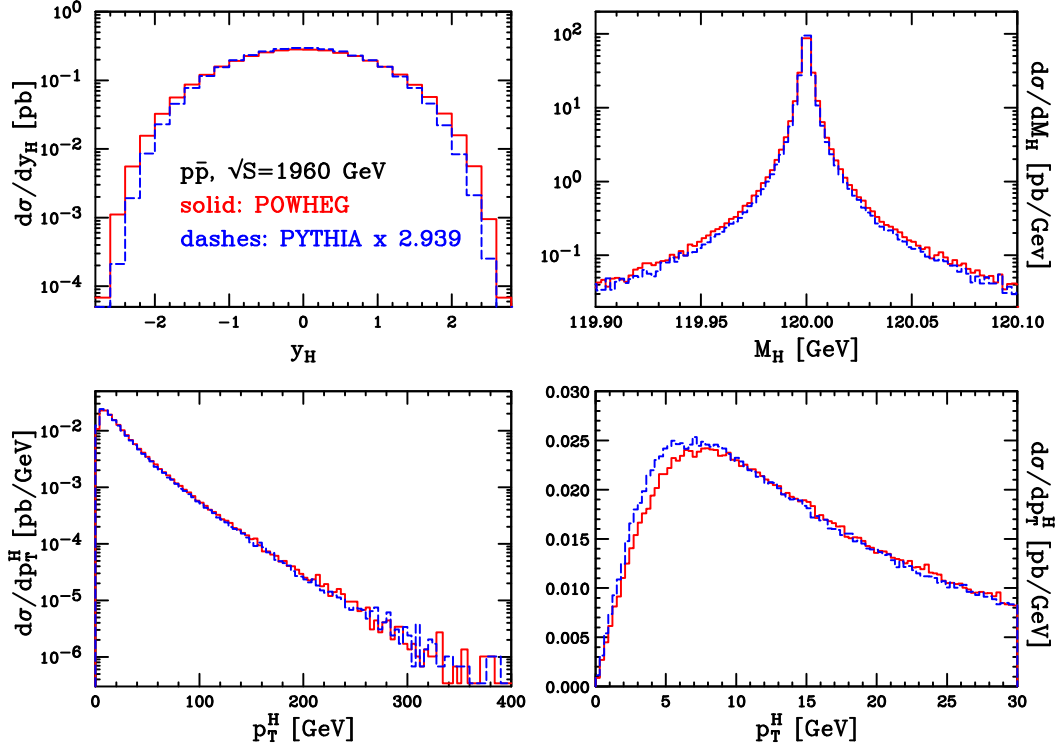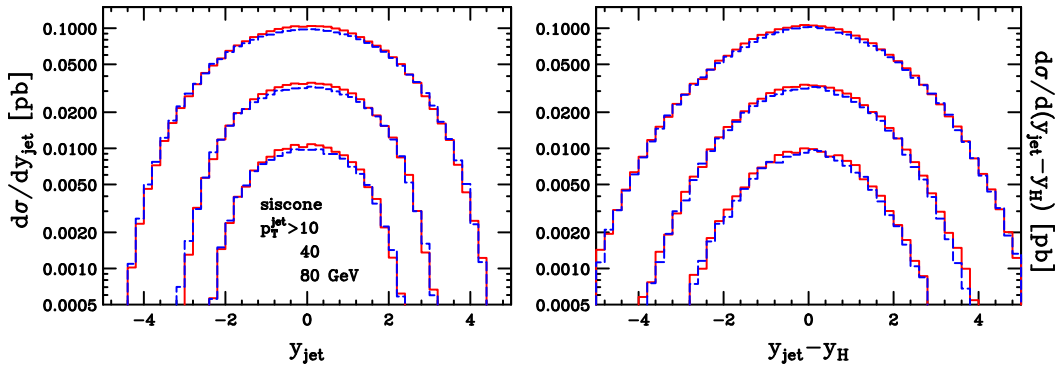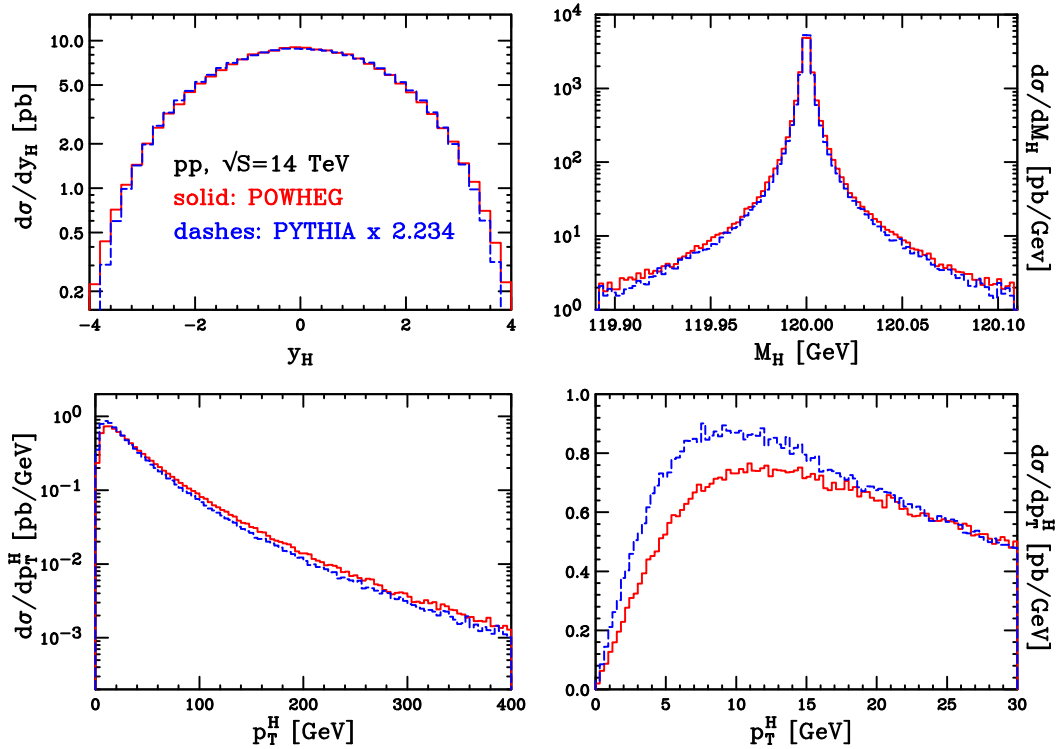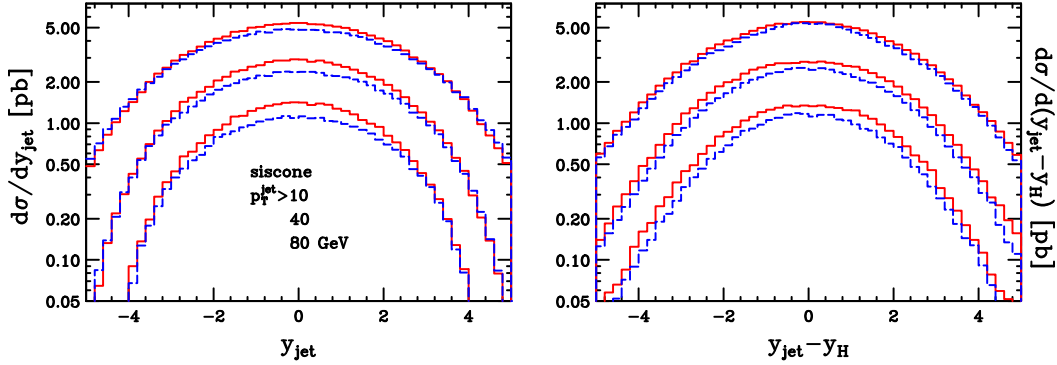

Figure 5.2: *Comparison between* POWHEG *and* MC@NLO *for the rapidity of the leading jet and the rapidity difference of the Higgs boson and the leading jet, defined according to the* SISCONE *algorithm, with different jet cuts.*

LHC results

From fig. 5.4 to 5.6 we carry out a similar analysis for the LHC pp collider. The difference in the hardness of the p_T distributions is more evident here than at the
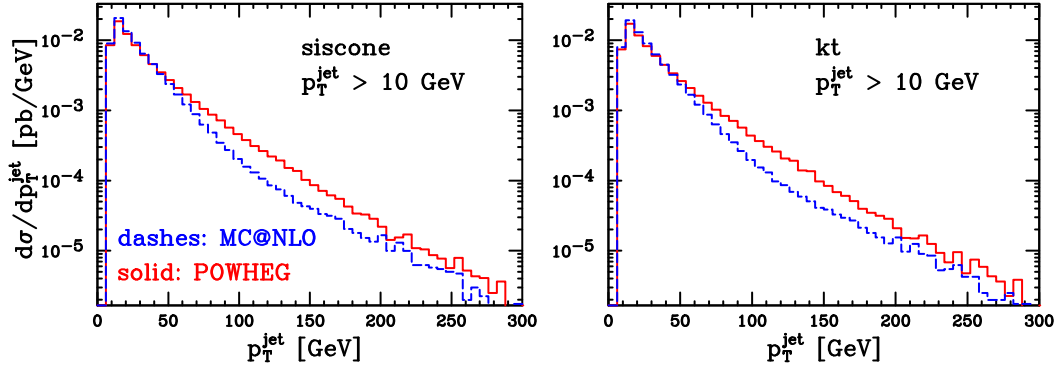
Figure 5.3: *Comparison between* POWHEG *and* MC@NLO *for the transverse-momentum distributions of the leading jet, defined according to the* SISCONE *and the* KT *jet algorithms.*
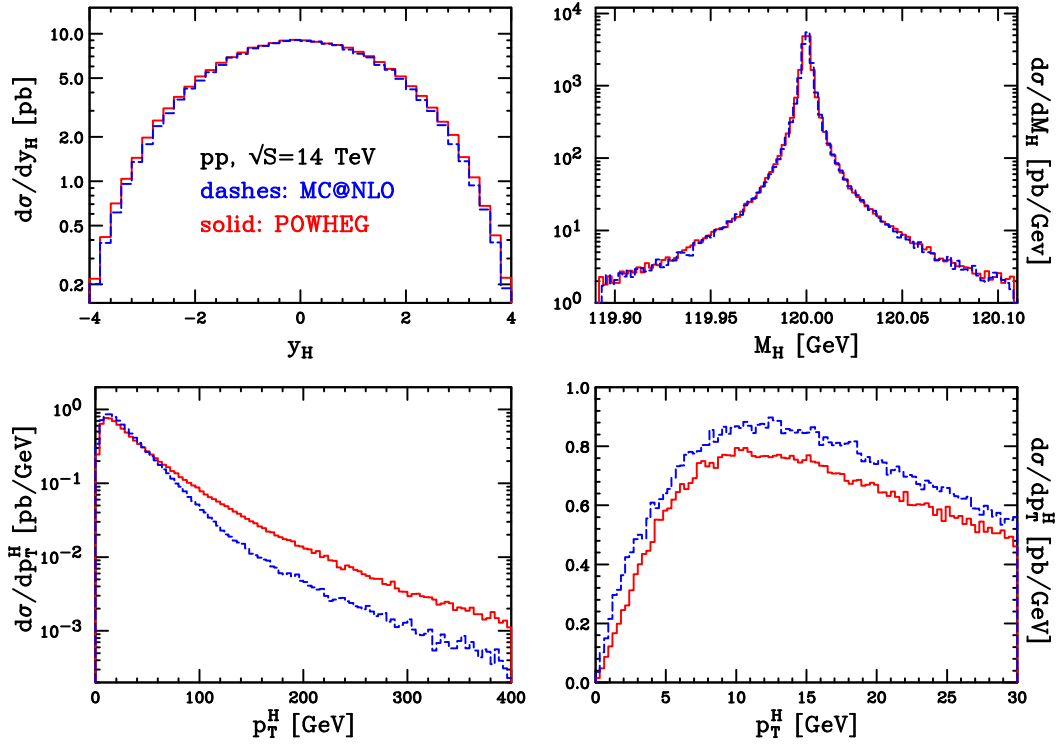
Figure 5.4: *Comparison between* POWHEG *and* MC@NLO *for the rapidity, invariant mass and transverse-momentum distributions of a Higgs boson with* $m_H = 120$ *GeV, at the LHC pp collider.*

Tevatron. The other plots show instead a good agreement between the two codes, apart from the aforementioned dip in the leading-jet rapidity distributions.

We have also made some comparisons with a different value of the Higgs boson
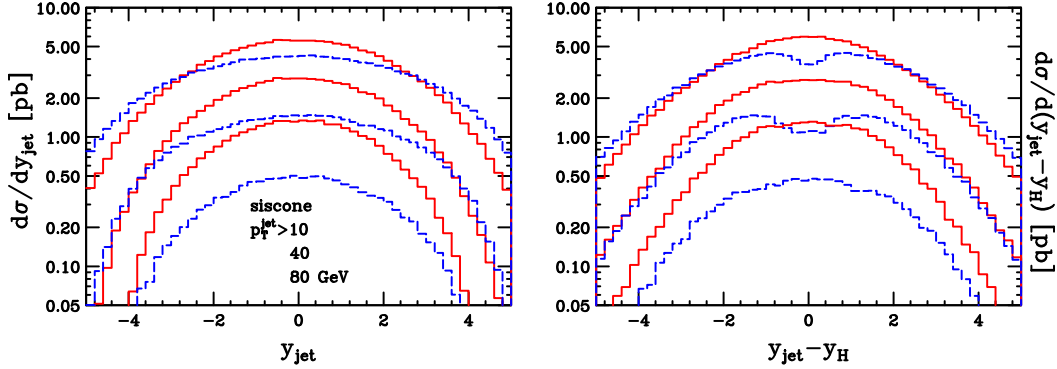
Figure 5.5: *Comparison between* POWHEG *and* MC@NLO *for the rapidity of the leading jet and the rapidity difference of the Higgs boson and the leading jet, defined according to the* SISCONE *algorithm, with different jet cuts.*
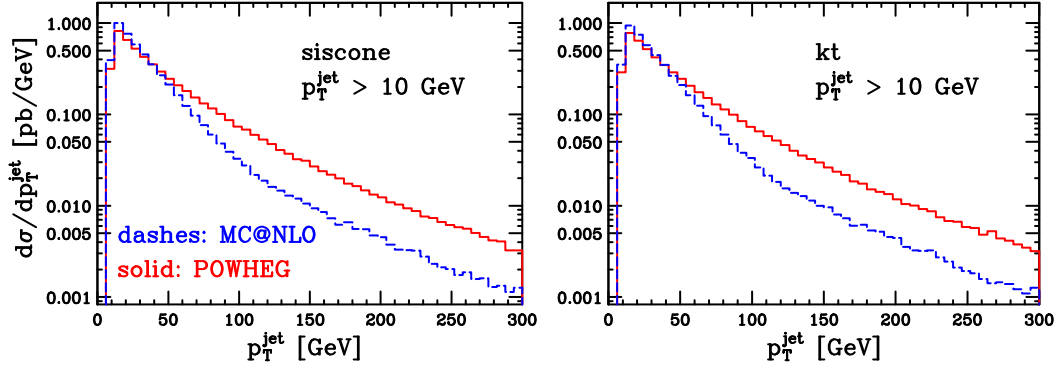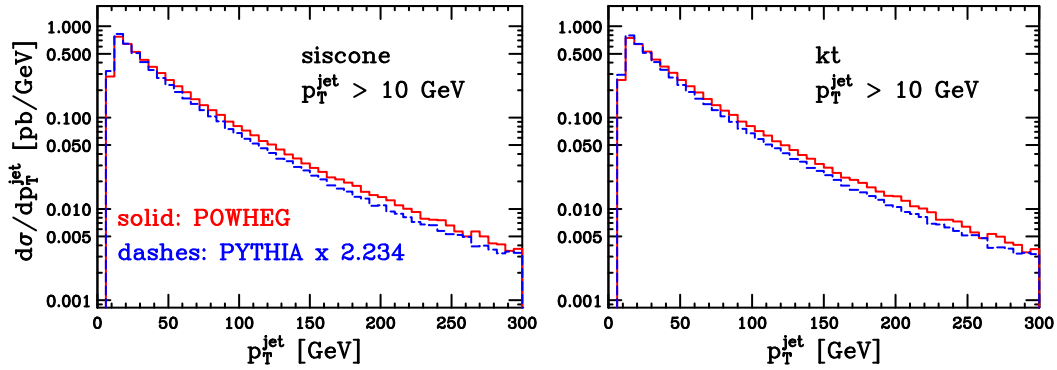

Figure 5.6: *Comparison between* POWHEG *and* MC@NLO *for the transverse-momentum distributions of the leading jet, defined according to the* SISCONE *and the* KT *algorithms.*

mass. We have chosen $m_H = 400$ GeV, where the ratio between the Born cross sections evaluated with $m_t = 171$ GeV and $m_t \to \infty$ is close to its maximum value and roughly equals 3. The results are shown in fig. 5.7 and 5.8. We see that, in this case, the dip in the rapidity of the hardest jet in MC@NLO is extremely marked. As already anticipated, we will comment more about this feature in sec. 5.5.

5.4.2   POWHEG - PYTHIA comparison

We now compare POWHEG and PYTHIA. The Higgs boson production implementation in PYTHIA includes matrix-element corrections, so that the p_T distribution of the Higgs boson is accurate at large p_T. In our comparisons, we always normalize the
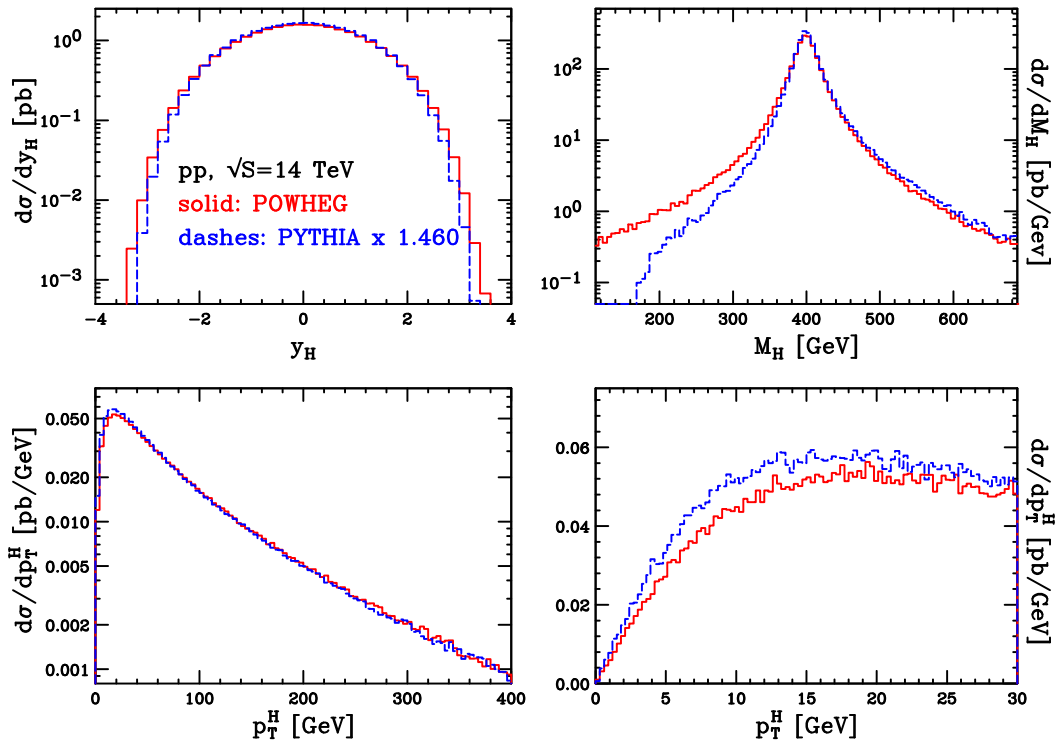
Figure 5.7: *Comparison between* POWHEG *and* MC@NLO *for the rapidity, invariant mass and transverse-momentum distributions of a Higgs boson with* $m_H = 400$ *GeV, at the LHC pp collider.*

Figure 5.8: *Comparison between* POWHEG *and* MC@NLO *for the rapidity of the leading jet and the rapidity difference of the Higgs boson and the leading jet, defined according to the* SISCONE *algorithm, with different jet cuts.*

PYTHIA results to the full NLO cross section of POWHEG. We use the new p_T-ordered shower defined in the PYEVNW routine of PYTHIA, that should be more appropriate when interfacing to POWHEG.

Figure 5.9: *Comparison between* POWHEG *and* PYTHIA *for the rapidity, invariant mass and transverse-momentum distributions of a Higgs boson with* $m_H = 120$ *GeV, at Tevatron* $p\bar{p}$ *collider.* PYTHIA *outputs normalized to the* POWHEG *cross section.*

Figure 5.10: *Comparison between* POWHEG *and* PYTHIA *for the rapidity of the leading jet and the rapidity difference of the Higgs boson and the leading jet, defined according to the* SISCONE *algorithm, with different jet cuts.* PYTHIA *outputs are normalized to the* POWHEG *cross section.*

The only difference with respect to the POWHEG-MC@NLO comparisons is in the
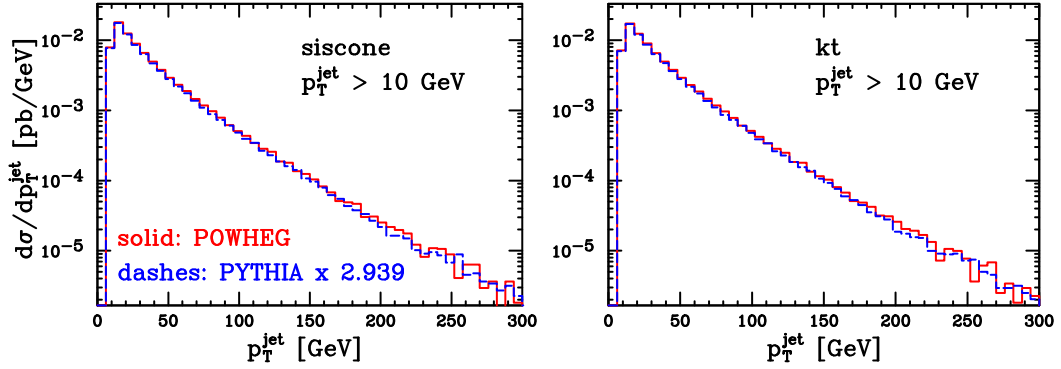
Figure 5.11: *Comparison between* POWHEG *and* PYTHIA *for the transverse-momentum distributions of the leading jet, defined according to the* SISCONE *and the* KT *algorithms.* PYTHIA *outputs are normalized to the* POWHEG *cross section.*

Figure 5.12: *Comparison between* POWHEG *and* PYTHIA *for the rapidity, invariant mass and transverse-momentum distributions of a Higgs boson with* $m_H = 120$ *GeV, at the LHC.* PYTHIA *outputs are normalized to the* POWHEG *cross section.*

generation of the Higgs boson virtuality, distributed now according to

$$\frac{1}{\pi} \frac{\bar{M}^2 \, \Gamma_H / m_H}{\left(\bar{M}^2 - m_H^2\right)^2 + (\bar{M}^2 \, \Gamma_H / m_H)^2} , \qquad (5.76)$$

Figure 5.13: *Comparison between* POWHEG *and* PYTHIA *for the rapidity of the leading jet and the rapidity difference of the Higgs boson and the leading jet, defined according to the* SISCONE *algorithm, with different jet cuts.* PYTHIA *outputs are normalized to the* POWHEG *cross section.*

Figure 5.14: *Comparison between* POWHEG *and* PYTHIA *for the transverse-momentum distributions of the leading jet, defined according to the* SISCONE *and the* KT *algorithms.* PYTHIA *outputs are normalized to the* POWHEG *cross section.*

which is very similar to the form used in PYTHIA, except for the fact that PYTHIA includes threshold effects in the calculation of the Higgs boson width. In fact, PYTHIA uses a running $\Gamma_H(\bar{M}^2)$, that increases when a decay channel opens up. The effects of using a fixed or a running Γ_H are more evident for a heavy Higgs boson, as will be shown in the following.

In figs. 5.9 through 5.11 we compare results for the Tevatron $p\bar{p}$ collider, while in figs. 5.12 through 5.14 we present results for the LHC. In all the plots we have set $m_H = 120$ GeV. Results are in an impressive good agreement, both for inclusive quantities and for more exclusive ones. The only visible difference is in the transverse Higgs boson momentum distribution at low p_{T} at the LHC. This could be due

Figure 5.15: *Comparison between* POWHEG *and* PYTHIA *for the rapidity, invariant mass and transverse-momentum distributions of a Higgs boson with* $m_H = 400$ *GeV, at the LHC.* PYTHIA *outputs are normalized to the* POWHEG *cross section.*

to the different choice of the renormalization and factorization scale in the generation of radiation, our choice being constrained by the requirement of next-to-leading logarithmic accuracy in the Sudakov form factor.

In fig. 5.15 we present a comparison with $m_H = 400$ GeV. Mass thresholds effects in Γ_H are evident in the invariant-mass distribution generated by PYTHIA. Below $2\,m_t$ the total width is smaller than the fixed one we are using, and PYTHIA results are accordingly lower than ours. All other plots show instead good agreement with POWHEG.

The good agreement between POWHEG and PYTHIA was to some extent expected. As already observed in refs. [30, 34], the matrix-element correction method used in PYTHIA [84, 53] bears considerable similarities to POWHEG.

5.5 Hardest-jet rapidity distributions

The discrepancy of POWHEG and MC@NLO in the rapidity distribution of the hardest jet deserves further discussions. In ref. [73], the rapidity distribution of the hardest jet in $t\bar{t}$ production was considered, and a dip was found in MC@NLO results at Tevatron energies. Neither the ALPGEN results, neither the $t\bar{t} + jet$ NLO calculation of ref. [97] shows the same dip in that distribution, as can be seen in fig. 5.16
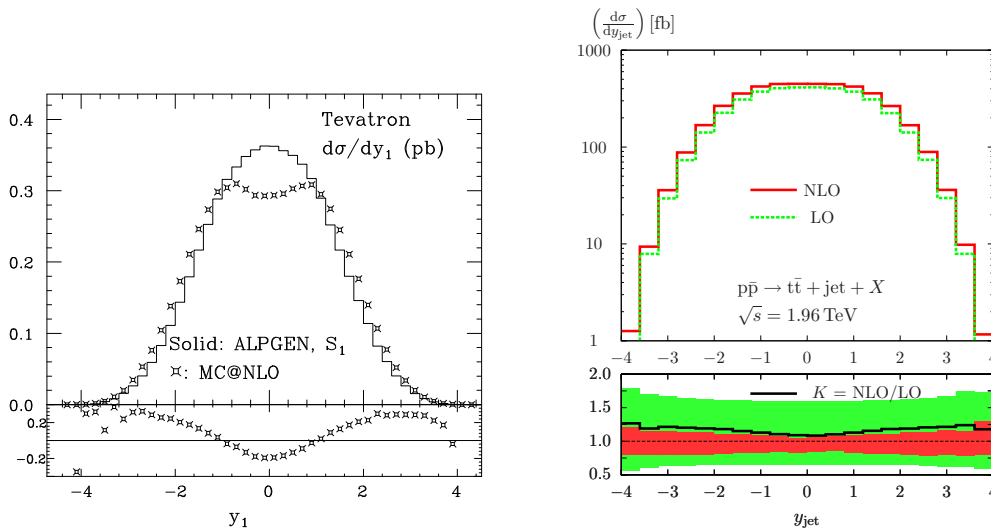
Figure 5.16: *Rapidity distributions of the hardest jet at Tevatron energies found in ref. [73] in the context of a* MC@NLO *-* ALPGEN *comparison (left) and the NLO* $t\bar{t} + jet$ *result of ref. [97] (right).*

In the analysis of chapter 4, in the context of single vector boson production, we found no dip in the rapidity distribution of the hardest jet, for both the MC@NLO and the POWHEG approaches (see left panels of figs. 4.3, 4.6, 4.17, 4.20 and 4.29). Neither we found any dip in the hardest-jet rapidity distribution, in the case of Higgs production via gluon fusion studied in this chapter (see left panels of figs. 5.2, 5.5 and 5.8).

We found instead a dip in the MC@NLO distributions in the rapidity difference between the jet and the vector boson and between the jet and the Higgs boson (see right panels of the aforementioned figures), which is not present in POWHEG results. The distribution in the pseudorapidity difference of the hardest jet with respect to the vector boson was also considered in ref. [95], in the context of a comparison of several matrix-element programs. Although noticeable differences are found among the generators considered there, none of them exhibit a dip at zero pseudorapidity.

It is reasonable to assume that a dip in the rapidity distribution of the jet may be inherited from the dip in the rapidity difference, if the kinematics production regime is forced to be central, like in the case of top-pair production at the Tevatron. We thus also reconsider Z pair production and $t\bar{t}$ production at the Tevatron, obtained through previous POWHEG implementations [26, 27], and compare POWHEG and MC@NLO results for the rapidity distribution of the hardest jet, and for the distribution in the rapidity difference. The results are shown in figs. 5.17 and 5.18. From fig. 5.17 we see
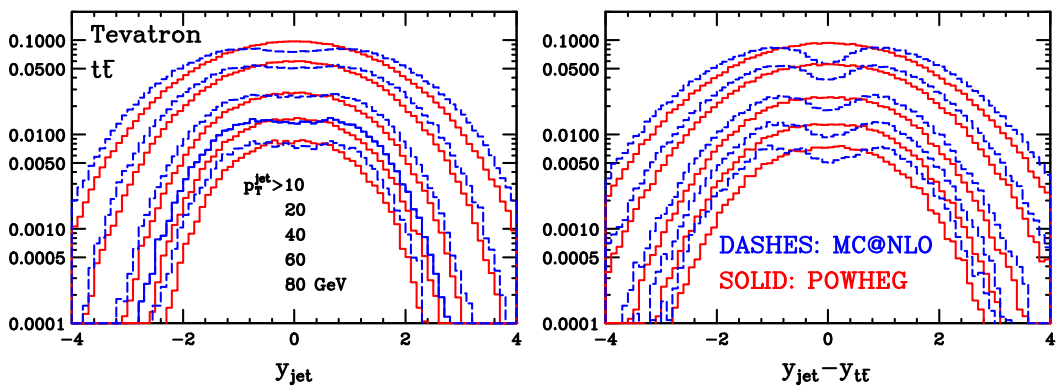
Figure 5.17: *Rapidity distribution of the hardest jet and of the rapidity difference between the hardest jet and the $t\bar{t}$ system at Tevatron energies.*
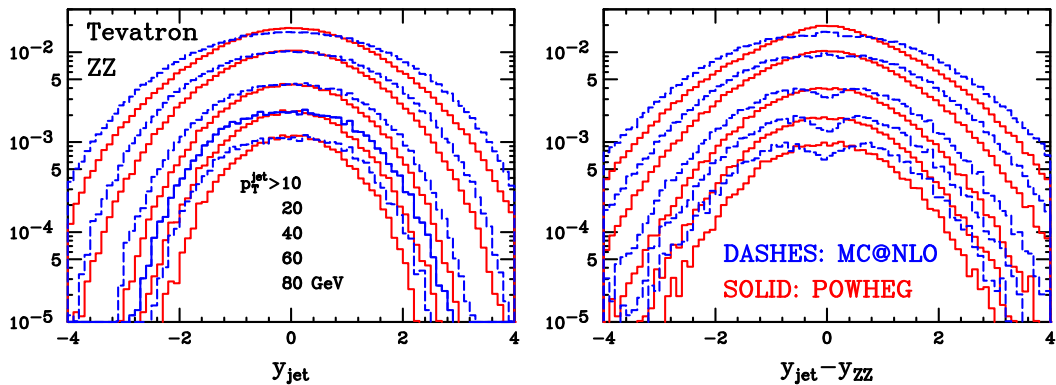
Figure 5.18: *Rapidity distribution of the hardest jet and of the rapidity difference between the hardest jet and the ZZ system at Tevatron energies.*

that the dip present in the $y_{\text{jet}} - y_{t\bar{t}}$ distribution is even deeper than the dip observed in the y_{jet} distribution. Furthermore, in fig. 5.18, we see no particular features in the y_{jet} distribution. The $y_{\text{jet}} - y_{ZZ}$ distribution displays instead a tiny tower and a dip, depending upon the transverse-momentum cut on the jet.

The same authors of ref. [73] performed a deeper analysis of these features, always in case of $t\bar{t}$ production, showing that the `HERWIG` Monte Carlo displays an even stronger dip than `MC@NLO`. A detailed study of this problem was also performed in ref. [38], in the context of Higgs boson production. There, it was shown that both `HERWIG` and `HERWIG++` have a dead radiation region corresponding to central rapidity at high energy. We report their findings in fig. 5.19.
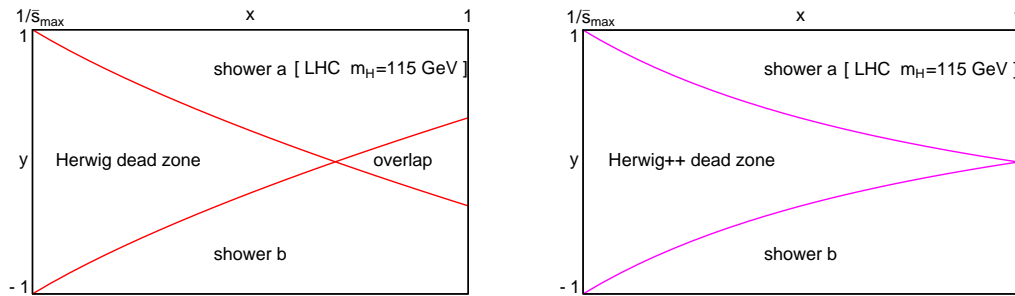
Figure 5.19: `HERWIG` *(left) and* `HERWIG++` *(right) dead zones in the full radiative phase space at LHC energies, as found by the authors of ref. [38]. In the plots, the energy fraction available after radiation is reported onto the x-axis (the soft limit is $x \to 1$), while the cosine of the emission angle (with respect to the beam-axis) is reported onto the y-axis (collinear limits are $y \to \pm 1$).*

The dip in central region in `HERWIG` and `HERWIG++` SMC implementations may thus be attributed to these dead zones. The `MC@NLO` generator provides more events that partially fill the dip, thus correcting the NLO inaccuracies of the LO shower Monte Carlo, but these are not enough to fill the dip.

The same pattern is also observed in the context of Higgs production via gluon fusion, as can be seen in fig. 5.20. There, we show the distributions for the rapidity of the leading jet and the rapidity difference of the Higgs boson and the leading jet, for a Higgs boson of $m_H = 400$ GeV, at the LHC collider. We remark, however, that these features do not mean that `HERWIG` is inaccurate at the LO level, or that `MC@NLO` is inaccurate at the NLO. In fact, a Shower Monte Carlo is accurate in the radiation of the hardest jet only in the collinear regions.

On the other hand, the `POWHEG` program, generate themselves the full NLO result, and thus are not sensitive to this feature of `HERWIG`. In fact, these dips are absent in the `POWHEG` approach, either when interfacing with `HERWIG`, either with `PYTHIA` (see figs. 4.9, 4.12, 4.23, 4.26, 4.32 for single vector boson and figs. 5.10, 5.13 for Higgs boson production.) This is the reason why also in programs which include matrix-
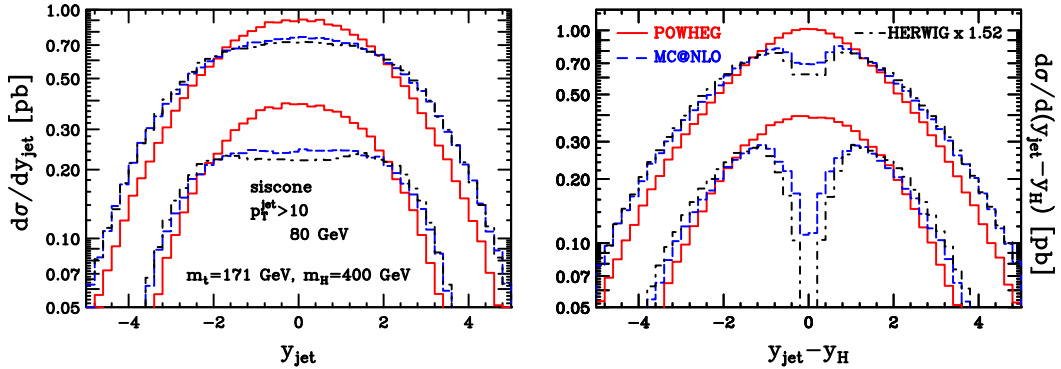
Figure 5.20: *Comparison of* POWHEG, MC@NLO *and* HERWIG *(without matrix-element corrections), for the rapidity of the leading jet and the rapidity difference of the Higgs boson and the leading jet, defined according to the* SISCONE *algorithm, with different jet cuts.*

element matching, and therefore generates their own real NLO contributions, this feature is not observed [95].

In chapter 4 we argued that the dip in the MC@NLO result is compatible with an effect beyond NLO. Following the ideas presented in recent talks [98, 99, 100], we give here a possible explanation of the presence of these dips in the MC@NLO results. According to sec. 3.2.3, we can schematically represent the MC@NLO cross section for the hardest emission with eq. (3.21)

$$
d\sigma = \underbrace{\bar{B}^{\mathrm{MC}}(\bar{\boldsymbol{\Phi}}_n)\, d\bar{\boldsymbol{\Phi}}_n}_{\mathbb{S}\ \mathrm{event}} \underbrace{\left[\Delta^{\mathrm{MC}}(\bar{\boldsymbol{\Phi}}_n, t_0) + \Delta^{\mathrm{MC}}(\bar{\boldsymbol{\Phi}}_n, t)\, \frac{R^{\mathrm{MC}}(\boldsymbol{\Phi}_{n+1})}{B(\bar{\boldsymbol{\Phi}}_n)}\, d\Phi^{\mathrm{MC}}_{\mathrm{rad}} \right]}_{\mathrm{MC\ shower}}
$$

$$
+ \underbrace{\left[R(\boldsymbol{\Phi}_{n+1}) - R^{\mathrm{MC}}(\boldsymbol{\Phi}_{n+1}) \right] d\bar{\boldsymbol{\Phi}}_n\, d\Phi^{\mathrm{MC}}_{\mathrm{rad}}}_{\mathbb{H}\ \mathrm{event}} . \tag{5.77}
$$

The terminology "$\mathbb{S}$" and "$\mathbb{H}$ events" is defined in the original MC@NLO papers [2, 17] and reported in sec. 3.2.1. The functions $\bar{B}^{\mathrm{MC}}(\bar{\boldsymbol{\Phi}}_n)$, $R^{\mathrm{MC}}(\boldsymbol{\Phi}_{n+1})$ and $\Delta^{\mathrm{MC}}(\bar{\boldsymbol{\Phi}}_n, t)$ are instead defined in eqs. (3.22), (3.11) and (3.23), respectively.

We remind that the "MC shower" factor in eq. (5.77) shows that the hardest emission is produced by running the HERWIG shower Monte Carlo, starting with the event kinematics $\bar{\boldsymbol{\Phi}}_n$. According to ref. [4], however, formula (5.77) does correctly represent the hardest emission probability, because of the transverse-momentum-ordered Sudakov form factor $\Delta^{\mathrm{MC}}(\bar{\boldsymbol{\Phi}}_n, t)$, even if the Monte Carlo may not generate the hardest radiation as its first emission.

In the production of a high-p_{T} parton, formula (5.77) yields

$$d\sigma \quad \approx \quad \bar{B}^{\mathrm{MC}}(\bar{\bm{\Phi}}_n) \frac{R^{\mathrm{MC}}(\bm{\Phi}_{n+1})}{B(\bar{\bm{\Phi}}_n)} \, d\bar{\bm{\Phi}}_n \, d\Phi_{\mathrm{rad}}^{\mathrm{MC}} + \left[R(\bm{\Phi}_{n+1}) - R^{\mathrm{MC}}(\bm{\Phi}_{n+1}) \right] d\bar{\bm{\Phi}}_n \, d\Phi_{\mathrm{rad}}^{\mathrm{MC}}$$

$$\approx \quad \overbrace{R(\bm{\Phi}_{n+1}) \, d\bar{\bm{\Phi}}_n \, d\Phi_{\mathrm{rad}}^{\mathrm{MC}}}^{\text{No dip}} + \underbrace{\left(\frac{\bar{B}^{\mathrm{MC}}(\bar{\bm{\Phi}}_n)}{B(\bar{\bm{\Phi}}_n)} - 1 \right)}_{\mathcal{O}(\alpha_{\mathrm{S}})} \overbrace{R^{\mathrm{MC}}(\bm{\Phi}_{n+1}) \, d\bar{\bm{\Phi}}_n \, d\Phi_{\mathrm{rad}}^{\mathrm{MC}}}^{\texttt{HERWIG dip}}, \qquad (5.78)$$

where we have used the fact that $\Delta^{\mathrm{MC}}(\bar{\bm{\Phi}}_n, t) \approx 1$ in this limit. The first term correctly describes the hard radiation in the whole phase space. The second term, while formally subleading in α_{s}, is responsible for the dip. In fact, the dip present in `HERWIG` propagates here with a weight proportional to $(\bar{B}^{\mathrm{MC}}/B - 1)$. Although subleading, this term can be significant for processes with large K factors.

In the processes studied so far, this ratio was significantly higher than 1. For example, for the $gg \to H$ process studied in this chapter, the effect is particularly visible owing to the fact that NLO corrections are of the same order of the LO result.

On the other hand, it easy to show that, modifying the `MC@NLO` code, replacing $\bar{B}^{\mathrm{MC}}(\bar{\bm{\Phi}}_n) \to B(\bar{\bm{\Phi}}_n)$ in eq. (5.77) (thus canceling the $(\bar{B}^{\mathrm{MC}}/B - 1)$ factor of eq. (5.78)), one obtain a formula which, although normalized only at the leading order, does not lead to any dip in the rapidity difference distributions.

5.6   The p_{T} distribution in POWHEG

In this section we address the discrepancy in the Higgs boson p_{T} distributions in `POWHEG` and in `MC@NLO`. First of all, we show in fig. 5.21 a comparison between the p_{T} spectrum of `POWHEG`, `MC@NLO` and the NLO calculation. For sake of comparison, we have used in `POWHEG` and in the NLO calculation the same scale choice adopted in `MC@NLO`. We point out, however, that using a scale that depends upon the transverse momentum of radiation in `POWHEG` can only affect the $\bar{B}$ function. More specifically, one ends up using a transverse momentum dependent scale only in calculation of the real contributions in $\bar{B}$, since the transverse momentum is zero for the Born, virtual and collinear remnant terms. Thus, this scale does not depend upon the transverse momentum of the real radiation, that is generated afterward using the
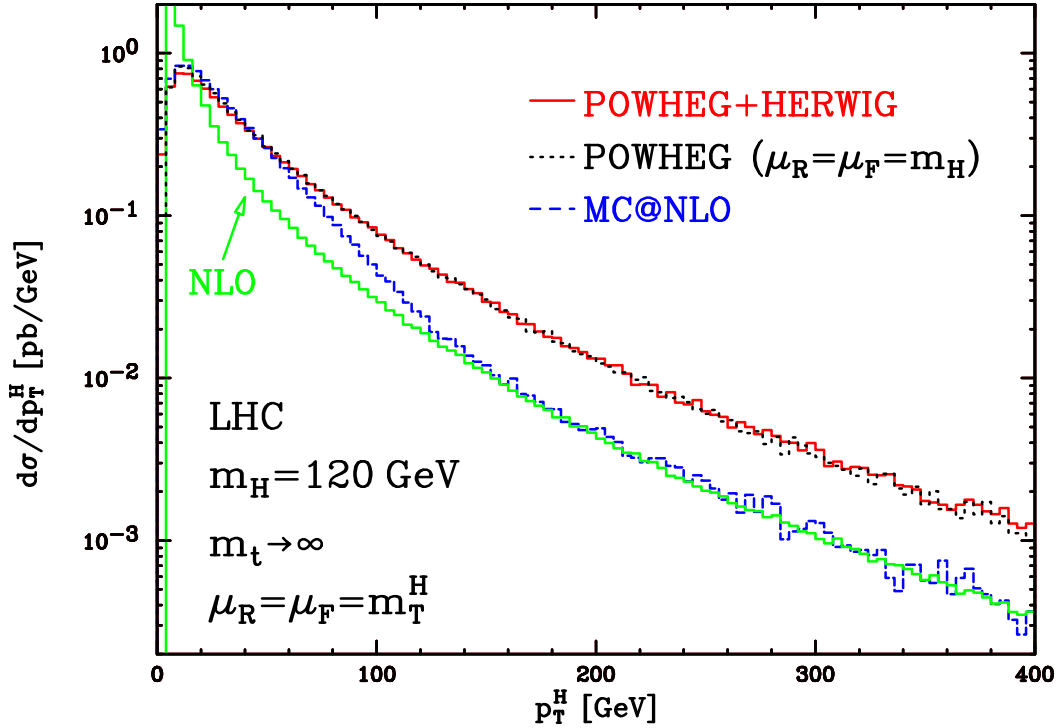
Figure 5.21: *Comparison between* POWHEG, MC@NLO *and the NLO calculation, for* $m_H = 120$ *GeV at the LHC. All calculations are performed in the* $m_t \to \infty$ *approximation. Shower and hadronization are included in the MC results. The* POWHEG *result is also presented without shower and hadronization, and with a fixed-scale choice.*

POWHEG Sudakov form factor. The choice of scale for radiation affects instead a single power of the coupling constant, since the Sudakov exponent is proportional to α_s. At low transverse momentum, this scale cannot be changed without spoiling the NLL accuracy of the Sudakov form factor. It can be changed, however, at large transverse momentum to explore further uncertainties. However, we have preferred not to implement this possibility. One should recall, in fact, that this scale only affects a single power of α_s, and it thus has a much smaller effect than a scale change in the NLO cross section.

We see from fig. 5.21 that MC@NLO agrees better than POWHEG with the NLO calculation at large p_T. Since the difference between MC@NLO and POWHEG should be of next-to-next-to-leading order (NNLO), the difference between POWHEG and the NLO result should also be of NNLO. In fact we can easily trace the origin of this difference. From eq. (5.74), we infer that, at large p_T, the POWHEG differential cross section can
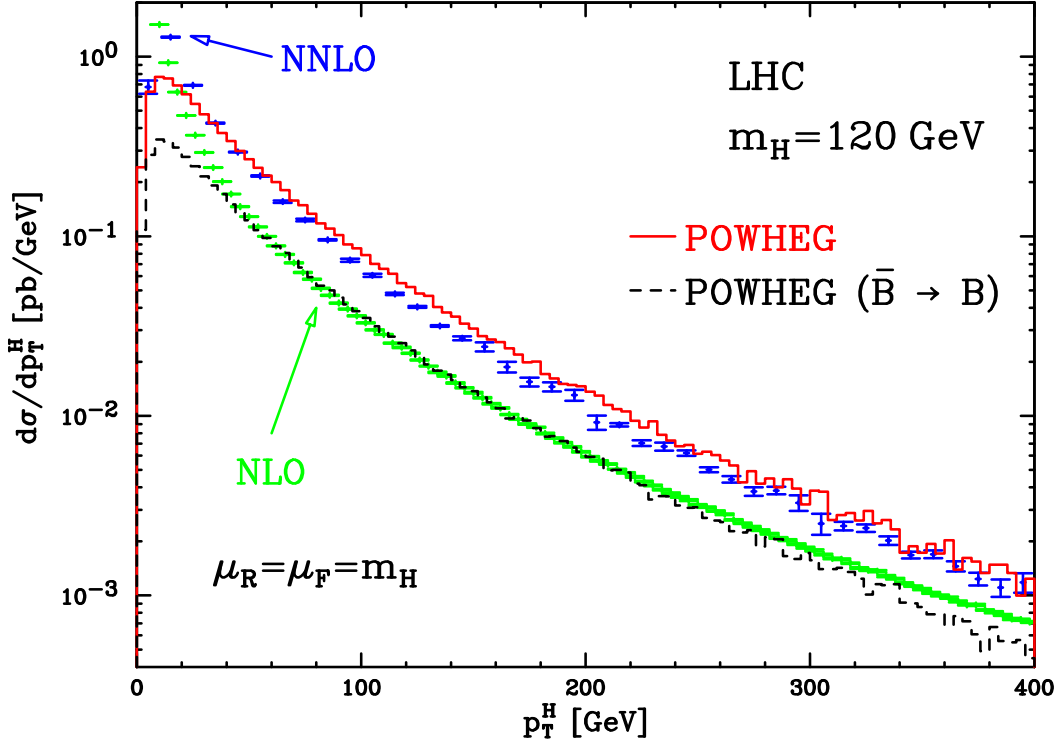
Figure 5.22: *Comparison between* POWHEG *and fixed NLO and NNLO distri-butions for the transverse-momentum of the Higgs boson. Plots are done for* $m_H = 120$ *GeV at the LHC.*

be written as

$$d\sigma = \left[\bar{B}(\bar{\mathbf{\Phi}}_1) \frac{R(\mathbf{\Phi}_2)}{B(\bar{\bar{\mathbf{\Phi}}}_1)} + \sum_q R_{q\bar{q}}(\mathbf{\Phi}_2) \right] d\bar{\mathbf{\Phi}}_1 \, d\Phi_{\text{rad}} , \qquad (5.79)$$

since the Sudakov form factor approaches 1 in this region. Neglecting the subdominant $q\bar{q}$ real contribution, this differs from the pure NLO result because of the presence of the factor

$$\frac{\bar{B}(\bar{\bar{\mathbf{\Phi}}}_1)}{B(\bar{\bar{\mathbf{\Phi}}}_1)} = 1 + \mathcal{O}(\alpha_{\text{s}}) . \qquad (5.80)$$

It is known that radiative corrections in Higgs boson production are large, so that the $\mathcal{O}(\alpha_{\text{s}})$ term is in fact of order 1, and thus we find an enhancement that approaches a factor of two.[3] We have performed a clear cut test of this interpretation of the

---

[3]We recall that normally the numerator and denominator in this factor are evaluated at different scales, since in $\bar{B}$ one uses a scale of the order of the Higgs boson transverse mass, while in the B term, one uses the transverse momentum. However, at large p_{T}, the two scales become of the same order.

discrepancy. We have replaced the $\bar{B}$ function with the Born term B in the POWHEG program. The result of this calculation is shown in comparison with the NLO curve in fig. 5.22. Since, as shown in fig. 5.21, the shower and hadronization are irrelevant for this distribution, we do not include them in the figure. In fig. 5.22 we have chosen to use p_{T} independent renormalization and factorization scales, in order to perform a consistent comparison. Notice that, with this choice of scales, the NLO distribution is harder than the one shown in fig. 5.21. This is easily explained by the fact that the NLO process is proportional to $\alpha_{\mathrm{S}}^3(\mu_{\mathrm{R}})$, and thus a p_{T} dependent renormalization scale can alter significantly the p_{T} distribution.

At this point, we can ask whether the higher order terms included in POWHEG with the mechanism illustrated above do in fact give a reasonable estimate of true NNLO effects. We thus include in fig. 5.22 the NNLO result, obtained from the HNNLO program of ref. [94]. The result shows a rather good agreement between the NNLO result and POWHEG. Thus, our seemingly large corrections to the Higgs boson p_{T} distributions are in fact very similar in size to the full NNLO result. Observe that in fig. 5.22 we have used a fixed scale choice for all the results. We were forced to do this, since the HNNLO program does not allow for other choices. However, because of the good agreement of the two POWHEG results in fig. 5.21, and because of the smaller scale dependence of the NNLO result, this should not make a severe difference.

Because of a fortuitous circumstance, we did not need to worry about correcting for the large difference between the POWHEG and the NLO result at large radiation transverse momentum, since the known NNLO result seems to support the POWHEG one. We remark, however, that, had this not been the case, it is very easy to modify the POWHEG algorithm so to obtain a p_{T} spectrum that agrees with the NLO calculation at large p_{T}. This can be done as follows. As shown in sec. 3.3.5, instead of using the full real cross section for the computation of the $\bar{B}$ function and of the Sudakov form factor, we can instead use a reduced real contribution

$$R^{\mathrm{red}} = R \times F \,, \tag{5.81}$$

where F is a function of the real phase space, with $F < 1$ everywhere, such that F approaches 1 for small transverse momenta, and approaches zero for large transverse momenta. We perform the POWHEG generation using R^{red} instead of R, and treat the remaining $R \times (1 - F)$ contribution to the cross section with the same method that we used for the $R_{q\bar{q}}$ contribution. This can be done, since $R \times (1 - F)$ is damped by the $1 - F$ factor in the singular region. It will then follow that, for

large transverse momentum, the result would agree with the NLO calculation, since
it would be dominated by the $R \times (1 - F)$ contribution. It turned out that, in all
previous implementations, it was not necessary to use such procedure. As remarked
before, thanks to the known properties of the NNLO result, this was not necessary
even in this case. We have however performed such study, just in order to illustrate
the flexibility of the POWHEG method. We have chosen for F the following form

$$F = \frac{h^2}{p_{\mathrm{T}}^2 + h^2} \, . \qquad (5.82)$$

The resulting transverse-momentum distribution at the LHC, for a Higgs boson mass
of 400 GeV, is shown in fig. 5.23 for $h \to \infty$ (standard POWHEG), $h = 120$ GeV and
$h = 400$ GeV. One can see that it is not difficult to get distributions that undershoot
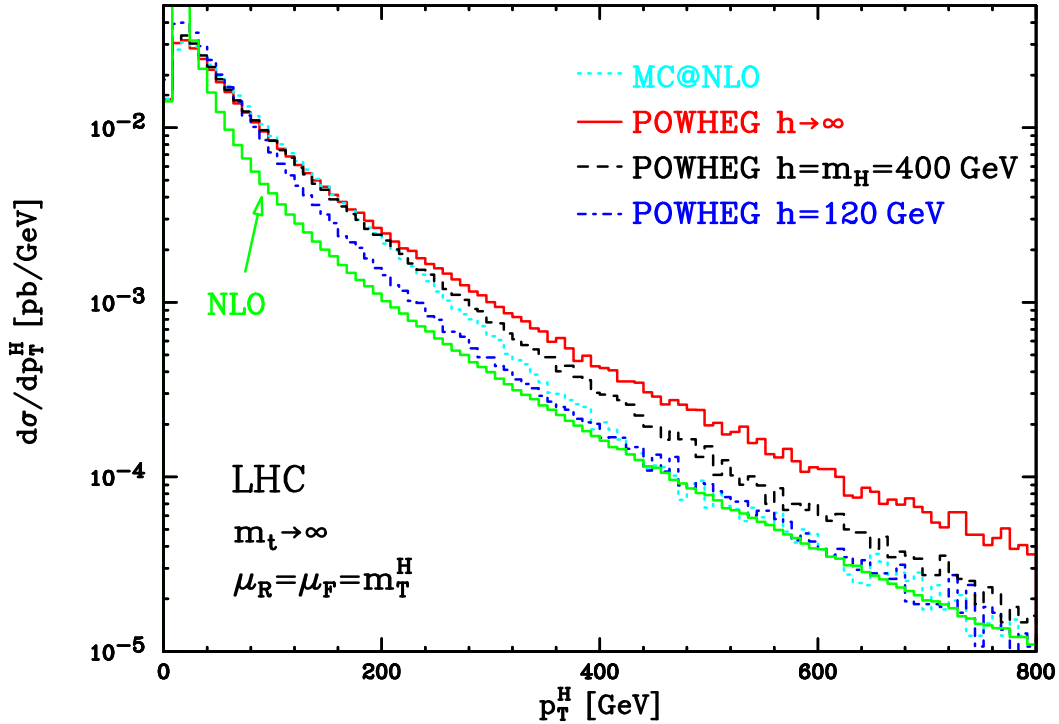
Figure 5.23: *Comparison of the predictions of* MC@NLO, *standard* POWHEG *($h \to \infty$) and* POWHEG *with two different values of the parameter h ($h = 120$ GeV and $h = m_H = 400$ GeV) in the function F of eq. (5.82), for the transverse-momentum distributions of a Higgs boson, at the LHC pp collider.*

the MC@NLO one in the intermediate range of p_{T}. We also observe that, with this
procedure, no undesired features of other distributions appear. In particular, the
distribution in the rapidity of the hardest jet, and in the rapidity difference between

the hardest jet and the Higgs boson remain qualitatively the same, as shown in fig. 5.24. We remark that the large $\bar{B}/B$ factor responsible for the harder Higgs boson $p_{\rm T}$ spectrum cannot generate any dip in POWHEG, since here HERWIG has no role in the generation of the hardest radiation. Thus the dip, which we show in sec. 5.5 to be inherited from HERWIG, does not appear in the POWHEG approach.
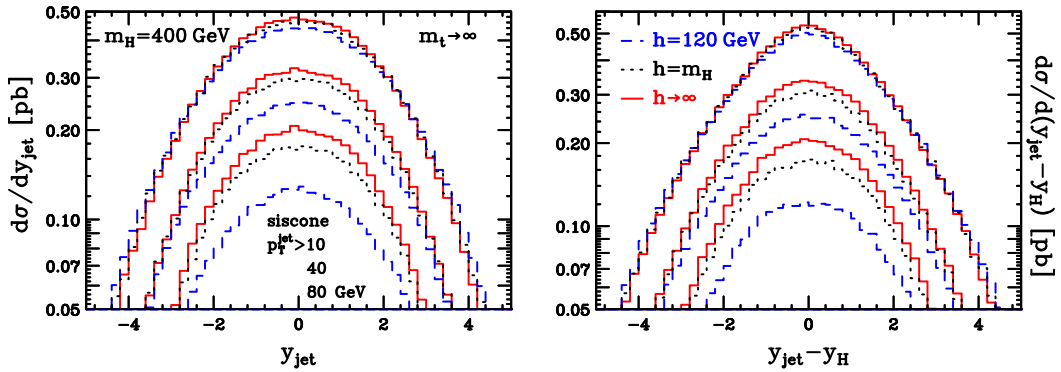
Figure 5.24: *Comparison of the predictions of the standard POWHEG ($h \to \infty$), and POWHEG with two different values of the parameter h ($h = 120$ GeV and $h = m_H = 400$ GeV) in the function F of eq. (5.82), for the rapidity of the leading jet and the rapidity difference of the Higgs boson and the leading jet, defined according to the SISCONE algorithm, with different jet cuts, at the LHC.*

5.6.1 Reduction of real contributions in the Sudakov form factor

In the previous section we showed how the reduction of the real contributions that enters the Sudakov form factor may be performed through the inclusion of an F function, in order to get that the high-$p_{\rm T}$ behaviour of Higgs boson transverse-momentum distribution approaches the NLO result.

In this section we test two functional form of F. The first is those reported in eq. (5.82), while the other is

$$F = (1 - \beta^{\alpha})^{\gamma}, \qquad (5.83)$$

where β can be expressed in terms of real radiation variables (see eqs. (5.10), (5.14) and (5.56)) as

$$\beta = \tilde{\xi}\sqrt{1 - y^2} \qquad (5.84)$$

and α, γ are real positive parameters. In any case, one can always recover *unreduced* results simply by setting $F = 1$.

In the following, we show some comparisons of various distributions obtained using both of these functions, changing the values of some parameters. In all the following figures the large top-mass limit is enforced.

The first comparison is run for a Higgs boson mass of $m_H = 120$ GeV at the LHC pp collider. In this case we consider only the first reducing F function, choosing $h = m_H$ and performing the calculation in the large-m_t limit. Results are shown in figs. 5.25 through 5.27.
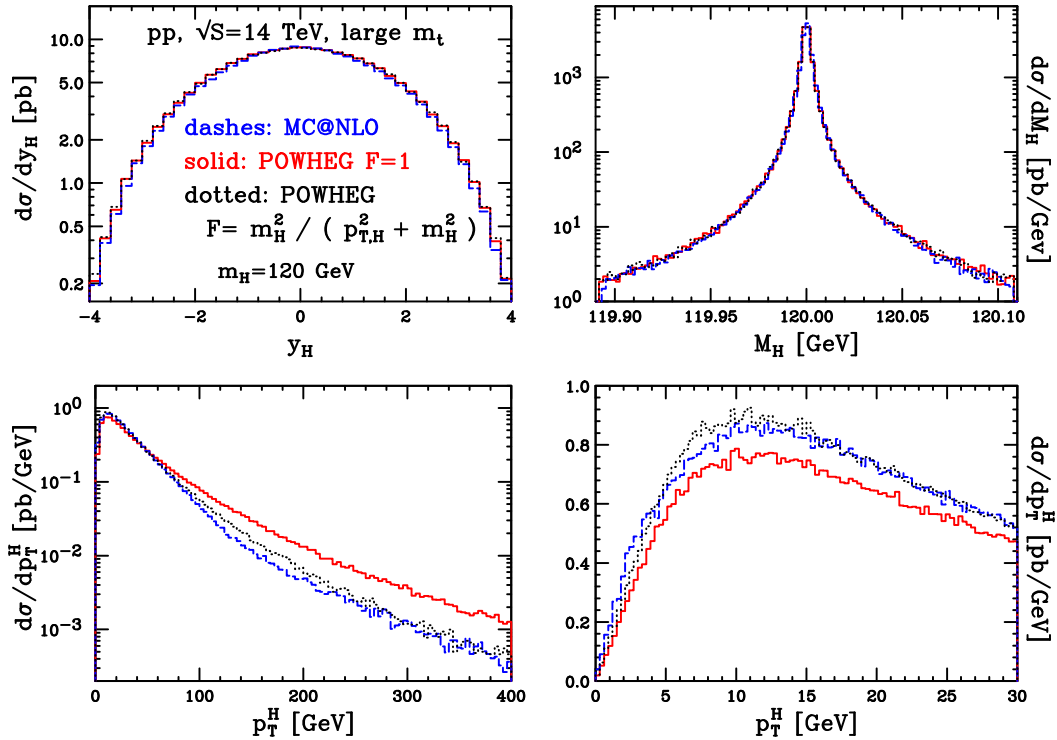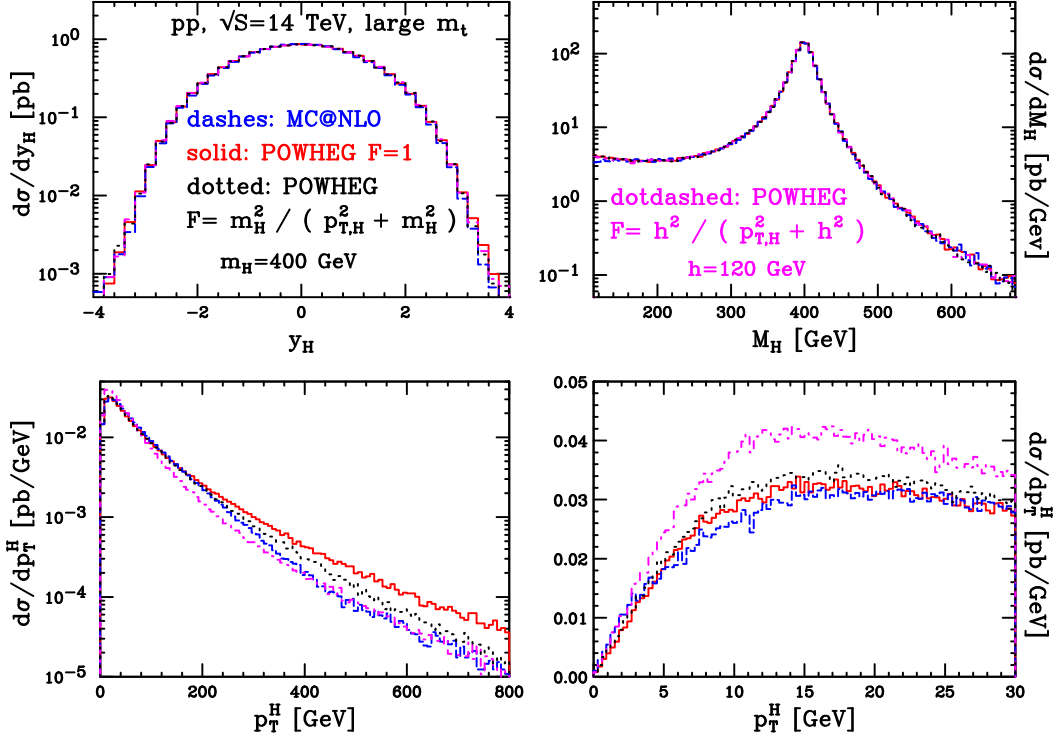

Figure 5.25: *Comparison between* POWHEG *and* MC@NLO *for the rapidity, invariant mass and transverse-momentum distributions of a Higgs boson with* $m_H = 120$ *GeV, at the LHC pp collider.*

The second comparison is run for a Higgs boson mass of $m_H = 400$ GeV at the LHC pp collider. We compare here the effect of different reducing functions, changing either the functional form of F, either its parameters. From fig. 5.28 to 5.30 we show the results for $F = \frac{h^2}{p_T^2 + h^2}$, with $h = m_H = 400$ GeV and $h = 120$ GeV. From fig. 5.31 to 5.33 we instead change the definition of F, adopting $F = (1 - \beta^\alpha)^\gamma$, with $\beta = \tilde{\xi}\sqrt{1 - y^2}$ and varying $\alpha = \gamma = 1, 2$.
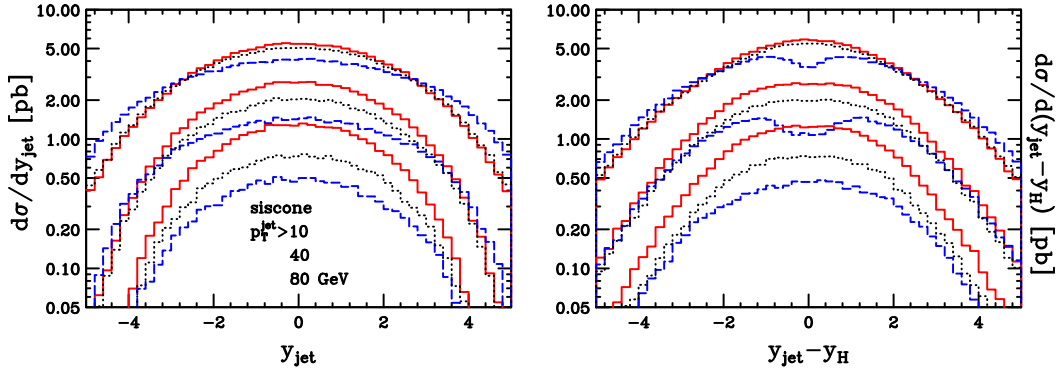
Figure 5.26: *Comparison between* `POWHEG` *and* `MC@NLO` *for the rapidity of the leading jet and the rapidity difference of the Higgs boson and the leading jet, defined according to the* `SISCONE` *algorithm, with different jet cuts.*
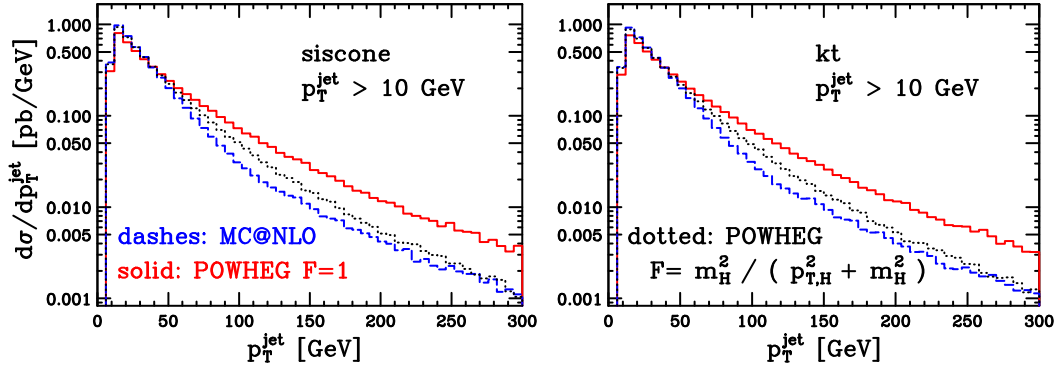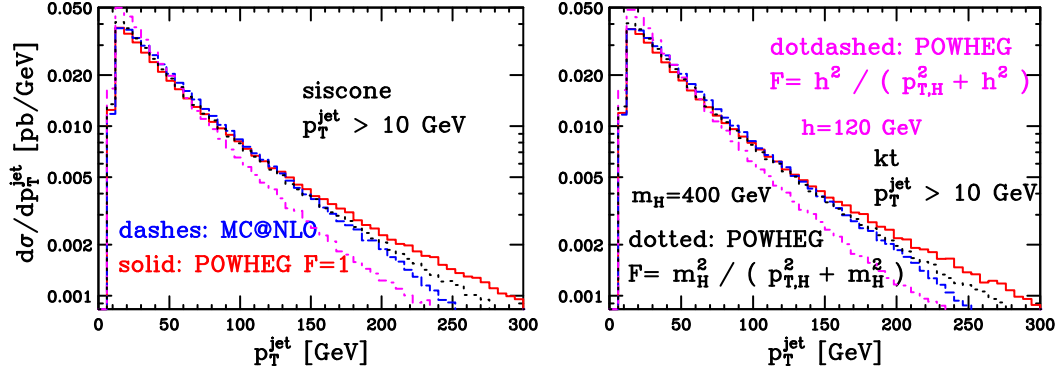

Figure 5.27: *Comparison between* `POWHEG` *and* `MC@NLO` *for the transverse-momentum distributions of the leading jet, defined according to the* `SISCONE` *and the* `KT` *algorithms.*

From the previous plots it is clear that the `POWHEG` approach is flexible enough to tune the part of real contributions which is then dealt with the shower technique. The important thing is to maintain the correct behaviour of the Sudakov form factor when singular limits are approached. On the contrary, in the `MC@NLO` approach this freedom is not present, since the part of the real contribution which is then showered is fixed by the shower itself, as one can evince looking at eq. (5.77).
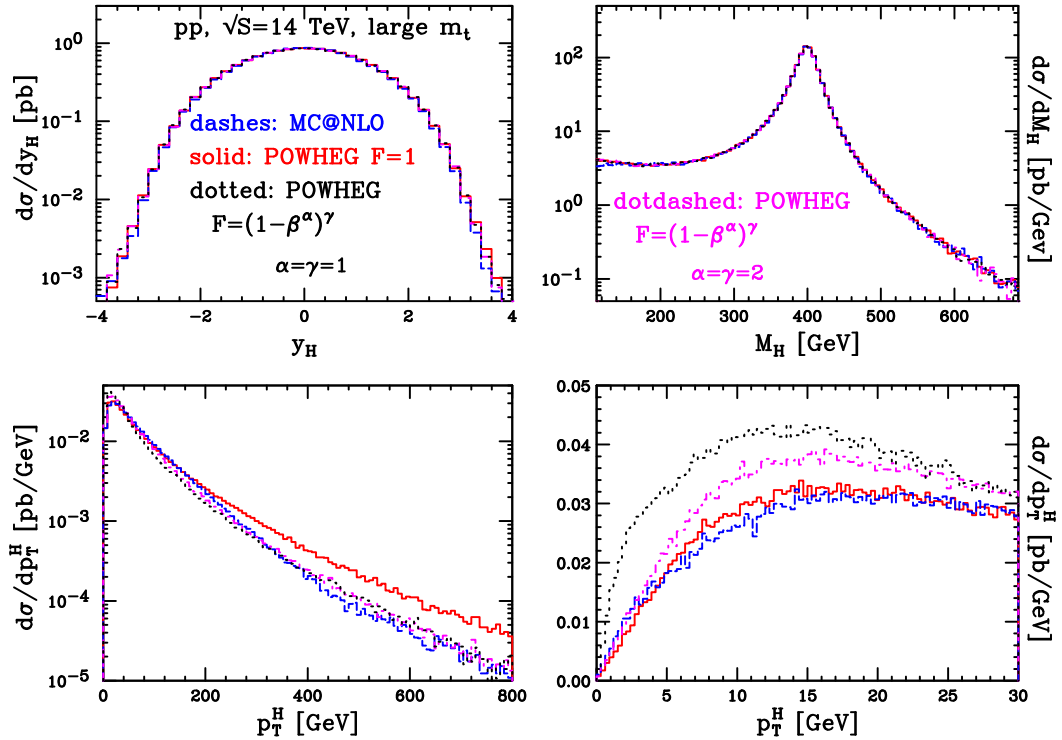
Figure 5.28: *Comparison between* POWHEG *and* MC@NLO *for the rapidity, invariant mass and transverse-momentum distributions of a Higgs boson with* $m_H = 400$ *GeV, at the LHC pp collider.*
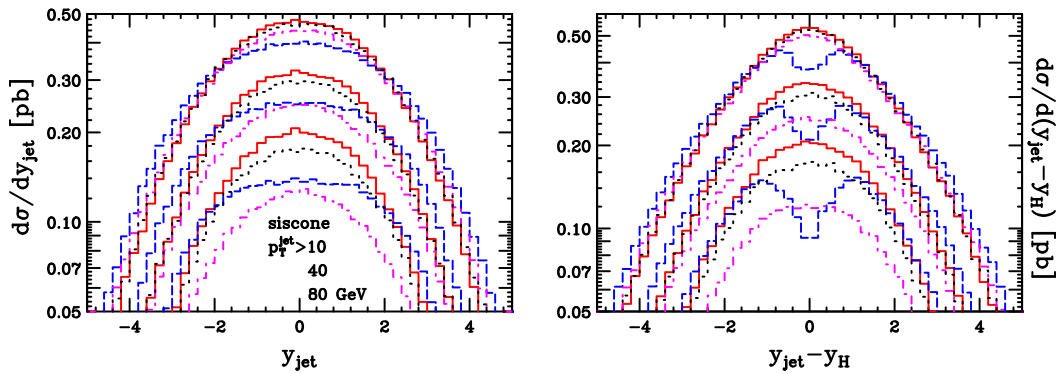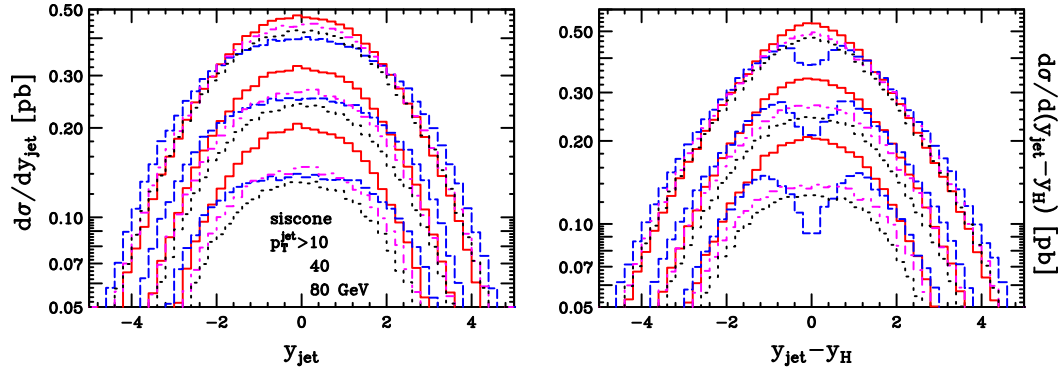

Figure 5.29: *Comparison between* POWHEG *and* MC@NLO *for the rapidity of the leading jet and the rapidity difference of the Higgs boson and the leading jet, defined according to the* SISCONE *algorithm, with different jet cuts.*
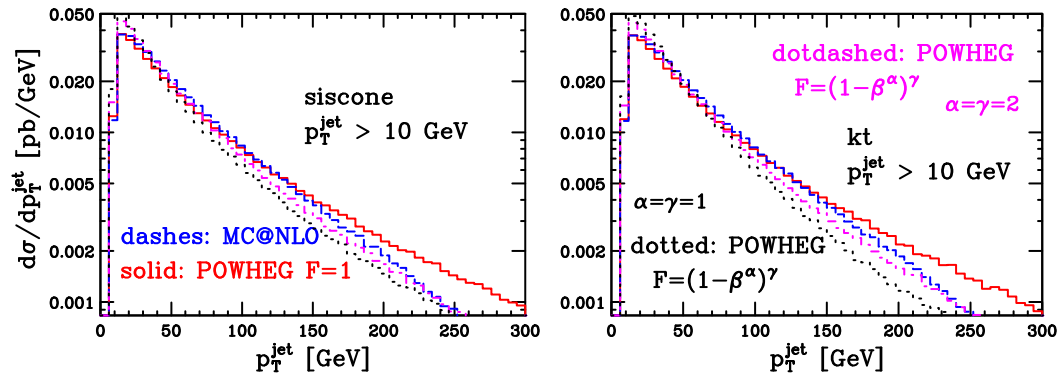
Figure 5.30: *Comparison between* POWHEG *and* MC@NLO *for the transverse-momentum distributions of the leading jet, defined according to the* SISCONE *and the* KT *algorithms.*

Figure 5.31: *Comparison between* POWHEG *and* MC@NLO *for the rapidity, invariant mass and transverse-momentum distributions of a Higgs boson with* $m_H = 400$ *GeV, at the LHC pp collider.*

Figure 5.32:   *Comparison between* POWHEG *and* MC@NLO *for the rapidity of the leading jet and the rapidity difference of the Higgs boson and the leading jet, defined according to the* SISCONE *algorithm, with different jet cuts.*

Figure 5.33:   *Comparison between* POWHEG *and* MC@NLO *for the transverse-momentum distributions of the leading jet, defined according to the* SISCONE *and the* KT *algorithms.*
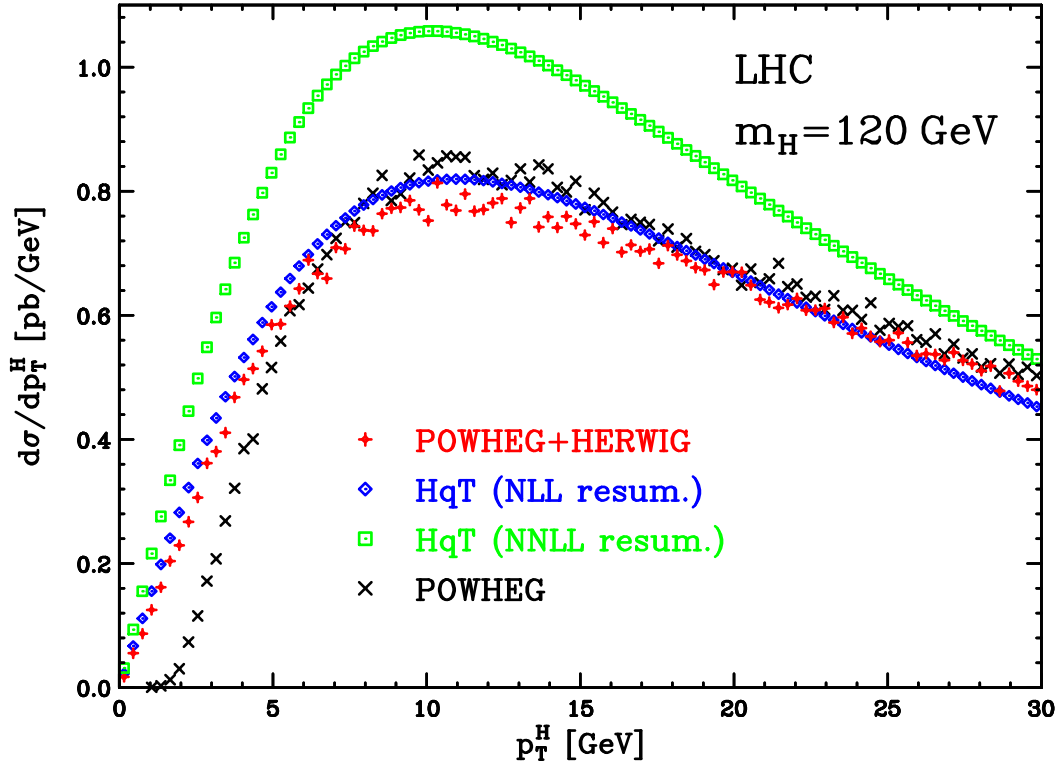
5.7 Next-to-leading logarithmic resummation

Figure 5.34: *Comparison between* POWHEG *and* HqT *for the transverse-momentum distributions of a Higgs boson, at the LHC. The* POWHEG *result without shower and hadronization is also shown.*

As summarized in section 3.3.3, and explained in sec. 4.4 of ref. [30], one can reach next-to-leading logarithmic (NLL) accuracy of soft gluon resummation if the number of coloured partons involved in the hard scattering is less or equal to three. This can be obtained by replacing the strong coupling constant in the Sudakov exponent with [61]

$$\alpha_{\rm S} \to A\left(\alpha_{\rm S}\left(k_{\rm T}^2\right)\right), \qquad A(\alpha_{\rm S}) = \alpha_{\rm S}\left\{1 + \frac{\alpha_{\rm S}}{2\pi}\left[\left(\frac{67}{18} - \frac{\pi^2}{6}\right)C_{\rm A} - \frac{5}{9}n_{\rm f}\right]\right\}, \qquad (5.85)$$

where the $\overline{\rm MS}$, 1-loop expression of $\alpha_{\rm S}$ should be used. The previous replacement may also be implemented by a simple redefinition of the strong scale Λ, which, for five active flavours ($n_{\rm f} = 5$), becomes $\Lambda_{\rm MC} \equiv 1.569\,\Lambda_{\overline{\rm MS}}^{(5)}$. We have exploited this possibility in our code, so that our result should agree with the NLL resummed one. A comparison has been thus carried out with the HqT [101] program, that performs such

a resummation. We have adopted fixed renormalization and factorization scales. Results are shown in fig. 5.34, together with next-to-next-to-leading logarithmic (NNLL) resummation, always from `HqT`, just for reference purposes. We see a fair agreement between the `POWHEG` result and the NLL analytic one, as expected. The different behaviour of the `POWHEG` result without shower and hadronization at very low p_{T} may be ascribed to the particular implementation of the minimum transverse momentum that we use, that is, to a large extent, arbitrary.

We observe that, in all cases, we do not expect full agreement between the `POWHEG` result without shower, and the NLL calculation. In fact, the `POWHEG` curve without shower represents the Sudakov form factor for the p_{T} of the hardest emission, while, in the NLL calculation, the total p_{T} distribution (i.e. the sum of the transverse momenta of all emissions) is considered. Thus, it is only after the inclusion of the full shower effects that the two distributions have a meaningful comparison.

5.8   Renormalization and factorization scale dependence

In this section we address the issue of renormalization and factorization scales dependence of our results, comparing them with available codes that perform similar tasks. All programs have been run with fixed renormalization and factorization scales, starting from $\mu_{\mathrm{F}} = \mu_{\mathrm{R}} = m_H/2$ and then varying them by a factor two, in both directions, between subsequent runs. This should give a *naïve* estimate of the size of higher order corrections. We choose for the Higgs boson mass the value $m_H = 120$ GeV. We show comparisons among distributions from different programs: we consider the $gg \rightarrow H$ implementation of `POWHEG`, `MC@NLO` and the pure fixed order result with NLO accuracy, which we obtained sampling phase space points, with the corresponding weight, during thee valuation of the total cross section at the NLO. We instead used the program `HNNLO` [94] for the NNLO results. Furthermore the p_{T} distribution away from the origin has been checked against the MCFM implementation for the $H + 1j$ production process, being this distribution affected only by real contributions, i.e. those corresponding to $H + 2j$ matrix elements. All the following figures are obtained in the large top-mass limit, for the pp LHC collider, running at $\sqrt{S} = 14$ TeV.

In figs. 5.35, 5.36 and 5.37 we show the Higgs boson p_{T} distributions of `POWHEG` compared with the NLO, `MC@NLO`and `MCFM` (for the $H + jet$ process) results. The
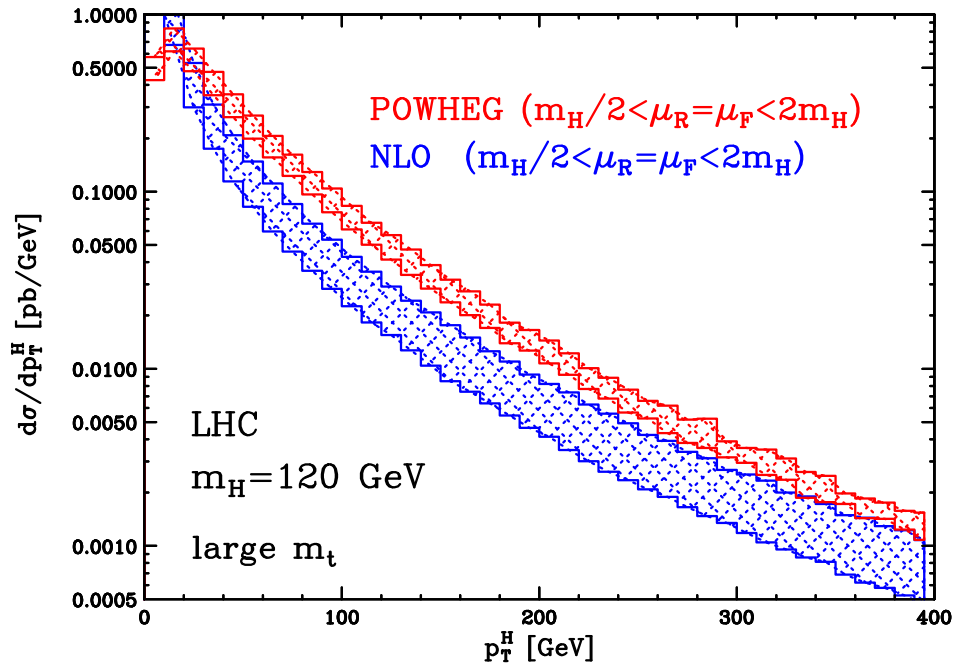
Figure 5.35: *Comparison between* POWHEG *and fixed NLO results for the transverse-momentum distributions of a Higgs boson with $m_H = 120$ GeV, at the LHC pp collider.*

magnitude of different variations may be explained considering that the MC@NLO and the NLO results away from the first bin receive real contributions of order $\alpha_s^3(\mu)$ only. Due to formula (3.43), the POWHEG high-transverse-momentum distributions are instead affected by terms proportional to $\alpha_s^2(\mu)\alpha_s(p_T)$, thus showing a reduced μ-dependence. Finally, the contributions to high-p_T distributions in MCFM for the $H + jet$ process start from order $\alpha_s^4(\mu)$. In this case, however also virtuals can give contributions away from $p_T = 0$, thus lowering the resulting variations. Looking at those figures, the good agreement which we previously found with the results of MCFM is still present. In fig. 5.38 we go even further showing that the good agreement at higher order is present event for an inclusive observable such as the rapidity of the Higgs boson, for which we compare our results against those of HNNLO, that also includes the two-loop virtual contributions. Finally, in figs. 5.39 and 5.40 we return to the issue of the dip in the rapidity difference between the Higgs boson and the hardest-jet, showing that the POWHEG and MC@NLO results are still clearly distinguishable, even when scale variation effects are taken into account.
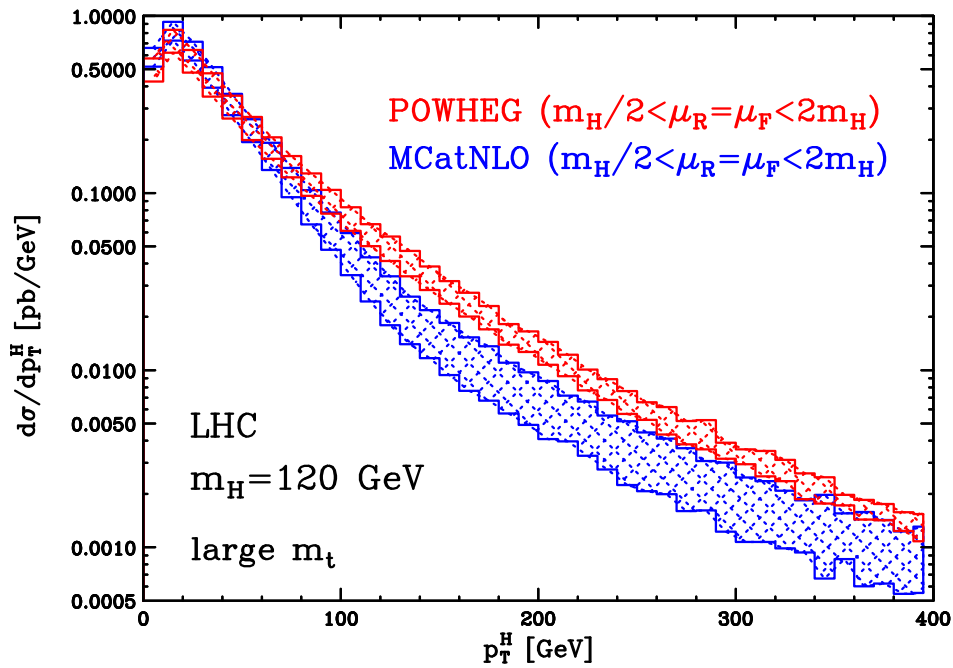
Figure 5.36: *Comparison between* POWHEG *and* MC@NLO *results for the transverse-momentum distributions of a Higgs boson with* $m_H = 120$ *GeV, at the LHC pp collider.*
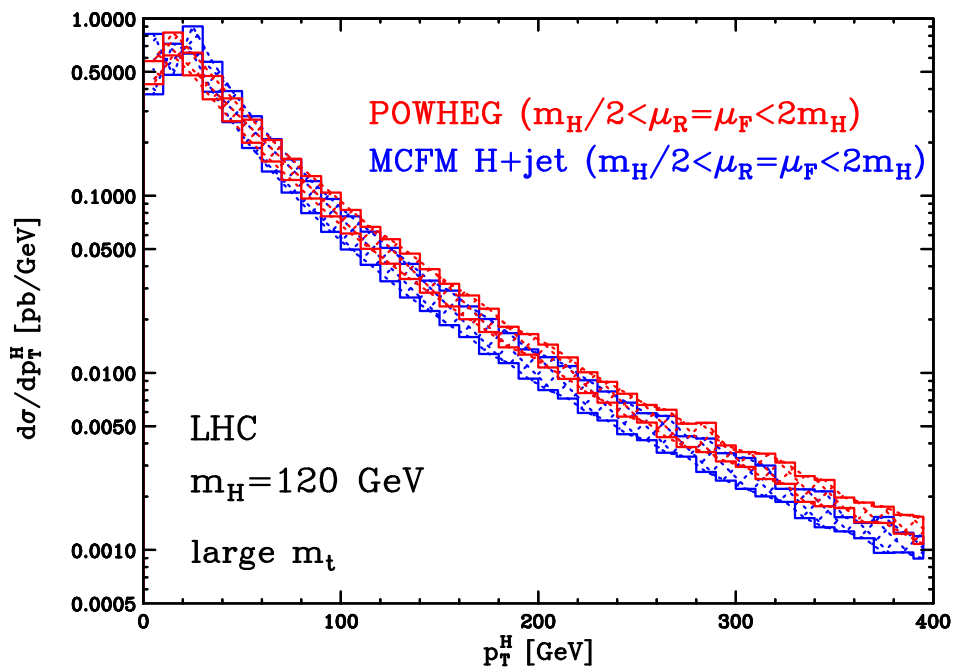

Figure 5.37: *Comparison between* POWHEG *and MCFM results for the transverse-momentum distributions of a Higgs boson with* $m_H = 120$ *GeV, at the LHC pp collider.*
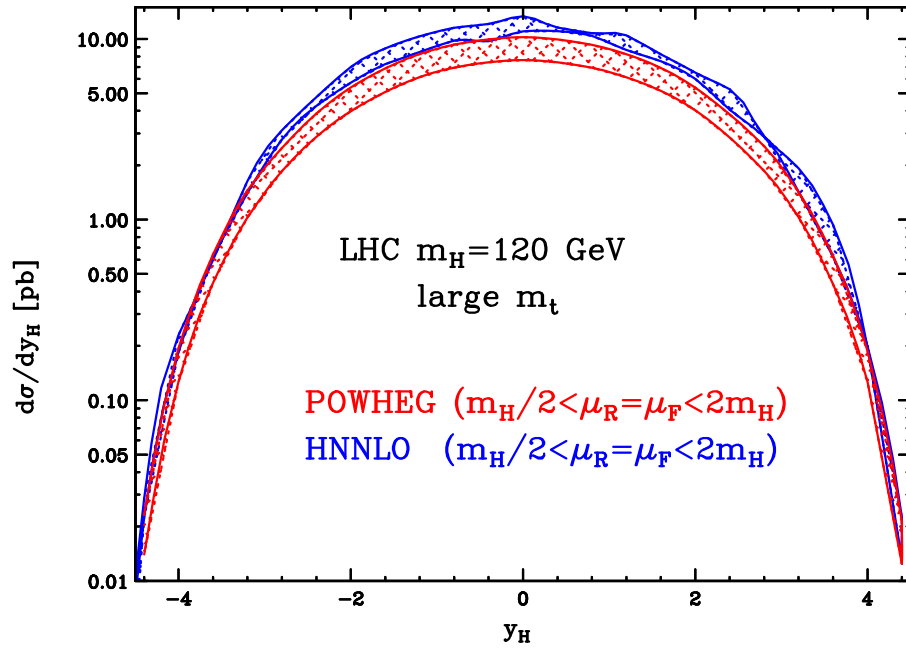
Figure 5.38: *Comparison between* POWHEG *and HNNLO results for the rapidity of the Higgs boson, with* $m_H = 120$ *GeV, at the LHC pp collider.*
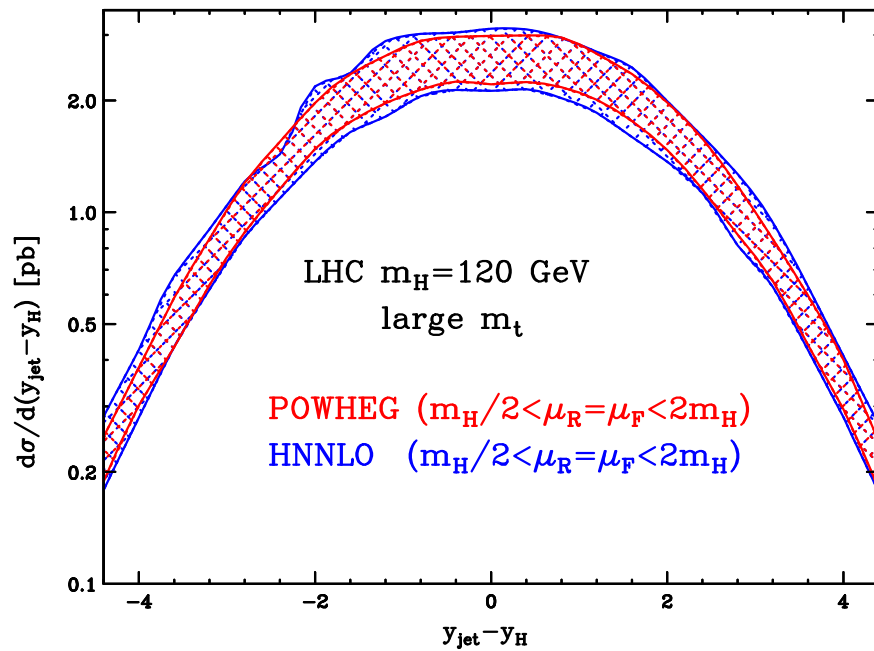

Figure 5.39: *Comparison between* POWHEG *and HNNLO results for the rapidity difference distributions of the Higgs boson, with* $m_H = 120$ *GeV, and the leading jet, defined according to the* SISCONE *algorithm, at the LHC pp collider.*

Figure 5.40: *Comparison between* POWHEG *and* MC@NLO *results for the rapidity difference distributions of the Higgs boson, with* $m_H = 120$ *GeV, and the leading jet, defined according to the* SISCONE *algorithm, at the LHC pp collider.*
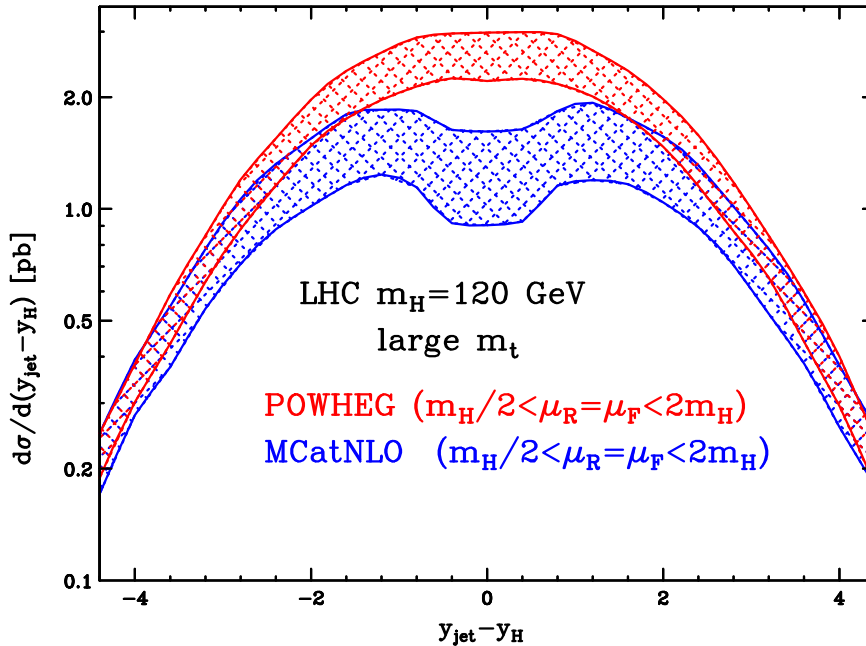
5.9   Conclusions

In this chapter we have reported on a complete implementation of Higgs boson production via gluon fusion at next-to-leading order in QCD, in the POWHEG framework. Following the work published in ref. [37], the calculation was performed within the Frixione-Kunszt-Signer [32, 33] subtraction approach. We have also shown how to deal with non-singular real contributions, that do not present a valid underlying Born matrix element.

The results of our work have been compared extensively with MC@NLO and PYTHIA shower Monte Carlo programs. The PYTHIA results, normalized to the total NLO cross section, are in good agreement with POWHEG, except for differences in the low transverse-momentum distributions of the Higgs boson at the LHC. The MC@NLO results are in fair agreement with POWHEG, except for the p_T distribution of the Higgs boson, and consequently of the hardest jet, in the high-p_T region. In this region the POWHEG distributions are generally harder. We have shown that this is due to NNLO

effects in the POWHEG formula for the differential cross section. We checked that these effects actually bring our result closer to the NNLO one [94]. We have also deepened the study of the high-p_{T} mismatch with respect to fixed order and MC@NLO programs, understanding the origin of these NNLO effects that enhance the POWHEG tail. We show that the POWHEG framework allows enough flexibility to get rid of them, if it is needed. The low-p_{T} region was instead tested against the q_T analytic resummed calculations. We find again good agreement up to NLL accuracy. Furthermore, we have also examined the distributions in the difference of the hardest jet and the Higgs boson rapidity. The MC@NLO dip found in other implementations [26, 27, 34] is still present. We have also examined analogous distributions for ZZ and $t\bar{t}$ production, and again found dips for these distributions. We remark that this seems to be a general feature of MC@NLO, for which we gave a possible explanation, since other calculations do not find effects of this kind [73, 95, 96]. In the final part we have studied the renormalization and factorization scales dependence of our results, comparing with other programs at the same accuracy.

Conclusion

In the recent past, next-to-leading order (NLO) QCD computations have become standard tools for phenomenological studies at lepton and hadron colliders, since the inclusion of NLO terms provides more reliable estimates of the production cross sections. The problem of merging NLO calculations with parton shower simulations, which usually implement LO calculation and resum dominant QCD effects at the leading logarithm level, is basically that of avoiding overcounting. In fact, because of the shower, the SMC programs already implement approximate NLO corrections. Two general solutions of this problem have become available in recent years: the one adopted by the `MC@NLO` program and the `POWHEG` method. The second solution is believed to improve the first one, since it is no more strongly dependent on the SMC which is interfaced to, and, moreover, does not assign events negative weights, spoiling their probabilistic interpretation.

In this thesis we gave a detailed description of the `POWHEG` method and a report on the complete implementations of two next-to-leading order calculations into the `POWHEG` framework: single vector boson hadroproduction and Higgs boson production via gluon fusion. We have also carried out extensive comparisons between the `POWHEG` and `MC@NLO` results, and reasonable agreement has been found, which nicely confirms the validity of both approaches.

We have first presented the features of a general subtraction scheme in chapter 1. There, we have also illustrated in detail two such schemes, adopted in calculations appearing in this thesis: the Catani and Seymour (CS) and the Frixione, Kunszt and Signer (FKS) one. Then in chapter 2, we gave an introductory review of SMC programs. In chapter 3, instead, we have presented the `MC@NLO` and `POWHEG` methods in detail.

Next, in chapter 4, we concentrated on the application of the `POWHEG` method to the process of single vector boson production, where, in the `POWHEG` framework,

the Catani-Seymour subtraction approach was employed for the first time. We also employed a generalization of the method in order to deal with vanishing Born cross sections, as in the case of $W^\pm$ production. Matrix elements were evaluated from scratch using helicity amplitude methods, including finite width effects, Z/γ interference and angular correlations of decay products. Our program has been interfaced both with `HERWIG` and with `PYTHIA`, two of the most popular Shower Monte Carlo used in simulations. Results were found in remarkable agreement both with Tevatron data and with the `MC@NLO` program. We have also discussed results at the LHC collider.

The implementation of the Higgs boson production via gluon fusion process in the `POWHEG` framework, has been then presented in chapter 5, with applications to both Tevatron and LHC colliders. Gluon fusion is the predominant Higgs boson production channel over a wide range of masses. Matrix elements were evaluated analytically and regularized according to the FKS subtraction formalism. The results of our work have been compared extensively with `MC@NLO` and `PYTHIA` shower Monte Carlo programs. Most of the results obtained are in remarkably good agreement with other programs and we gave detailed explanation of the difference found when comparing with `MC@NLO`. In particular we addressed the `POWHEG` higher tail in the Higgs boson transverse-momentum distribution, which brings our results closer to the NNLO ones, and discussed the source of dips in the Higgs-boson – hardest-jet rapidity difference distributions in `MC@NLO` (and in `HERWIG`). We have also studied the renormalization and factorization scales dependence of our results.

Summarizing, in view of the advent of the LHC collider, which will open up several exciting possibilities for new measurements, at energies higher than those previously probed, the merging of NLO calculations with the parton shower approach will be a great advantage for experimentalist collaborations. In this way, indeed, NLO corrections are made directly available, in a flexible form that could be easily used for simulations, therefore improving the reliability of results and the ability to disentangle signals from backgrounds.

The computer codes for the `POWHEG` implementations presented in this thesis are available, together with their manuals, at the site

$$\texttt{http://moby.mib.infn.it/~nason/POWHEG}.$$

Notations and Convenctions

In this appendix we summarize the notations and convections used throughout this thesis.

A.1 Feynman Rules for QCD

External lines

For each external fermion of momentum p, spin s and colour index i running in the fundamental representation $\mathbf{3}$ of $SU(3)$ $i = 1, \ldots, 3$, entering or leaving a graph, include, respectively, the spinor
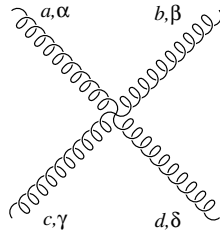
$$u(p, s)_i \qquad \text{or} \qquad \bar{u}(p, s)_i\,. \tag{A.1}$$

For each external anti-fermion of momentum p, spin s and colour $i = 1, \ldots, 3$ (anti-fundamental $\overline{\mathbf{3}}$ of $SU(3)$) entering or leaving a graph, include, respectively, the spinor

$$\bar{v}(p, s)_i \qquad \text{or} \qquad v(p, s)_i\,. \tag{A.2}$$

For each external gluon of momentum k, polarization λ and color index $a = 1, \ldots, 8$ running in the adjoint representation $\mathbf{8}$ of $SU(3)$, entering or leaving a graph, include, respectively, the Lorentz four-vector

$$\epsilon_\mu(k, \lambda)_a \qquad \text{or} \qquad \epsilon_\mu^*(k, \lambda)_a\,. \tag{A.3}$$

Propagators

There are three free-particle propagators: the fermion propagator, the gluon propagator and the ghost propagator. For the gluon (and ghost) propagator we choose the usual covariant gauge-fixing condition eq. (1.24), with λ gauge parameter. With this choice, they read respectively

$$
\underset{i \quad\quad p \quad\quad k}{\longrightarrow} \quad = \quad \delta^{ik} \frac{i}{\not{p} - m + i\epsilon} , \tag{A.4}
$$

$$
\underset{a,\alpha \quad\quad p \quad\quad b,\beta}{\sim\!\sim\!\sim\!\sim} \quad = \quad \delta^{ab} \frac{i}{p^2 + i\epsilon} \left(-g^{\alpha\beta} + (1-\lambda)\frac{p^\alpha p^\beta}{p^2} \right) , \tag{A.5}
$$

$$
\underset{a \quad\quad p \quad\quad b}{-\,-\,-\,\blacktriangleright\,-\,-\,-} \quad = \quad \delta^{ab} \frac{i}{p^2 + i\epsilon} . \tag{A.6}
$$

Vertexes

In QCD, with the choice of a covariant gauge-fixing condition eq. (1.24), four kinds of vertexes may appear: the fermion-gluon vertex, the 3-gluon vertex, the 4-gluon vertex and also the ghost-gluon vertex. They are given by

$$
= \quad -ig\gamma^\alpha t^a_{ij} , \tag{A.7}
$$

$$
= \quad -gf^{abc} \left[g^{\alpha\beta} \left(p_a - p_b \right)^\gamma + g^{\beta\gamma} \left(p_b - p_c \right)^\alpha + g^{\gamma\alpha} \left(p_c - p_a \right)^\beta \right] ,
$$

$$
\tag{A.8}
$$

$$= -ig^2 \Big[f^{eac} f^{ebd} \left(g^{\alpha\beta} g^{\gamma\delta} - g^{\alpha\delta} g^{\gamma\beta} \right) + f^{ead} f^{ebc} \left(g^{\alpha\beta} g^{\gamma\delta} - g^{\alpha\gamma} g^{\beta\delta} \right)$$

$$+ f^{eab} f^{ecd} \left(g^{\alpha\gamma} g^{\beta\delta} - g^{\alpha\delta} g^{\beta\gamma} \right) \Big] ,$$

<div align="right">(A.9)</div>

$$= g f^{abc} p_c^\alpha .$$

<div align="right">(A.10)</div>

Loops

For each loop, integrate (in d dimensions) over the loop momentum ℓ with

$$\int \frac{d^d \ell}{(2\pi)^d} \times S$$

<div align="right">(A.11)</div>

where S is -1 if a fermion or a ghost loop, whilst S is 1 if a gluon or a ghost loop and if a quark-gluon or a ghost-gluon loop.

A.2 Colour Algebra and Useful Relations

$$i, j, k, \ldots = 1, \ldots, N_c , \qquad a, b, c, \ldots = 1, \ldots, N_c^2 - 1 , \qquad N_c = 3 \qquad \text{(A.12)}$$

$$\left[t^a, t^b \right] = i f^{abc} t^c \qquad (t^a)_{ij} = \frac{\lambda^a{}_{ij}}{2} \qquad \text{(A.13)}$$

$$\left[T^a, T^b \right] = i f^{abc} T^c \qquad (T^b)_{ac} = i f^{abc} \qquad \text{(A.14)}$$

$$f^{abc} = -2i \, \text{Tr}\{ \left[t^a, t^b \right] t^c \} \qquad \text{(A.15)}$$

$$\text{Tr}\left\{t^a t^b\right\} = \text{Tr}\left\{T^a T^b\right\} = T_{\text{F}}\delta^{ab} \qquad T_{\text{F}} = \frac{1}{2} \tag{A.16}$$

$$\sum_a (t^a)_{ij}(t^a)_{jk} = C_{\text{F}}\delta_{ik} \qquad C_{\text{F}} = \frac{N_{\text{c}}^2 - 1}{2N_{\text{c}}} = \frac{4}{3} \tag{A.17}$$

$$\sum_{b,c} f^{abc} f^{ebc} = C_{\text{A}}\delta^{ae} \qquad C_{\text{A}} = N_{\text{c}} = 3 \tag{A.18}$$

$$\left\{t^a, t^b\right\}_{ij} = d^{abc} t_{ij}^c + \frac{\delta^{ab}}{N_{\text{c}}} \mathbb{1}_{ij} \tag{A.19}$$

$$\sum_{b,c} d^{abc} d^{ebc} = 4B_{\text{F}}\delta^{ae} \qquad B_{\text{F}} = \frac{N_{\text{c}}^2 - 4}{4N_{\text{c}}} = \frac{5}{12} \tag{A.20}$$

$$\sum_{a,b,c} d^{abc}\left(t^a t^b t^c\right)_{ij} = C_{2,\text{F}}\delta_{ij} \qquad C_{2,\text{F}} = \frac{(N_{\text{c}}^2 - 4)(N_{\text{c}}^2 - 1)}{4N_{\text{c}}^2} = \frac{10}{9} \tag{A.21}$$

$$\sum_a (t^a)_{ij}(t^a)_{kl} = \frac{1}{2}\left(\delta_{il}\delta_{kj} - \frac{1}{N_{\text{c}}}\delta_{ij}\delta_{kl}\right) \tag{A.22}$$

$$(t^a)_{ij}(t^b)_{jk} = \frac{1}{2N_{\text{c}}}\left(\delta_{ik}\delta^{ab}\right) + \frac{1}{2}\left(d^{abc} + if^{abc}\right)t_{ik}^c \tag{A.23}$$

A.3 Gell-Mann Matrices

$$\lambda^1 = \begin{pmatrix} 0 & 1 & 0 \\ 1 & 0 & 0 \\ 0 & 0 & 0 \end{pmatrix}, \quad \lambda^2 = \begin{pmatrix} 0 & -i & 0 \\ i & 0 & 0 \\ 0 & 0 & 0 \end{pmatrix}, \quad \lambda^3 = \begin{pmatrix} 1 & 0 & 0 \\ 0 & -1 & 0 \\ 0 & 0 & 0 \end{pmatrix},$$

$$\lambda^4 = \begin{pmatrix} 0 & 0 & 1 \\ 0 & 0 & 0 \\ 1 & 0 & 0 \end{pmatrix}, \quad \lambda^5 = \begin{pmatrix} 0 & 0 & -i \\ 0 & 0 & 0 \\ i & 0 & 0 \end{pmatrix}, \quad \lambda^6 = \begin{pmatrix} 0 & 0 & 0 \\ 0 & 0 & 1 \\ 0 & 1 & 0 \end{pmatrix},$$

$$\lambda^7 = \begin{pmatrix} 0 & 0 & 0 \\ 0 & 0 & -i \\ 0 & i & 0 \end{pmatrix}, \quad \lambda^8 = \frac{1}{\sqrt{3}}\begin{pmatrix} 1 & 0 & 0 \\ 0 & 1 & 0 \\ 0 & 0 & -2 \end{pmatrix}. \tag{A.24}$$

Useful Integrals and Functions

In this appendix, we want to collect some useful functions and integrals, togheter with their properties, which have been extensively used throughout our computations. We start calculating the generic d–dimensional scalar integrals I resulting from one–loop Feynman diagrams,

$$
I = \int \frac{d^d \ell}{(2\pi)^d} \frac{1}{(\ell + p_1)^2 - m_1^2 + i\eta} \frac{1}{(\ell + p_1 + p_2)^2 - m_2^2 + i\eta} \cdots
$$
$$
\cdots \frac{1}{(\ell + p_1 + p_2 + \cdots + p_n)^2 - m_n^2 + i\eta} \,, \tag{B.1}
$$

where $(+i\eta)$, with $\eta > 0$, gives the prescription of how the contour integral has to be deformed around the poles, and momentum conservation gives

$$
\sum_{i=1}^{n} p_i = 0 \,. \tag{B.2}
$$

We can rewrite I as

$$
I = \int \frac{d^d \ell}{(2\pi)^d} \prod_{i=1}^{n} \frac{1}{D_i} \,, \tag{B.3}
$$

where D_i's are the single denominators in eq. (B.1).

At this point it is useful to employ the Feynman parametrization, which, in the most general form, reads

$$
\prod_{i=1}^{n} \frac{1}{D_i^{c_i}} = \frac{\Gamma(c)}{\prod\limits_{i=1}^{n} \Gamma(c_i)} \int_0^1 \prod_{i=1}^{n} d\alpha_i \, \alpha_i^{c_i - 1} \, \delta\left(1 - \sum_{j=1}^{n} \alpha_j\right) \frac{1}{\left(\sum\limits_{k=1}^{n} \alpha_k D_k\right)^c} \,, \tag{B.4}
$$

where c_i are arbitrary complex numbers and

$$c = \sum_{i=1}^{n} c_i \ . \tag{B.5}$$

In our case one simply has $c_i = 1$ $(i = 1, 2, \dots, n)$, $c = n$.

Using the identity (B.4) and integrating over ℓ, we can rewrite I in the following way

$$
\begin{aligned}
I &= (-1)^n \frac{i}{(4\pi)^{\left(\frac{d}{2}\right)}} \Gamma\left(n - \frac{d}{2}\right) \int_0^1 \prod_{i=1}^{n} d\alpha_i \ \delta\left(1 - \sum_{j=1}^{n} \alpha_j\right) \frac{1}{D^{n-\frac{d}{2}}} \\
&\equiv (-1)^n \frac{i}{(4\pi)^{\left(\frac{d}{2}\right)}} \Gamma\left(n - \frac{d}{2}\right) \int \frac{[d\alpha]}{D^{n-\frac{d}{2}}} \ ,
\end{aligned}
\tag{B.6}
$$

where

$$D = -\sum_{i>j} \alpha_i \, \alpha_j \, s_{ij} + \sum_i \alpha_i \, m_i^2 - i\eta \ , \tag{B.7}$$

s_{ij} is the square of the momentum flowing through the i-j cut of the diagram representing I, and the notation $[d\alpha]$ stands for $\prod_{i=1}^{n} d\alpha_i \ \delta\left(1 - \sum_{j=1}^{n} \alpha_j\right)$.

The Euler Gamma function appearing in eq. (B.6) is defined, for any complex z, by

$$\Gamma(z) = \int_0^\infty dx \, \mathrm{e}^{-x} x^{z-1} \ , \qquad \mathrm{Re}\, z > 0 \ . \tag{B.8}$$

The requirement of $\mathrm{Re}\, z > 0$ is needed to insure the convergence of the integral. A useful expansion is given by

$$\Gamma(1 + \epsilon) = 1 - \gamma_E \, \epsilon + \frac{6\, \gamma_E^2 + \pi^2}{12} \, \epsilon^2 + \mathcal{O}\left(\epsilon^3\right) \ , \tag{B.9}$$

where $\gamma_E = 0.5772157\dots$ is the Euler-Mascheroni constant.

From eq. (B.8), it is easy to obtain the relation with the Euler Beta function, that is

$$
\begin{aligned}
B(\alpha + 1, \beta + 1) = \int_0^1 dx \, x^\alpha (1 - x)^\beta &= 2 \int_0^{\frac{\pi}{2}} d\phi \, (\sin\phi)^{2\alpha+1} (\cos\phi)^{2\beta+1} \\
&= \frac{\Gamma(\alpha + 1)\, \Gamma(\beta + 1)}{\Gamma(\alpha + \beta + 2)} \ .
\end{aligned}
\tag{B.10}
$$

Another important function, often encountered in loop calculations, is the dilogarithm function, defined as

$$\text{Li}_2\left(z\right) = -\int_0^z dt\, \frac{\log(1-t)}{t} = \sum_{k=0}^{\infty} \frac{z^k}{k^2}\,, \qquad |z| \le 1\,, \tag{B.11}$$

where $|z| \le 1$ is the radius of convergence of the series. An immediate consequence of this definition is the following expansion in powers of ϵ

$$
\begin{aligned}
\int_0^1 dx\, x^{-1-\gamma\epsilon} \left(1 - \alpha\, x\right)^{\beta\epsilon} &= \int_0^1 dx\, x^{-1-\gamma\epsilon} \left[1 + \beta\,\epsilon \log(1-\alpha\,x) + \mathcal{O}\left(\epsilon^2\right)\right] \\
&= -\frac{1}{\gamma\,\epsilon} - \beta\,\epsilon\,\text{Li}_2\left(\alpha\right) + \mathcal{O}\left(\epsilon^2\right)\,.
\end{aligned}
\tag{B.12}
$$

One of the most used properties is the analytic continuation of the dilogarithm function

$$\text{Li}_2\left(x \pm i\eta\right) = -\text{Li}_2\left(\frac{1}{x}\right) - \frac{1}{2}\log^2 x + \frac{\pi^2}{3} \pm i\pi \log x \qquad \text{for} \quad x > 1\,, \tag{B.13}$$

that can be demonstrated with the help of

$$\log(-x \pm i\eta) = \log x \pm i\pi\,, \qquad x > 0\,. \tag{B.14}$$

Finally, we introduce the Riemann ζ-function by means of the functional equation

$$\zeta(z) = 2^z \pi^{z-1} \sin\left(\frac{z\pi}{2}\right) \Gamma\left(1-z\right) \zeta\left(1-z\right)\,, \tag{B.15}$$

which evaluated on integers gives

$$\zeta(n) = \sum_{k=1}^{\infty} \frac{1}{k^n}\,. \tag{B.16}$$

Common useful values are

$$\zeta(0) = -\frac{1}{2}\,, \quad \zeta(1) = \infty\,, \quad \zeta(2) = \frac{\pi^2}{6}\,, \tag{B.17}$$

$$\zeta(3) = 1.202056903\ldots\,, \quad \zeta(4) = \frac{\pi^4}{90}\,. \tag{B.18}$$

Monte Carlo Techniques

In this appendix, we want to detail some well-known Monte Carlo techniques, which are frequently adopted in SMC programs.

C.1   The veto technique

In this section we describe a method to generate a set of d variables x, distributed according to

$$f(x)\,\Delta(h(x)) \tag{C.1}$$

where

$$\Delta(h) = \exp\left\{-\int d^dx'\, f(x')\,\theta(h(x') - h)\right\}. \tag{C.2}$$

We assume, as usual, that f and h are non-negative functions, and that the unrestricted integral of f is divergent, that is

$$\Delta(0) = \exp\left\{-\int d^dx'\, f(x')\right\} = 0\,. \tag{C.3}$$

Within these assumptions, upon multiplying the infinitesimal probability

$$f(x)\,\Delta(h(x))\,d^dx \tag{C.4}$$

by $\delta(h - h(x))\,dh$, we can integrate over d^dx and interpret it as the infinitesimal probability for the variable h

$$dh \int d^dx\, \delta(h - h(x))\, f(x) \exp\left\{-\int d^dx'\, f(x')\,\theta(h(x') - h)\right\} = dh\,\frac{d\Delta(h)}{dh} = d\Delta(h)\,, \tag{C.5}$$

179

that shows that the probability is uniform in $\Delta(h)$. In principle, the generation of events is therefore straightforward: one generates a uniform random number r between 0 and 1, and solves the equation $\Delta(H) = r$ for H (here we have used the fact that $\Delta(0) = 0$). At this point, the variables x have distribution function equal to

$$\delta(H - h(x))\, f(x) \exp \left\{ - \int d^d x'\, f(x')\, \theta(h(x') - H) \right\}, \tag{C.6}$$

where the exponent is now just a number (a normalization factor), so that the variables x are on the surface $\delta(H - h(x))$, with a distribution function proportional to $f(x)\,\delta(H - h(x))$. The generation of these variables can be done, for example, with a hit-and-miss technique, or, if the integration can be performed analytically, by generating $(d-1)$ random numbers r_i, uniformly distributed between 0 and 1, and solving

$$\int_{x_{i,0}}^{X_i} dx_i \prod_{k \neq i} \int dx_k\, \delta(H - h(x))\, f(x) = r_i \tag{C.7}$$

for X_i, where $x_{i,0}$ is the lower limit for the variable x_i, and all the other variables are integrated over their full range of validity.

In practice, however, the solution of the equation $\Delta(H) = r$ is, in most cases, very heavy, from a numerical point of view. This difficulty can be overcome by means of the so-called veto method. We assume that there is a function $F(x) \geq f(x)$ for all x values, and that

$$\Delta_F(h) = \exp \left[- \int d^d x'\, F(x')\, \theta(h(x') - h) \right] \tag{C.8}$$

has a simple form, so that the solution of the equation $\Delta_F(H) = r$ and the generation of the distribution $F(x)\,\delta(H - h(x))$ are reasonably simple. Then, we implement the following procedure:

1. Set $H_{\max}$ equal to the maximum allowed value, such that $\Delta_F(H_{\max}) = 1$.

2. Generate a flat random number $0 < r < 1$ and solve the equation

$$\frac{\Delta_F(H)}{\Delta_F(H_{\max})} = r \tag{C.9}$$

   for H (a solution with $0 < H < H_{\max}$ always exists for $0 < r < 1$).

3. Generate x according to $F(x)\,\delta(h(x) - H)$.

4. Generate a new random number r'.

5. If $r' > f(x)/F(x)$ then the event is vetoed, we set $H_{\max} = H$, go to step 2 and continue. Otherwise the event is accepted, and the procedure stops.

The resulting events are distributed according to eq. (C.1). The proof of this statement goes as follows.

First consider that at the end of the vetoing procedure, the event distribution will be given by the sum of the distribution for the case in which there is no veto, there is one veto applied, two vetoes, etc.. The probability distribution of events generated with no veto applied is given by

$$P_0(x) = \int_0^{H_{\max}} dh_1 \, \frac{\Delta_F(h_1)}{\Delta_F(H_{\max})} \, F(x) \, \delta(h(x) - h_1)) \, \frac{f(x)}{F(x)}$$
$$= f(x) \, \Delta_F(h(x)) \,. \tag{C.10}$$

We have used the fact that $\Delta_F(H_{\max}) = 1$, and we have inserted a factor of $f(x)/F(x)$, corresponding to the acceptance probability.

When one veto is applied, we have

$$
\begin{aligned}
P_1(x) &= \int_0^{H_{\max}} dh_1 \, \frac{\Delta_F(h_1)}{\Delta_F(H_{\max})} \int d^d x_1 \, F(x_1) \, \delta(h(x_1) - h_1) \left(1 - \frac{f(x_1)}{F(x_1)} \right) \\
&\quad \times \int_0^{h_1} dh_2 \, \frac{\Delta_F(h_2)}{\Delta_F(h_1)} \, F(x) \, \delta(h(x) - h_2)) \, \frac{f(x)}{F(x)} \\
&= f(x) \, \Delta_F(h(x)) \int_{h(x)}^{H_{\max}} dh_1 \, g(h_1) \,, \tag{C.11}
\end{aligned}
$$

where we have defined

$$g(h_1) = \int d^d x_1 \, F(x_1) \, \delta(h(x_1) - h_1) \left(1 - \frac{f(x_1)}{F(x_1)} \right) \,. \tag{C.12}$$

The factor $1 - f(x_1)/F(x_1)$ is the rejection probability, which must be inserted at each vetoed step. Note that the result is nonzero only for $h_1 \geq h(x)$, because of the δ function in the h_2 integration.

It will be useful to perform one more step explicitly; for two vetoes, we find

$$
\begin{aligned}
P_2(x) &= \int_0^{H_{\max}} dh_1 \, \frac{\Delta_F(h_1)}{\Delta_F(H_{\max})} \, g(h_1) \int_0^{h_1} dh_2 \, \frac{\Delta_F(h_2)}{\Delta_F(h_1)} \, g(h_2) \\
&\quad \times \int_0^{h_2} dh_3 \, \frac{\Delta_F(h_3)}{\Delta_F(h_2)} \, F(x) \, \delta(h(x) - h_3)) \, \frac{f(x)}{F(x)} \\
&= f(x) \, \Delta_F(h(x)) \, \frac{1}{2} \left[\int_{h(x)}^{H_{\max}} dh \, g(h) \right]^2 ,
\end{aligned}
\tag{C.13}
$$

where we have used symmetric integration. It is now easy to obtain the generic term of this infinite sum, namely the term with n vetoes applied. We get

$$
P_n(x) = \Delta_F(h(x)) \, h(x) \, \frac{1}{n!} \left[\int_{h(x)}^{H_{\max}} dh \, g(h) \right]^n .
\tag{C.14}
$$

The sum over n yields

$$
\begin{aligned}
\sum_{n=0}^{\infty} P_n(x) &= f(x) \, \Delta_F(f(x)) \, \exp\left[\int_{f(x)}^{H_{\max}} dh \, g(h) \right] \\
&= f(x) \, \Delta_F(h(x)) \, \exp\left[\int d^d x' \, [F(x') - f(x')] \, \theta(h(x') - h(x)) \right] \\
&= f(x) \, \exp\left[- \int d^d x' \, f(x') \, \theta(h(x') - h(x)) \right] ,
\end{aligned}
\tag{C.15}
$$

which is the announced result.

C.2   The highest-p_{T} bid procedure

Our aim is to generate (k, x_k) pairs with a probability

$$
f_k(x_k) \prod_i \Delta_i(h_k(x_k)) \, d^d x_k ,
\tag{C.16}
$$

where

$$
\Delta(h) = \prod_i \Delta_i(h) ,
\tag{C.17}
$$

and

$$
\Delta_i(h) = \exp\left\{ - \int d^d x_i' \, f_i(x_i') \, \theta(h_i(x_i') - h) \right\} .
\tag{C.18}
$$

We assume, as in the previous section, that the f_i and h_i are non-negative functions, and that the unrestricted integral of the f_i is divergent, that is

$$\Delta_i(0) = \exp\left\{ - \int d^d x'_i \, f_i(x'_i) \right\} = 0 \,. \tag{C.19}$$

Under these conditions, we have the identity

$$\int d^d x_k \, \Delta_k(h_k(x_k)) \, f_k(x_k) \, \delta(h_k(x_k) - h) = \frac{d}{dh} \Delta_k(h) \,, \tag{C.20}$$

so that

$$\int d^d x_k \, \Delta_k(h_k(x_k)) \, f_k(x_k) \, \theta(h - h_k(x_k))$$

$$= \int_0^\infty dh' \int d^d x_k \, \Delta_k(h_k(x_k)) \, f_k(x_k) \, \delta(h' - h_k(x_k)) \, \theta(h - h')$$

$$= \int_0^\infty dh' \, \frac{d}{dh'} \Delta_k(h') \, \theta(h - h') = \int_0^h dh' \, \frac{d}{dh'} \Delta_k(h') = \Delta_k(h) \,, \tag{C.21}$$

where we have used the fact that $\Delta_k(0) = 0$. If we interpret h and h_k as transverse momenta, then $\Delta_k(h)$ in eq. (C.21) corresponds to the probability of not emitting a parton with transverse momentum bigger than h.

The procedure to generate the distribution in eq. (C.16), using the highest-bid method, is the following. For each k, we generate an x_k value with probability

$$\Delta_k(h_k(x_k)) \, f_k(x_k) \, d^d x_k \,, \tag{C.22}$$

as described in Appendix C.1, and then we pick the k value with the largest $h_k(x_k)$. In fact, the probability that the generated (k, x_k) has the largest $h_k(x_k)$ is precisely given by the product of its generation probability (eq. (C.22)) times the probability that all the other $h_i(x_i)$ are less then $h_k(x_k)$, which is given by the product

$$\prod_{i \neq k} \Delta_i(h_k(x_k)) \,, \tag{C.23}$$

and together they reconstruct eq. (C.16).

C.3 Generation of radiation according to an upper bounding function

In this section we document the generation of radiation according to an upper bounding function. In the following , we present the case of single vector boson production, but the case of Higgs boson production is fully analogous, once the change of variables $\xi = 1 - x$, $y = (1 - 2v - x)/(1 - x)$ is performed, and the different definitions of $d\Phi_{\text{rad}}$ are properly taken into account (see also Appendix D of [26]). We thus start from eq. (4.44),

$$U = \frac{16\pi^2}{\bar{M}^2} N \frac{\alpha_s(k_T^2)}{2v} \frac{x^2}{1 - x - v}. \tag{C.24}$$

Using the definitions of eqs. (4.22) and (4.17)

$$d\Phi_{\text{rad}} = \frac{\bar{M}^2}{16\pi^2} \frac{d\phi}{2\pi} dv \frac{dx}{x^2} \theta(v) \theta\left(1 - \frac{v}{1 - x}\right) \theta(x(1 - x)) \theta(x - \bar{x}_\oplus), \tag{C.25}$$

$$k_T^2 = \frac{\bar{M}^2}{x}(1 - x - v) v, \tag{C.26}$$

and calling $\Delta_U(p_T^2)$ the resulting Sudakov form factor, we write

$$
\begin{aligned}
\frac{\log \Delta_U(p_T^2)}{-N} &= \int_{\bar{x}}^1 \frac{dx}{x^2} \int_0^{1-x} dv \frac{\alpha_s(k_T^2)}{2v} \frac{x^2}{1 - x - v} \theta\left(k_T^2 - p_T^2\right) \\
&= \int_{\bar{x}}^1 \frac{dx}{x} \int_0^{1-x} dv \frac{\alpha_s(k_T^2)}{2} \frac{\bar{M}^2}{k_T^2} \theta\left(k_T^2 - p_T^2\right) \\
&= \int_{p_T^2}^\infty \frac{dk_T^2}{k_T^2} \frac{\alpha_s(k_T^2)}{2} \int_0^1 dv \\
&\quad \times \int_{\bar{x}}^1 \frac{dx}{x} \theta(1 - x - v) \bar{M}^2 \delta\left(\frac{\bar{M}^2}{x}(1 - x - v)v - k_T^2\right), \tag{C.27}
\end{aligned}
$$

where, for ease of notation, we have dropped the $\oplus$ and $q\bar{q}$ labels on N and $\bar{x}$. We perform the x integration using the δ function

$$\int \frac{dx}{x} \bar{M}^2 \delta\left(\frac{\bar{M}^2}{x}(1 - x - v)v - k_T^2\right) = \frac{1}{k_T^2/\bar{M}^2 + v}, \qquad x = \frac{\bar{M}^2 v(1 - v)}{k_T^2 + \bar{M}^2 v}. \tag{C.28}$$

Notice that $x < 1$, and

$$\theta\left(1 - v - \frac{\bar{M}^2 v(1 - v)}{k_T^2 + \bar{M}^2 v}\right) = \theta\left(1 - v \frac{k_T^2 + \bar{M}^2}{k_T^2 + \bar{M}^2 v}\right) = 1. \tag{C.29}$$

The only remaining condition on x is $x \geqslant \bar{x}$. We thus get

$$\frac{\log \Delta_U(p_T^2)}{-N} = \int_{p_T^2}^{\infty} \frac{dk_T^2}{k_T^2} \frac{\alpha_s(k_T^2)}{2} \int_0^1 \frac{dv}{k_T^2/\bar{M}^2 + v} \theta\left(\frac{\bar{M}^2 v(1-v)}{k_T^2 + \bar{M}^2 v} - \bar{x}\right). \qquad \text{(C.30)}$$

We must find the conditions implied by the theta function upon v. For

$$k_T^2 < k_{T\,\text{max}}^2 = \frac{\bar{M}^2(1-\bar{x})^2}{4\bar{x}}, \qquad \text{(C.31)}$$

the θ function is satisfied if $v_- < v < v_+$, where

$$v_\pm = \frac{1 - \bar{x} \pm \sqrt{(1-\bar{x})^2 - 4\,\bar{x}\,\frac{k_T^2}{M^2}}}{2}. \qquad \text{(C.32)}$$

We thus have

$$\frac{\log \Delta_U(p_T^2)}{-N} = \int_{p_T^2}^{k_{T\,\text{max}}^2} \frac{dk_T^2}{k_T^2} \frac{\alpha_s(k_T^2)}{2} \log \frac{\frac{k_T^2}{M^2} + v_+}{\frac{k_T^2}{M^2} + v_-}. \qquad \text{(C.33)}$$

The k_T^2 integral is still too complex to be performed analytically. We thus resort another time to the veto method, by finding an upper bound to the integrand. We have

$$\frac{\frac{k_T^2}{M^2} + v_+}{\frac{k_T^2}{M^2} + v_-} \leqslant \frac{\frac{k_T^2}{M^2} + 1}{\frac{k_T^2}{M^2}} = \frac{\bar{M}^2}{k_T^2} + 1 \leqslant \frac{\bar{M}^2}{k_T^2} + \frac{k_{T\,\text{max}}^2}{k_T^2} = \frac{\bar{M}^2(1+\bar{x})^2}{4\,\bar{x}\,k_T^2}. \qquad \text{(C.34)}$$

We thus define

$$q^2 = \frac{\bar{M}^2(1+\bar{x})^2}{4\,\bar{x}\,k_T^2}, \qquad \text{(C.35)}$$

and introduce a new Sudakov form factor

$$\frac{\log \tilde{\Delta}_U(p_T^2)}{-N} = \int_{p_T^2}^{k_{T\,\text{max}}^2} \frac{dk_T^2}{k_T^2} \frac{\alpha_U(k_T^2)}{2} \log \frac{q^2}{k_T^2}, \qquad \text{(C.36)}$$

where $\alpha_U(k_T^2)$ has the form of the one-loop running coupling constant

$$\alpha_U(k_T^2) = \frac{1}{b_0 \log \frac{k_T^2}{\Lambda_U^2}}, \qquad \text{(C.37)}$$

and is required to satisfy the bound $\alpha_U(k_T^2) \geqslant \alpha_s(k_T^2)$ in the allowed range for k_T^2. The integral in eq. (C.36) is now easily performed, and we get

$$\tilde{\Delta}_U(p_T^2) = \exp\left\{ -\frac{N}{2b} \left[\log \frac{q^2}{\Lambda_U^2} \log \frac{\log \frac{k_{T\,\text{max}}^2}{\Lambda_U^2}}{\log \frac{p_T^2}{\Lambda_U^2}} - \log \frac{k_{T\,\text{max}}^2}{p_T^2} \right] \right\}. \qquad \text{(C.38)}$$

The generation of the radiation variables is then performed starting with $\tilde{\Delta}_U(p_T^2)$, using the veto procedure to obtain the $\Delta_U(p_T^2)$ distribution. Further vetoing is then used to obtain the correct R/B generated distribution.

Bibliography

[1] M. Dobbs, *Phase space veto method for next-to-leading order event generators in hadronic collisions*, *Phys. Rev.* **D65** (2002) 094011, [`hep-ph/0111234`].

[2] S. Frixione and B. R. Webber, *Matching NLO QCD computations and parton shower simulations*, *JHEP* **06** (2002) 029, [`hep-ph/0204244`].

[3] Y. Kurihara *et al.*, *QCD event generators with next-to-leading order matrix-elements and parton showers*, *Nucl. Phys.* **B654** (2003) 301–319, [`hep-ph/0212216`].

[4] P. Nason, *A new method for combining NLO QCD with shower Monte Carlo algorithms*, *JHEP* **11** (2004) 040, [`hep-ph/0409146`].

[5] Z. Nagy and D. E. Soper, *Matching parton showers to nlo computations*, *JHEP* **10** (2005) 024, [`hep-ph/0503053`].

[6] M. Kramer, S. Mrenna, and D. E. Soper, *Next-to-leading order qcd jet production with parton showers and hadronization*, *Phys. Rev.* **D73** (2006) 014022, [`hep-ph/0509127`].

[7] C. W. Bauer and M. D. Schwartz, *Event generation from effective field theory*, *Phys. Rev.* **D76** (2007) 074004, [`hep-ph/0607296`].

[8] C. W. Bauer and F. J. Tackmann, *Gaining analytic control of parton showers*, `arXiv:0705.1719`.

[9] Z. Nagy and D. E. Soper, *Parton showers with quantum interference*, *JHEP* **09** (2007) 114, [`arXiv:0706.0017`].

[10] W. T. Giele, D. A. Kosower, and P. Z. Skands, *A simple shower and matching algorithm*, `arXiv:0707.3652`.

[11] M. Dinsdale, M. Ternick, and S. Weinzierl, *Parton showers from the dipole formalism*, `arXiv:0709.1026`.

[12] S. Schumann and F. Krauss, *A parton shower algorithm based on catani-seymour dipole factorisation*, `arXiv:0709.1027`.

[13] S. Platzer and S. Gieseke, *Coherent Parton Showers with Local Recoils*, `arXiv:0909.5593`.

[14] G. Marchesini *et al.*, *HERWIG: A Monte Carlo event generator for simulating hadron emission reactions with interfering gluons. Version 5.1 - April 1991*, *Comput. Phys. Commun.* **67** (1992) 465–508.

[15] G. Corcella *et al.*, *HERWIG 6: An event generator for hadron emission reactions with interfering gluons (including supersymmetric processes)*, *JHEP* **01** (2001) 010, [`hep-ph/0011363`].

[16] G. Corcella *et al.*, *Herwig 6.5 release note*, `hep-ph/0210213`.

[17] S. Frixione, P. Nason, and B. R. Webber, *Matching NLO QCD and parton showers in heavy flavour production*, *JHEP* **08** (2003) 007, [`hep-ph/0305252`].

[18] S. Frixione, E. Laenen, P. Motylinski, and B. R. Webber, *Single-top production in MC@NLO*, *JHEP* **03** (2006) 092, [`hep-ph/0512250`].

[19] E. Boos *et al.*, *Generic user process interface for event generators*, `hep-ph/0109068`.

[20] M. Bahr *et al.*, *Herwig++ Physics and Manual*, *Eur. Phys. J.* **C58** (2008) 639–707, [`arXiv:0803.0883`].

[21] L. Lonnblad, *Ariadne version 4: A program for simulation of qcd cascades implementing the color dipole model*, *Comput. Phys. Commun.* **71** (1992) 15–31.

[22] T. Sjostrand, S. Mrenna, and P. Skands, *Pythia 6.4 physics and manual*, *JHEP* **05** (2006) 026, [`hep-ph/0603175`].

[23] G. Gustafson and U. Pettersson, *Dipole Formulation of QCD Cascades*, *Nucl. Phys.* **B306** (1988) 746.

[24] U. Pettersson, *ARIADNE: A Monte Carlo for QCD cascades in the color dipole formulation*, . LU-TP-88-5.

[25] L. Lonnblad and U. Pettersson, *ARIADNE 2: A Monte Carlo for QCD cascades in the color dipole formulation: An update*, . LU-TP-88-15.

[26] P. Nason and G. Ridolfi, *A positive-weight next-to-leading-order Monte Carlo for Z pair hadroproduction*, *JHEP* **08** (2006) 077, [`hep-ph/0606275`].

[27] S. Frixione, P. Nason, and G. Ridolfi, *A Positive-Weight Next-to-Leading-Order Monte Carlo for Heavy Flavour Hadroproduction*, *JHEP* **09** (2007) 126, [`arXiv:0707.3088`].

[28] O. Latunde-Dada, S. Gieseke, and B. Webber, *A positive-weight next-to-leading-order Monte Carlo for e^+e^- annihilation to hadrons*, *JHEP* **02** (2007) 051, [`hep-ph/0612281`].

[29] O. Latunde-Dada, *Applying the POWHEG method to top pair production and decays at the ILC*, *Eur. Phys. J.* **C58** (2008) 543–554, [`arXiv:0806.4560`].

[30] S. Frixione, P. Nason, and C. Oleari, *Matching NLO QCD computations with Parton Shower simulations: the POWHEG method*, *JHEP* **11** (2007) 070, [`arXiv:0709.2092`].

[31] S. Catani and M. H. Seymour, *A general algorithm for calculating jet cross sections in NLO QCD*, *Nucl. Phys.* **B485** (1997) 291–419, [`hep-ph/9605323`].

[32] S. Frixione, Z. Kunszt, and A. Signer, *Three-jet cross sections to next-to-leading order*, *Nucl. Phys.* **B467** (1996) 399–442, [`hep-ph/9512328`].

[33] S. Frixione, *A general approach to jet cross sections in QCD*, *Nucl. Phys.* **B507** (1997) 295–314, [`hep-ph/9706545`].

[34] S. Alioli, P. Nason, C. Oleari, and E. Re, *NLO vector-boson production matched with shower in POWHEG*, *JHEP* **07** (2008) 060, [`arXiv:0805.4802`].

[35] K. Hamilton, P. Richardson, and J. Tully, *A Positive-Weight Next-to-Leading Order Monte Carlo Simulation of Drell-Yan Vector Boson Production*, *JHEP* **10** (2008) 015, [`arXiv:0806.0290`].

[36] A. Papaefstathiou and O. Latunde-Dada, *NLO production of W ' bosons at hadron colliders using the MC@NLO and POWHEG methods*, JHEP **07** (2009) 044, [`arXiv:0901.3685`].

[37] S. Alioli, P. Nason, C. Oleari, and E. Re, *NLO Higgs boson production via gluon fusion matched with shower in POWHEG*, JHEP **04** (2009) 002, [`arXiv:0812.0578`].

[38] K. Hamilton, P. Richardson, and J. Tully, *A Positive-Weight Next-to-Leading Order Monte Carlo Simulation for Higgs Boson Production*, JHEP **04** (2009) 116, [`arXiv:0903.4345`].

[39] S. Alioli, P. Nason, C. Oleari, and E. Re, *NLO single-top production matched with shower in POWHEG: s- and t-channel contributions*, `arXiv:0907.4076`.

[40] D. J. Gross and F. Wilczek, *Ultraviolet behaviour of non-abelian gauge theories*, Phys. Rev. Lett. **30** (1973) 1343–1346.

[41] H. D. Politzer, *Reliable perturbative results for strong interactions?*, Phys. Rev. Lett. **30** (1973) 1346–1349.

[42] T. van Ritbergen, J. A. M. Vermaseren, and S. A. Larin, *The four-loop beta function in quantum chromodynamics*, Phys. Lett. **B400** (1997) 379–384, [`hep-ph/9701390`].

[43] S. Bethke, *The 2009 Wolrd Average of $\alpha_s(M_Z)$*, `arXiv:0908.1135`.

[44] F. Bloch and A. Nordsieck, *Note on the Radiation Field of the electron*, Phys. Rev. **52** (1937) 54–59.

[45] D. R. Yennie, S. C. Frautschi, and H. Suura, *The infrared divergence phenomena and high-energy processes*, Ann. Phys. **13** (1961) 379–452.

[46] T. Kinoshita, *Mass singularities of Feynman amplitudes*, J. Math. Phys. **3** (1962) 650–677.

[47] T. D. Lee and M. Nauenberg, *Degenerate Systems and Mass Singularities*, Phys. Rev. **133** (1964) B1549–B1562.

[48] K. Fabricius, I. Schmitt, G. Kramer, and G. Schierholz, *Higher Order Perturbative QCD Calculation of Jet Cross- Sections in e+ e- Annihilation*, *Zeit. Phys.* **C11** (1981) 315.

[49] R. K. Ellis, D. A. Ross, and A. E. Terrano, *The perturbative calculation of jet structure in e+ e- annihilation*, *Nucl. Phys.* **B178** (1981) 421.

[50] A. Bassetto, M. Ciafaloni, and G. Marchesini, *Jet Structure and Infrared Sensitive Quantities in Perturbative QCD*, *Phys. Rept.* **100** (1983) 201–272.

[51] Y. L. Dokshitzer, V. A. Khoze, A. H. Mueller, and S. I. Troian, *Basics of perturbative QCD*, . Gif-sur-Yvette, France: Ed. Frontieres (1991) 274 p. (Basics of).

[52] B. R. Webber, *Monte Carlo Simulation of Hard Hadronic Processes*, *Ann. Rev. Nucl. Part. Sci.* **36** (1986) 253–286.

[53] T. Sjostrand, *Monte Carlo generators*, `hep-ph/0611247`.

[54] F. Ambroglini *et al.*, *Proceedings of the Workshop on Monte Carlo's, Physics and Simulations at the LHC PART I*, `arXiv:0902.0293`.

[55] A. H. Mueller, *On the Multiplicity of Hadrons in QCD Jets*, *Phys. Lett.* **B104** (1981) 161–164.

[56] H.-U. Bengtsson and T. Sjostrand, *PYTHIA: The Lund Monte Carlo for hadronic processes*, . To appear in Proc. of 1986 Summer Study on Physics of the Superconducting Super Collider, Snowmass, CO, Jun 23 - Jul 11, 1986.

[57] H.-U. Bengtsson and T. Sjostrand, *The Lund Monte Carlo for Hadronic Processes: Pythia Version 4.8*, *Comput. Phys. Commun.* **46** (1987) 43.

[58] T. Sjostrand, S. Mrenna, and P. Z. Skands, *A brief introduction to pythia 8.1*, `arXiv:0710.3820`.

[59] W. Furmanski and R. Petronzio, *Singlet parton densities beyond leading order*, *Phys. Lett.* **B97** (1980) 437.

[60] G. Curci, W. Furmanski, and R. Petronzio, *Evolution of parton densities beyond leading order: The nonsinglet case*, *Nucl. Phys.* **B175** (1980) 27.

[61] S. Catani, B. R. Webber, and G. Marchesini, *QCD coherent branching and semiinclusive processes at large x*, *Nucl. Phys.* **B349** (1991) 635–654.

[62] S. Catani, F. Krauss, R. Kuhn, and B. R. Webber, *QCD matrix elements + parton showers*, *JHEP* **11** (2001) 063, [`hep-ph/0109231`].

[63] F. Krauss, *Matrix elements and parton showers in hadronic interactions*, *JHEP* **08** (2002) 015, [`hep-ph/0205283`].

[64] M. L. Mangano, *presentation at the FNAL Matrix Element/Monte Carlo Tuning Working Group*, `http://www-cpd.fnal.gov/personal/mrenna/tuning/nov2002/mlm.pdf`.

[65] T. Gleisberg *et al.*, *SHERPA 1.alpha, a proof-of-concept version*, *JHEP* **02** (2004) 056, [`hep-ph/0311263`].

[66] A. Schalicke and F. Krauss, *Implementing the ME+PS merging algorithm*, *JHEP* **07** (2005) 018, [`hep-ph/0503281`].

[67] M. L. Mangano, M. Moretti, F. Piccinini, R. Pittau, and A. D. Polosa, *ALPGEN, a generator for hard multiparton processes in hadronic collisions*, *JHEP* **07** (2003) 001, [`hep-ph/0206293`].

[68] T. Stelzer and W. F. Long, *Automatic generation of tree level helicity amplitudes*, *Comput. Phys. Commun.* **81** (1994) 357–371, [`hep-ph/9401258`].

[69] F. Maltoni and T. Stelzer, *MadEvent: Automatic event generation with MadGraph*, *JHEP* **02** (2003) 027, [`hep-ph/0208156`].

[70] A. Kanaki and C. G. Papadopoulos, *HELAC: A package to compute electroweak helicity amplitudes*, *Comput. Phys. Commun.* **132** (2000) 306–315, [`hep-ph/0002082`].

[71] A. Cafarella, C. G. Papadopoulos, and M. Worek, *Helac-Phegas: a generator for all parton level processes*, *Comput. Phys. Commun.* **180** (2009) 1941–1955, [`0710.2427`].

[72] S. Mrenna and P. Richardson, *Matching matrix elements and parton showers with HERWIG and PYTHIA*, *JHEP* **05** (2004) 040, [`hep-ph/0312274`].

[73] M. L. Mangano, M. Moretti, F. Piccinini, and M. Treccani, *Matching matrix elements and shower evolution for top-quark production in hadronic collisions*, *JHEP* **01** (2007) 013, [`hep-ph/0611129`].

[74] S. Frixione, E. Laenen, P. Motylinski, B. R. Webber, and C. D. White, *Single-top hadroproduction in association with a W boson*, *JHEP* **07** (2008) 029, [`arXiv:0805.3067`].

[75] Y. L. Dokshitzer, D. Diakonov, and S. I. Troian, *Hard Processes in Quantum Chromodynamics*, *Phys. Rept.* **58** (1980) 269–395.

[76] S. Kawabata, *A New version of the multidimensional integration and event generation package BASES/SPRING*, *Comp. Phys. Commun.* **88** (1995) 309–326.

[77] P. Nason, *MINT: a Computer Program for Adaptive Monte Carlo Integration and Generation of Unweighted Distributions*, `arXiv:0709.2085`.

[78] G. P. Lepage, *Vegas: An adaptive multidimensional integration program*, . CLNS-80/447.

[79] K. Hagiwara and D. Zeppenfeld, *Helicity Amplitudes for Heavy Lepton Production in e^+e^- Annihilation*, *Nucl. Phys.* **B274** (1986) 1.

[80] K. Hagiwara and D. Zeppenfeld, *Amplitudes for Multiparton Processes Involving a Current at e^+e^-, $e^\pm p$, and Hadron Colliders*, *Nucl. Phys.* **B313** (1989) 560.

[81] J. Pumplin *et al.*, *New generation of parton distributions with uncertainties from global QCD analysis*, *JHEP* **07** (2002) 012, [`hep-ph/0201195`].

[82] G. P. Salam and G. Soyez, *A practical Seedless Infrared-Safe Cone jet algorithm*, *JHEP* **05** (2007) 086, [`arXiv:0704.0292`].

[83] M. Cacciari and G. P. Salam, *Dispelling the N^3 myth for the k_T jet-finder*, *Phys. Lett.* **B641** (2006) 57–61, [`hep-ph/0512210`].

[84] M. Bengtsson and T. Sjostrand, *Coherent Parton Showers Versus Matrix Elements: Implications of PETRA - PEP Data*, *Phys. Lett.* **B185** (1987) 435.

[85] C. Anastasiou, L. J. Dixon, K. Melnikov, and F. Petriello, *High-precision QCD at hadron colliders: Electroweak gauge boson rapidity distributions at NNLO*, *Phys. Rev.* **D69** (2004) 094008, [`hep-ph/0312266`].

[86] **CTEQ** Collaboration, H. L. Lai *et al.*, *Global QCD analysis of parton structure of the nucleon: CTEQ5 parton distributions*, *Eur. Phys. J.* **C12** (2000) 375–392, [`hep-ph/9903282`].

[87] **D0** Collaboration, V. M. Abazov *et al.*, *Measurement of the shape of the boson transverse momentum distribution in* $p\bar{p} \to Z/\gamma^* \to e^+e^- + X$ *events produced at* $\sqrt{s} = 1.96$ *TeV*, *Phys. Rev. Lett.* **100** (2008) 102002, [`arXiv:0712.0803 [hep-ex]`].

[88] **CDF** Collaboration, A. A. Affolder *et al.*, *The transverse momentum and total cross section of* e^+e^- *pairs in the Z boson region from* $p\bar{p}$ *collisions at* $\sqrt{s} = 1.8$ *TeV*, *Phys. Rev. Lett.* **84** (2000) 845–850, [`hep-ex/0001021`].

[89] **D0** Collaboration, B. Abbott *et al.*, *Measurement of the inclusive differential cross section for Z bosons as a function of transverse momentum in* $\bar{p}p$ *collisions at* $\sqrt{s} = 1.8$ *TeV*, *Phys. Rev.* **D61** (2000) 032004, [`hep-ex/9907009`].

[90] **D0** Collaboration, B. Abbott *et al.*, *Differential production cross section of Z bosons as a function of transverse momentum at* $\sqrt{s} = 1.8$ *TeV*, *Phys. Rev. Lett.* **84** (2000) 2792–2797, [`hep-ex/9909020`].

[91] S. Dawson, *Radiative corrections to Higgs boson production*, *Nucl. Phys.* **B359** (1991) 283–300.

[92] A. Djouadi, M. Spira, and P. M. Zerwas, *Production of Higgs bosons in proton colliders: QCD corrections*, *Phys. Lett.* **B264** (1991) 440–446.

[93] M. Spira, A. Djouadi, D. Graudenz, and P. M. Zerwas, *Higgs boson production at the LHC*, *Nucl. Phys.* **B453** (1995) 17–82, [`hep-ph/9504378`].

[94] S. Catani and M. Grazzini, *An NNLO subtraction formalism in hadron collisions and its application to Higgs boson production at the LHC*, *Phys. Rev. Lett.* **98** (2007) 222002, [`hep-ph/0703012`].

[95] J. Alwall *et al.*, *Comparative study of various algorithms for the merging of parton showers and matrix elements in hadronic collisions*, Eur. Phys. J. **C53** (2008) 473–500, [arXiv:0706.2569].

[96] S. Dittmaier, P. Uwer, and S. Weinzierl, *Hadronic top-quark pair production in association with a hard jet at next-to-leading order QCD: Phenomenological studies for the Tevatron and the LHC*, Eur. Phys. J. **C59** (2009) 625–646, [arXiv:0810.0452].

[97] S. Dittmaier, P. Uwer, and S. Weinzierl, *Nlo qcd corrections to t anti-t + jet production at hadron colliders*, Phys. Rev. Lett. **98** (2007) 262002, [hep-ph/0703120].

[98] P. Nason, *Shower Monte Carlo at Next-to-Leading Order*, http://theory.fi.infn.it/research/nason.pdf. Talk given at the Università degli Studi di Firenze, Florence, Italy, 2009.

[99] P. Nason, *MC at NLO tools*, http://indico.cern.ch/getFile.py/access?contribId=2&resId=0&materialId= slides&confId=49675. Talk given at *MC4LHC Meeting*, CERN, Switzerland, 2009.

[100] P. Nason, *POWHEG*, http://agenda.hep.wisc.edu/materialDisplay.py?contribId=13&materialId= slides&confId=189. Talk given at *LoopFest Symposium*, Madison, WI, USA, 2009.

[101] G. Bozzi, S. Catani, D. de Florian, and M. Grazzini, *Transverse-momentum resummation and the spectrum of the Higgs boson at the LHC*, Nucl. Phys. **B737** (2006) 73–120, [hep-ph/0508068].